Stellingen

behorende bij het proefschrift

TURBULENT FREE-SURFACE FLOW OVER A SILL

P. Blom, Delft 1993

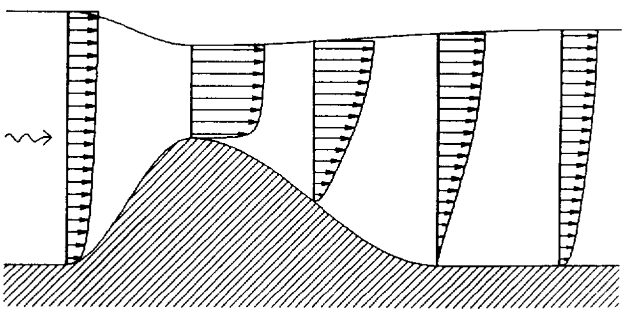

1) Stromingen met een vrij oppervlak kunnen in civiel-technische toepassingen veelal als hydrostatisch beschouwd worden.

2) Het gebruik van convectie- en wrijvingscoëfficiënten in de langegolfvergelijkingen kan de berekende waterspiegel meer in overeenstemming brengen met de in werkelijkheid optredende waterspiegel.

3) De energieverliezen die optreden in een vertragingsgebied, de z.g.n. Carnotverliezen, kunnen in de langegolfvergelijkingen gesimuleerd worden door toepassing van convectiecoëfficiënten met geschikte waarden.

4) De diepte-gemiddelde waarden voor de turbulentie-viscositeit gebaseerd op de diepte-gemiddelde snelheid zijn in een versnellingsgebied te hoog en in een vertragingsgebied te laag in vergelijking tot de waarden berekend met een *ke*-turbulentie model.

5) De bodemschuifspanning berekend met de methode van gewogen residuen geeft een goede benadering van de werkelijk optredende bodemschuifspanning. Toepassing van deze methode in sediment-transport-formules kan een betere voorspelling geven van het lokale sediment-transport dan formules gebaseerd op de conventionele diepte-gemiddelde impulsvergelijkingen alleen.

6) De methode van de asymptotische benaderingen leidt niet altijd tot praktisch bruikbare oplossingen, maar wel tot veel rekenwerk.

7) Stromingsmodellen die een goede snelheidsverdeling berekenen voor situaties waarvan de analytische oplossing bekend is, hoeven dit niet te doen voor meer gecompliceerde stromingssituaties.

8) Ondanks de grote mate van accuratesse en bedieningsgemak van geavanceerde laser-Doppler snelheidsmeters, blijft de nauwkeurigheid van de metingen afhankelijk van deskundige bediening.

9) Omdat een mens vijf vingers aan één hand heeft is het logisch een vijftallig getallenstelsel te gebruiken. Met de vingers van twee handen kan dan tot vijfentwintig worden geteld, hetgeen een voordeel is ten opzichte van het huidige tientallig stelsel.

10) Maatregelen ter bevordering van de wegverkeersveiligheid zijn veelal bedoeld om het *auto*verkeer veiliger te maken. Door dit eenzijdige doel wordt het overige verkeer onnodig in gevaar gebracht.

11) De kans op het aantreffen van beschermde planten en dieren in de Alpen is recht evenredig met de afstand tot de kabelbaan, c.q. tot bewoonde gebieden.

12) Bij de keuze tussen ATV-dagen of verlofdagen in de periode tussen kerst en nieuwjaar is het, i.v.m. de dan meestal heersende griepepidemie, aanbevelenswaardig te kiezen voor verlofdagen.

TURBULENT FREE-SURFACE FLOW OVER A SILL

Proefschrift

ter verkrijging van de graad van doctor aan de
Technische Universiteit Delft, op gezag van de
Rector Magnificus, prof. drs. P.A. Schenck, in
het openbaar te verdedigen ten overstaan van een
commissie aangewezen door het College van Dekanen
op maandag 25 januari 1993 te 16.00 uur

door

Pieter Blom,
geboren te Schiedam
civiel ingenieur

1993

Dit proefschrift is goedgekeurd door de promotor
prof. dr. ir. J.A. Battjes

This thesis is also published as Communications on Hydraulic and Geotechnical Engineering No. 93-1.

Summary

To predict the effects of the closure of the Eastern Scheldt, an estuary in The Netherlands, with a storm surge barrier, two-dimensional computations in a horizontal plane were made to predict the flow velocities and water levels in the area during construction stages of the works. The calculated water levels and flow velocities did not match the measured ones for all situations, especially for flow over a sill (dam under construction). Apparently, the set of equations used in the numerical model, the shallow-water equations, are not adequate for the flow situations considered. These equations are derived by depth-averaging the continuity and momentum equations, in which the uniform-flow velocity and hydrostatic pressure distributions are substituted.

The problem of turbulent free-surface flow over a sill has been investigated in this study. The treatment is restricted to two dimensions in a vertical plane.

For different situations of flow over a sill, two-dimensional numerical calculations have been made. From the results of these two-dimensional calculations modifications in the one-dimensional shallow-water equations are derived. To check the correctness of the velocities obtained by the numerical two-dimensional model, the results of a computation with this model are compared with the results of laser-Doppler velocity measurements in a flume. The similarity between the measured and calculated velocities is good, which gives confidence in the reliability of the calculated velocities and water levels obtained from the numerical model for other situations.

Routine calculations of modifications to the one-dimensional equations from results of two-dimensional models is not practicable. Therefore two analytical methods were used to obtain the modifications. One of these was the method of asymptotic expansions. Unfortunately the modifications derived with this method are only valid for extremely mild slopes.

The other method used, the method of weighted residuals, has a larger range of applicability. For slopes up to $^1/_5$ the water levels obtained by means of this method show good agreement with the water levels obtained from the two-dimensional model.

Nevertheless much work has still to be done to improve this method and to extend it to two dimensions in the horizontal plane. A proposal for such extension (the modifications of the two-dimensional shallow-water equations) is described.

Samenvatting

Om de effecten van het afsluiten van de Oosterschelde met een stormvloedkering te voorspellen, zijn er twee-dimensionale berekeningen gemaakt om de waterstanden en stroomsnelheden te voorspellen voor verschillende uitvoeringsstadia van de werkzaamheden. De berekende waterstanden en stroomsnelheden kwamen niet altijd overeen met gemeten waterstanden of snelheden, met name bij stroming over een drempel (een in aanbouw zijnde dam). Blijkbaar zijn de, in het numerieke model, gebruikte vergelijkingen niet geschikt voor deze stromingssituaties. Deze vergelijkingen zijn afgeleid voor situaties met een vlakke bodem, door de continuïteit- en impulsvergelijkingen over de diepte te middelen. In deze vergelijkingen zijn uitdrukkingen voor het snelheidsprofiel voor uniforme stroming en de hydrostatische drukverdeling gesubstitueerd.

Het probleem van turbulente stroming met vrij water oppervlak over een drempel is in deze studie onderzocht. De beschouwing is beperkt tot twee dimensies in een verticaal vlak.

Voor verschillende situaties van stroming over een heuvel zijn twee-dimensionale computer berekeningen gemaakt. Uit de resultaten van deze berekeningen zijn aanpassingen van de één-dimensionale langegolf vergelijkingen afgeleid. Om de juistheid van de met het twee-dimensionale model berekende snelheden te controleren zijn de uitkomsten van het model vergeleken met de uitkomsten van laser-Doppler snelheidsmetingen in een goot. De overeenkomst tussen de gemeten en berekende snelheden is goed, wat vertrouwen geeft in de betrouwbaarheid van de snelheden berekend met het numerieke model in andere situaties.

Berekeningen van aanpassingen van één-dimensionale vergelijkingen door middel van twee-dimensionale berekeningen is niet erg praktisch. Daarom zijn er twee analytische methoden gebruikt om deze modificaties te bepalen. Eén hiervan was de methode van de asymptotische ontwikkelingen. Helaas zijn de aanpassingen berekend met deze methode alleen geldig voor extreem flauwe hellingen.

De andere gebruikte methode, die van de gewogen residuen, heeft een groter toepasbaarheidsgebied. Voor hellingen tot $^1/_5$ vertonen de waterhoogtes bepaald met deze methode grote overeenkomst met de waterstanden bepaald met het twee-dimensionale numerieke model.

Desalniettemin moet er nog veel werk verricht worden om deze methode te verbeteren en uit te breiden naar twee dimensies in een horizontaal vlak. Een voorstel voor zo'n uitbreiding (aanpassing van de twee-dimensionale langegolf vergelijkingen) wordt in dit proefschrift beschreven.

Acknowledgements

This study has been conducted at the Delft University of Technology, Faculty of Civil Engineering, section Hydraulic and Geotechnical Engineering. It was supported in part by Delft Hydraulics and Rijkswaterstaat. Offices and laboratory facilities were provided by the Laboratory of Fluid Mechanics of the Delft University of Technology.

I wish to thank prof. dr. ir. J.A. Battjes for his valuable comments, sharing his experience on fluid mechanics and his stimulating support. Dr. ir. J.P. Th. Kalkwijk is acknowledged for his guidance during the initial phase of the study.

I wish to thank drs. R. Booij for his constructive attitude, his valuable comments, his stimulating suggestions, for his critical reading and sharing his experience on turbulent flows.

The members of the supervision committee, ir. A. Langerak, ir. C. Flokstra, ir. L. Klatter and prof. dr. ir. G.S. Stelling are gratefully acknowledged for their stimulating ideas, suggestions, constructive criticism and fruitful cooperation.

I wish to express my gratitude to the personnel and the staff of the Laboratory of Fluid Mechanics for their support.

I wish to thank the PhD researchers working in the Laboratory of Fluid Mechanics: G.J.C.M. Hofmans, X.-Y. Jin, E.J. Langedoen, A.M. Talmon, A.S. Tijsseling, and P.J. de Wit for being such fine colleagues. Especially Eddy Langedoen is acknowledged for the many fruitful discussions and his critical comments, which often helped to gain insight in fluid mechanics.

Contents page

Symbols

a	height of stagnant water	[m]
a	height of the sill	[m]
a_{cr}	critical sill height	[m]
$a_E, a_H, a_L, a_N, a_P, a_S, a_T, a_W$	coefficients in finite volume model	[-]
a_1, a_2, a_3, a_4	arbitrary coefficients	[-]
a_{10}, a_{11}, a_{12}	arbitrary coefficients	[-]
a_{20}, a_{21}, a_{22}	arbitrary coefficients	[-]
A	area	[m^2]
b	height of mixing layer	[m]
b	arbitrary coefficient	[-]
B	width of flume	[m]
c	coefficient determining the importance of the diffusion part	[-]
c_μ	coefficient in ke-viscosity model	[-]
c_{BE}	coefficient in ke-viscosity model	[-]
d	water depth	[m]
d_r	scaled water depth to 1^{st}-order/2^{nd}-order	[-]
d_0, d_1, d_i	0^{th}-order water depth, 1^{st}-order water depth, i^{th}-order water depth	[-]
D	characteristic vertical length	[m]
f	Coriolis parameter	[-]
f	arbitrary function	[-]
f	frequency	[Hz]
Fr	Froude number	[-]
g	gravitational acceleration	[m/s^2]
i	hydraulic gradient	[-]
k	turbulence energy	[m^2/s^2]
k_N	roughness according to Nikuradse	[m]
L	characteristic horizontal length	[m]
L_{crown}	length of sill's crown	[m]
L_m	length scale of turbulence	[m]
L_{slope}	length of sill's slope	[m]
$L_{\sigma 0}$	$\ln(1/\sigma_0)$	[-]
L_σ	$\ln(d/z_0)$	[-]
$\dot{m}$	mass flux	[kgm/s]
p	water pressure	[Pa]
p_0, p_1, p_i	0^{th}-order, 1^{st}-order, i^{th}-order water pressure	[-]
q	discharge per unit width	[m^2/s]
q_0, q_1, q_i	0^{th}-order, 1^{st}-order, i^{th}-order discharge per unit width	[-]
Q	discharge	[m^3/s]
r	volume fraction	[-]

S	source	[m/s^2]
S_{10}, S_{11}, S_{12}	coefficients in the convective term of the momentum equation	[-]
$S_{20}, S_{21}, S_{22}, S_{23}$	coefficients in the convective term of the energy equation	[-]
S_{30}, S_{31}, S_{32}	coefficients in the friction term of the energy equation	[-]
S_{40}, S_{41}	coefficients in the friction term of the momentum equation	[-]
t	time	[s]
u	flow velocity in x-direction	[m/s]
u_c	maximum horizontal velocity in the boundary layer	[m/s]
u_0	velocity outside mixing layer	[m/s]
u_1	velocity inside mixing layer	[m/s]
u_0, u_1, u_i	0th-order, 1st-order, ith-order flow velocity in x-direction	[-]
$\bar{u}$	depth-averaged velocity in x-direction	[m/s]
u_*	friction velocity	[-]
$\overline{u'^2}$	turbulence energy component	[m^2/s^2]
$\overline{u'w'}$	Reynolds shear stress	[m^2/s^2]
U	characteristic horizontal velocity	[m/s]
v	flow velocity in y-direction	[m/s]
$\bar{v}$	depth-averaged velocity in y-direction	[m/s]
$\overline{v'^2}$	turbulence energy component	[m^2/s^2]
V	volume	[m^3]
w	flow velocity in z-direction	[m/s]
w_0, w_1, w_i	0th-order, 1st-order, ith-order flow velocity in z-direction	[-]
$\overline{w'^2}$	turbulence energy component	[m^2/s^2]
W	characteristic vertical velocity	[m/s]
x	horizontal spatial coordinate	[m]
y	horizontal spatial coordinate	[m]
z	vertical spatial coordinate	[m]
z_b	bottom level	[m]
z_0	roughness length	[m]

α	convection coefficient in momentum equation	[-]
β	coriolis coefficient or convection coefficient in energy equation	[-]
γ	friction coefficient in momentum equation	[-]
γ_1	friction coefficient in energy equation	[-]
Γ	parameter defining the magnitude of the perturbation velocity profile in the method of weighted residuals	[-]
Γ_ϕ	exchange coefficient	[m^2/s]
δ_{ij}	Kronecker delta	[-]
ϵ	dissipation rate of the turbulence energy	[m^3/s^2]
ε	perturbation quantity	[-]
κ	Von Kármán parameter	[-]
λ	friction parameter	[-]
λ	wave length	[m]
ν	kinematic viscosity of fluid	[m^2/s]
ν_L	horizontal viscosity	[m^2/s]
ν_t	eddy-viscosity	[m^2/s]
$\nu_{t0}, \nu_{t1}, \nu_{ti}$	0^{th}-order, 1^{st}-order, i^{th}-order eddy viscosity	[-]
ρ	water density	[kg/m^3]
σ	vertical spatial coordinate in transformed coordinate system	[-]
σ_0	dimensionless roughness length (z_0/d_0)	[-]
ζ	water pressure coefficient	[-]
τ_{ij}	Reynolds stress	[Pa]
τ_{xw}	wind shear stress in x-direction	[Pa]
τ_{yw}	wind shear stress in y-direction	[Pa]
ϕ	arbitrary function	[-]
ϕ	conserved property	[m/s]
χ	ratio of the discharge per unit width to the eddy-viscosity	[-]
$\vec{a}$	arbitrary vector	[-]
$\vec{n}$	normal vector	[-]
$\vec{v}$	velocity vector	[m/s]

1. Introduction

1.1 Background

In civil engineering practice, flows in seas, estuaries, harbours and rivers are usually predicted by making use of hydraulic scale models or numerical models. The prediction of the effects of the Dutch Delta plan is one of the most important applications of these models in the Netherlands. After the catastrophic flood disaster in 1953 the Delta plan was made to protect the Rhine-Meuse-Scheldt delta for future disasters. According to this plan all estuaries of the delta had to be closed, except the approaches to the harbours of Rotterdam and Antwerp. In the beginning of the implementation of the Delta plan the influences of these closures on the flow and water levels in the delta were examined with hydraulic scale models.

After 1970 numerical models were also employed in the examination of these influences. At first 1DH (one-dimensional horizontal) numerical models were used. In these models an estuary is schematized as a system of channels and nodes. The locations of these channels and nodes are defined by the flow pattern, known from observations in the prototype or hydraulic scale models, or by channels in the prototype, separated by relatively high tidal flats. In each channel the 1DH shallow-water equations are solved with an implicit method. Using boundary values as measured in the prototype, it is possible to compute the water levels and discharges in the channels of the estuary. It is possible only to calculate cross sectionally averaged velocities in a channel. A full 2DH (two-dimensional horizontal) flow field cannot be calculated with these models.

In the seventies the development of 2DH numerical models (Leendertse [1970], Gustafsson [1971], Elvius & Sundström [1973]) made it possible to solve the 2DH shallow-water equations. With these models it is possible to compute 2DH flow fields. In the first discretisation schemes used in these models, the inertia and convection terms were approximated with lower order difference schemes. The results of these models were disappointing because instabilities could only be counteracted by imposing unrealistic large eddy-viscosities. These large eddy-viscosities caused inaccurate results, especially if the flow contains circulations (Stelling [1984]). Small time steps increased the stability and accuracy but made the computations less efficient. An important improvement was the use of more

accurate difference schemes, e.g. the scheme developed by Stelling [1984].

The last project of the Delta plan was the partial closure of the Eastern Scheldt (Fig. 1.1.1) with a storm surge barrier. In this estuary the water motion is dominated by tidal flow. As a consequence the Eastern Scheldt has special environmental conditions. Its aquatic life and its function as nursery for flat- and shell-fishes are unique for the Netherlands.

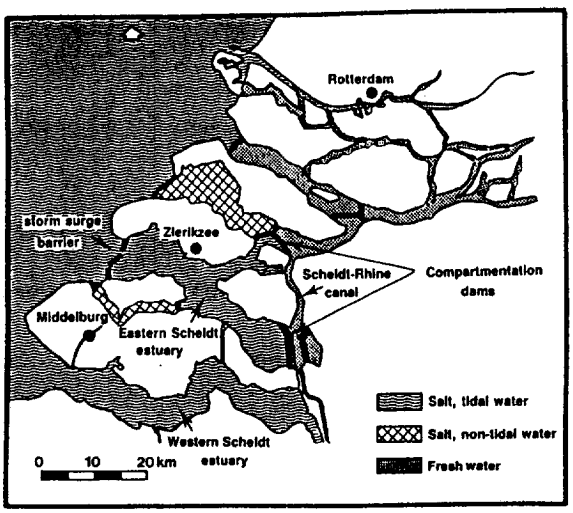

Figure 1.1.1 The Eastern Scheldt estuary after the completion of works

In 1976 the Dutch Government decided to build a storm surge barrier in the mouth of the Eastern Scheldt instead of a massive dam to preserve this unique environment. This change in the Delta plan implied the division of the Eastern Scheldt estuary in compartments. In the western compartment the tide is maintained, but the eastern part has a tide-free fresh water lake to prevent salt intrusion into the agricultural hinterland and to provide a tide-free Scheldt-Rhine canal (Fig. 1.1.1).

Before the construction of the storm surge barrier and the dams started, 2DH calculations were made to predict the water levels and flow velocities for several construction stages in the Eastern Scheldt. During these construction stages many measuring programs took place. The measured water levels and flow velocities were compared with results of the 2DH calculations. In a major part of the basin the measured water levels and flow velocities were found to agree very well with the calculated ones. Only in the vicinity of the storm surge barrier (RWS [1989]) and in the vicinity of dams under construction (RWS [1988]) significant deviations occurred between the calculated and measured water levels and flow

velocities.

In the next section these deviations are discussed, because these deviations determine the aim of this study.

1.2 Aim and scope of the present study

Hydraulic structures in the flow field lead to energy losses other than those generated by the bottom stresses. The flow pattern is basically three-dimensional, often with flow separation and vertical and horizontal eddies directly downstream from the structures. These three-dimensional effects and the additional dissipation of energy in the deceleration zone of the flow are responsible for the additional energy losses. Such hydraulic structures may be a weir, a structure with a gate, e.g. the storm surge barrier, or a series of piers for a bridge. In the context of 2DH flow simulation, such a hydraulic structure is called a barrier. When locating barriers in the 2DH numerical models, special measures have to be taken to introduce the correct energy loss at the barriers.

Barriers are generally schematized as internal boundaries, for which discharge coefficients are prescribed. When the results of the water levels and flow velocities, using barrier boundaries, are compared with measurements in the prototype, some deviations in the results of the calculations can be noticed. According to RWS [1989], these deviations are:

- The flow pattern directly downstream from the barrier is incorrect.
- The spreading of the main flow is much stronger than in the prototype.
- Downstream from the barrier the absence of large eddies in the computed flow field is obvious.

A cause of these deviations is the schematisation of the barriers as 1DH internal boundary elements. In these 1DH elements the relation between the discharge and the head difference over the barrier is described by an empirical relationship, the weir or gate formula. This relationship is based on Bernoulli's principle of preservation of energy in an acceleration zone.

When the current flows towards a barrier under a small angle (in a horizontal plane), the barrier will give a reduction of this angle and downstream from the barrier the flow becomes nearly perpendicular to the barrier (Akkermans [1984]). This reduction of the angle is described very well when using the above-described 1DH barrier boundary elements, but

downstream from the barrier the current is influenced too much by the reduction of the angle. The expected eddies downstream from the barriers are absent or, if they appear, are too small due to the small convection just downstream from the barriers.

The reproduction of the flow patterns can be improved (RWS [1988]) by a different schematization of the energy losses over the barrier. In this schematization the shallow-water equations are used throughout; the effect of the barriers is only schematized by an adjustment of the local bottom roughness. To do this the discharge coefficient in the weir formula is expressed in the local roughness of the open channel formula. The discharges, which can be calculated with the weir and open channel formulas, are equalized to obtain the modified local roughness.

In the computational grid one barrier element can be replaced by one or two grid elements in flow-direction with modified roughness. The barrier is no longer an internal boundary in the model. The roughness is continuously adapted to the water level during the computations.

The downstream flow patterns calculated with this schematisation give a fairly good reproduction of the patterns in the prototype. The spreading of the flow and the velocity gradients are nearly equal to the prototype ones and large eddies are present downstream from the abutments. In Fig. 1.2.2 the flow patterns of the Hammen channel are shown for maximum flood flow, using the barrier boundary elements (Fig. 1.2.2a) and using the adjustment local roughness (Fig. 1.2.2b). The barrier in this channel is for protection against storm surges; a row of piers (for support of movable gates) offers resistance to the tidal flow.

Because the flow patterns in the vicinity of barriers are reproduced well using the schematization of the energy losses at the barrier by means of the adjustment of local depth and roughness (RWS [1989]), barriers are not discussed further.

Deviations also appeared in the vicinity of dams under construction (RWS [1988]). The dams needed to divide the Eastern Scheldt estuary into compartments are sandfill dams. During the construction of these dams, sills were created by depositing sand into the closure gaps. These sills had mild slopes, $^1/_{15}$ or flatter. 2DH numerical models were used for the prediction of the water levels and flow velocities in the vicinity of the sills for different construction stages. These 2DH models were based upon equations derived for flat bottom situations. Due to the mild slopes of the sill, no separation of the flow was expected and a 2DH model seemed appropriate to calculate flow across such structures. But, when the

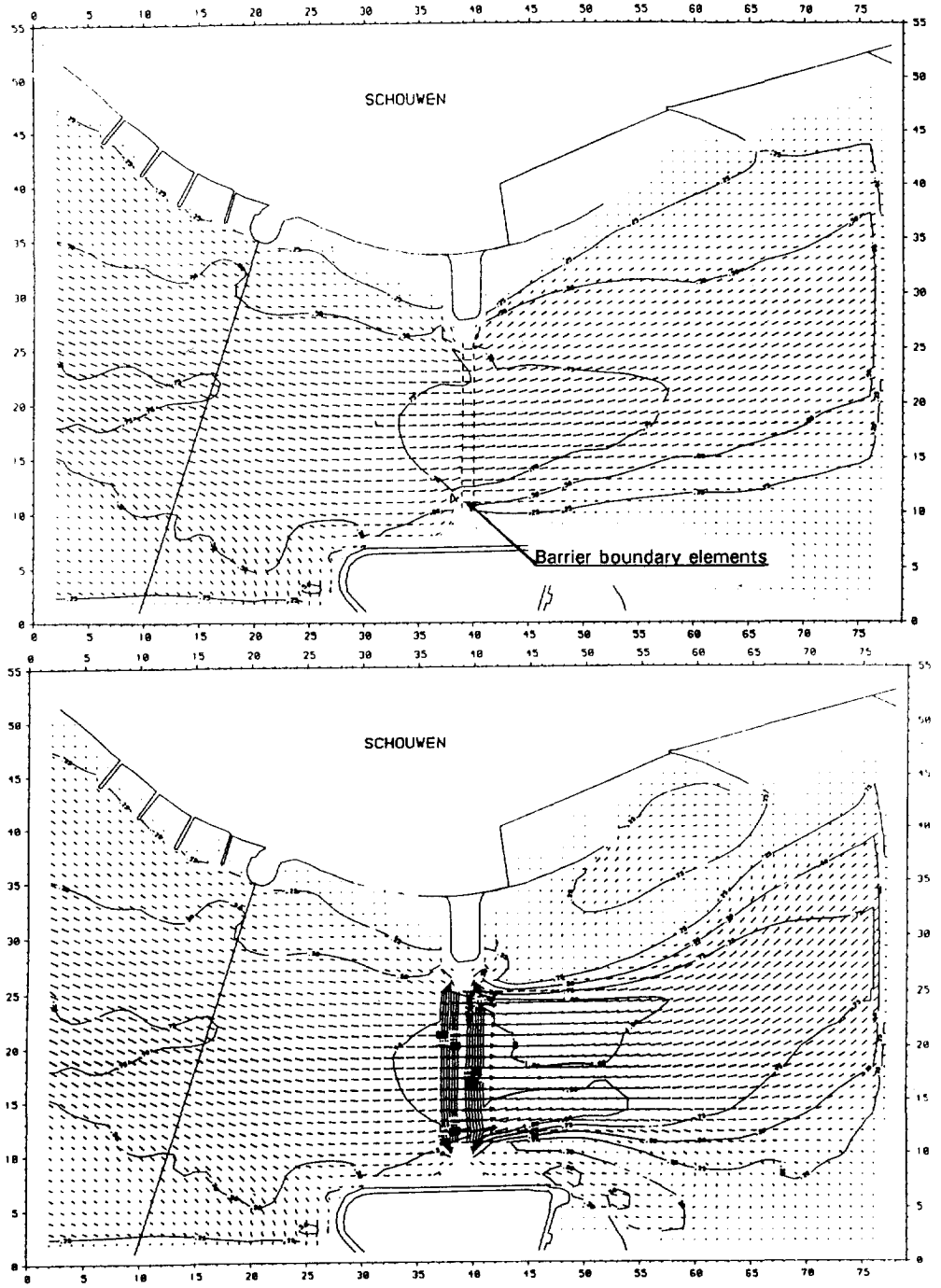

Figure 1.2.2 Flow pattern for maximum flood in the Hammen channel
a) using the barrier boundary elements, b) using adjustment of local depth and roughness

results of computations were compared with measurements in the prototype, some deviations were noticed (RWS [1988]). The main conclusions in this report read:

- The flow levels, discharges and phases of the tide are reproduced well.
- The flow velocities are reproduced well upstream from the sill but the reproduction of the flow velocities downstream from the sill is insufficient.
- The calculated water levels just downstream from the sill are too high (Fig. 1.2.3).

Different methods for the improvement of the reproduction in the vicinity of a sill under construction were tried by Rijkswaterstaat (RWS [1988]):

- Increasing the bottom roughness of the sill.
- Varying the magnitude of the convective terms in the equations of motion.
- Adapting the eddy-viscosity in the equations of motion.

Increasing the bottom roughness upstream from the sill, to improve the simulation of the energy losses, improves the computed water levels. Unfortunately, the modification of the roughness required is not known beforehand.

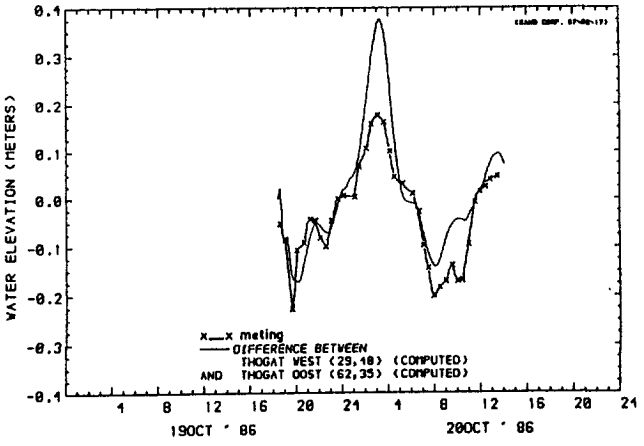

Figure 1.2.3 The difference in water level upstream and downstream from the sill
x——x measurements, ———— calculations

Introducing variations in the convective terms has a very large influence on the water level and on the flow velocities. Accurate values for the convective terms are very important because underestimating the momentum flux causes a too low dissipation of kinetic energy. The resulting head difference across the sill is too low then. The choice of a too high value for the convective terms leads to the opposite effect, a too large decrease of the water level. The correct value of this modification is also not known beforehand.

Decreasing the eddy-viscosity does not lead to an improvement in the locations of the eddies, but it improves the spreading of the mixing layer at both sides of the main flow.

In this section the applicability of 2DH models was discussed. In general the water levels and flow velocities obtained by 2DH models agree very well with the measured water levels and flow velocities in the prototype. There are deviations in the vicinity of barriers and on locations where the bottom gradient becomes important, e.g. at slopes of sills. The cause of the deviations is known for the barriers. An improved schematization was developed for this case. For flows over a sill the cause of these deviations was not completely clear and a way to improve the shallow-water equations was yet to be developed. Therefore the aim of this study is:

- To explain the differences in the water levels and flow velocities calculated with 2DH numerical models and the measured water levels and flow velocities for flow over a sill.
- To modify the shallow-water equations for flow over a sill.

1.3 Approach in the present study

In general research of flows can be performed using analytical approaches, numerical approaches, physical models and observations in the field. In this study analytical approaches, numerical approaches and observations in a physical model are used.

Conventional numerical models for calculation of water levels and flow patterns in seas, estuaries and harbours are based on the shallow-water equations, which are derived on the assumption of hydrostatic pressure and a uniform-flow velocity profile. Differences between results of numerical models, based on these shallow-water equations, and measurements in the field are probably due to wrong assumptions made in the derivation of the shallow-water equations.

For flow over a sill the velocity profiles become more uniform in the acceleration zone and less uniform in the deceleration zone. For very steep, downward-faced slopes separation even occurs, in which case a recirculation flow behind the sill appears. 2DH numerical models are depth-averaged models and it is not possible to simulate these changes in the velocity profile with these depth-averaged numerical models.

The approach taken in the present study to investigate and to model the effects of a

sill in the flow is to evaluate the above-mentioned effects and to express modifications to the convection term, the pressure term and the bottom stress term in the shallow-water equations through multiplication factors. This is done both analytically (chapter 2) and numerically (chapter 3), with an empirical check (chapter 4).

This study is restricted to flows that are subcritical, even on the sill. In estuaries supercritical flow can occur if the sill's crown is sufficiently high, e.g. in the last phase of closure with sandfill dams.

Studying 3D (three-dimensional) flow is rather complex and time-consuming both experimentally (laser-Doppler) and numerically. 2DV (two-dimensional in the vertical plane, uniform in transverse-direction) flow can be studied more easily. In 2DV steady flow the most important effects, adaption of the velocity profile and separation, also appear. For that reason only 2DV steady flows are studied in this investigation.

In chapters 2 and 3 results of analytical and numerical calculations for 2DV flows over a sill are presented and discussed. Starting point is the set of exact 2DV equations.

The 1DH shallow-water equations can be derived by depth-averaging the 2DV equations, in which the expressions for the horizontal velocity and pressure distribution have to be substituted. For uniform flow, the velocity profile can be approximated by a logarithmic velocity profile and the water pressure distribution by a hydrostatic water distribution. Substitution of these expressions yields the commonly used shallow-water equations.

In non-uniform flows the velocity profile and pressure distribution are not exactly known, but they deviate from the logarithmic velocity profile and the hydrostatic pressure distribution. Due to these deviations the convection, pressure and friction terms of the shallow-water equations change slightly.

Exact analytical solutions of the horizontal velocity and the water pressure distribution derived from the Navier-Stokes and continuity equations are only possible for special flow cases. Only if the non-linear convective terms are unimportant in comparison to the pressure and Reynolds shear stress terms (mildly non-uniform flow), analytical solutions can be found. However, it is possible to find approximations using the method of asymptotic expansions (chapter 2.2). Unfortunately, the approximations in this method are only valid for extremely mild bed slopes. Another approximation method used is the method of weighted residuals (chapter 2.3). The latter method is valid for more realistic slopes. The maximum gradient

is about $^1/_5$.

Approximate solutions can also be obtained from numerical computations. Chapter 3 describes results of 2DV-applications of the PHOENICS flow simulation system of CHAM Ltd. There are no restrictions to the maximum slope using such a numerical system. Several computations are made for different bottom geometries. The results of these 2DV computations are used to calculate appropriate modifications for the 1DH shallow-water equations. The analytical approximations of the water levels, horizontal velocities and modifications of the shallow-water equations from chapter 2 are compared with the ones obtained by the numerical model to verify the correctness and applicability of the analytical modifications.

In chapter 4 measurements of the flow over a sill in a flume are described. Results of these measurements are compared with those of numerical calculations and results described elsewhere in the literature, to check the correctness of the numerical model.

Possible improvements of 2DH shallow-water models are described in chapter 5. The analytically derived modifications for the 1DH shallow-water equations of chapter 2 are used to suggest modifications for the 2DH shallow-water equations.

Conclusions are given in chapter 6.

2. Analytic approximations for the 2DV Navier-Stokes and the 1DH shallow-water equations

2.1 Introduction

As mentioned in section 1.2, the 2DH (two-dimensional horizontal) shallow-water equations do not give a satisfactory prediction of the observed water levels and flow velocities in places where the bottom has a medium or a steep slope. The reason for the differences can be the fact that the 2DH shallow-water equations are derived for quasi-uniform flow. To improve these shallow-water equations, solutions for the velocities and pressure distribution valid for non-uniform flow over medium or steep slopes have to be taken into account. Therefore 3D (three-dimensional) flows have to be studied, but these studies are rather complex and time-consuming. 2DV (two-dimensional vertical) flow can be studied more easily. In 2DV flows, uniform in transverse direction, the most important bottom-slope effects already appear. So 2DV flows are studied in this investigation.

In this chapter, 1DH (one-dimensional horizontal) shallow-water equations are derived by substituting velocity and pressure profiles for mildly non-uniform flow into the Navier-Stokes and continuity equations, and by integrating these with respect to the depth.

It is rather difficult to find exact solutions for the velocity and pressure profiles because the Navier-Stokes equations are non-linear second-order differential equations. Therefore, it is only possible to find approximative profiles.

The first method used to approximate the velocity and pressure profiles, described in section 2.2, is the method of asymptotic expansions or the perturbation method (van Dyke [1963]). Unfortunately, the solutions of the velocity and pressure profiles found are only valid for extremely mild slopes, which severely limits the applicability.

The second method, described in section 2.3, is the method of weighted residuals in which velocity profiles of prescribed shape are used, with multiplication factors which are calculated as a function of the streamwise coordinate only (as in boundary layer approximations).

2.2 Method of asymptotic expansions

In this section the method of asymptotic expansions is used to derive approximate analytical solutions of the continuity equation and the Navier-Stokes equations. The Navier-Stokes equations are non-linear differential equations. This non-linearity does not make it possible to find an exact solution. Under certain circumstances however, it is possible to find an approximation by using this method. In this method all the terms in the differential equations are scaled, in the following way:

$$(\text{term}) = \begin{pmatrix}\text{order of magnitude}\\ \text{of the term}\end{pmatrix} \cdot \begin{pmatrix}\text{dimensionless variable with the}\\ \text{order of magnitude of unity}\end{pmatrix}$$

Scaling makes it more simple to estimate the relative magnitude of the terms in the equations and thus to determine the relative importance.

The next step is to write the dependent variables as asymptotic expansions, e.g:

$$y = y_0 + \varepsilon y_1 + \varepsilon^2 y_2 + \varepsilon^3 y_3 + \cdots \qquad (2.1.1)$$

The variable y is written as a sum of partial variables. Each term of the variable has a different order of magnitude. The order of magnitude is described by the power of ε, the perturbation quantity. The perturbation quantity, ε, has to be chosen in such a way that it is at least an order of magnitude smaller than 1, while all y_i are of order $O(1)$. The contributions of the terms $\varepsilon^i y_i$ become smaller and smaller for larger i's. This is a convergent series for which the assumption is made that there is an i for which $\varepsilon^i y_i$ is so small that the contribution of the terms with powers above i can be omitted.

If the value of $\varepsilon^i y_i$ does not decrease or decreases very slowly, the choice of the perturbation quantity is wrong and the method of asymptotic expansions is not valid for the decomposition of the variables used.

The asymptotic expansions of the dependent variables are substituted into the equations. These equations are rearranged into partial equations containing terms with perturbation quantities to an equal power, which are solved separately. The ultimate approximation for the variable is found by substituting the partial variables in the asymptotic expansion, such as eq. (2.1.1).

2.2.1 The fundamental set of equations

The equations to which the method of asymptotic solutions is applied, are the continuity equation and the Navier-Stokes equations for two-dimensional steady flow:

Continuity equation:

$$\frac{\partial u}{\partial x} + \frac{\partial w}{\partial z} = 0 \tag{2.2.1}$$

Navier-Stokes equations:

$$u\frac{\partial u}{\partial x} + w\frac{\partial u}{\partial z} + \frac{1}{\rho}\frac{\partial p}{\partial x} = -\frac{1}{\rho}\frac{\partial \tau_{xx}}{\partial x} - \frac{1}{\rho}\frac{\partial \tau_{xz}}{\partial z} + \nu\frac{\partial^2 u}{\partial x^2} + \nu\frac{\partial^2 u}{\partial z^2} \tag{2.2.2a}$$

$$u\frac{\partial w}{\partial x} + w\frac{\partial w}{\partial z} + \frac{1}{\rho}\frac{\partial p}{\partial z} + g = -\frac{1}{\rho}\frac{\partial \tau_{zx}}{\partial x} - \frac{1}{\rho}\frac{\partial \tau_{zz}}{\partial z} + \nu\frac{\partial^2 w}{\partial x^2} + \nu\frac{\partial^2 w}{\partial z^2} \tag{2.2.2b}$$

with the boundary conditions:

$$p = 0 \qquad \text{at } z = z_b + d \tag{2.2.3a}$$

$$u\frac{\mathrm{d}(z_b + d)}{\mathrm{d}x} - w = 0 \qquad \text{at } z = z_b + d \tag{2.2.3b}$$

$$\tau_{xz} = 0 \qquad \text{at } z = z_b + d \tag{2.2.3c}$$

$$u\frac{\mathrm{d}z_b}{\mathrm{d}x} - w = 0 \qquad \text{at } z = z_b \tag{2.2.3d}$$

plus a slip / partial slip / no slip condition at $z = z_b$ (see below).

In these equations g is the gravitational acceleration, z_b is the bottom level, p is the fluid pressure, u is the horizontal and w is the vertical velocity, x is the horizontal and z is the vertical coordinate, d is the water depth, ν is the molecular kinematic viscosity and ρ is the density of the fluid, τ_{xx} and τ_{zz} are the Reynolds normal stresses and τ_{xz} and τ_{zx} are the Reynolds shear stresses (see Fig. 2.2.1).

To solve the set of equations, eq. (2.2.1) and eq. (2.2.2), it is convenient to use the depth-integrated continuity equation. This yields (after substitution of expression (2.2.3b) and (2.2.3d)):

$$\frac{\mathrm{d}}{\mathrm{d}x}\int_{z_b}^{z_b+d} u\,\mathrm{d}z = 0 \tag{2.2.4a}$$

Designating the volume flux per unit width as q, eq. (2.2.4a) gives:

$$\frac{\mathrm{d}q}{\mathrm{d}x} = 0 \text{ or } q = \int_{z_b}^{z_b+d} u\,\mathrm{d}z \text{ is constant in the calculation domain.} \tag{2.2.4b}$$

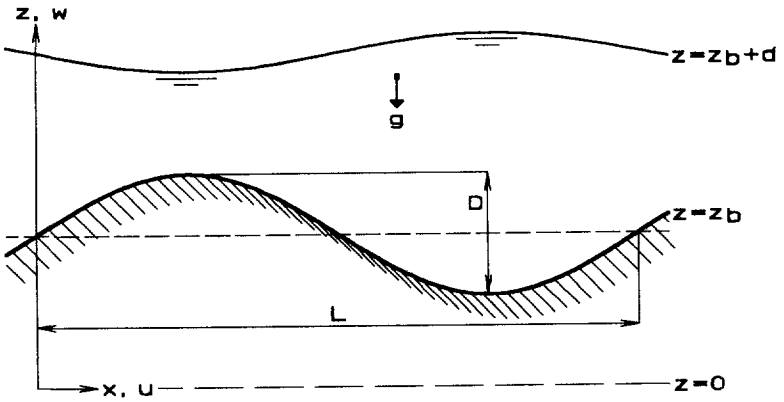

Figure 2.2.1 The basic situation

This discharge condition is used instead of the kinematical conditions of eq. (2.2.3b) and eq. (2.2.3d).

The Reynolds stress terms in the Navier-Stokes equations can be approximated by many methods. These are usually based on the assumption of a gradient-type of diffusion, which means that the flux of a transferable property can be expressed in terms of the local gradient of the mean property. This assumption was applied first by Boussinesq [1877]. He made the assumption that the turbulent stresses, or Reynolds stresses, act like viscous stresses and that they are directly proportional to the corresponding mean velocity gradient. He introduced the concept of the eddy-viscosity. According to Boussinesq the Reynolds stresses read:

Reynolds normal stress in x-direction: $$\tau_{xx} = -2\rho\nu_t\frac{\partial u}{\partial x} \qquad (2.2.5a)$$

Reynolds shear stresses: $$\tau_{zx} = \tau_{xz} = -\left(\rho\nu_t\frac{\partial u}{\partial z} + \rho\nu_t\frac{\partial w}{\partial x}\right) \qquad (2.2.5b)$$

and Reynolds normal stress in z-direction: $$\tau_{zz} = -2\rho\nu_t\frac{\partial w}{\partial z} \qquad (2.2.5c)$$

For high Reynolds number flows, as assumed here, the molecular kinematic viscosity, ν, is much smaller than the eddy-viscosity, ν_t, therefore the molecular kinematic viscosity is neglected.

In this chapter two different models are used to describe the vertical variation of the eddy-viscosity, a model with a constant eddy-viscosity and a model with a parabola-shaped eddy-viscosity, while in chapter 3 the kε-model is used in the numerical calculations.

Scaling

In uniform flows the convective terms are zero; in that case the Reynolds stress terms balance the pressure gradient. In other words the pressure gradient due to the fall of the water level is in equilibrium with the bottom friction.

In flow over sills the convective terms are not equal to zero, but for mild depth variations ($D/L \ll 0$) they are assumed to be small in comparison to the Reynolds stresses and the pressure gradient. D and L are the characteristic vertical and horizontal length scale of depth variations (Fig. 2.2.1).

The assumption about the magnitude of the terms is taken into account in the scaling of the variables of eq. (2.2.1) and eq. (2.2.2), which is necessary to use the method of asymptotic expansions.

All the dependent length variables in x-direction are scaled by a characteristic length, L, for which the length of the sill is chosen (see Fig. 2.2.1). The changes in the variables in x-direction are influenced by the longitudinal changes of the bottom level. The variations of the variables in z-direction are influenced by the height of the sill. Therefore the dependent variables in z-direction are scaled with D, the characteristic vertical length, for which the height of the sill is chosen. Of course some of the variables in z-direction could have been scaled with the water depth. In that case an extra perturbation quantity has to be introduced determining the proportions between the water depth and D. In this investigation the ratio of these two characteristic lengths is of order 1, which means that the characteristic lengths are equal and that the importance of changes in both variables are equal.

The two terms in the continuity equation have to be of the same order of magnitude. This yields the characteristic vertical velocity, W, in comparison to the characteristic horizontal velocity, U:

$$W = \frac{D}{L} U$$

The characteristic horizontal velocity, U, is defined as the averaged flow velocity.

To estimate the magnitudes of the terms in the Navier-Stokes equation in flow direction, the coordinates x and z are scaled with a characteristic length L and D respectively, while the velocities and pressure are estimated by the characteristic horizontal velocity, U, and the characteristic pressure, P. The eddy-viscosity is scaled with the characteristic horizontal velocity, U, multiplied by the characteristic vertical length, D, and a small

coefficient χ, which is dependent on the turbulent Reynolds number. Substitution of these characteristic values into the Navier-Stokes equation in flow direction yields:

$$u\frac{\partial u}{\partial x} + w\frac{\partial u}{\partial z} + \frac{1}{\rho}\frac{\partial p}{\partial x} = 2\frac{\partial}{\partial x}\nu_t\frac{\partial u}{\partial x} + \frac{\partial}{\partial z}\nu_t\frac{\partial u}{\partial z} + \frac{\partial}{\partial z}\nu_t\frac{\partial w}{\partial x} \qquad (2.2.6a)$$

with the orders of magnitude:

$$\frac{U^2}{L} \quad \frac{U^2}{L} \quad \frac{P}{\rho L} \quad 2\frac{\chi D U^2}{L^2} \quad \frac{\chi D U^2}{D^2} \quad \frac{\chi D U^2}{L^2} \qquad (2.2.6b)$$

In rapidly varied flows the third term, the pressure term, should have the same order of magnitude as the first and second term of eq. (2.2.6), the convection terms, while in gradually varied flows the pressure term should have the same order of magnitude as the fifth term, the Reynolds shear stress term. Only this last case is worked out to arrive at the set of dimensionless equations. The reason for this is that it is tried to modify the shallow-water equations, e.g. with an adjustment of the local bottom friction, just like was done to simulate barriers (chapter 1).

For **gradually varied flows** the leading term is the friction term. Dividing eq. (2.2.6b) by $\chi U^2/D$ yields the orders of magnitude of the terms in eq. (2.2.6) relative to that of the friction term. These orders of magnitude are:

$$\frac{D}{\chi L}, \quad \frac{D}{\chi L}, \quad \frac{PD}{\rho\chi L U^2}, \quad \frac{D^2}{L^2}, \quad 1, \quad \frac{D^2}{L^2}$$

The method of asymptotic expansions concerns the development of terms to a perturbation quantity of which the magnitude approaches the value zero, although its actual value remains finite. The pressure term is supposed to be of the same order of magnitude as the friction term and the other terms are supposed to be at least one order of magnitude smaller. Therefore the characteristic pressure is taken $P = \chi\rho L U^2/D$ and the perturbation quantity, ε, is taken: $\varepsilon = D/(\chi L)$. The choice of the perturbation quantity determines the order of magnitude of the ratio D/L and with this ratio the validity range of the solutions. ε has to be small, therefore the order of magnitude of D/L has to be much smaller than χ. This means that the length of the sill has to be much larger than the height of the sill.

Recapitulating, the variables are scaled in the following way:

$$x^* = \frac{x}{L} \qquad (2.2.7a)$$

$$z^* = \frac{z}{D} \tag{2.2.7b}$$

$$z_b^* = \frac{z_b}{D} \tag{2.2.7c}$$

$$d^* = \frac{d}{D} \tag{2.2.7d}$$

$$p^* = \frac{p}{P} = \frac{p}{\frac{\rho \chi L U^2}{D}} \tag{2.2.7e}$$

$$u^* = \frac{u}{U} \tag{2.2.7f}$$

$$w^* = \frac{w}{\frac{D}{L}U} \tag{2.2.7g}$$

$$\nu_t^* = \frac{\nu_t}{\chi U D} \tag{2.2.7h}$$

To scale the Navier-Stokes equation in vertical direction it is convenient to introduce a dimensionless gravity:

$$g^* = \frac{g}{\frac{\chi L U^2}{D^2}} \tag{2.2.7i}$$

Substituting these dimensionless variables into eq. (2.2.1) and eq. (2.2.2), the dimensionless equations become (omitting the * and taking $\varepsilon = D/(\chi L)$):

$$\frac{\partial u}{\partial x} + \frac{\partial w}{\partial z} = 0 \tag{2.2.8}$$

$$\varepsilon\left(u\frac{\partial u}{\partial x} + w\frac{\partial u}{\partial z}\right) + \frac{\partial p}{\partial x} = 2\chi^2\varepsilon^2\frac{\partial}{\partial x}\left(\nu_t\frac{\partial u}{\partial x}\right) + \frac{\partial}{\partial z}\left(\nu_t\left(\frac{\partial u}{\partial z} + \chi^2\varepsilon^2\frac{\partial w}{\partial x}\right)\right) \tag{2.2.9a}$$

$$\chi^2\varepsilon^3\left(u\frac{\partial w}{\partial x} + w\frac{\partial w}{\partial z}\right) + \frac{\partial p}{\partial z} + g = \chi^2\varepsilon^2\frac{\partial}{\partial x}\left(\nu_t\left(\frac{\partial u}{\partial z} + \chi^2\varepsilon^2\frac{\partial w}{\partial x}\right)\right) + 2\chi^2\varepsilon^2\frac{\partial}{\partial z}\left(\nu_t\frac{\partial w}{\partial z}\right) \tag{2.2.9b}$$

The validity range of solutions of the eq. (2.2.8) and eq. (2.2.9) is determined by the perturbation coefficient ε, which is dependent on the sill slope and the coefficient χ. The value of χ is nearly independent on the flow circumstances and its magnitude is about $^1/_{225}$ (Blom [1988]). Since $D/L = \varepsilon\chi$, $\chi \ll 1$ and $\varepsilon \ll 1$, the solutions are only valid for extremely mild slopes. Therefore the solutions of eq. (2.2.8) and eq. (2.2.9) are not presented in this chapter. Interested readers can find the analysis in appendix A.

In an attempt to find approximate solutions valid for more realistic, steeper slopes a different approach was taken, using the method of weighted residuals. This is discussed in

the next section.

2.3 Method of weighted residuals

One of the conclusions of the previous section is that it is not possible to solve the Navier-Stokes equations analytically with the method of asymptotic expansions, for flows in which the turbulent friction terms are not dominating. The flow is only friction dominated at very mild non-uniformities, which are not important in this study. For that reason another approximation method was used, the method of weighted residuals. This method is a generalization of the method introduced by Von Kármán [1930] for boundary-layer problems. Madsen & Svendsen [1983] used this method to compute the velocity distribution in a hydraulic jump. The results of the latter analysis showed good agreement with measurements in flumes.

The method of weighted residuals makes use of similarity of velocity profiles. The choice of the shape of the similarity profile is more or less free, but such a profile has to consist of a zeroth-order profile and a first-order profile multiplied with a profile parameter. The similarity profile is substituted in the momentum and energy equations and these equations are depth-averaged. The profile parameter is one of the variables to be solved. The solution found for the velocity distribution with this method is not exact, but the best fit for the chosen similarity profile.

In many shear layer problems the assumption of similarity has also been used (Abramovich [1963], Rajaratham [1976], and Fischer [1979]). If a uniform flow of water meets an abrupt change in depth (Fig. 2.3.1), an intense shear stress at the surface of velocity discontinuity occurs due to turbulence. Due to the shear stress the stagnant fluid is accelerated, which causes some momentum loss of the mean flow. The fluid layer affected by this exchange of momentum is known as the free shear layer; its thickness (b) (Fig. 2.3.1) increases continuously with the downstream distance (x). If the velocity distribution is observed (Liepmann & Laufer [1947]) at different x-stations, it appears that they have the same shape but are not symmetrical with respect to the x-axis. The flow in this shear layer can be described by the following general expression:

$$u(x,z) = u_0(x)\left(1 + \Gamma(x) f(\sigma)\right) \qquad (0 \le \sigma \le 1) \qquad (2.3.1a)$$

$$\sigma = \frac{z - a(x)}{b(x)} \qquad (2.3.1b)$$

in which four parameters u_0, Γ, a and b appear (Fig. 2.3.1). The velocity $u_0(x)$ is the horizontal velocity outside the turbulent region, b is the width of the turbulent region, and $z-a$ is its lower edge.

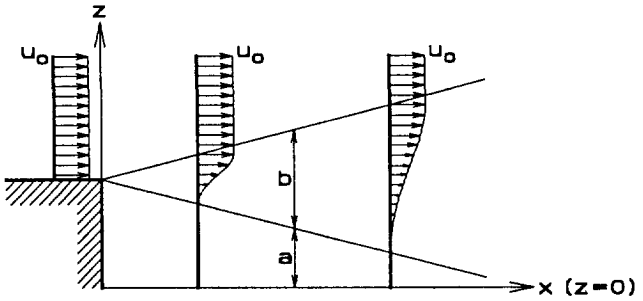

Figure 2.3.1 The similarity velocity profiles in mixing layer problems.

Such solutions exist only for certain types of flow, in which the pressure gradients and the friction at its lower edge are neglected, but not for the flow considered in this investigation, in which these quantities are important. Thus it cannot be expected that a flow field for which an expression like eq. (2.3.1) applies can be found which satisfies the equation of motion in all detail.

In the present study, it was tried at first to satisfy the continuity and Navier-Stokes equations in the depth-integrated form, following Madsen & Svendsen [1983]. In their method a suitable form of $f(\sigma)$ is specified and the development of $\Gamma(x)$ is obtained from the requirements that the depth-integrated versions of the continuity and the Navier-Stokes equations are satisfied for all x. Unfortunately, it was not possible to use this method with a velocity u_0 which only depends on the x-coordinate, as was used by Madsen & Svendsen. Writing the shear stress as an eddy-viscosity multiplied by the vertical gradient of the horizontal velocity does not yield a satisfactory bottom shear stress because due to the uniform initial velocity profile the bottom shear stress becomes zero. Introducing a bottom shear stress dependent on the average velocity yields velocity profiles without a vertical variation on the downward-faced slope of the sill. These solutions were not wanted. Therefore the zeroth-order horizontal velocity was chosen to be dependent on both the x and the z-coordinate. This velocity profile u_0 can be parabolic or logarithmic.

For flows over a sill the velocity profile becomes more nearly uniform in the

acceleration zone and less so in the deceleration zone. This change in the velocity profile can be simulated by subtraction or addition of a first-order velocity profile, u_1, to a zeroth-order velocity profile, u_0. The magnitude of the velocity profile to be subtracted or added is determined by a multiplication coefficient, $\Gamma(x)$. This coefficient depends on the bathymetry. The shapes of the velocity profiles u_0 and u_1 are assumed not to change due to changes in the bottom profile. Only an adaptation of the depth-averaged velocity to the changes in the bottom profile takes place. The turbulent layer is assumed to be fully developed and to reach from the bottom up to the water surface. Therefore the height of the turbulent region $b(x)$ is chosen as the entire water depth, d, and the lower edge, $z = a(x)$, is chosen in the bottom, $z = z_b(x)$ (Fig. 2.3.2). The equation used for the horizontal velocity reads:

$$u(x,z) = u_0(x,\sigma) + \Gamma(x)u_1(x,\sigma) \qquad (0 \le \sigma \le 1) \tag{2.3.2a}$$

$$\sigma = \frac{z - z_b}{d} \tag{2.3.2b}$$

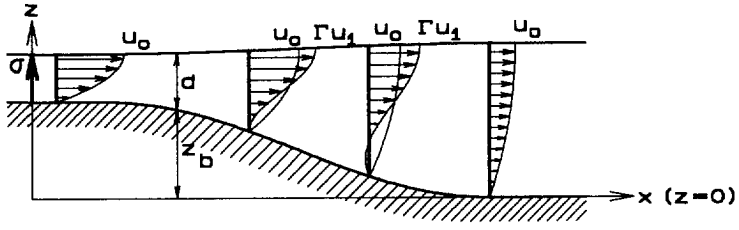

Figure 2.3.2 The similarity velocity profiles for flow over sills.

The shapes of the velocity profiles u_0 and u_1 are dependent on the eddy-viscosity model used. In section 2.3.1 a constant eddy-viscosity model is used and in section 2.3.2 a parabola-shaped eddy-viscosity model is used.

The coordinate σ defined in eq. (2.3.2b) is used below as the new vertical coordinate in the differential equations. Using σ all equations have to be transformed. This transformation is called the σ-transformation and was first used by Phillips [1957].

The equations used to determine the shape of the velocity profile and, with this shape, the modifications in the shallow-water equations, are the equations (2.2.1) and (2.2.2). Only some unimportant terms are omitted, such as the viscous stress terms and the Reynolds normal stress terms in both Navier-Stokes equations and the convection terms and Reynolds shear stress terms in the Navier-Stokes equations in σ-direction. The neglect of these terms

is permissible because it is assumed that the horizontal length scale for the flow is much larger than the vertical scale. The set of transformed equations is:

the continuity equation:

$$\frac{\partial u}{\partial x} - \frac{1}{d}\left(\frac{\mathrm{d}z_b}{\mathrm{d}x} + \sigma\frac{\mathrm{d}d}{\mathrm{d}x}\right)\frac{\partial u}{\partial \sigma} + \frac{1}{d}\frac{\partial w}{\partial \sigma} = 0 \tag{2.3.3}$$

and the Navier-Stokes equations:

$$u\frac{\partial u}{\partial x} - \frac{u}{d}\left(\frac{\mathrm{d}z_b}{\mathrm{d}x} + \sigma\frac{\mathrm{d}d}{\mathrm{d}x}\right)\frac{\partial u}{\partial \sigma} + \frac{w}{d}\frac{\partial u}{\partial \sigma} + \frac{1}{\rho}\frac{\partial p}{\partial x} - \frac{1}{d\rho}\left(\frac{\mathrm{d}z_b}{\mathrm{d}x} + \sigma\frac{\mathrm{d}d}{\mathrm{d}x}\right)\frac{\partial p}{\partial \sigma} = -\frac{1}{d\rho}\frac{\partial \tau_{x\sigma}}{\partial \sigma} \tag{2.3.4a}$$

$$\frac{1}{d\rho}\frac{\partial p}{\partial \sigma} + g = 0 \tag{2.3.4b}$$

Integrating the Navier-Stokes equation in σ-direction yields the hydrostatic water pressure distribution:

$$p = \rho g d(1-\sigma) \tag{2.3.5}$$

Substitution of the expressions for the water pressure distribution, eq. (2.3.5), and the velocity profile, eq. (2.3.2), into eq. (2.3.4a) yields an equation containing three unknown variables: d, Γ and w. The vertical distribution of the vertical velocity can be solved by using the continuity equation eq. (2.3.3), but there still remain two unknown variables for the solution of which only one differential equation remains. The energy equation can be used as an additional equation. The energy equation is derived by adding eq. (2.3.4a) multiplied by u and eq. (2.3.4b) multiplied by w. The hydrostatic water pressure distribution, eq. (2.3.5), has to be substituted into this sum to get this additional, but dependent, differential equation. The three equations read:

$$\frac{\partial u}{\partial x} - \frac{1}{d}\left(\frac{\mathrm{d}z_b}{\mathrm{d}x} + \sigma\frac{\mathrm{d}d}{\mathrm{d}x}\right)\frac{\partial u}{\partial \sigma} + \frac{1}{d}\frac{\partial w}{\partial \sigma} = 0 \tag{2.3.6a}$$

$$u\frac{\partial u}{\partial x} - \frac{u}{d}\left(\frac{\mathrm{d}z_b}{\mathrm{d}x} + \sigma\frac{\mathrm{d}d}{\mathrm{d}x}\right)\frac{\partial u}{\partial \sigma} + \frac{w}{d}\frac{\partial u}{\partial \sigma} + g\frac{\mathrm{d}(z_b+d)}{\mathrm{d}x} + \frac{1}{d\rho}\frac{\partial \tau_{x\sigma}}{\partial \sigma} = 0 \tag{2.3.6b}$$

$$u^2\frac{\partial u}{\partial x} - \frac{u^2}{d}\left(\frac{\mathrm{d}z_b}{\mathrm{d}x} + \sigma\frac{\mathrm{d}d}{\mathrm{d}x}\right)\frac{\partial u}{\partial \sigma} + \frac{uw}{d}\frac{\partial u}{\partial \sigma} + ug\frac{\mathrm{d}(z_b+d)}{\mathrm{d}x} + \frac{u}{d\rho}\frac{\partial \tau_{x\sigma}}{\partial \sigma} = 0 \tag{2.3.6c}$$

This set of equations is solved in their depth-integrated form. This gives a depth-averaged energy equation, which is independent of the depth-averaged momentum equation, because of the non-uniform vertical distribution of the horizontal velocity.

Depth-integrating the continuity equation, eq. (2.3.6a), yields:

$$\frac{\mathrm{d}q}{\mathrm{d}x} = 0 \tag{2.3.7}$$

This is the continuity equation of the 1DH shallow-water equations.

The shallow-water equation for motion is derived by depth-averaging the momentum equation (2.3.6b) after adding the continuity equation, eq. (2.3.6a), multiplied by the horizontal velocity, u. This yields:

$$d\int_0^1\left(2u\frac{\partial u}{\partial x}-2\frac{u}{d}\left(\frac{\mathrm{d}z_b}{\mathrm{d}x}+\sigma\frac{\mathrm{d}d}{\mathrm{d}x}\right)\frac{\partial u}{\partial\sigma}+\frac{w}{d}\frac{\partial u}{\partial\sigma}+\frac{u}{d}\frac{\partial w}{\partial\sigma}+g\frac{\mathrm{d}(z_b+d)}{\mathrm{d}x}+\frac{1}{d\rho}\frac{\partial\tau_{x\sigma}}{\partial\sigma}\right)\mathrm{d}\sigma = 0$$

or

$$\int_0^1\left(d\frac{\partial u^2}{\partial x}-\frac{\mathrm{d}z_b}{\mathrm{d}x}\frac{\partial u^2}{\partial\sigma}-\sigma\frac{\mathrm{d}d}{\mathrm{d}x}\frac{\partial u^2}{\partial\sigma}+\frac{\partial uw}{\partial\sigma}+gd\frac{\mathrm{d}(z_b+d)}{\mathrm{d}x}+\frac{1}{\rho}\frac{\partial\tau_{x\sigma}}{\partial\sigma}\right)\mathrm{d}\sigma = 0$$

which is equal to

$$d\frac{\mathrm{d}}{\mathrm{d}x}\left(\int_0^1 u^2\mathrm{d}\sigma\right)-\frac{\mathrm{d}z_b}{\mathrm{d}x}\left[u^2\right]_0^1-\frac{\mathrm{d}d}{\mathrm{d}x}\left[\sigma u^2\right]_0^1+\frac{\mathrm{d}d}{\mathrm{d}x}\left(\int_0^1 u^2\mathrm{d}\sigma\right)+\left[uw\right]_0^1+gd\frac{\mathrm{d}(z_b+d)}{\mathrm{d}x}+\frac{1}{\rho}\left[\tau_{x\sigma}\right]_0^1 = 0$$

which can be worked out into

$$\frac{\mathrm{d}}{\mathrm{d}x}\left(d\int_0^1 u^2\mathrm{d}\sigma\right)+gd\frac{\mathrm{d}(z_b+d)}{\mathrm{d}x}-\frac{1}{\rho}\tau_{x\sigma}\Big|_{\sigma=0} = 0 \tag{2.3.8}$$

The boundary conditions (2.2.3b) and (2.2.3d) are used in this integration.

To integrate the energy equation, the continuity equation, eq. (2.3.6a), multiplied by $\left(\frac{1}{2}u^2+g(z_b+d)\right)$, is added before the integration. This yields:

$$\int_0^1\left(\tfrac{3}{2}du^2\frac{\partial u}{\partial x}-\tfrac{3}{2}u^2\left(\frac{\mathrm{d}z_b}{\mathrm{d}x}+\sigma\frac{\mathrm{d}d}{\mathrm{d}x}\right)\frac{\partial u}{\partial\sigma}+\tfrac{1}{2}u^2\frac{\partial w}{\partial\sigma}+uw\frac{\partial u}{\partial\sigma}+ugd\frac{\mathrm{d}(z_b+d)}{\mathrm{d}x}+\right.$$

$$\left.+gd(z_b+d)\frac{\partial u}{\partial x}-g(z_b+d)\left(\frac{\mathrm{d}z_b}{\mathrm{d}x}+\sigma\frac{\mathrm{d}d}{\mathrm{d}x}\right)\frac{\partial u}{\partial\sigma}+g(z_b+d)\frac{\partial w}{\partial\sigma}+\frac{u}{\rho}\frac{\partial\tau_{x\sigma}}{\partial\sigma}\right)\mathrm{d}\sigma = 0$$

which is equal to

$$\int_0^1\left(\tfrac{1}{2}\left(d\frac{\partial u^3}{\partial x}-\left(\frac{\mathrm{d}z_b}{\mathrm{d}x}+\sigma\frac{\mathrm{d}d}{\mathrm{d}x}\right)\frac{\partial u^3}{\partial\sigma}+\frac{\partial u^2w}{\partial\sigma}\right)+gd\frac{\partial}{\partial x}\left(u(z_b+d)\right)+\right.$$

$$\left.-g(z_b+d)\left(\frac{\mathrm{d}z_b}{\mathrm{d}x}+\sigma\frac{\mathrm{d}d}{\mathrm{d}x}\right)\frac{\partial u}{\partial\sigma}+g(z_b+d)\frac{\partial w}{\partial\sigma}+\frac{u}{\rho}\frac{\partial\tau_{x\sigma}}{\partial\sigma}\right)\mathrm{d}\sigma = 0$$

or

$$\frac{1}{2}\left(d\frac{\mathrm{d}}{\mathrm{d}x}\left(\int_0^1 u^3\,\mathrm{d}\sigma\right)-\frac{\mathrm{d}z_b}{\mathrm{d}x}\left[u^3\right]_0^1-\frac{\mathrm{d}d}{\mathrm{d}x}\left[\sigma u^3\right]_0^1+\frac{\mathrm{d}d}{\mathrm{d}x}\left(\int_0^1 u^3\,\mathrm{d}\sigma\right)+\left[u^2w\right]_0^1\right)+gd\frac{\mathrm{d}}{\mathrm{d}x}\left(\int_0^1 u(z_b+d)\,\mathrm{d}\sigma\right)+$$

$$-g(z_b+d)\left(\frac{\mathrm{d}z_b}{\mathrm{d}x}\left[u\right]_0^1+\frac{\mathrm{d}d}{\mathrm{d}x}\left[\sigma u\right]_0^1-\frac{\mathrm{d}d}{\mathrm{d}x}\left(\int_0^1 u\,\mathrm{d}\sigma\right)\right)+g(z_b+d)\left[w\right]_0^1+\int_0^1\left(\frac{u}{\rho}\frac{\partial\tau_{x\sigma}}{\partial\sigma}\right)\mathrm{d}\sigma=0$$

which can be worked out into

$$\frac{1}{2}\frac{\mathrm{d}}{\mathrm{d}x}\left(d\int_0^1 u^3\,\mathrm{d}\sigma\right)+g\frac{\mathrm{d}}{\mathrm{d}x}\left(d\int_0^1 (z_b+d)u\,\mathrm{d}\sigma\right)+\int_0^1\left(\frac{u}{\rho}\frac{\partial\tau_{x\sigma}}{\partial\sigma}\right)\mathrm{d}\sigma=0 \qquad (2.3.9)$$

Again the two boundary conditions, eq. (2.2.3b) and eq. (2.2.3d), are used in this integration.

The modifications for the 1DH shallow-water and depth-averaged energy equations can be found by calculating the convection and the friction term of eq. (2.3.8) and eq. (2.3.9).

The convection terms of the equations eq. (2.3.8) and eq. (2.3.9) can be written in abbreviated form as:

$$d\int_0^1 u^2\,\mathrm{d}\sigma=\alpha\frac{q^2}{d} \qquad (2.3.10a)$$

in which α is the convection coefficient in the momentum equation, and

$$d\int_0^1 u^3\,\mathrm{d}\sigma=\beta\frac{q^3}{d^2} \qquad (2.3.10b)$$

in which β is the convection coefficient in the energy equation or the Coriolis coefficient.

The friction term in the momentum equation can be written as:

$$\frac{1}{\rho}\tau_{x\sigma}\Big|_{\sigma=0}=\frac{1}{\rho}\gamma\,\tau_{bx} \qquad (2.3.10c)$$

in which γ is the friction coefficient in the momentum equation and τ_{bx} the bottom friction for uniform flow over a flat bottom with the same discharge and bottom roughness. The friction term in the energy equation can be written as:

$$\frac{1}{\rho}\int_0^1\left(u\frac{\partial\tau_{x\sigma}}{\partial\sigma}\right)\mathrm{d}\sigma=-\frac{1}{\rho}\gamma_1\frac{q}{d}\tau_{bx} \qquad (2.3.10d)$$

in which γ_1 is the friction coefficient in the energy equation.

The magnitudes of the convection and the friction coefficients in these equations are dependent on the velocity profile and eddy-viscosity model used.

In the next section the equations (2.3.8) and (2.3.9) are solved for a constant eddy-viscosity model (parabolic velocity profile). In the last section of this chapter the solutions are derived for a parabolic eddy-viscosity model (logarithmic velocity profile).

2.3.1 The constant eddy-viscosity model.

In this section the appropriate modifications of the shallow-water equations are derived for a constant eddy-viscosity. This choice is physically not realistic but this relatively simple analysis was carried out as a first step.

The uniform-flow velocity profile which corresponds to a constant eddy-viscosity is parabolic. Such a profile can be written as:

$$u = \frac{q}{d}\left(-\tfrac{3}{2}\sigma^2 + 3\sigma\right) \tag{2.3.11}$$

For non-uniform flows, the velocity profile of expression (2.3.2a) has to be substituted into the equations (2.3.8) and (2.3.9). But before substituting this velocity profile, the expressions of the two parts of the velocity, u_0 and u_1, of eq. (2.3.2a) have to be specified. The assumption is made that these still unknown velocity profiles can be written as power series of σ. The number of terms in this series is determined by the number of independent conditions to be fulfilled. There are three independent conditions:

1) The no-slip condition at the bottom, $u(0)=0$.
2) The boundary condition of zero friction at the water surface. This condition implies that the gradient of the velocity profile has to be zero.
3) The discharge condition. This condition can be derived from the continuity equation. Choosing the discharge, q, equal to the depth-integrated zeroth-order velocity, yields that the depth-integrated first-order velocity is equal to zero.

In addition, a constraint is imposed by letting $\Gamma=1$ correspond to uniform flow; this implies that u_0+u_1 is given by eq. (2.3.11).

Due to the three independent conditions the highest power in σ of the terms should be two. But the magnitude of the velocity profile u_1 is determined by the coefficient Γ. Therefore one unknown parameter of the velocity profile can be chosen freely, and the maximum power of terms containing σ in the velocity profiles can be increased with one. The velocity u_0 is therefore written as:

$$u_0 = \frac{q}{d}\left(a_0\sigma^3 + b_0\sigma^2 + c_0\sigma + d_0\right)$$

and the velocity u_1 is written as:

$$u_1 = \frac{q}{d}\left(a_1\sigma^3 + b_1\sigma^2 + c_1\sigma + d_1\right)$$

The above described conditions yield the following set of equations:

$$\left\{\begin{array}{rcl}
d_0 = 0 \\
d_1 = 0
\end{array}\right] \text{ condition 1}$$

$$\left\{\begin{array}{rcl}
3a_0 + 2b_0 + c_0 = 0 \\
3a_1 + 2b_1 + c_1 = 0
\end{array}\right] \text{ condition 2}$$

$$\left\{\begin{array}{rcl}
\frac{1}{4}a_0 + \frac{1}{3}b_0 + \frac{1}{2}c_0 + d_0 = 1 \\
\frac{1}{4}a_1 + \frac{1}{3}b_1 + \frac{1}{2}c_1 + d_1 = 0
\end{array}\right] \text{ condition 3}$$

$$\left\{\begin{array}{rcl}
a_0 + a_1 = 0 \\
b_0 + b_1 = -\frac{3}{2} \\
c_0 + c_1 = 3 \\
d_0 + d_1 = 0
\end{array}\right] \text{ condition 4}$$

These equations can be reduced to three independent equations with four unknown variables, of which one can be chosen freely. Choosing b_0=1 yields:

$$\left\{\begin{array}{rcl}
a_0 = -\frac{4}{3} \\
b_0 = 1 \\
c_0 = 2 \\
d_0 = 0
\end{array}\right. \quad \text{and} \quad \left\{\begin{array}{rcl}
a_1 = \frac{4}{3} \\
b_1 = -\frac{5}{2} \\
c_1 = 1 \\
d_1 = 0
\end{array}\right.$$

and for the velocity:

$$u(x,z) = u_0(x,\sigma) + \Gamma(x)u_1(x,\sigma) \qquad (2.3.12a)$$

$$\text{with} \quad u_0(x,\sigma) = \frac{q}{d}\left(-\frac{4}{3}\sigma^3 + \sigma^2 + 2\sigma\right) \qquad (2.3.12b)$$

$$u_1(x,\sigma) = \frac{q}{d}\left(\frac{4}{3}\sigma^3 - \frac{5}{2}\sigma^2 + \sigma\right) \qquad (2.3.12c)$$

Graphs of these velocity profiles are plotted in Fig. 2.3.3, using normalised velocities, $\widetilde{u}=ud/q$.

The value of the constant eddy-viscosity is expressed as a function of the friction parameter λ. For a steady flow in a open channel the bed friction can be written as:

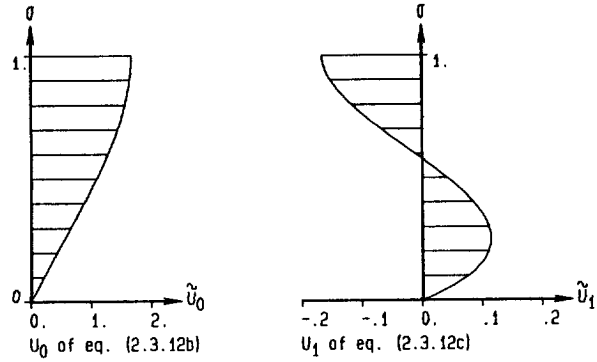

Figure 2.3.3 The velocity profiles of eq. (2.3.12) ($\tilde{u}=ud/q$)

$$-\frac{1}{\rho}\tau_{bx} = u_*^2 = \lambda(q/d)^2$$

in which τ_{bx} is the bottom friction and u_* is the friction velocity. Substituting the Reynolds stress term, eq. (2.2.5b), and neglecting the vertical velocity, w, gives:

$$-\frac{1}{\rho}\tau_{bx} = u_*^2 = \frac{\nu_t}{d}\frac{\partial u}{\partial \sigma}\bigg|_{\sigma=0}$$

in which ν_t is the eddy-viscosity. The gradient of the velocity at the bottom is $\partial u/\partial\sigma|_{\sigma=0}=3q/d$ for the parabolic velocity profile of expression (2.3.11). Substitution of the friction velocity, $u_*=\sqrt{\lambda}(q/d)$, yields:

$$\nu_t = \tfrac{1}{3}\lambda q \qquad (2.3.13)$$

in which λ is a friction parameter defined for the bottom friction by $\tau_{bx}=-\lambda\rho(q/d)^2$. The friction parameter λ depends on the roughness length of the bottom.

The two unknown variables Γ and d are solved by substituting the velocity profile, eq. (2.3.12), and the eddy-viscosity, eq. (2.3.13), into the equations (2.3.8) and (2.3.9). It is convenient to calculate the coefficients of eq. (2.3.10) first. This yields for the convection coefficient in the momentum equation, α:

$$\alpha = S_{10} + S_{11}\Gamma + S_{12}\Gamma^2 \qquad (2.3.14a)$$

with $S_{10} = \frac{134}{105}$

$$S_{11} = -\frac{9}{105}$$

$$S_{12} = \frac{1}{105},$$

for the convection coefficient in the energy equation, β:

$$\beta = S_{20} + S_{21}\Gamma + S_{22}\Gamma^2 + S_{23}\Gamma^3 \qquad (2.3.14b)$$

with $S_{20} = \frac{4484}{2520}$

$S_{21} = -\frac{680}{2520}$

$S_{22} = \frac{85}{2520}$

$S_{23} = -\frac{1}{2520}$,

for the friction coefficient in the energy equation, γ_1:

$$\gamma_1 = S_{30} + S_{31}\Gamma + S_{32}\Gamma^2 \qquad (2.3.14c)$$

with $S_{30} = \frac{16}{15}$

$S_{31} = -\frac{2}{15}$

$S_{32} = \frac{1}{15}$,

and for the friction coefficient in the momentum equation, γ:

$$\gamma = S_{40} + S_{41}\Gamma \qquad (2.3.14d)$$

with $S_{40} = \frac{2}{3}$

$S_{41} = \frac{1}{3}$.

Substitution of these coefficients into the equations (2.3.8) and (2.3.9) yields:

$$-\alpha\frac{q^2}{d^2}\frac{\mathrm{d}d}{\mathrm{d}x} + \frac{q^2}{d}\frac{\mathrm{d}\alpha}{\mathrm{d}\Gamma}\frac{\mathrm{d}\Gamma}{\mathrm{d}x} + gd\frac{\mathrm{d}(z_b+d)}{\mathrm{d}x} + \gamma\lambda\frac{q^2}{d^2} = 0 \qquad (2.3.15)$$

$$-\beta\frac{q^3}{d^3}\frac{\mathrm{d}d}{\mathrm{d}x} + \frac{1}{2}\frac{q^3}{d^2}\frac{\mathrm{d}\beta}{\mathrm{d}\Gamma}\frac{\mathrm{d}\Gamma}{\mathrm{d}x} + gq\frac{\mathrm{d}(z_b+d)}{\mathrm{d}x} + \gamma_1\lambda\frac{q^3}{d^3} = 0 \qquad (2.3.16)$$

The differential equations (2.3.15) and (2.3.16) are worked out to obtain the differential equations for the profile parameter, Γ, and the water depth, d:

$$\frac{\mathrm{d}\Gamma}{\mathrm{d}x} = \frac{\frac{q^2\lambda}{gd^4}F_{10} + \frac{1}{d}\frac{\mathrm{d}z_b}{\mathrm{d}x}F_{11} + \frac{\lambda}{d}F_{12}}{\frac{q^2}{gd^3}T_1 + T_2} \qquad (2.3.17a)$$

$$\frac{\mathrm{d}d}{\mathrm{d}x} = \frac{\frac{q^2\lambda}{gd^3}F_{20} - \frac{\mathrm{d}z_b}{\mathrm{d}x}T_2}{\frac{q^2}{gd^3}T_1 + T_2} \qquad (2.3.17b)$$

with $F_{10} = \alpha\gamma_1 - \beta\gamma$ (2.3.17c)

$F_{11} = \alpha - \beta$ (2.3.17d)

$F_{12} = \gamma - \gamma_1$ (2.3.17e)

$F_{20} = \gamma_1 \frac{d\alpha}{d\Gamma} - \frac{1}{2}\gamma \frac{d\beta}{d\Gamma}$ (2.3.17f)

$T_1 = \beta \frac{d\alpha}{d\Gamma} - \frac{1}{2}\alpha \frac{d\beta}{d\Gamma}$ (2.3.17g)

$T_2 = \frac{1}{2}\frac{d\beta}{d\Gamma} - \frac{d\alpha}{d\Gamma}$ (2.3.17h)

Some calculations of flow over a sill were made with these equations for a discharge of 13 m^2/s. The initial water depth was 20 m. The length of the sinusoidal slope of the sill was 100 m, while the crown's length was 50 m. The maximum allowable height of the sill appeared to be 4 m. Choosing higher (or steeper) sills, the coefficient Γ becomes unstable near the top of the sill, which causes unstable solutions of the coefficients α, β, γ and γ_1, but also for the water level.

Graphs of the velocity profiles and the coefficients α, β, γ, γ_1, and Γ are plotted for the maximum sill height in the Fig. 2.3.4. In this figure the water depth derived with the common shallow-water equations, $\alpha=\beta=\gamma=\gamma_1=1$, is also plotted.

Downstream from the sill the water level obtained by the method of weighted residuals is lower than the water level obtained by the common model. This effect was to be achieved (chapter 1), but unfortunately the used similarity velocity profiles do not allow sills higher than 4.0 m. To make the analysis suitable for steep slopes, a slightly modified similarity velocity profile is chosen instead of eq. (2.3.12). Higher order terms in σ have to be added to get an increase of gradient near the bottom. This increases the bottom shear stress and increases the value of α in the acceleration zone. For $\Gamma=1$ an expression for such a velocity profile has to agree with the expression for the velocity profile of eq. (2.3.11), the velocity profile for uniform flow. The following velocity profile satisfies the last condition: $u(x,\sigma) = u_0(x,\sigma) + \Gamma(x)\,u_1(x,\sigma)$ (2.3.18a)

with $u_0 = \frac{q}{d}\left(\phi(\sigma) + \sigma^2 + 2\sigma\right)$ (2.3.18b)

and $u_1 = \frac{q}{d}\left(-\phi(\sigma) - \frac{5}{2}\sigma^2 + \sigma\right)$ (2.3.18c)

The unknown part of the velocity profile is called $\phi(\sigma)$. The function $\phi(\sigma)$ contains terms

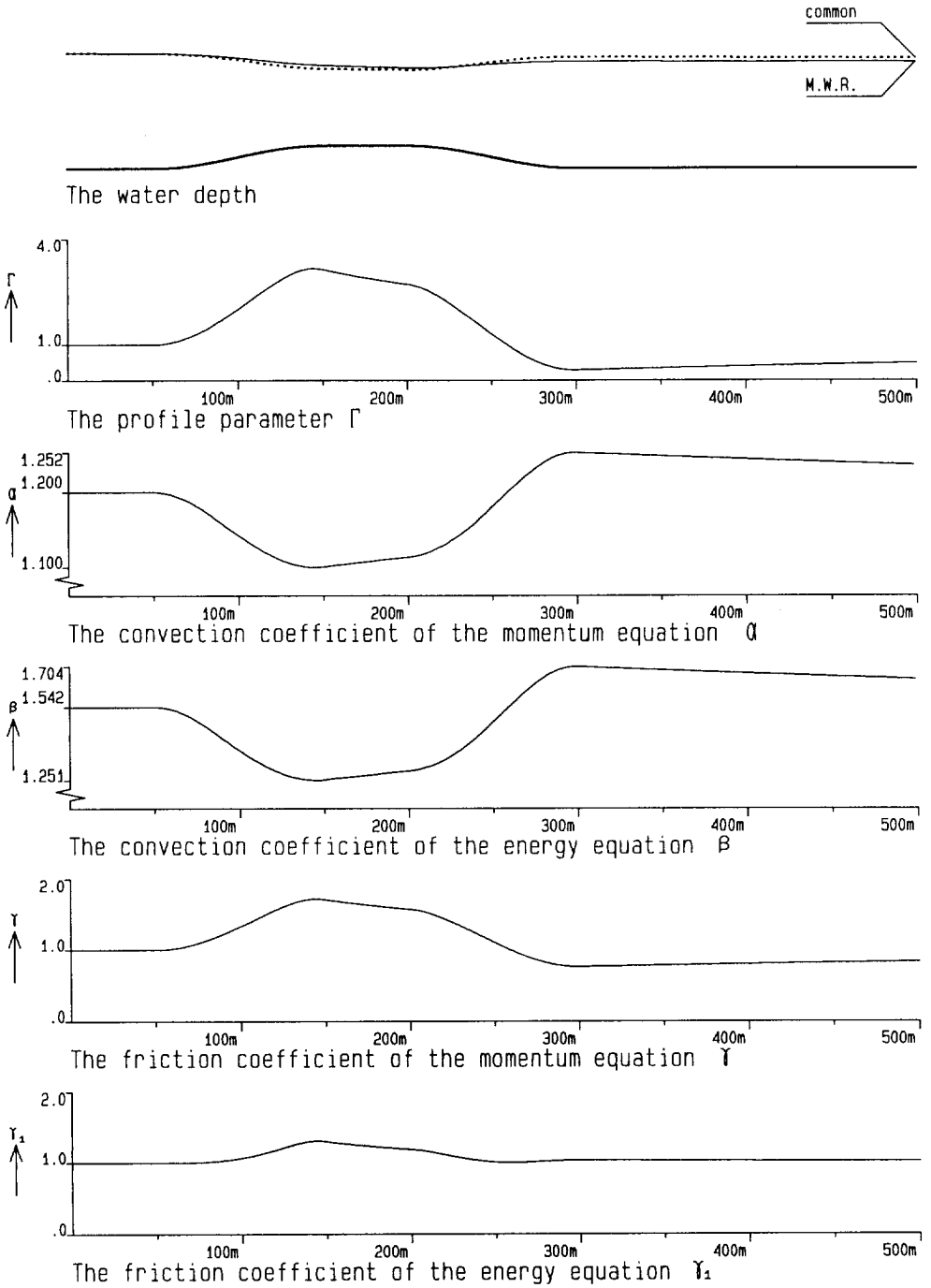

Figure 2.3.4 The coefficients and water level derived for eq. (2.3.12)

—— water level obtained by the method of weighted residuals, ····· water level obtained by the common model

with powers in σ of at least 1 to satisfy the no-slip condition. The value of the function $\phi(\sigma)$ integrated with respect to σ from $\sigma=0$ to $\sigma=1$ must be equal to $-1/3$ to satisfy the discharge condition. The last condition that $\phi(\sigma)$ has to fulfil is the zero friction condition at the water surface. Therefore the gradient of $\phi(\sigma)$ must be zero at the water surface.

There are many functions $\phi(\sigma)$, which satisfy these conditions. To come to a more specific assumption concerning the function $\phi(\sigma)$ it is convenient to use a different similarity coefficient Γ^* instead of Γ:

$$\Gamma^* = 1 - \Gamma$$

Substitution of this new coefficient in the velocity profile (2.3.18), yields:

$$u = \frac{q}{d}\left(\left(-\tfrac{3}{2}\sigma^2+3\sigma\right)+\Gamma^*\left(\phi(\sigma)+\tfrac{5}{2}\sigma^2-\sigma\right)\right) \qquad (2.3.19)$$

The first term of expression (2.3.19), is equal to the zeroth-order velocity profile obtained by the method of asymptotic expansions, expression (A.3.8), while the function $\phi(\sigma)$ can be chosen in such a way that the second part of expression (2.3.19) is equal to σ-terms of the main part of the first-order velocity profile obtained with this method, expression (A.3.12). The σ-terms of this first-order velocity profile are used for the first-order velocity profile in eq. (2.3.19). The velocity profile used reads:

$$u(x,\sigma) = u_0(x,\sigma)+\Gamma^*(x)u_1(x,\sigma) \qquad (2.3.20a)$$

$$\text{with} \quad u_0 = \frac{q}{d}\left(-\tfrac{3}{2}\sigma^2+3\sigma\right) \qquad (2.3.20b)$$

$$\text{and} \quad u_1 = \frac{q}{d}\left(\frac{7\sigma^6-42\sigma^5+70\sigma^4-72\sigma^2+32\sigma}{21}\right) \qquad (2.3.20c)$$

A graph of these velocity profiles is plotted in Fig. 2.3.5.

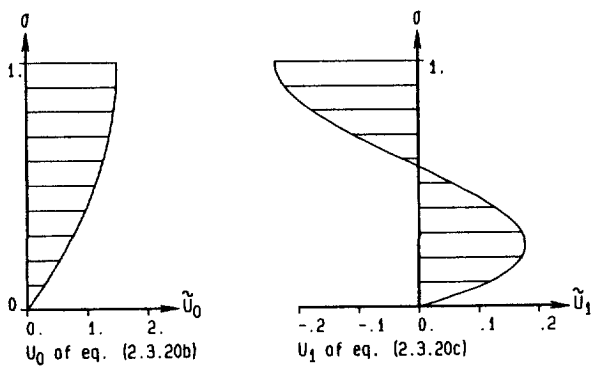

Figure 2.3.5 The velocity profiles of eq. (2.3.20) ($\tilde{u}=ud/q$)

From this point Γ^* is replaced by Γ, without changing the meaning of Γ^*. It only

means that the * is dropped.

To obtain the modified shallow-water equations derived using this velocity profile, the velocity profile defined by eq. (2.3.20) has to be substituted into the equations (2.3.10a) up to (2.3.10d). This yields for the convection coefficient, α:

$$\alpha = S_{10} + S_{11}\Gamma + S_{12}\Gamma^2 \tag{2.3.21a}$$

with $$S_{10} = \frac{6}{5} \tag{2.3.21b}$$

$$S_{11} = -\frac{32}{315} \tag{2.3.21c}$$

$$S_{12} = \frac{8704}{405405} \tag{2.3.21d}$$

for the Coriolis coefficient, β:

$$\beta = S_{20} + S_{21}\Gamma + S_{22}\Gamma^2 + S_{23}\Gamma^3 \tag{2.3.22a}$$

with $$S_{20} = \frac{54}{35} \tag{2.3.22b}$$

$$S_{21} = -\frac{832}{2695} \tag{2.3.22c}$$

$$S_{22} = \frac{159232}{2207205} \tag{2.3.22d}$$

$$S_{23} = -\frac{48381952}{44914414545} \tag{2.3.22e}$$

for the friction coefficient in the energy equation, γ_1:

$$\gamma_1 = S_{30} + S_{31}\Gamma + S_{32}\Gamma^2 \tag{2.3.23a}$$

with $$S_{30} = 1 \tag{2.3.23b}$$

$$S_{31} = 0 \tag{2.3.23c}$$

$$S_{32} = \frac{6656}{43659} \tag{2.3.23d}$$

and for the friction coefficient in the momentum equation, γ:

$$\gamma = S_{40} + S_{41}\Gamma \tag{2.3.24a}$$

with $$S_{40} = 1 \tag{2.3.24b}$$

$$S_{41} = \frac{32}{63} \tag{2.3.24c}$$

The coefficients S_{10} to S_{41} are substituted into eq. (2.3.17) to calculate the water depth, d, and the coefficient Γ. With velocity profile (2.3.20), some calculations were made for flow over sinusoidal sills with slope lengths of 100 m, an average initial velocity of .65 m/s and an initial water depth of 20 m. The maximum sill height appears to be 4.3 m. (For higher sills the coefficient Γ becomes unstable.) For this maximum sill height the coefficients α, β, γ

and γ_1 and the water depth are plotted in the Fig. 2.3.6. In this figure the water depth derived with the common shallow-water equations, $\alpha=\beta=\gamma=\gamma_1=1$, is also plotted.

Comparing the water depth calculated with both models, it can be concluded that the fall of the water level due to the sill is increased in the modified model. This is qualitatively what was to be achieved (chapter 1).

Using the velocity profiles of eq. (2.3.20) the maximum sill height has only slightly increased, compared to the maximum sill height using the velocity profiles of eq. (2.3.12). The calculated modifications of both velocity profiles give an increase of the fall of the water level over the sill in comparison to the water level fall obtained by the common shallow-water equations, but the maximum sill height remains low in comparison to the water depth. The maximum dimensions of the sill can be improved by choosing other velocity profiles for u_1, but the disadvantage of the constant eddy-viscosity and the parabolic velocity profile is too great. The value of the convection coefficient α is too large for turbulent flows in open channels, for which it is better to use a logarithmic velocity profile and, as a first estimate, a parabolic eddy-viscosity distribution. This analysis is discussed in the last section of this chapter.

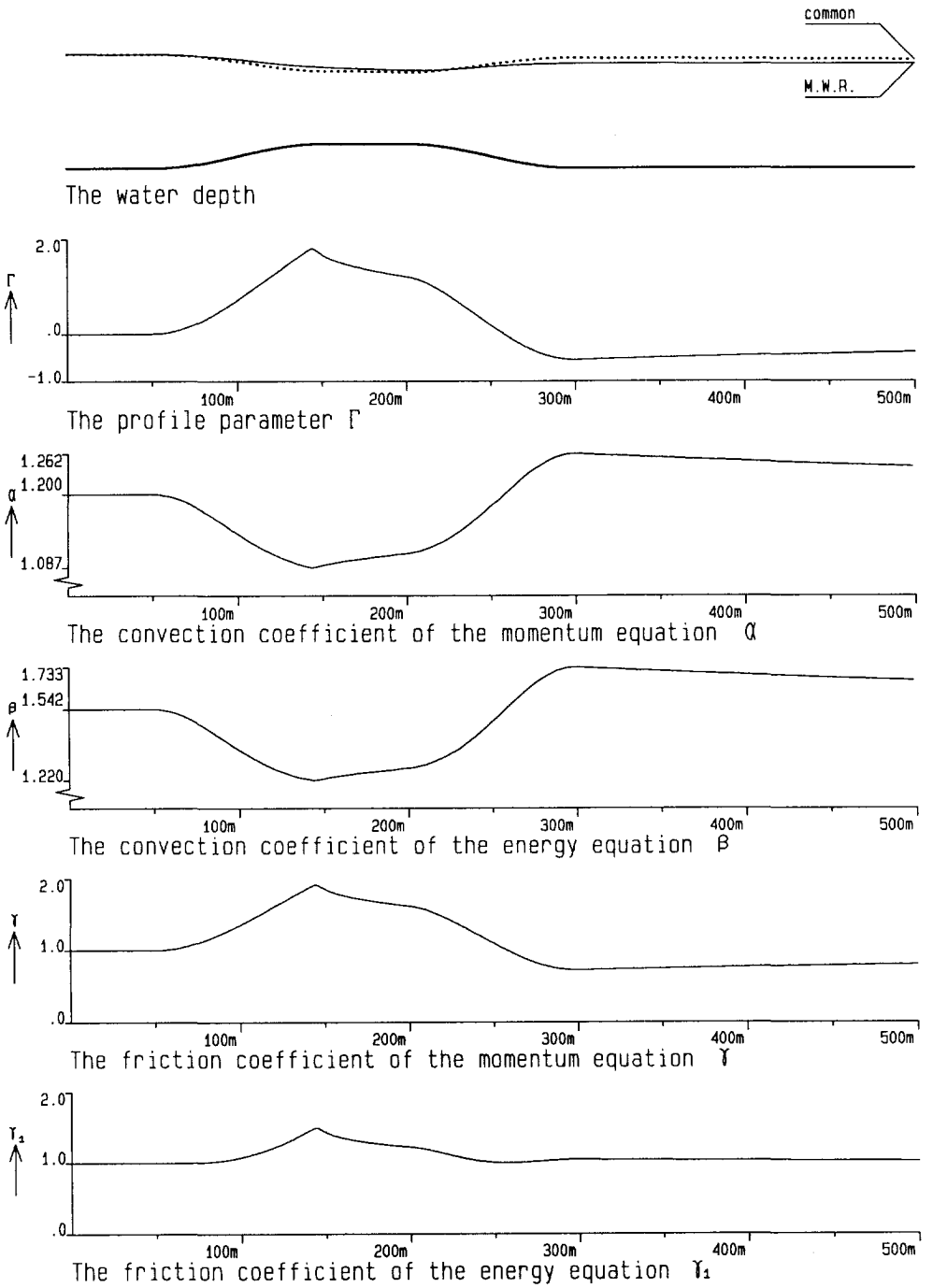

Figure 2.3.6 The coefficients and water level derived for eq. (2.3.20)

—— *water level obtained by the method of weighted residuals,* ····· *water level obtained by the common model*

2.3.2 The parabolic eddy-viscosity model

In this section the modified shallow-water equations are derived using a parabolic eddy-viscosity model and a logarithmic velocity profile for uniform flow. This eddy-viscosity can be written as:

$$\nu_t = \kappa u_* d\,\sigma(1-\sigma)$$

Starting-point is again eq. (2.3.20a) with uniform flow for Γ=0:

$$u(x,z) = u_0(x,\sigma) + \Gamma(x)\,u_1(x,\sigma) \tag{2.3.25a}$$

In the present case, the uniform-flow profile is logarithmic:

$$u_0 = \frac{q}{d}\left(\frac{\ln(\sigma/\sigma_0)}{L_{\sigma 0}-1}\right) \tag{2.3.25b}$$

in which $L_{\sigma 0}$ is defined by:

$$L_{\sigma 0} = \ln(1/\sigma_0)$$

and σ_0 is the elevation where the logarithmic velocity is zero in the σ-x coordinate system, $\sigma_0=z_0/d$, with z_0 dependent on the roughness according to expression (A.4.1).

To find the velocity profile u_1 of eq. (2.3.25a) almost the same procedure as in the previous section can be used, except that the velocity profile given by eq. (2.3.20c) and obtained by the method of asymptotic expansions using a constant eddy-viscosity model, is replaced by the velocity profile derived using a parabolic eddy-viscosity model, expression (A.4.10). Unfortunately, this first-order velocity profile contains series which make the calculations much more complicated. The shape of the first-order profile can be approximated by some terms containing powers of logarithms (appendix C and Fig. 2.3.7), up to second order:

$$u_1(x,\sigma) = \frac{q}{d}\left(\frac{\ln^2(\sigma/\sigma_0)}{\left(L_{\sigma 0}^{\,2}-2L_{\sigma 0}+2\right)} - \frac{\ln(\sigma/\sigma_0)}{(L_{\sigma 0}-1)}\right) \tag{2.3.26}$$

and up to third order:

$$u_1(x,\sigma) = \frac{q}{d}\left(\frac{\ln^3(\sigma/\sigma_0)-5\ln^2(\sigma/\sigma_0)}{\left(L_{\sigma 0}^{\,3}-8L_{\sigma 0}^{\,2}+16L_{\sigma 0}-16\right)} - \frac{\ln(\sigma/\sigma_0)}{(L_{\sigma 0}-1)}\right) \tag{2.3.27}$$

The first velocity profile of u_1, eq. (2.3.26), has a steeper gradient near the bottom than u_1

of eq. (2.3.27) (Fig. 2.3.7). Therefore this profile is expected to be better for simulating flows in acceleration zones.

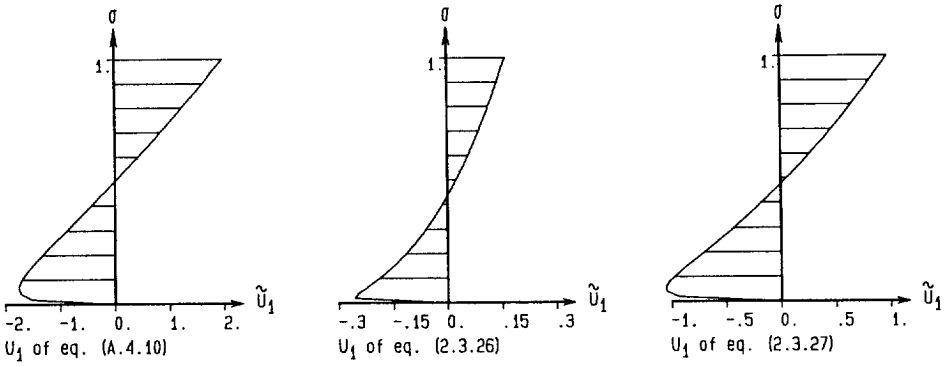

Figure 2.3.7 Several first order velocity profiles

The expressions for the eddy-viscosity and the horizontal velocity can be substituted into the expression for the Reynolds shear stress, eq. (2.2.5b). Neglecting the vertical velocity in this expression yields for the Reynolds shear stress:

$$-\frac{1}{\rho}\tau_{x\sigma} = \frac{q\, u_*\kappa(1-\sigma)}{d(L_{\sigma 0}-1)}$$

The bottom shear stress in open channels for flat bottom situations can be written as:

$$-\frac{1}{\rho}\tau_{x\sigma}\bigg|_{\sigma=0} = u_*^2$$

Combining these last two equations gives an alternative way of writing the parabolic eddy-viscosity, which is used in this analysis:

$$\nu_t = \frac{q\kappa^2}{(L_{\sigma 0}-1)}\sigma(1-\sigma) \qquad (2.3.28)$$

These equations also determine the friction parameter, λ, for a logarithmic velocity profile:

$$\lambda = -\frac{\tau_{x\sigma}}{\rho(q/d)^2} = \frac{\kappa^2}{(L_{\sigma 0}-1)^2}$$

Substitution of this first-order velocity profile, eq. (2.3.26), into eq. (2.3.25) yields the velocity profile used to determine the modified shallow-water equations. Substitution of this velocity profile, eq. (2.3.25), and the eddy-viscosity distribution, eq. (2.3.28), into the depth-averaged momentum equation, eq. (2.3.8), and the depth-averaged energy equation, eq. (2.3.9), yields:

$$-\alpha\frac{q^2}{d^2}\frac{\mathrm{d}d}{\mathrm{d}x} + \frac{q^2}{d}\frac{\partial\alpha}{\partial L_{\sigma 0}}\frac{\mathrm{d}L_{\sigma 0}}{\mathrm{d}d}\frac{\mathrm{d}d}{\mathrm{d}x} + \frac{q^2}{d}\frac{\partial\alpha}{\partial\Gamma}\frac{\mathrm{d}\Gamma}{\mathrm{d}x} + gd\frac{\mathrm{d}(z_b+d)}{\mathrm{d}x} + \gamma\frac{q^2\lambda}{d^2} = 0 \qquad (2.3.29a)$$

$$-\beta\frac{q^3}{d^3}\frac{\mathrm{d}d}{\mathrm{d}x}+\frac{1}{2}\left(\frac{q^3}{d^2}\frac{\partial\beta}{\partial L_{\sigma 0}}\frac{\mathrm{d}L_{\sigma 0}}{\mathrm{d}d}\frac{\mathrm{d}d}{\mathrm{d}x}+\frac{q^3}{d^2}\frac{\partial\beta}{\partial\Gamma}\frac{\mathrm{d}\Gamma}{\mathrm{d}x}\right)+gq\frac{\mathrm{d}(z_b+d)}{\mathrm{d}x}+\gamma_1\frac{q^3\lambda}{d^3}=0 \quad (2.3.29b)$$

with the convection coefficient α:

$$\alpha = S_{10}+S_{11}\Gamma+S_{12}\Gamma^2 \quad (2.3.30a)$$

in which:

$$S_{10} = \frac{L_{\sigma 0}-2L_{\sigma 0}+2}{(L_{\sigma 0}-1)^2} = 1+\frac{1}{(L_{\sigma 0}-1)^2} \quad (2.3.30b)$$

$$S_{11} = \frac{2(L_{\sigma 0}{}^2-4L_{\sigma 0}+2)}{(L_{\sigma 0}-1)^2\,(L_{\sigma 0}{}^2-2L_{\sigma 0}+2)} \quad (2.3.30c)$$

$$S_{12} = \frac{L_{\sigma 0}{}^4-8L_{\sigma 0}{}^3+24L_{\sigma 0}{}^2-24L_{\sigma 0}+8}{(L_{\sigma 0}-1)^2\,(L_{\sigma 0}{}^2-2L_{\sigma 0}+2)^2} \quad (2.3.30d)$$

with the Coriolis coefficient β:

$$\beta = S_{20}+S_{21}\Gamma+S_{22}\Gamma^2+S_{23}\Gamma^3 \quad (2.3.31a)$$

in which:

$$S_{20} = \frac{L_{\sigma 0}{}^3-3L_{\sigma 0}{}^2+6L_{\sigma 0}-6}{(L_{\sigma 0}-1)^3} \quad (2.3.31b)$$

$$S_{21} = \frac{6(L_{\sigma 0}{}^3-6L_{\sigma 0}{}^2+12L_{\sigma 0}-6)}{(L_{\sigma 0}-1)^3\,(L_{\sigma 0}{}^2-2L_{\sigma 0}+2)} \quad (2.3.31c)$$

$$S_{22} = \frac{3(L_{\sigma 0}{}^5-11L_{\sigma 0}{}^4+56L_{\sigma 0}{}^3-144L_{\sigma 0}{}^2+144L_{\sigma 0}-48)}{(L_{\sigma 0}-1)^3\,(L_{\sigma 0}{}^2-2L_{\sigma 0}+2)^2} \quad (2.3.31d)$$

$$S_{23} = \frac{-2(L_{\sigma 0}{}^6-18L_{\sigma 0}{}^5+132L_{\sigma 0}{}^4-464L_{\sigma 0}{}^3+708L_{\sigma 0}{}^2-480L_{\sigma 0}+120)}{(L_{\sigma 0}-1)^3\,(L_{\sigma 0}{}^2-2L_{\sigma 0}+2)^3} \quad (2.3.31e)$$

with the friction coefficient γ_1:

$$\gamma_1 = S_{30}+S_{31}\Gamma+S_{32}\Gamma^2 \quad (2.3.32a)$$

in which:

$$S_{30} = 1 \quad (2.3.32b)$$

$$S_{31} = 0 \quad (2.3.32c)$$

$$S_{32} = \frac{\left(L_{\sigma 0}{}^4 - 4L_{\sigma 0}{}^3 + 12L_{\sigma 0}{}^2 - 24L_{\sigma 0} + 12\right)}{3\left(L_{\sigma 0}{}^2 - 2L_{\sigma 0} + 2\right)^2} \tag{2.3.32d}$$

with the friction coefficient γ:

$$\gamma = S_{40} + S_{41}\Gamma \tag{2.3.33a}$$

in which:

$$S_{40} = 1 \tag{2.3.33b}$$

$$S_{41} = -1 \tag{2.3.33c}$$

Substitution of $dL_{\sigma 0}/dd = 1/d$ and rewriting the expressions (2.3.29a) and (2.3.29b) yields the differential equations for the profile parameter, Γ, and the water depth, d:

$$\frac{d\Gamma}{dx} = \frac{\frac{q^2\lambda}{gd^4}F_{10} + \frac{1}{d}\frac{dz_b}{dx}F_{11} + \frac{\lambda}{d}F_{12}}{\frac{q^2}{gd^3}T_1 + T_2} \tag{2.3.34a}$$

$$\frac{dd}{dx} = \frac{\frac{q^2\lambda}{gd^3}F_{20} - \frac{dz_b}{dx}T_2}{\frac{q^2}{gd^3}T_1 + T_2} \tag{2.3.34b}$$

with the definition of the factors F_{12}, F_{20}, and T_2 as in eq. (2.3.17). Due to the dependence of $L_{\sigma 0}$ on the water depth the factors F_{10}, F_{11} and T_1 are slightly different from the ones of eq. (2.3.17):

$$F_{10} = \left(\alpha - \frac{\partial\alpha}{\partial L_{\sigma 0}}\right)\gamma_1 - \left(\beta - \tfrac{1}{2}\frac{\partial\beta}{\partial L_{\sigma 0}}\right)\gamma \tag{2.3.34c}$$

$$F_{11} = \alpha - \frac{\partial\alpha}{\partial L_{\sigma 0}} - \beta + \tfrac{1}{2}\frac{\partial\beta}{\partial L_{\sigma 0}} \tag{2.3.34d}$$

$$T_1 = \left(\beta - \tfrac{1}{2}\frac{\partial\beta}{\partial L_{\sigma 0}}\right)\frac{\partial\alpha}{\partial\Gamma} - \tfrac{1}{2}\left(\alpha - \frac{\partial\alpha}{\partial L_{\sigma 0}}\right)\frac{\partial\beta}{\partial\Gamma} \tag{2.3.34e}$$

Graphs of the velocity profiles u_0 and u_1 are plotted in Fig. 2.3.8. Several calculations were made of flow over a sill with an average approach velocity of 0.65 m/s, an initial water depth of 20 m, a length of the sinusoidal slope is 75 m and a crown length of 50 m. The

maximum crown height appeared to be 7.5 m (maximum slope about $^1/_6$). Graphs of the water level and the coefficients α, β, γ and γ_1 are plotted in Fig. 2.3.9 for this maximum sill height. In this figure the water level derived with the common shallow-water equations, $\alpha=\beta=\gamma=\gamma_1=1$, is also plotted. The rise of the water level in the deceleration zone is much less in the modified model than in the common model, but further downstream the water levels of both models hardly deviate from each other, contrary to what was to be achieved. The developments of the convection and friction coefficients are as expected in the acceleration zone. In the deceleration zone the friction coefficient, γ, is already negative somewhere high on the sill (indicating flow reversal).

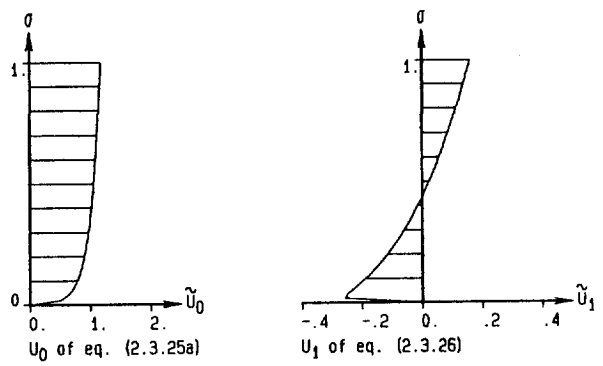

Figure 2.3.8 The velocity profiles of eq. (2.3.25a) and eq. (2.3.26)

The velocity profile u_1 given in eq. (2.3.26) is a good approximation in the acceleration zone but apparently less good in the deceleration zone. In this zone the gradient of this first-order profile is too large near the bottom and near the water surface. The large gradient near the bottom can be improved by using eq. (2.3.27). The large gradient near the water surface can be improved by adding some terms of powers of σ to the first-order profile of eq. (2.3.27):

$$u_1(x,\sigma) = \frac{q}{d}\left(\frac{\ln^3(\sigma/\sigma_0) - 5\ln^2(\sigma/\sigma_0)}{3\left(L_{\sigma 0}{}^3 - 8L_{\sigma 0}{}^2 + 16L_{\sigma 0} - 16\right)} + \frac{10}{9}\sigma^2\left(3\sigma^2 - 8\sigma + 6\right) - \frac{\ln(\sigma/\sigma_0)}{(L_{\sigma 0} - 1)} \right) \qquad (2.3.35)$$

The first term on the right-hand side shows good similarity with the first term of the first-order velocity profile of the perturbation method (Fig. 2.3.7). The factor $^1/_3$ is introduced to reduce the discharge caused by this first and the second term. (The depth-integrated value for the first term is $^1/_3 q$, for the second term $^2/_3 q$ and for the third term $-q$.) Near the water

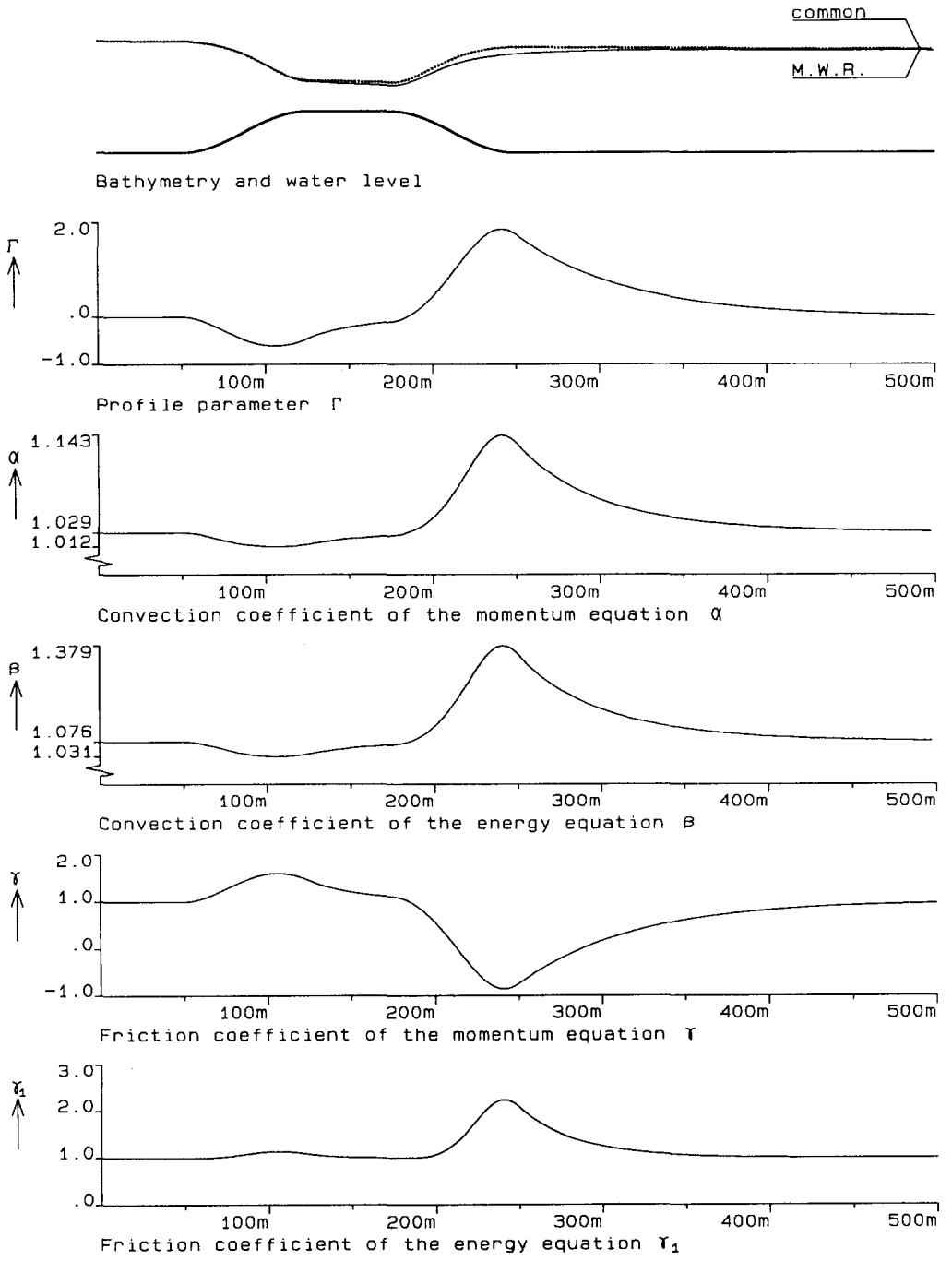

Figure 2.3.9 The coefficients and water level derived from eq. (2.3.25a) and eq. (2.3.26)

—— water level obtained by the method of weighted residuals, ····· water level obtained by the common model

surface this velocity profile is almost linear. This is not expected, because numerical calculations of flows over sills (chapter 3) and measurements in a flume (chapter 4) show a decrease of the total horizontal velocity gradient near the water surface, although the gradient remains positive. This can be simulated with a uniform section in the velocity profile. To calculate the width of this uniform section a third momentum equation can be used, as done by Madsen & Svendsen [1983]. But, a decrease of the velocity gradient can also be simulated by the second term of the right hand side of eq. (2.3.35). The velocity gradient of this part approaches the value zero at the water surface, and adding this term to the first term makes the velocity gradient decrease approaching the water surface. The third part of this velocity profile is the logarithmic part which causes the discharge of the first-order profile to be zero. The total velocity profile, which is used in the deceleration zone, can be written as:

$$u(x,\sigma)=\frac{q}{d}\left(\frac{\ln(\sigma/\sigma_0)}{L_{\sigma 0}-1}+\Gamma\left(\frac{\ln^3(\sigma/\sigma_0)-5\ln^2(\sigma/\sigma_0)}{3\left(L_{\sigma 0}{}^3-8L_{\sigma 0}{}^2+16L_{\sigma 0}-16\right)}+\frac{10}{9}\sigma^2(3\sigma^2-8\sigma+6)-\frac{\ln(\sigma/\sigma_0)}{L_{\sigma 0}-1}\right)\right) \qquad (2.3.36)$$

Graphs of this velocity profile is plotted in Fig. 2.3.10.

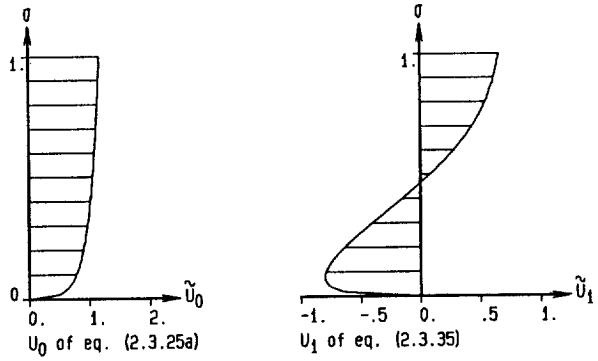

Figure 2.3.10 The velocity profiles of eq. (2.3.25a) and eq. (2.3.35)

Substitution of this velocity and the viscosity profile of eq. (2.3.28) into the depth-averaged momentum equation, eq. (2.3.8), and the depth-averaged energy equation, eq. (2.3.9), yield the same differential equations for the profile parameter, Γ, and the water depth, d, as in eq. (2.3.34). The only differences are the values of the coefficients S_{10} up to S_{41} in the deceleration zone. In this case these coefficients read:

$$S_{10} = \frac{L_{\sigma 0}{}^2-2L_{\sigma 0}+2}{\left(L_{\sigma 0}-1\right)^2} = 1+\frac{1}{\left(L_{\sigma 0}-1\right)^2} \qquad (2.3.37a)$$

$$S_{11} = \frac{0.6963L_{\sigma 0}^{\ 4} - 6.2667L_{\sigma 0}^{\ 3} + 16.044L_{\sigma 0}^{\ 2} - 14.281L_{\sigma 0} + 17.807}{\left(L_{\sigma 0} - 1\right)^2 \left(L_{\sigma 0}^{\ 3} - 8L_{\sigma 0}^{\ 2} + 16L_{\sigma 0} - 16\right)} \tag{2.3.37b}$$

$$S_{12} = \frac{0.1552L_{\sigma 0}^{\ 8} - 2.7937L_{\sigma 0}^{\ 7} + 20.446L_{\sigma 0}^{\ 6} - 81.498L_{\sigma 0}^{\ 5} + 2.0942\cdot 10^2 L_{\sigma 0}^{\ 4}}{\left(L_{\sigma 0} - 1\right)^2 \left(L_{\sigma 0}^{\ 3} - 8L_{\sigma 0}^{\ 2} + 16L_{\sigma 0} - 16\right)^2} + \frac{-4.0752\cdot 10^2 L_{\sigma 0}^{\ 3} + 6.1391\cdot 10^2 L_{\sigma 0}^{\ 2} - 5.2732\cdot 10^2 L_{\sigma 0} + 2.2418\cdot 10^2}{\left(L_{\sigma 0} - 1\right)^2 \left(L_{\sigma 0}^{\ 3} - 8L_{\sigma 0}^{\ 2} + 16L_{\sigma 0} - 16\right)^2} \tag{2.3.37c}$$

$$S_{20} = \frac{L_{\sigma 0}^{\ 3} - 3L_{\sigma 0}^{\ 2} + 6L_{\sigma 0} - 6}{\left(L_{\sigma 0} - 1\right)^3} \tag{2.3.37d}$$

$$S_{21} = \frac{2.0889L_{\sigma 0}^{\ 5} - 21.992L_{\sigma 0}^{\ 4} + 76.860L_{\sigma 0}^{\ 3} - 1.0345\cdot 10^2 L_{\sigma 0}^{\ 2} + 39.561L_{\sigma 0} - 35.070}{\left(L_{\sigma 0} - 1\right)^3 \left(L_{\sigma 0}^{\ 3} - 8L_{\sigma 0}^{\ 2} + 16L_{\sigma 0} - 16\right)} \tag{2.3.37e}$$

$$S_{22} = \frac{\left(4.6561\cdot 10^{-1} L_{\sigma 0}^{\ 9} - 9.0893L_{\sigma 0}^{\ 8} + 74.090L_{\sigma 0}^{\ 7} - 3.3370\cdot 10^2 L_{\sigma 0}^{\ 6} + 9.3986\cdot 10^2 L_{\sigma 0}^{\ 5}\right)}{\left(L_{\sigma 0} - 1\right)^3 \left(L_{\sigma 0}^{\ 3} - 8L_{\sigma 0}^{\ 2} + 16L_{\sigma 0} - 16\right)^2} + \frac{\left(-1.9466\cdot 10^2 L_{\sigma 0}^{\ 4} + 3.6036\cdot 10^3 L_{\sigma 0}^{\ 3} - 6.1323\cdot 10^3 L_{\sigma 0}^{\ 2} + 5.2974\cdot 10^3 L_{\sigma 0} - 1.8264\cdot 10^3\right)}{\left(L_{\sigma 0} - 1\right)^3 \left(L_{\sigma 0}^{\ 3} - 8L_{\sigma 0}^{\ 2} + 16L_{\sigma 0} - 16\right)^2} \tag{2.3.37f}$$

$$S_{23} = \frac{\left(-2.3746\cdot 10^{-2} L_{\sigma 0}^{\ 12} + 6.4114\cdot 10^{-1} L_{\sigma 0}^{\ 11} - 7.3144L_{\sigma 0}^{\ 10} + 46.223L_{\sigma 0}^{\ 9} - 1.8647\cdot 10^2 L_{\sigma 0}^{\ 8}\right)}{\left(L_{\sigma 0} - 1\right)^3 \left(L_{\sigma 0}^{\ 3} - 8L_{\sigma 0}^{\ 2} + 16L_{\sigma 0} - 16\right)^3} + \frac{\left(6.0476\cdot 10^2 L_{\sigma 0}^{\ 7} - 1.9749\cdot 10^3 L_{\sigma 0}^{\ 6} + 4.5093\cdot 10^3 L_{\sigma 0}^{\ 5} + 1.6392\cdot 10^4 L_{\sigma 0}^{\ 4}\right)}{\left(L_{\sigma 0} - 1\right)^3 \left(L_{\sigma 0}^{\ 3} - 8L_{\sigma 0}^{\ 2} + 16L_{\sigma 0} - 16\right)^3} + \frac{\left(-3.5617\cdot 10^4 L_{\sigma 0}^{\ 3} + 6.4506\cdot 10^4 L_{\sigma 0}^{\ 2} - 4.5263\cdot 10^4 L_{\sigma 0} + 1.1057\cdot 10^4\right)}{\left(L_{\sigma 0} - 1\right)^3 \left(L_{\sigma 0}^{\ 3} - 8L_{\sigma 0}^{\ 2} + 16L_{\sigma 0} - 16\right)^3} \tag{2.3.37g}$$

$$S_{30} = 1 \tag{2.3.37h}$$

$$S_{31} = 0 \tag{2.3.37i}$$

$$S_{32} = \frac{3.5273\cdot 10^{-1} L_{\sigma 0}^{\ 7} - 5.4631L_{\sigma 0}^{\ 6} + 32.773L_{\sigma 0}^{\ 5} - 1.0309\cdot 10^2 L_{\sigma 0}^{\ 4}}{\left(L_{\sigma 0}^{\ 3} - 8L_{\sigma 0}^{\ 2} + 16L_{\sigma 0} - 16\right)^2} + \frac{2.0458\cdot 10^2 L_{\sigma 0}^{\ 3} - 2.6637\cdot 10^2 L_{\sigma 0}^{\ 2} + 2.1202\cdot 10^2 L_{\sigma 0} - 1.2379\cdot 10^2}{\left(L_{\sigma 0}^{\ 3} - 8L_{\sigma 0}^{\ 2} + 16L_{\sigma 0} - 16\right)^2} \tag{2.3.37j}$$

$$S_{40} = 1 \qquad (2.3.37k)$$

$$S_{41} = -1 \qquad (2.3.37l)$$

The transition from the velocity profile used in the acceleration zone to the velocity profile in the deceleration zone, is imposed at the downstream edge of the crown.

Some calculations were made of flow over a sill with an average approach velocity of 0.65 m/s, an initial water depth of 20 m, a length of the sinusoidal slope of 75 m and a crown length of 50 m. For sills higher than about 10 m the calculated water surface elevation downstream from the sill showed unrealistic features.

Graphs of the water level and the coefficients α, β, γ and γ_1 are plotted in Fig. 2.3.11 for a sill height of 9.6 m. In this figure the water level derived with the common shallow-water equations, $\alpha=\beta=\gamma=\gamma_1=1$, is also plotted.

Nothing has changed in the acceleration zone compared to the solutions of the previous velocity profile used (Fig. 2.3.9). In the deceleration zone the friction coefficient remains positive (absence of flow reversal), and the maximum value of the convection coefficient is higher.

Small jumps arise in the graphs of the convection coefficients and the friction coefficient of the energy equation at the transition point of the velocity profiles (downstream edge of the sill crown). These jumps are small due to the near-zero value of the profile parameter, Γ, at this point. At the transition point the profile parameter, Γ, and the friction coefficient, γ, are continuous because the expressions for both coefficients do not change. The velocity profile has nearly reached its shape corresponding to uniform-flow over flat bottoms.

Due to the modifications the downstream water level calculated with the method of weighted residuals is significantly lower than the water level calculated with the common shallow-water equations. This is qualitatively what was to be achieved (chapter 1).

In the next chapter several 2DV calculations are made for flow over different sills using a finite-volume numerical computer model, which solves the 2DV Navier-Stokes and continuity equation. From these solutions modifications of the 1DH shallow-water equations

are calculated. The modifications and horizontal velocity profiles calculated with the method of weighted residuals are compared with those obtained from the 2DV numerical model.

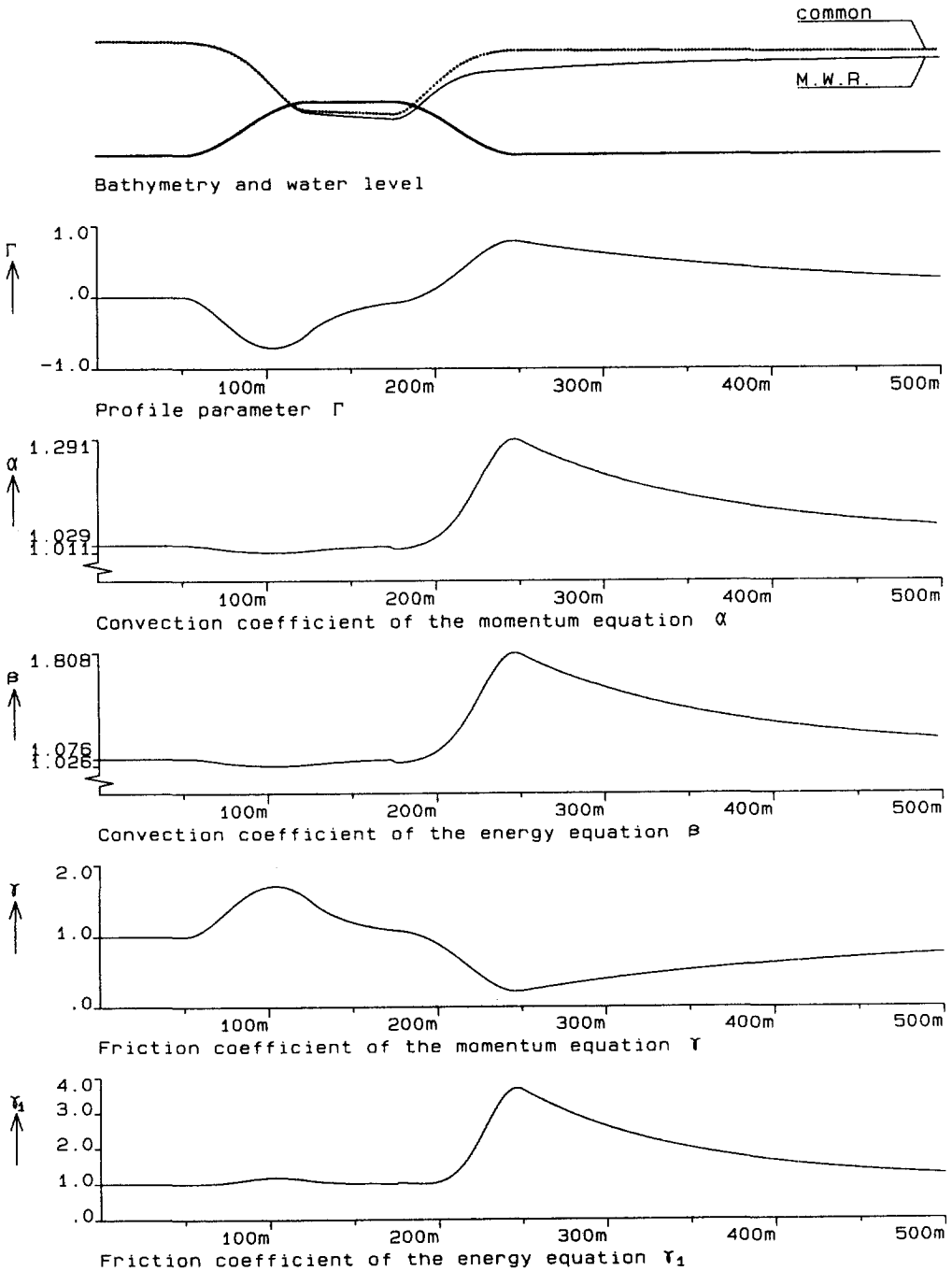

Figure 2.3.11 The coefficients and water level derived from eq. (2.3.25a), eq. (2.3.26) and eq. (2.3.35)
—— water level obtained by the method of weighted residuals, ····· water level obtained by the common model

3. Numerical modelling

3.1 Introduction

Using the method of weighted residuals, velocity profiles were calculated in the previous chapter by adding perturbation profiles of assumed shape to a logarithmic or parabolic velocity profile. The magnitude of this perturbation profile depends on the bathymetry. The velocity profiles found in this way were used to calculate modifications in the 1DH (one-dimensional horizontal) shallow-water equations. The exact perturbation profile to be imposed, is not known. The present chapter presents results of calculations with a 2DV (two-dimensional vertical) numerical model, which were made to verify the velocity profiles, the ones obtained by the method of weighted residuals and to get a better insight in the reliability of the modifications.

In this study the PHOENICS flow-simulation system of CHAM Ltd was used. This model is based on a 3D (three-dimensional) finite-volume method that solves transport equations, e.g. the Navier-Stokes equations. With PHOENICS only 2DV calculations have been made in this study. Some of the results of the calculations, the horizontal velocity and the pressure field, are used to calculate modifications of the conventional 1DH shallow-water equations.

Several computations are made for different bottom geometries. These flow situations are described in the next section. In the third section, the PHOENICS flow-simulation system is described with the boundary conditions used. The results of the flow-simulations are described in the second part of this section. In the fourth section a 1DH numerical model is described. This model is based on the 1DH shallow-water equations and contains modified terms calculated from the results of the 2DV flow-simulation system PHOENICS. The water levels derived with this 1DH model are compared with the water levels derived with the 2DV flow-simulation system PHOENICS and with the commonly used shallow-water equations. For two cases the water levels derived with the flow-simulation system PHOENICS are also compared with the water levels derived by the method of weighted residuals (chapter 2). In the last section the importance of each modification is discussed.

3.2 Description of the flow-situations

The flow-simulation system PHOENICS and the 1DH model described in section 3.4 are used to make some calculations of steady flow in a vertical plane over a sill. The proportions of the basic sill used in the calculations are based on those of a dam in the Tholense Gat, a closure gap located in the Eastern Scheldt (Fig. 3.2.1) in the south-west of the Netherlands. The bathymetry of the Eastern Scheldt is almost two-dimensional at that location. The flow in that part of the Eastern Scheldt is parallel to the straight natural channel. Therefore the water levels and flow velocities calculated with a 2DV model should not be much different from the ones in the prototype.

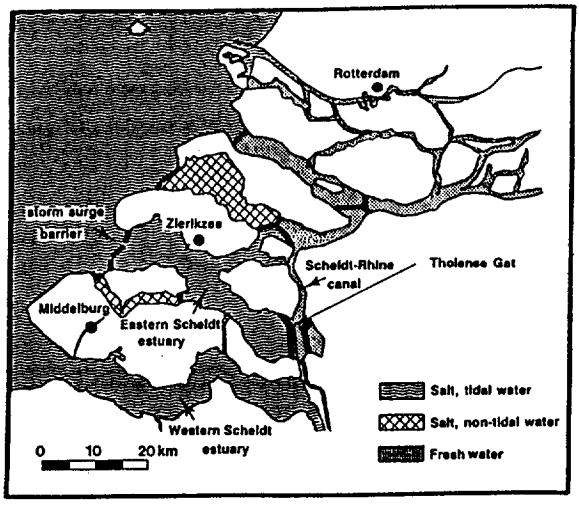

Figure 3.2.1 The Eastern Scheldt estuary

The water depth and the average flow velocity in the computations are based on the situation at maximum flood current. At this time the volume flux in the Tholense Gat is about 3800 m^3/s and the water depth, d, is approximately 20 m. The hydraulic cross-sectional area of the closure gap is 5985 m^2. This yields an average horizontal velocity of 0.65 m/s approximately.

The shape of the basic sill (Fig. 3.2.2) in the computations deviates slightly from the shape of the dam under construction in the prototype. The sill in the prototype has nominally the shape of a trapezoid. The sill in the calculations has a sinusoidal shape to avoid numerical inaccuracies due to the discontinuity of the bottom slope. In the basic situation, the length

of the crown (L_{crown}) is 50 m and the height of the crown (a) is taken about half the water depth. The maximum slope gradient of the sill is $^1/_5$, the maximum gradient for which no separation occurs. (The maximum slope gradient of the sill in the prototype is much smaller, $^1/_{15}$.) The roughness of the bottom is expressed by a roughness length according to Nikuradse of k_N=0.6 m, which corresponds approximately to small dunes of about 1.2 m height occurring at the bottom in the prototype.

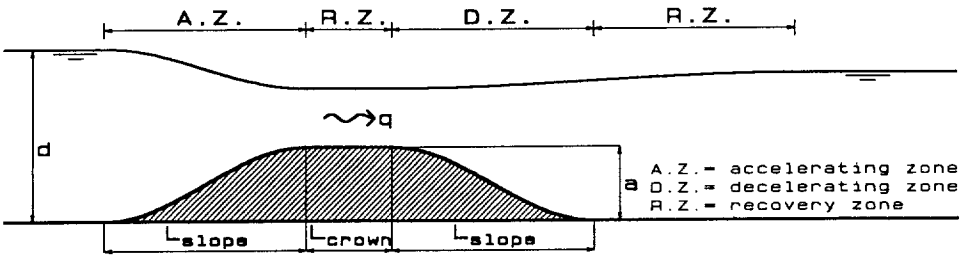

Figure 3.2.2 The basic sill.

Other flow situations were obtained by varying the length of the slope of the sill, the height of the sill, the length of the crown of the sill, the roughness of the sill and the average inflow velocity (Table 1). The purpose of these variations is to determine their influence on the flow and on appropriate modifications in the shallow-water equations. The latter are explained in section 3.3.

The different variations have in some cases been combined. Not all possible combinations were investigated. Unrealistic situations like a very smooth bottom of the sill, existing of sand with a small diameter, combined with a very steep slope of the sill were rejected. Combinations of a small roughness length and mild slopes were investigated.

The sill height corresponding to critical flow for the given inflow conditions is 13.6 m. The maximum height of the sill used in the computations is slightly lower (13.4 m), corresponding to a chosen slope length of 105 m and a maximum slope gradient of $^1/_5$ (Table 1).

For the situations described in Table 1, 2DV calculation of steady flow are made with the flow-simulation system PHOENICS. The results of these calculation are described in the next section. 1DH calculations are described in section 3.4.

run no.	Situation	slope length m	crown height m	maximum slope	crown length m	Froude number	roughness m
1	basic situation	75	9.6	$^1/_5$	50	0.046	0.60
2	mild slope	150	9.6	$^1/_{10}$	50	0.046	0.60
3	less roughness	150	9.6	$^1/_{10}$	50	0.046	0.10
4	milder slope	300	9.6	$^1/_{20}$	50	0.046	0.60
5	less rough. milder sl.	300	9.6	$^1/_{20}$	50	0.046	0.01
6	long crown	75	9.6	$^1/_5$	100	0.046	0.60
7	short crown	75	9.6	$^1/_5$	0	0.046	0.60
8	steep slope	50	9.6	$^3/_{10}$	50	0.046	0.60
9	higher Froude number	75	9.6	$^1/_5$	50	0.093	0.60
10	large roughness length	75	9.6	$^1/_5$	50	0.093	2.00
11	maximum sill height	105	13.4	$^1/_5$	50	0.093	0.60

Table 1 The calculated situations

3.3 The 2DV numerical model

3.3.1 The flow-simulation model PHOENICS

The 2DV numerical calculations are made with the PHOENICS flow-simulation system. Originally, PHOENICS is a 3D finite volume system. The domain is divided into computational cells. In the finite-volume system, differential equations are integrated over each computational cell. For this numerical integration, different approximation schemes can be used. PHOENICS uses the fully implicit upwind scheme. The result of these integrations for the transport equation of a variable is the dependency of a variable's value in a cell on the values of this variable in all neighbouring cells. If the cell is located at the boundary the

value in this cell is also dependent on the value at the boundary. The various equations of all the cells together form a set of equations. This set of equations can be solved because the unknown values of the field variables can be expressed in the known values at the boundaries. The equations and boundary values used are discussed in this section.

Field equations

It is possible to use PHOENICS for multi-phase flow conditions. The transport equations in PHOENICS have the form:

$$\frac{\partial}{\partial t}(r_i\ \rho_i\ \phi_i)\ +\ \nabla\cdot(r_i\ \rho_i\ \vec{v}_i\ \phi_i\ -\ r_i\ \Gamma_{\phi i}\ \nabla\phi_i)\ =\ r_i\ S_i \tag{3.3.1}$$

in which t is the time, r_i is the volume fraction of phase i, ρ_i is the density of phase i, ϕ_i is any conserved property of phase i, such as momentum per unit mass, mass fraction, turbulence energy, etc., $\vec{v}_i$ is the velocity vector of phase i, $\Gamma_{\phi i}$ is the exchange coefficient of the entity ϕ in phase i and S_i is a source rate of ϕ_i.

In this study only one-phase flow is considered and r is equal to 1, so the subscript i is dropped. The resulting differential equation stands for the Navier-Stokes equations, the continuity equation, the transport equation of the turbulence energy or the transport equation of the dissipation of the turbulence energy. For each element, this differential equation can be rewritten using the theorem of Gauss or the divergence theorem, which reads:

$$\int_V \nabla\cdot\vec{a}\,\mathrm{d}V\ =\ \oint_A \vec{a}\cdot\vec{n}\,\mathrm{d}A \tag{3.3.2}$$

in which V is the volume of the cell, A is the area of the surface bounding the cell, $\vec{a}$ is an arbitrary vector and $\vec{n}$ is the normal vector. The solution for $\vec{a}$ is fully determined by the values at the boundaries of that particular element. This couples the value of a variable ϕ in an element to the values of ϕ in surrounding elements. For the complete field the values of a variable ϕ are determined by the boundary values of the whole computational field, because the value of a variable ϕ in an element in the computational field is dependent on the value of that variable in the surrounding elements. Generally, eq. (3.3.1) can be written, for one-phase flow:

$$\nabla\cdot(\rho\vec{v}\,\phi\ -\ \Gamma_\phi\nabla\phi)\ =\ S_\phi\ -\ \frac{\partial}{\partial t}(\rho\,\phi)$$

or

$$\int_V \nabla\cdot(\rho\vec{v}\,\phi\ -\ \Gamma_\phi\nabla\phi)\mathrm{d}V\ =\ \int_V\left(S_\phi - \frac{\partial}{\partial t}(\rho\,\phi)\right)\mathrm{d}V$$

Using eq. (3.3.2) this equation can be written as:

$$\oint_A \left(\rho \vec{v}\phi - \Gamma_\phi \nabla\phi\right)\cdot\vec{n}\,dA = \int_V \left(S_\phi - \frac{\partial}{\partial t}(\rho\phi)\right)dV \qquad (3.3.3)$$

Simplifying the left-hand side of eq. (3.3.3) yields the relation between the value of a variable in a particular element and the values of variables in surrounding elements. This relation is expressed by coefficients. These coefficients are a measure for the interaction with the neighbouring elements and depend on the discretisation of the diffusive, convective and time-derivative terms. The result of the integrations can be written in an equation having the form (Rosten & Spalding, [1987]):

$$\phi_P = \frac{a_E\phi_E + a_W\phi_W + a_N\phi_N + a_S\phi_S + a_H\phi_H + a_L\phi_L + a_T\phi_T + S}{a_E + a_W + a_N + a_S + a_H + a_L + a_T + a_P} \qquad (3.3.4)$$

in which S is the volume-integrated source, ϕ is the dependent variable considered, a the coefficients expressing the interactions, and the subscripts E, W, N, S, H and L denote the locations of the neighbouring elements. These locations are called in the PHOENICS the East, West, North, South, High or Low side of element P. The subscript T denotes the value at the previous time step.

Boundary conditions

In PHOENICS all the boundary conditions are imposed by means of convective and diffusive transport terms. These are substituted into eq. (3.3.4) as a source term, which means that these convective and diffusive parts are derived from values of the variables in virtual elements located at the boundary just outside the computational grid. This source term by which the boundary condition is imposed reads:

$$\dot{m}\phi + c(\phi - \phi_P) = S_\phi \qquad (3.3.5)$$

in which c is the coefficient determining the relative importance of the diffusion part, $\dot{m}$ is the mass flux, ϕ_P is the actual value of the variable ϕ in that particular element and S_ϕ is the source term. A boundary condition in PHOENICS is set by specifying the value of the variable ϕ at that boundary and the coefficient c.

In the following, the boundary conditions used for steady 2DV flows in PHOENICS using a k-ϵ model are discussed. First the inflow conditions are discussed, then the outflow conditions, the bottom conditions and finally the water surface conditions.

The first boundary conditions discussed are the inflow conditions. The inflow velocity to be specified is the horizontal velocity. Due to the staggered grid the vertical velocity is

to be specified is the horizontal velocity. Due to the staggered grid the vertical velocity is not a velocity to be specified at the inflow boundary. The velocity profile used is an equilibrium profile for uniform flow over a flat bottom. This profile multiplied with the density is used as the inflow profile for the mass flux. The inflow profile for the turbulence energy and the dissipation of the turbulence energy are also equilibrium profiles for uniform flow over a flat bottom.

These equilibrium profiles were obtained by a PHOENICS computation of uniform flow over a horizontal bottom, using a logarithmic profile as the inflow condition. The inflow profiles for the turbulence energy and the dissipation of the turbulence energy were chosen in such a way that the eddy-viscosity had a parabola-shape. The equilibrium profiles were reached in the region where the shapes of the velocity, the turbulence energy and the dissipation of the turbulence energy profiles were uniform. Graphs of the equilibrium profiles are plotted in Fig. 3.3.1.

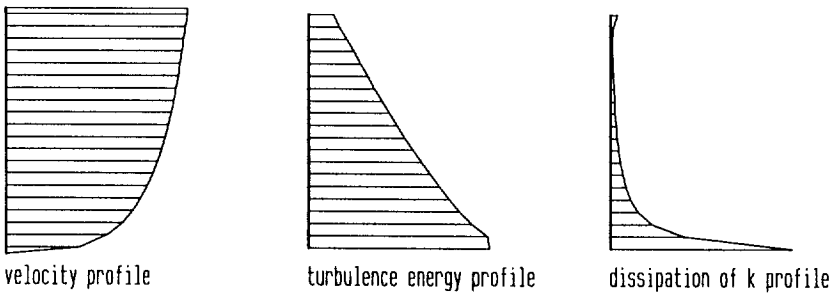

Figure 3.3.1 The equilibrium profiles

The outflow conditions are very simple. The outflow boundary has to be so far downstream from the place where the interesting flow phenomena occur that this boundary does not influence these phenomena. A convenient location for the outflow boundary is in the region where the flow is uniform again. In that region it is possible to choose the hydrostatic pressure distribution as the outflow condition. Prescribing a hydrostatic pressure at the outflow boundary corresponds to prescribing a Neumann boundary condition, $\partial u/\partial x=0$.

In PHOENICS it is convenient to work with the dynamic pressure, i.e. the pressure deviation from the hydrostatic pressure. The dynamic pressure at the outflow boundary has a constant value.

Four bottom boundary conditions have to be prescribed: two for the horizontal and the vertical velocities; and two for the variables in the k-ε model, the turbulence energy and

in flow direction in an element close to the bottom. In this case the transport equation must be integrated numerically through the viscous sublayer, which is undesirable, because the viscous sublayer is very thin so that many grid points have to be placed in this layer, and the computation becomes expensive. However, integrating through the sublayer is normally not necessary because empirical laws of sufficient generality are available that connect the bottom shear stress to the dependent variables just outside the viscous sublayer. Such an empirical law is the "law of the wall" (Rodi, [1980]). In this investigation this "law" is approximated by:

$$u_* = \frac{\underline{u}\kappa}{\ln(\Delta z/z_0) - 1} \tag{3.3.6}$$

in which u_* is the friction velocity, $\underline{u}$ is the velocity in the element closest to the bottom, Δz is the height of that element, z_0 is the roughness length (eq. (A.4.1)) and κ is the Von Kármán parameter. The friction velocity, u_*, is used to prescribe a source at the bottom in the momentum equation in flow direction, which is equal to the shear stress, τ_{bx}:

$$\tau_{bx} = -\rho u_*^2$$

The imposed vertical velocity is w=0 at the bottom.

The values for the boundary conditions of the turbulence energy and the dissipation of the turbulence energy also depend on the friction velocity, u_*. The one for the turbulence energy at the bottom reads (Rodi, [1980]):

$$k = \frac{u_*^2}{\sqrt{c_\mu}}$$

and the condition for the dissipation of the turbulence energy at the bottom is (Rodi, [1980]):

$$\epsilon = \frac{u_*^3}{\kappa(\Delta z/2)}$$

in which c_μ is a coefficient (c_μ = 0.09, Launder & Spalding [1972]) in the k-ϵ model.

At the water surface four boundary conditions have to be imposed: one for the horizontal velocity, one for the vertical velocity, one for the turbulence energy and one for the dissipation of the turbulence energy. The velocity in flow direction is parallel to the water surface and is not prescribed. Due to the staggered computational grid the vertical velocity is not a variable on the boundary. In the calculations the vertical velocity in the surface element is approximated by the vertical velocity in the element just below this element. Therefore the condition for the vertical velocity is approximated by $\partial w/\partial z$=0.

In the absence of wind-induced shear stresses a free surface can be considered to a

first approximation as a symmetry plane (Rodi, [1980]). This gives for the turbulence energy:

$$\frac{\partial k}{\partial z} = 0$$

The presence of a free surface reduces the length scale of the turbulence. A symmetry condition for the dissipation of turbulence energy, $\partial\epsilon/\partial z=0$, can cause large lengths scales. To counteract large length scales and to allow the same conditions to be used for a surface with and without wind-induced shear, Rodi [1980] proposes for the dissipation of the turbulence energy at the free surface:

$$\epsilon = \frac{\left(\sqrt{c_\mu}k\right)^{3/2}}{\kappa\left(\Delta z/2 + c_{BE}d\right)}$$

in which Δz is the height of the surface element, c_{BE} and c_μ are coefficients in the k-ϵ model (c_{BE} = 0.07, Hossain [1980]) and d is the water depth.

In PHOENICS it is only possible to calculate flows using a rigid water surface. This assumption is not important for free-surface flows with low Froude numbers. In such flows the level of the water surface does not vary considerably due to the small accelerations and decelerations generated by hydraulic structures, e.g. a sill, in the flow. In these cases, the velocity profiles calculated with a rigid, plane surface, do not deviate significantly from the velocity profiles calculated with a free surface. For flows with Froude numbers near 1, the critical flow condition, the influence of the flow on the position of the water surface is important. In such cases the differences between the velocities computed with a rigid, plane surface and a free surface can be considerable. It is possible to adapt iteratively the level of the rigid surface using the pressure at that surface, by an amount of:

$$\Delta d = \frac{\Delta p}{\rho g}$$

in which Δd is the rise of the water surface and Δp is the excess pressure with respect to the pressure in the inflow element at the rigid surface. Apart from the adaptation of the water surface another measure has to be taken to allow for the presence of the water surface. In the momentum equation a source term has to be introduced equivalent to the change of the hydrostatic water pressure due to the rise of the water. This source term, applied in all elements of a vertical, reads:

$$S = \rho g \Delta d$$

As mentioned before, a boundary condition in PHOENICS is set by specifying a value

of the variable at the boundary and a coefficient (eq. 3.3.5). The boundary values, sources and coefficients used are summarized in Table 2. (This Table is inserted especially for other PHOENICS users.) The values, sources and coefficients in Table 2 are specific for the treatment of the boundary conditions in PHOENICS.

Location	Variable	Value	c in eq. 3.3.5
Inflow boundary	u	coefficient from equilibrium profile u multiplied by q/d	0
	p	coefficient from equilibrium profile u multiplied by $\rho\, q/d$	10^{-10}
	k	coefficient from equilibrium profile multiplied by $u_*^2/\sqrt{c_\mu}$	0
	ϵ	coefficient from equilibrium profile multiplied by $u_*^3/(\kappa z)$	0
Outflow boundary	p	0	10^{10}
Bottom boundary	k	$k = u_*^2/\sqrt{c_\mu}$	10^{10}
	ϵ	$\epsilon = u_*^3/(\kappa z)$	10^{10}
Surface boundary	k	$\partial k/\partial z = 0$	10^{10}
	ϵ	$\epsilon = \left(\sqrt{c_\mu}k\right)^{3/2}/(\kappa(z + c_{BE}d))$	10^{10}
Source terms	u	Bottom boundary $\tau_{bx} = \rho u_* \lvert u_* \rvert$	10^{-10}
	u	Whole field $S = \rho g \Delta d$	10^{-10}

Table 2 Boundary conditions and sources used

Computational grid

The computational grid in the basic situation has the dimensions of a mesh of 20×2000 elements of about 1m×1m (Fig. 3.3.2), except for the elements on the sill whose heights are reduced. Studying the results of the computations of the basic situation, it was visible that the flow seems to be uniform again at a distance of approximately 60 water depths downstream from the sill. Therefore the computational domains in the other calculations were reduced, 20×1000 elements of about 1m×1m (Fig. 3.3.2), except for the calculation with the maximum sill height. In this situation the computational domain was 20×600 elements of about 1m×1.25m (Fig. 3.3.2). This calculation was made on a HP work station for which

the maximum number of elements in one direction was only 608. The other calculations were made on a CONVEX (near super computer), which had a larger memory.

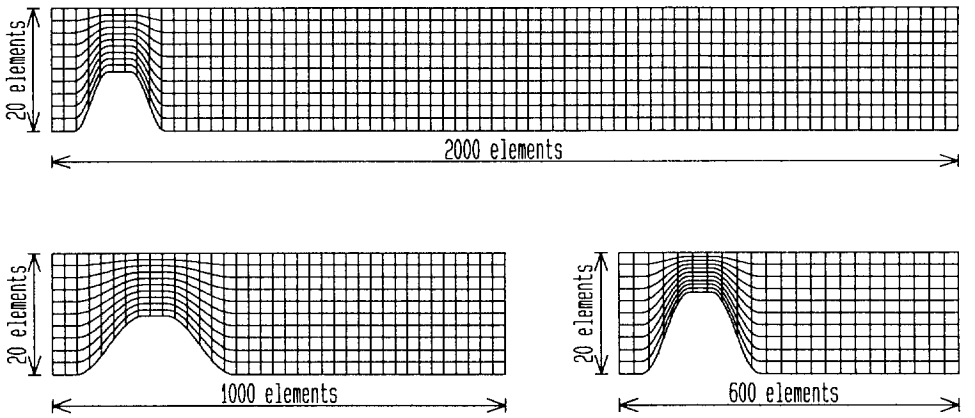

Figure 3.3.2 The computational grids of the basic situation and the other situations of table 2

The PHOENICS option of the body fitted coordinates is used. Using this option the equations have to be transformed into a contravariant coordinate system (Fig. 3.3.3), which means that the differentials transform like the normal vectors. Due to this transformation some inaccuracies appear in the calculated velocities, but these are less than those appearing in the other option, in which the sill is described by impermeable and partly permeable square elements. Due to the step-like shape of such a sill the accuracy of the velocities near the bottom is not very good.

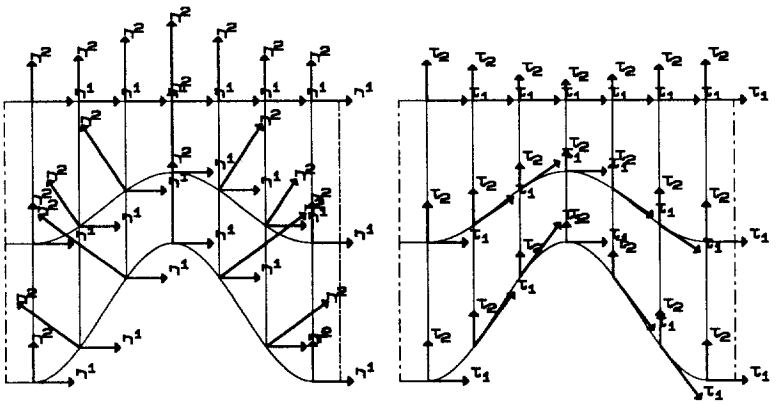

Figure 3.3.3 Contravariant (η^1,η^2) and covariant (τ_1,τ_2) base vectors in a grid on a sill.

With the computational grids and the boundary values described in this section, some calculations with PHOENICS were made for the situations of Table 1 described in the

previous section. The results of these computations are discussed in the next part of this section.

3.3.2 Results

The flows for the situations summarised in Table 1 are calculated with PHOENICS using the boundary conditions described in the previous part. The results are discussed in this section, in order of appearance in Table 1. The results are shown as drawings of the bottom profile with the calculated water level and vertical profiles of the horizontal velocity, the vertical velocity, the turbulence energy, the dissipation of the turbulence energy and the length scale of turbulence, L_m, defined by:

$$L_m = \frac{\left(\sqrt{c_\mu}\, k\right)^{3/2}}{\epsilon}$$

In all the drawings three scales are used. The first scale is the horizontal length scale. The second scale is the vertical length scale for the bottom profile. This scale is twice the horizontal length scale. The third scale used is different in all the drawings. The scales are defined in the figures. In the drawing of the calculated water level the third scale is the scale of the local water level with respect to the water level at the inflow boundary. This difference is plotted at a larger scale than the scale of the bottom profile. In the drawings of the profiles of velocities, turbulence energy, etc. the profiles are plotted every 25 m.

The results for the basic sill are shown in Fig. 3.3.4. This is a computation of the flow using a rigid, plane upper surface. The water level is calculated from the pressure against the rigid surface. The figure of the horizontal velocity profiles shows that these profiles become more uniform in the acceleration zone and less uniform in the deceleration zone. The vertical velocity is upward in the acceleration zone and downward in the deceleration zone. (The scale of the vertical velocities used is twice the scale of the horizontal velocities.) The profiles of the turbulence energy show that the production of the turbulence energy at the bottom is very large in the acceleration zone because of large velocity gradients there and consequently large values of the friction velocity, and that it is almost zero at the bottom in the deceleration zone. But, a large production of turbulence energy in the wake of the sill is obvious. Further downstream from the sill the production of the turbulence energy decreases and the turbulence energy profile becomes equal to the

profile upstream from the sill. In the recovery zone the turbulence energy in the bottom elements has almost the same value as in elements higher in the vertical, probably due to numerical inaccuracies in the computer code of PHOENICS. The dissipation at the bottom is very large in the acceleration zone and is almost zero in the deceleration zone. There is appreciable dissipation of turbulence energy in the wake of the sill. Large values occur in the water surface elements. This is caused by the boundary condition used, in which the turbulence energy to the power $^3/_2$ appears. The turbulence energy increases due to the dissipation of kinetic and potential energy in the recovery zone. The mixing lengths decrease in the acceleration zone. In the deceleration zone a new boundary layer appears. In the new boundary layer the mixing lengths are short. Where the new boundary layer has reached the water surface the mixing lengths increase. In the recovery zone the mixing lengths decrease until they have the same values as the ones upstream from the sill.

The next situation computed, Fig. 3.3.5, is a sill with the same height as in the basic situation but with **mild** slopes. The maximum gradient of the slope is $^1/_{10}$. The effect of this can be seen in the milder changes in the profiles of the horizontal velocity, vertical velocity, the turbulence energy, the dissipation of turbulence energy and the mixing length.

The influence of the reduction of the roughness length on the flow over a sill is shown in Fig. 3.3.6. Due to the smooth bottom of the sill and the smaller friction velocity, u_*, the water level on the sill is higher than in the previous situations. The influence on the shapes of the velocity profiles is small. The profiles are more uniform in the deceleration zone in comparison to the basic situation. The profiles of the turbulence energy, dissipation of turbulence energy and the mixing length are different from the previous profiles, the values of the quantities are smaller.

In Fig. 3.3.7 and Fig. 3.3.8 the results for even gentler slopes ($^1/_{20}$) are plotted. The changes in the velocity, turbulence energy, dissipation and mixing length profiles in comparison to the basic situation are less pronounced than in the situations discussed previously.

In the next two figures, Fig. 3.3.9 and Fig. 3.3.10, results are plotted for the basic situation except for the length of the crown. In Fig. 3.3.9 the length of the crown is twice the length of the crown in the basic situation and in Fig. 3.3.10 it is zero. Increasing the length of the crown has a very small influence on the flow field. On the top of the sill the adaptation length of the velocity profiles is very short and the changes in the velocity profiles

in the deceleration zone in comparison to the basic situation are very small. If the crown length is zero there are some changes in comparison to the basic situation. There is a large production of turbulence energy and dissipation near the bottom in the acceleration zone because of the large velocity gradient there and consequently large values of u_*. High-intensity turbulence flows into the deceleration zone, giving higher values of the turbulence energy in this zone. This effect is only noticeable just downstream from the crown.

The influence of a steeper slope ($^3/_{10}$) is shown in Fig. 3.3.11. The horizontal velocity profiles are much more uniform in the acceleration zone and less uniform in the deceleration zone. For this magnitude of the gradient of the slope separation occurs. The values of the turbulence energy, dissipation and mixing lengths are larger than in the basic situation due to the large friction velocity upstream from the crown and the separation downstream from the crown.

In Fig. 3.3.12 the influence of a higher Froude number is shown. The mean velocity and so the friction velocity are higher than in the basic situation, causing a larger fall of the water level and a higher production of the turbulence energy and dissipation.

For the higher-Froude number flow combined with increased roughness of the slope, Fig. 3.3.13, the fall of the water level increases. The influence of the larger roughness length can also be noticed in the velocity profiles at the deceleration zone. These profiles are less uniform in this situation in comparison to the ones in the situation discussed previously. Due to the larger friction and the larger friction velocity, the productions of turbulence energy and dissipation are larger too.

In Fig. 3.3.14 the influence of the height of the sill, close to the critical height, is shown. The maximum slope gradient of the sill has the same magnitude as in the basic situation. Nevertheless the flow separates. The whole amount of water has to flow through a narrow gap. This situation resembles almost a jet flowing into stagnant water. The turbulence energy and the dissipation of turbulence energy become very large in the acceleration zone, while the mixing length becomes very small in this zone. At the outflow boundary the equilibrium profiles are not yet reached, which means that the values near the outflow boundary can be influenced by this boundary.

In the next section results of 1DH computations of the flow situations of Table 1 are discussed. These results are obtained by solving two sets of shallow-water equations. One of these is the commonly used shallow-water equation derived for flat bottom situations. The

second is the set of modified shallow-water equations; in these equations terms of the commonly used shallow-water equation are multiplied by coefficients derived from the 2DV solutions shown in this section, obtained numerically.

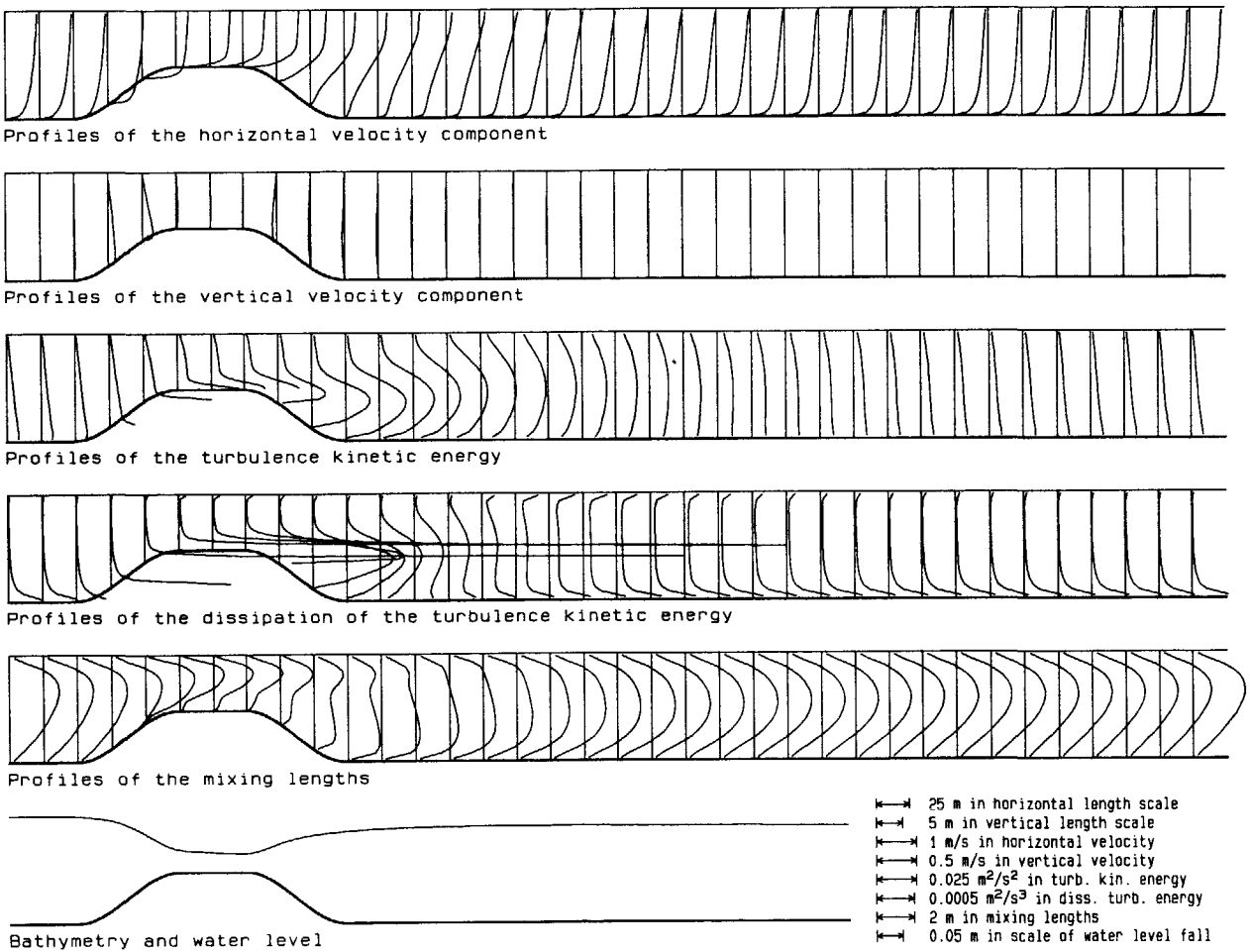

Figure 3.3.4 The basic situation (run 1)

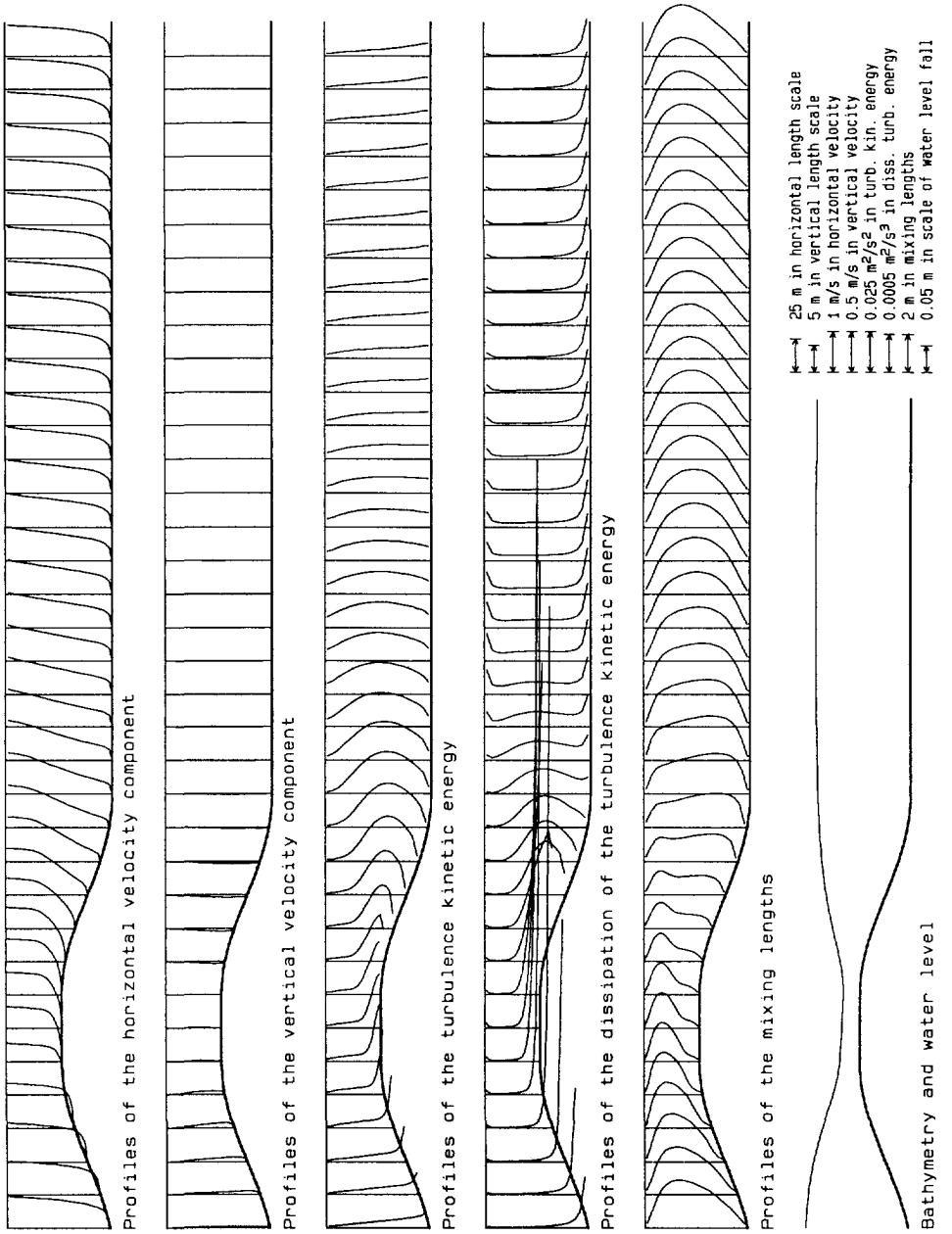

Figure 3.3.5 The situation with slopes $^{1}/_{10}$ (run 2)

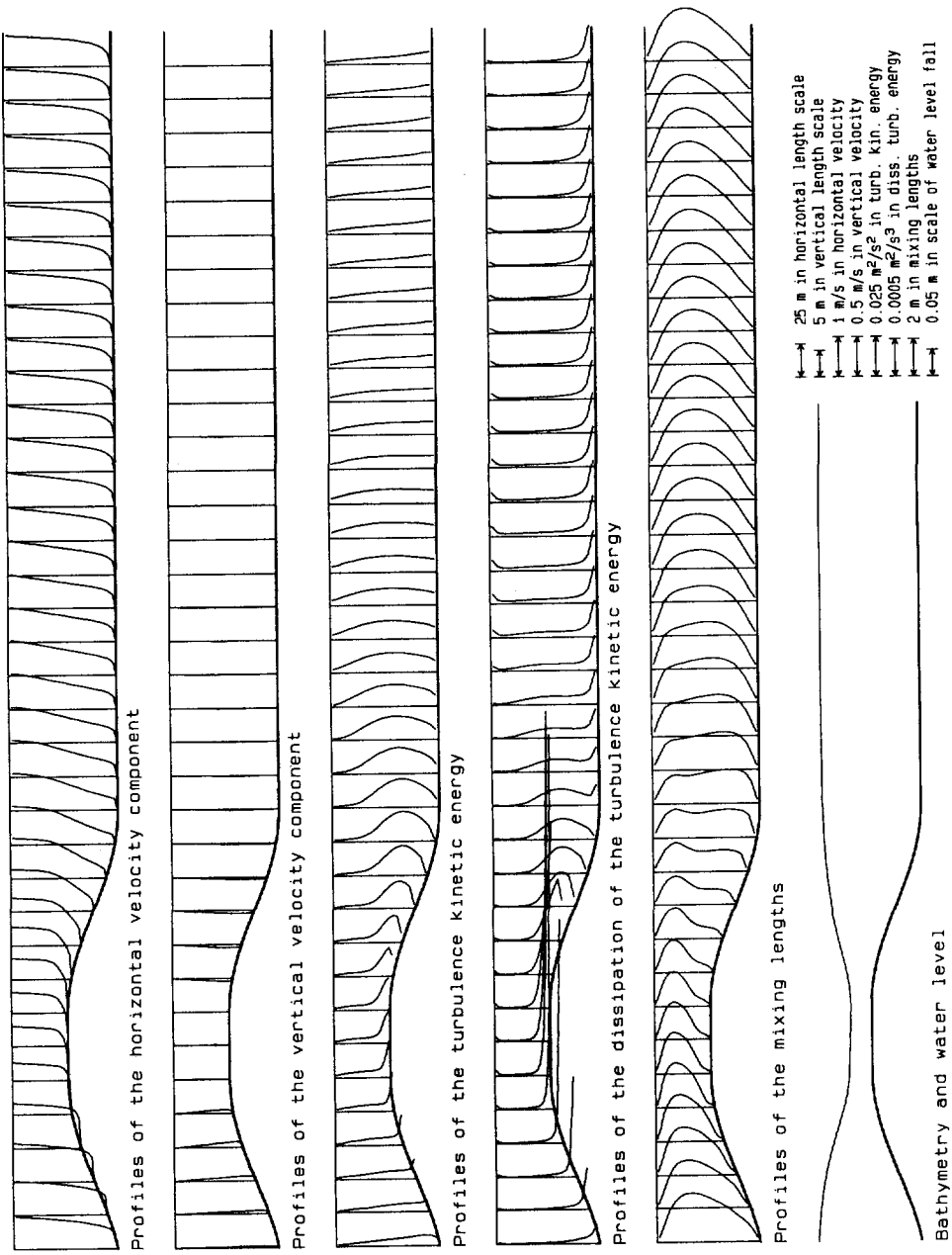

Figure 3.3.6 The situation with slopes $^{1}/_{10}$ and decreased roughness (run 3)

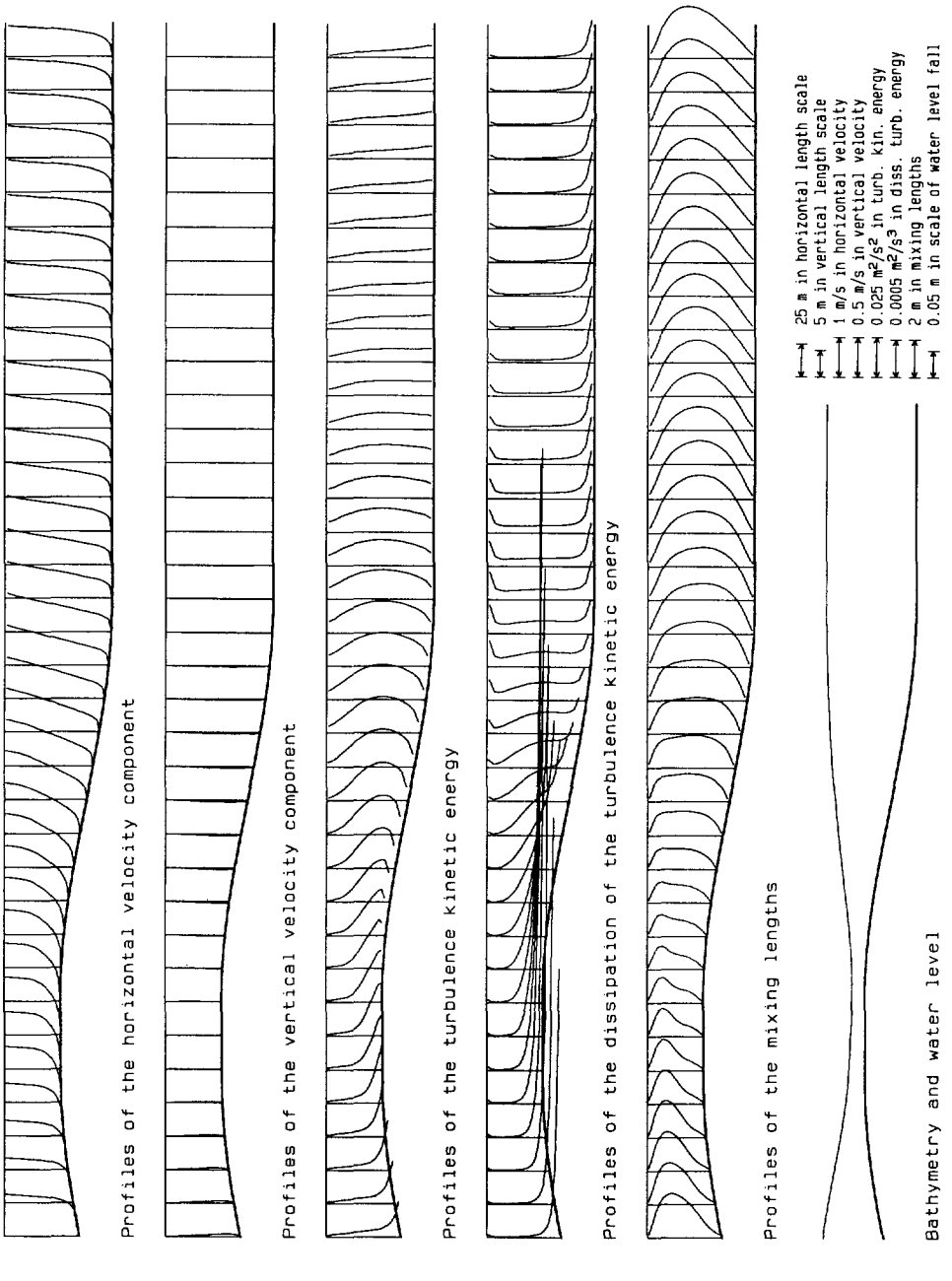

Figure 3.3.7 The situation with slopes $^{1}/_{20}$ (run 4)

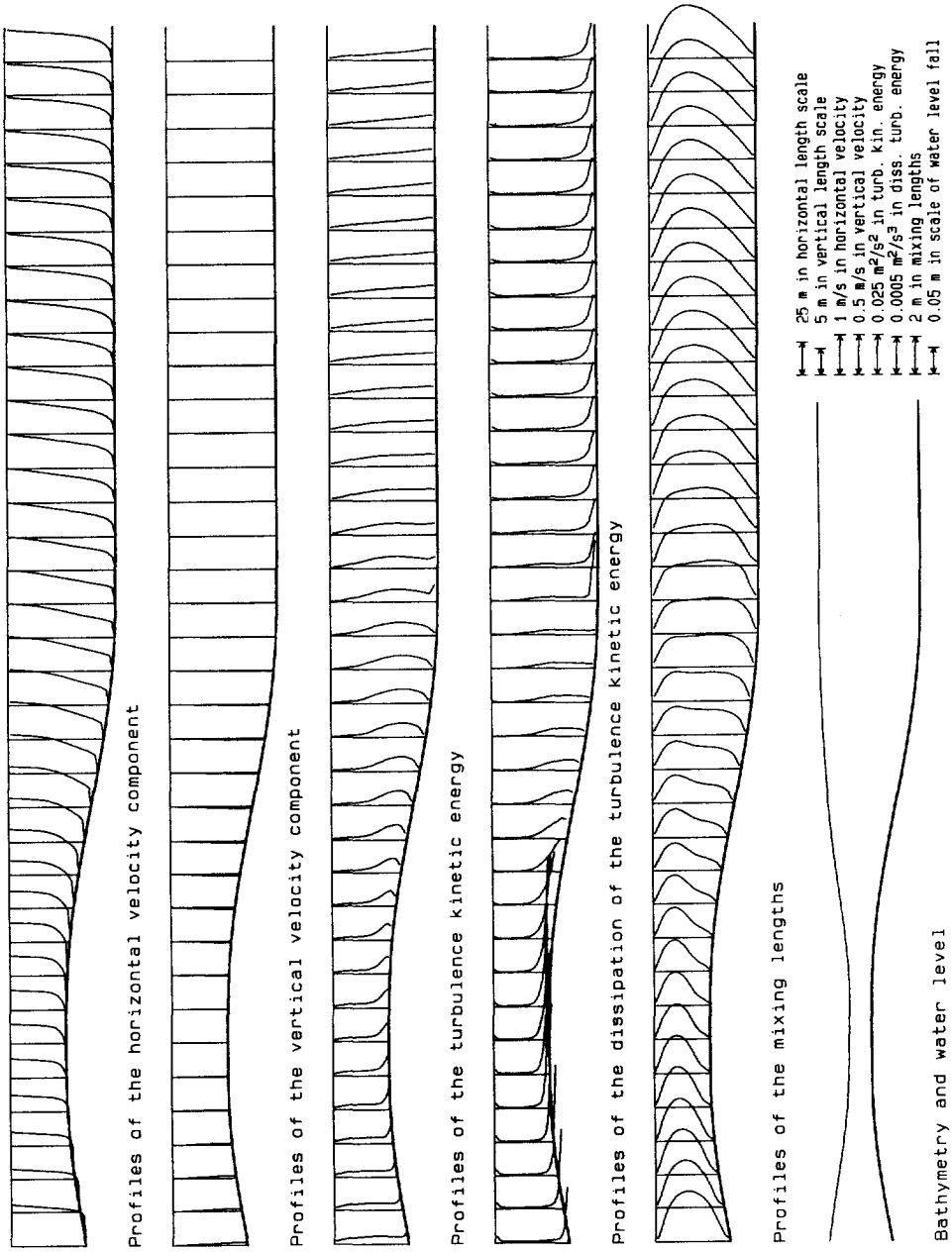

Figure 3.3.8 The situation with slopes $^1/_{20}$ and decreased roughness (run 5)

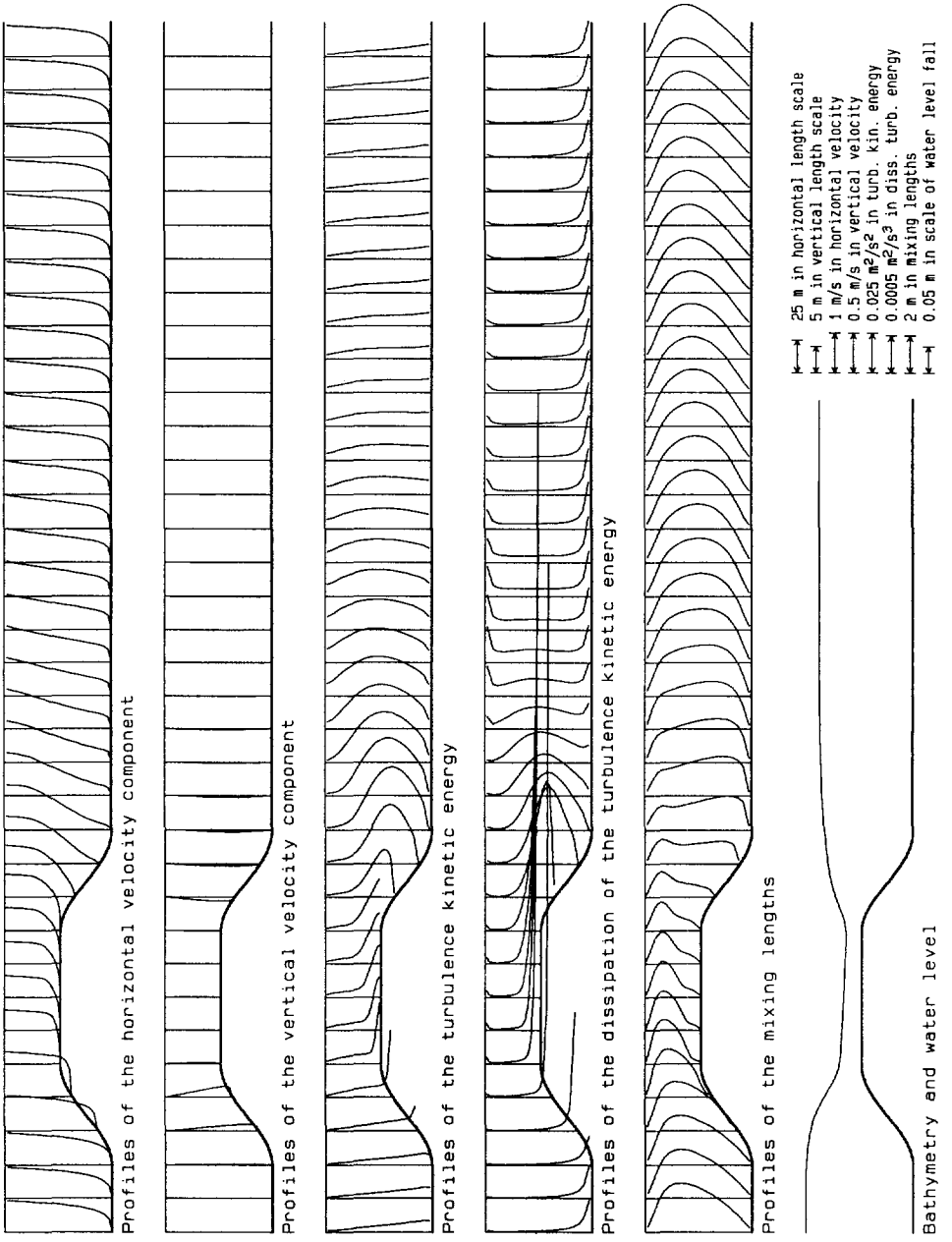

Figure 3.3.9 The situation with an increased crown length (run 6)

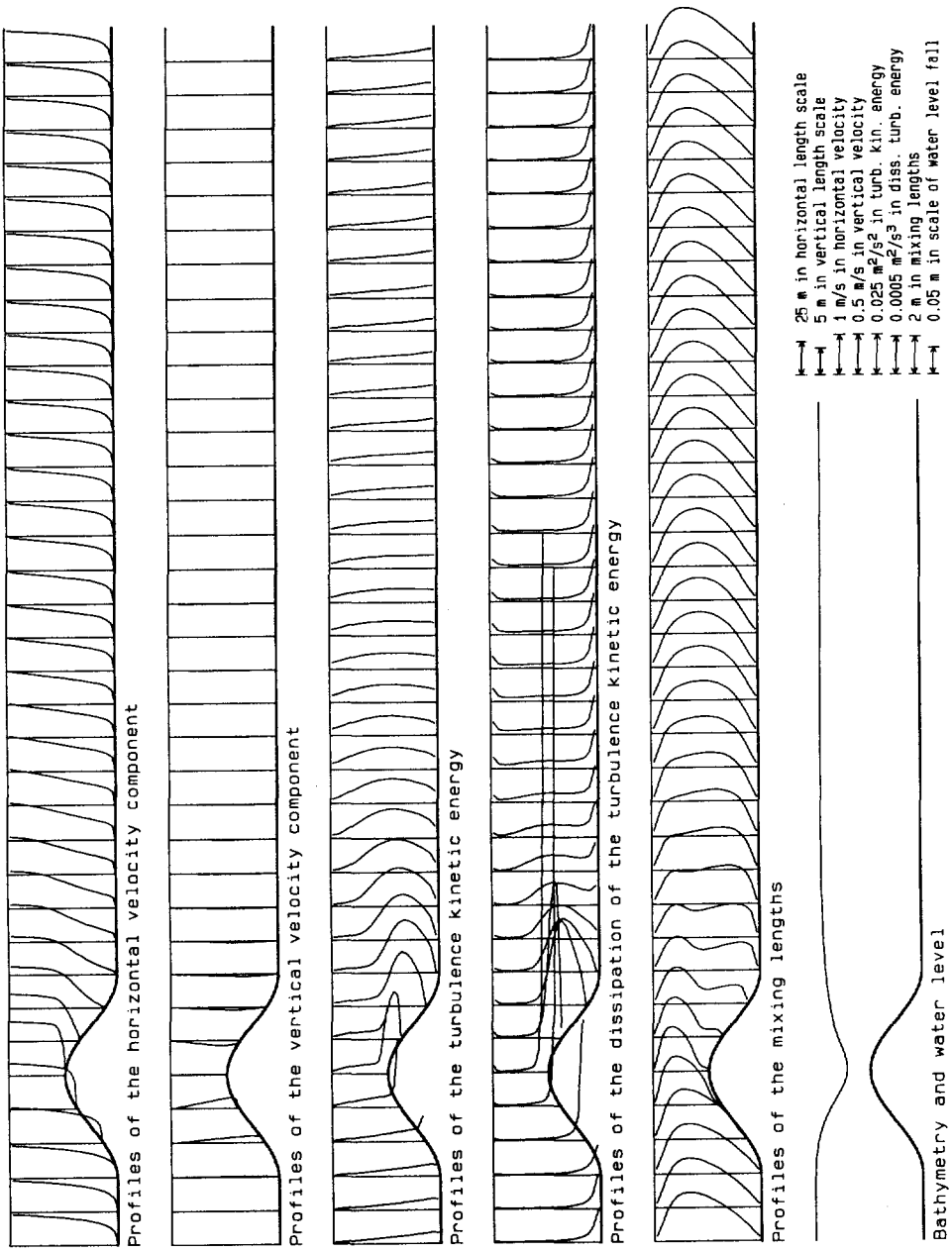

Figure 3.3.10 The situation with a decreased crown length (run 7)

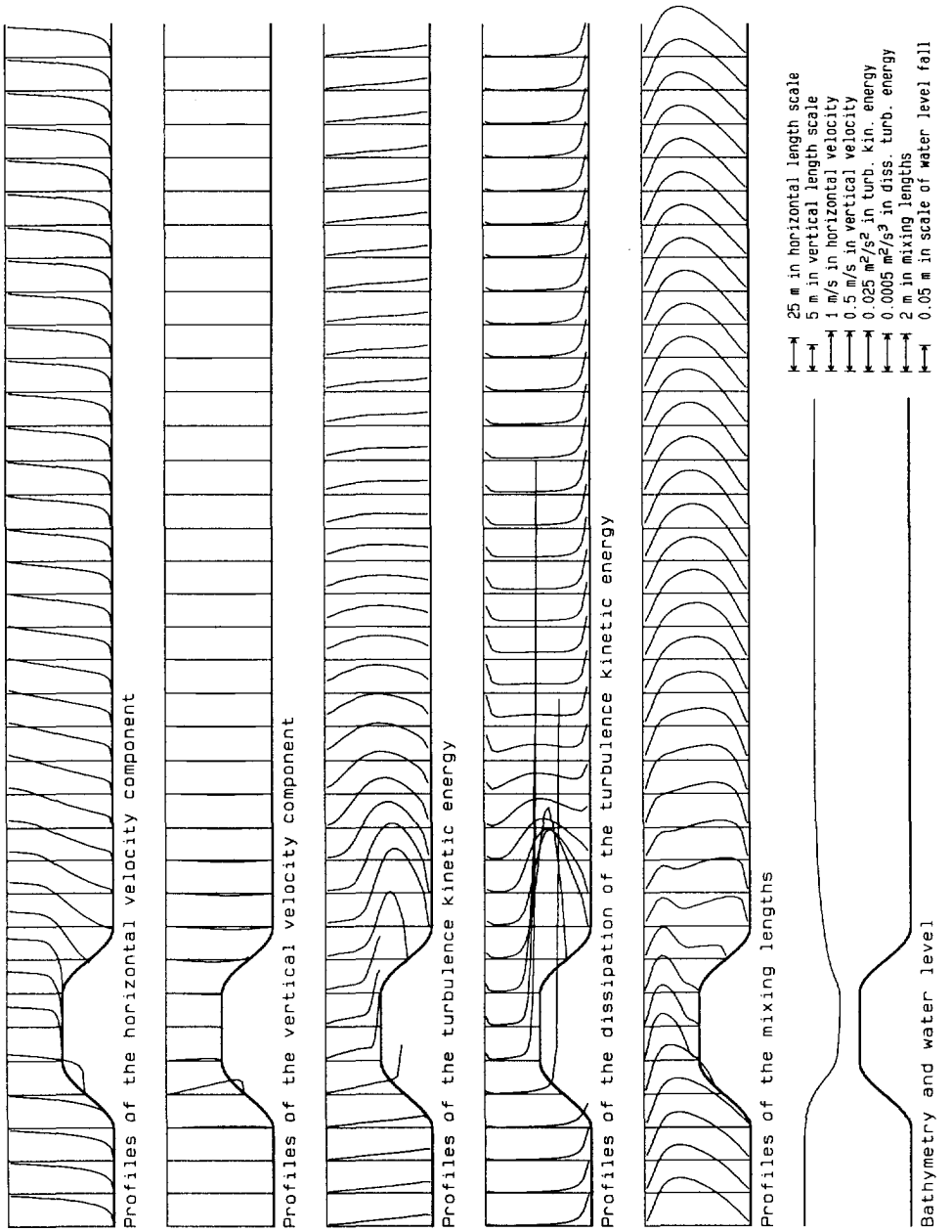

Figure 3.3.11 The situation with slopes $^{3}/_{10}$ (run 8)

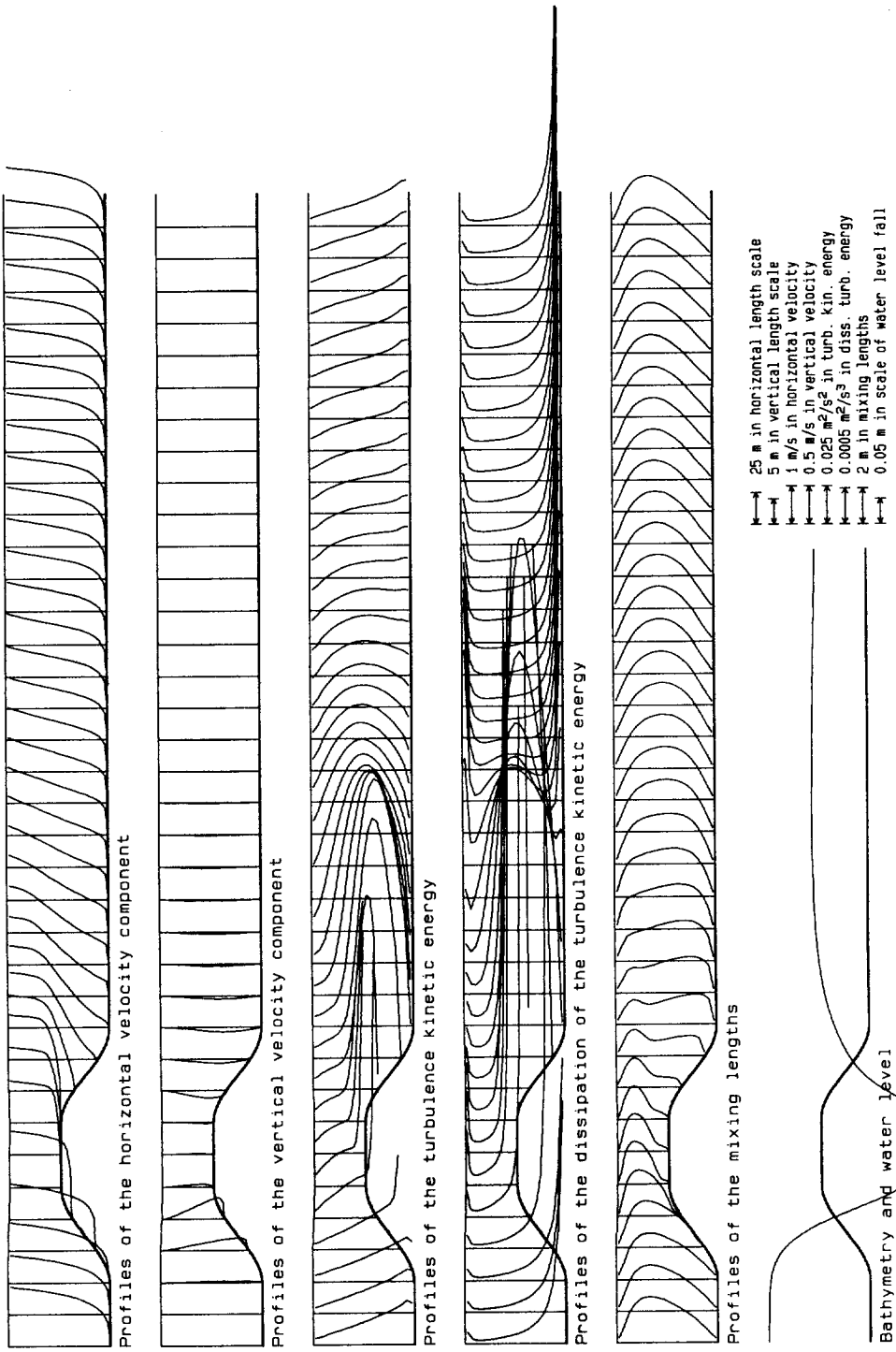

Figure 3.3.12 The basic situation with high Froude number (run 9)

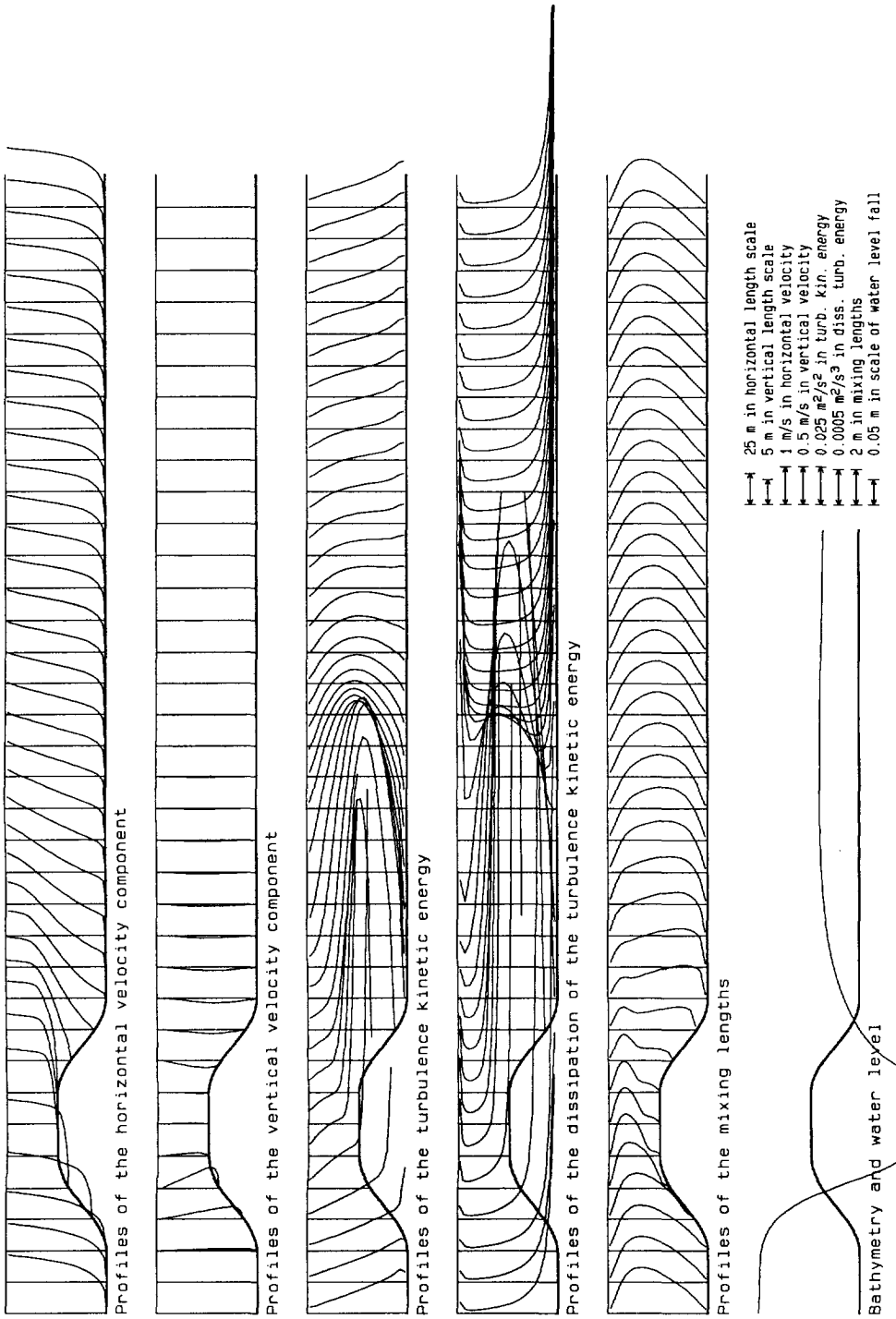

Figure 3.3.13 The situation with high Froude number and increased roughness (run 10)

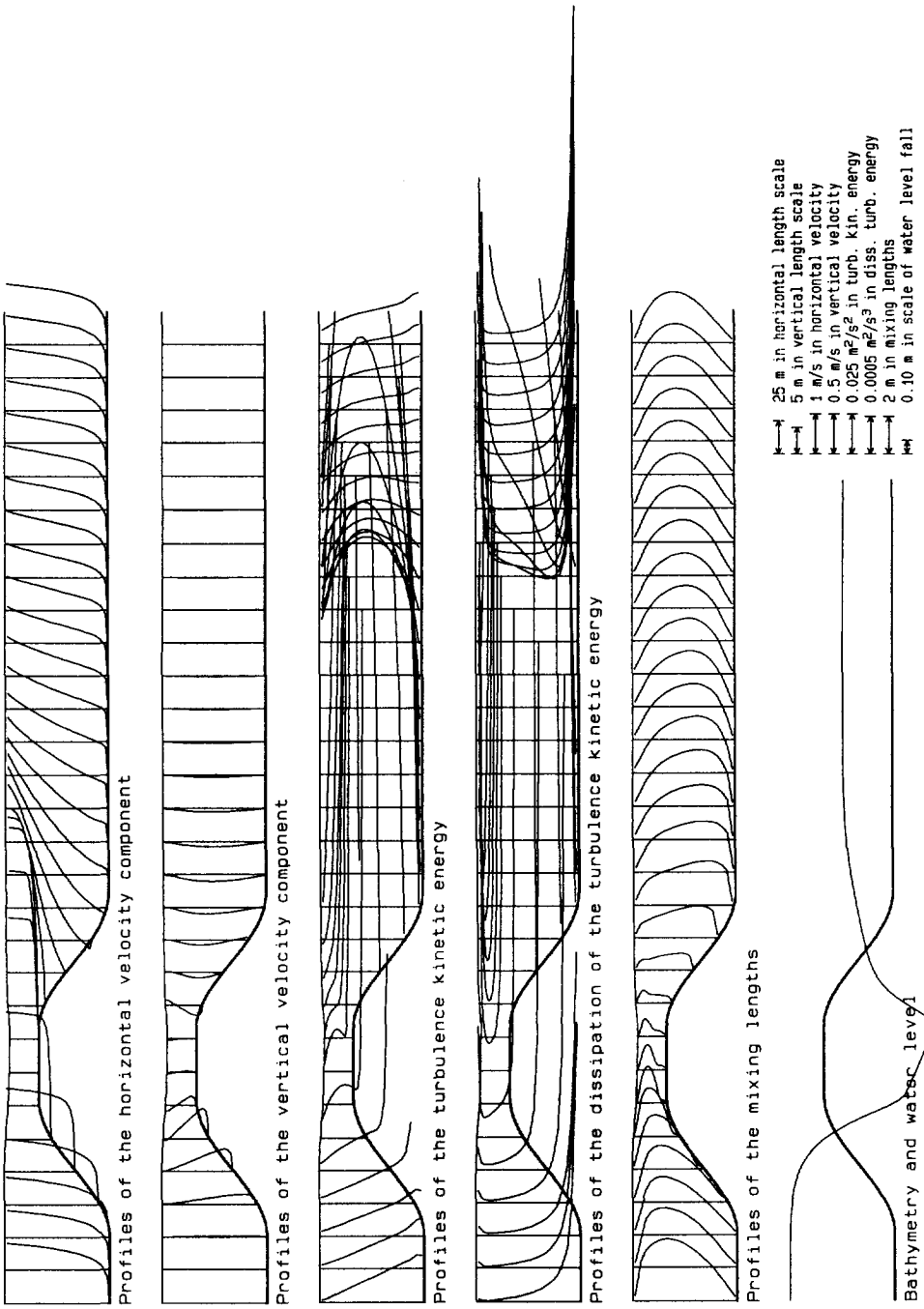

Figure 3.3.14 The situation with high Froude number and maximum height of the sill (run 11)

3.4 The 1DH numerical model

To calculate the water levels for flow over a sill in a 2DV plane, it is also possible to use 1DH numerical models. Such models are based on the shallow-water equations. The shallow-water equations are derived by integrating the continuity equation and the Navier-Stokes equation in flow direction with respect to the depth. These shallow-water equations were derived in chapter 2, eq. (2.3.7) and eq. (2.3.8), for a hydrostatic water pressure distribution. If the hydrostatic water pressure assumption is not made, the equation of motion, eq. (2.3.8), changes slightly. A coefficient in the pressure term can be introduced expressing the relation between the hydrostatic pressure and the actual pressure. This new shallow-water equation is derived in this section. The continuity equation, eq. (2.3.7), keeps the same form.

To derive the shallow-water equation of motion the Navier-Stokes equation in the flow direction has to be integrated over the depth. This yields:

$$\int_{z_b}^{z_b+d}\left(u\frac{\partial u}{\partial x}+w\frac{\partial u}{\partial z}+\frac{1}{\rho}\frac{\partial p}{\partial x}+\frac{1}{\rho}\frac{\partial \tau_{xz}}{\partial z}+\frac{1}{\rho}\frac{\partial \tau_{xx}}{\partial x}\right)dz = 0$$

or

$$\frac{d}{dx}\int_{z_b}^{z_b+d}u^2\,dz+\frac{1}{\rho}\frac{d}{dx}\int_{z_b}^{z_b+d}p\,dz+\frac{1}{\rho}\frac{dz_b}{dx}p\Big|_{z_b}-\frac{1}{\rho}\tau_{xz}\Big|_{z_b}+\frac{1}{\rho}\frac{d}{dx}\int_{z_b}^{z_b+d}\tau_{xx}dz = 0 \qquad (3.4.1)$$

The first and the fourth terms of eq. (3.4.1) already exist in eq. (2.3.8). The integral in the first term is again written as $\alpha q^2/d$. The fourth term is again written as the bottom shear stress, τ_{bx}, for uniform flat bottom flow situations (same q, d, λ, ρ) multiplied with a friction coefficient, γ, defined in expression (2.3.10c).

The second term of eq. (3.4.1) contains the unknown pressure distribution. The integration of the pressure with respect to the depth can be written as the hydrostatic pressure force multiplied with a coefficient, ζ;

$$\int_{z_b}^{z_b+d}p\,dz = \zeta\left(\tfrac{1}{2}\rho g d^2\right)$$

In the third term of eq. (3.4.1) the only unknown variable is the pressure at the bottom. This pressure is written as the hydrostatic pressure at the bottom multiplied with the coefficient ζ, although this is not completely correct. This assumption corresponds to the

coupling of the actual pressure with the hydrostatic pressure by the factor ζ in each point in the vertical. The actual water pressure is dependent on vertical accelerations, which are not distributed uniformly over the depth. However, the difference between the pressure at the bottom and the hydrostatic pressure at the bottom multiplied with the coefficient ζ is neglected. The last term, containing the Reynolds normal stress, is supposed to be very small and this term is neglected.

The shallow-water equations of motion now reads:

$$\frac{\mathrm{d}}{\mathrm{d}x}\left(\alpha \frac{q^2}{d}\right) + \zeta g d \frac{\mathrm{d}(z_b + d)}{\mathrm{d}x} + \tfrac{1}{2} g d^2 \frac{\mathrm{d}\zeta}{\mathrm{d}x} - \gamma \frac{1}{\rho} \tau_{bx} = 0 \tag{3.4.2a}$$

with $$\alpha = \frac{d}{q^2} \int_{z_b}^{z_b + d} u^2 \, \mathrm{d}z \tag{3.4.2b}$$

$$\zeta = \frac{\int_{z_b}^{z_b + d} p \, \mathrm{d}z}{\frac{1}{2} \rho g d^2} \tag{3.4.2c}$$

$$\gamma = \frac{\tau_{xz}(z_b)}{\tau_{bx}} = -\frac{\tau_{xz}(z_b)}{\lambda \rho (q/d)^2} \tag{3.4.2d}$$

and the continuity equation reads:

$$\frac{\mathrm{d}q}{\mathrm{d}x} = 0 \tag{3.4.3}$$

For flat bottom situations of flow in open channels the horizontal velocity and the pressure distribution can be approximated with a logarithmic velocity and a hydrostatic pressure distribution, respectively. Substituting these into the eq. (3.4.2b) until eq. (3.4.2d) yields the values $\zeta = 1$, $\gamma = 1$ and $\alpha \approx 1$. These values for the coefficients are frequently used in computer models solving the shallow-water equations. The set of equations with α, ζ and γ equal to 1 is called from now on the set of "common" shallow-water equations. The set of equations with these value of α, ζ and γ dependent on the flow conditions is called from now on the set of "modified" shallow-water equations.

Results

Values of the coefficients of α, ζ and γ were calculated according to eq. (3.4.2b) through eq. (3.4.2d) using results from the simulations with the 2DV PHOENICS computations. The situations are those described in Table 1. The results are plotted in Fig. 3.4.1 through Fig. 3.4.11. The coefficients obtained from PHOENICS were used to modify the common

shallow-water equations. With both sets of 1DH equations computations of flows over sills are made.

The same three scales as described in the previous section are used to plot the water levels. The water levels and three coefficients calculated are plotted in Fig. 3.4.1 for the basic situation. The differences between the water levels calculated with the modified 1DH model and the 2DV model PHOENICS are very small. These differences might be caused by the omission of the Reynolds normal stress term and by the approximation of the pressure at the bottom in eq. (3.4.2a). Below only the common and the modified 1DH shallow-water equations are compared (Fig. 3.4.2 through Fig. 3.4.11).

The differences between the water levels derived with the common and the modified models are remarkable. Especially in the deceleration zone and in the recovery zone significant differences exist. The main reason is the underestimation of the momentum flux in the common model in the deceleration region where α actually is considerably greater than 1. In the uniform flow region, only the bottom shear stress influences the water level. The water levels derived by the modified and the common model stay parallel in this region. (Fig. 3.4.1 through Fig. 3.4.11)

In the basic situation (Fig. 3.4.1), the coefficient in the convective term, α, approaches the value of $\alpha = 1$, which applies for a uniform velocity profile, in the acceleration zone; in the deceleration zone it approaches the value $\alpha = {}^4/_3$, which applies for a triangular velocity profile. In the recovery zone the value of α asymptotically approaches the inflow value of α.

Changes in the coefficient of the pressure term, ζ, are very small. The increase at the toe of the sill can be explained from the pressure gradient needed to accelerate the water in upward direction. At the bottom the pressure has to be higher than the hydrostatic pressure value, causing $\zeta > 1$. Near the top of the sill the opposite effect takes place. At the water surface a higher pressure than the hydrostatic pressure is necessary to accelerate the water in horizontal direction. This causes $\zeta < 1$.

Although it was expected that the deviations from the equilibrium value, $\zeta = 1$, are important (chapter 1), these deviations appear to be remarkably small. The use of this coefficient seems to be not necessary. The assumption of a hydrostatic pressure distribution made in section 2.3 appears to be a reasonable one.

The coefficient in the friction term, γ, increases in the acceleration zone, due to the

more nearly uniform profile of the horizontal velocity and, therefore, larger velocity gradients near the bottom. In the deceleration zone, the value decreases and it approaches the value $\gamma=0$. The flow at this point nearly separates. For the steep slope ($^3/_{10}$) situation the friction coefficient γ even becomes negative in the back-flow region, downstream from the point of separation (Fig. 3.4.8).

Fig. 3.4.2 shows results for flow over a sill with a gentler slope. Similar differences are observed as in the previous situation, although they are less pronounced. The variations in the coefficients α, ζ and γ are less due to the gentler slopes. As a consequence, smaller changes in the horizontal velocity profiles occur. The value of the pressure coefficient, ζ, in point $x=0$ is $\zeta > 1$ due to the short inflow length in this computation. The pressure deviates from the hydrostatic pressure to accelerate the flow in upward direction.

The influence of the reduction of the roughness length on the sill is shown in Fig. 3.4.3. Due to this smaller roughness the water level fall is less than in the previous situation for both models because the equilibrium horizontal velocity profile has a more uniform shape for a smaller roughness. In the acceleration zone the value of the coefficient α approaches the value $\alpha=1$ more closely than in the previous situation, due to the smaller roughness. The value of the pressure coefficient, ζ, is not very different in comparison to the pressure coefficient in the previous situations. This contrasts with the friction coefficient γ. The small jumps in Fig. 3.4.3 are caused by discontinuous changes in the roughness at the transition between the sill and the horizontal bottom. Where the roughness changes abruptly from rough to smooth, the horizontal velocity upstream from the change in roughness has an equilibrium profile corresponding to the large roughness length. If the roughness suddenly becomes less, the value of the horizontal velocity near the bottom is less than the equilibrium value for this shorter roughness length. This causes a smaller friction coefficient than just before the change in roughness. The opposite effect happens downstream from the sill where the roughness increases. These are very local effects which hardly influence the water levels.

In the next two figures, Fig. 3.4.4 and Fig. 3.4.5, the results calculated for gentler slopes are shown. The changes in the water levels are less pronounced in comparison to the previous situations. The differences between the water levels of both models are smaller than in the basic situation. The behaviour of the coefficients α, ζ and γ is not much different from that in the previous two situations.

The influence of the length of the crown is shown in Fig. 3.4.6 and Fig. 3.4.7. The

fall of the water levels is almost as large as in the basic situation, although the differences between the water levels of the two models are larger for the longer crown than for the shorter crown. The reason is the extra resistance to the flow over a longer crown with a higher friction due to the higher average velocity. The maximum and the minimum values of the friction coefficient γ are not different from those in the basic situation, just like the minimum value of the convection coefficient, α. The maximum value of α is lower for the shorter crown. The bottom friction velocity at the top of the sill, just before the downward slope, is higher in the case of the short crown than in the case of the longer crown. This causes a larger eddy-viscosity at the crown and downstream from the crown in the case of the short crown. The eddy-viscosity smoothes the velocity profiles. So, the velocity profiles are more uniform in the case of the short crown than in the case of a long crown.

Fig. 3.4.8 shows the influence of a steep slope. Differences between the two water levels for the two models are much greater in comparison to the differences between the two water levels in the basic situation. The minimum value of the convection coefficient, α, is a little closer to unity than in the basic situation, due to the larger accelerations. The maximum value for α is larger, even larger than $\alpha = {}^4/_3$ the value for a triangular velocity profile, due to separation of the flow. Separation of the flow is also recognizable in the graph of the friction coefficient γ. This coefficient even becomes negative due to the separation and back flow. Due to the large acceleration in the acceleration zone, the maximum value of γ in this situation is much larger than the maximum value in the basic situation.

The effects of higher Froude numbers, in comparison to the basic situation with a low Froude number, are noticeable in the water levels (Fig. 3.4.9). The modifications result in considerably lower water levels downstream. In this figure, the minimum value of the convection coefficient, α, has almost the same value as in the basic situation, but the maximum value of α is a little higher in comparison to the basic situation. The friction coefficient γ has the same differences in comparison to the basic situation as the convection coefficient α. The minimum values are equal and the maximum value has almost the same value as the maximum value in the basic situation.

The influence of increased roughness on the sill is shown in Fig. 3.4.10. Noticeable differences between both water levels appear on the crown of the sill. The fall of the water level is larger in the modified model than in the previous situation because the increase in friction due to a larger roughness length is larger for the modified equation, with stronger

near-bottom velocity gradients, than it is for the common equations, as discussed above. This effect is visible in the graph of the coefficient γ. The jumps appear due to the changes in roughness length. The convection coefficient α is smaller in the acceleration zone and larger in the deceleration zone in comparison to the basic situation. There is a small difference between the water levels derived by the modified model and PHOENICS.

In Fig. 3.4.11 the effects of the critical sill height are shown. The differences between the convection and the friction coefficients of this situation and the situation with the higher Froude number, Fig. 3.4.9, are not very large, although the extreme values are more pronounced. In the pressure coefficient some instabilities are recognizable, caused by the numerical inaccuracies at the transition between the horizontal crown and the curves slope. These instabilities hardly influence the modified water level, because the deviations from the hydrostatic value ($\zeta=1$) remain small. But there is a difference between the water levels derived by the modified model and those derived by PHOENICS. This may be due to the neglect of the Reynolds normal stresses in the modified shallow-water equations (the last term of eq. (3.4.1)). This can also cause the small difference between the water levels obtained by the modified model and those obtained by PHOENICS in Fig. 3.4.10. Another cause for the differences between these water levels can be the incorrect description of the pressure at the bottom, although the pressure coefficient hardly deviates from the hydrostatic value.

Discussion

In this section 1DH modified shallow-water equations were used to calculate flows over sills. The modifications appear in the equation of motion as convection, pressure and friction coefficients. These coefficients, α ζ and γ respectively, are obtained from 2DV calculations with the flow-simulation system PHOENICS.

The water levels derived with the modified shallow-water equations and 2DV model show a great similarity, even for steep slopes. Remarkable is the unimportance of the pressure coefficient. Even for steep slopes ($^3/_{10}$) this coefficient hardly deviates from $\zeta=1$, the value for the hydrostatic pressure distribution. For high Froude numbers the neglect of the Reynolds normal stress term may not be allowed.

Unfortunately, the method used here for purpose of investigation (calculation of 1DH coefficients from 2DV results) is not practicable for routine applications (it is easier to make

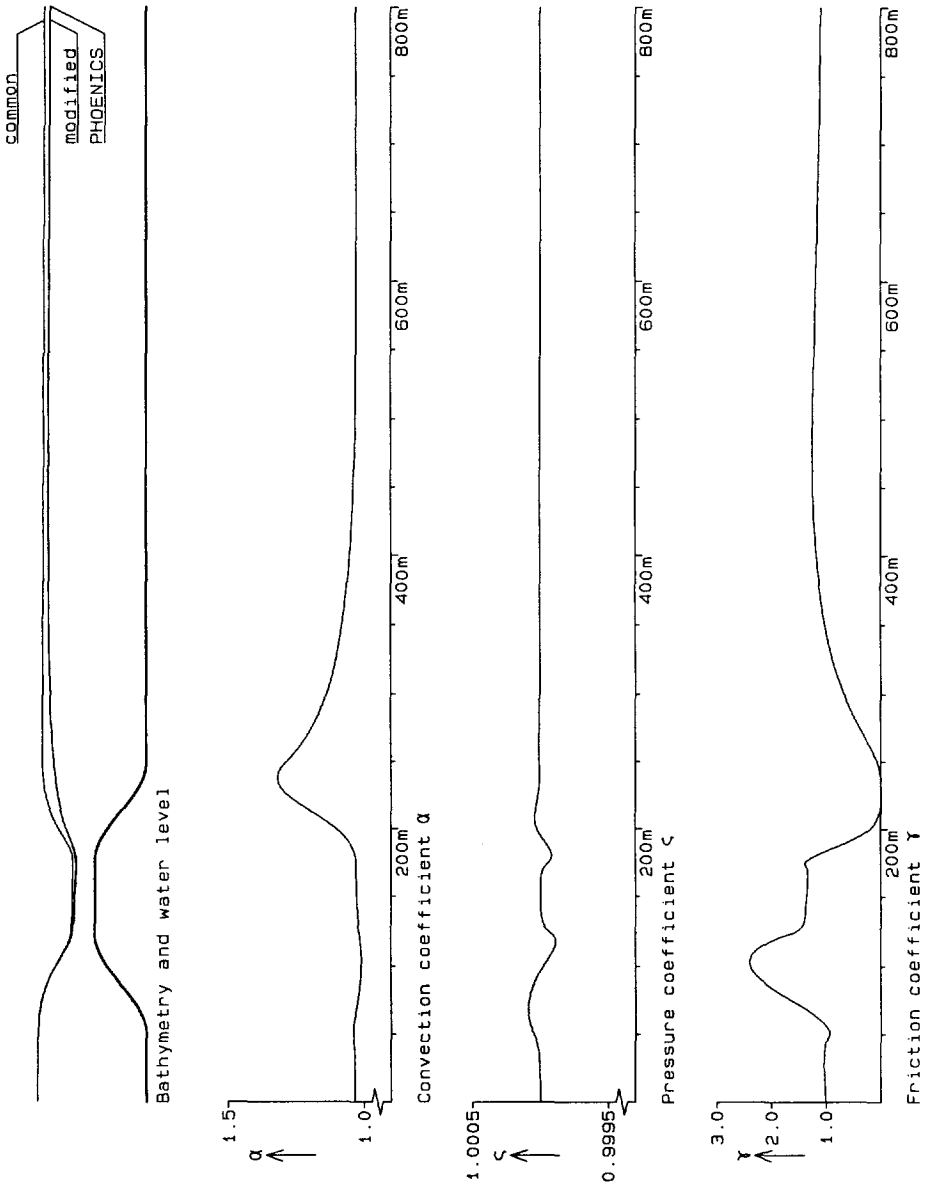

Figure 3.4.1 The basic situation (run 1)

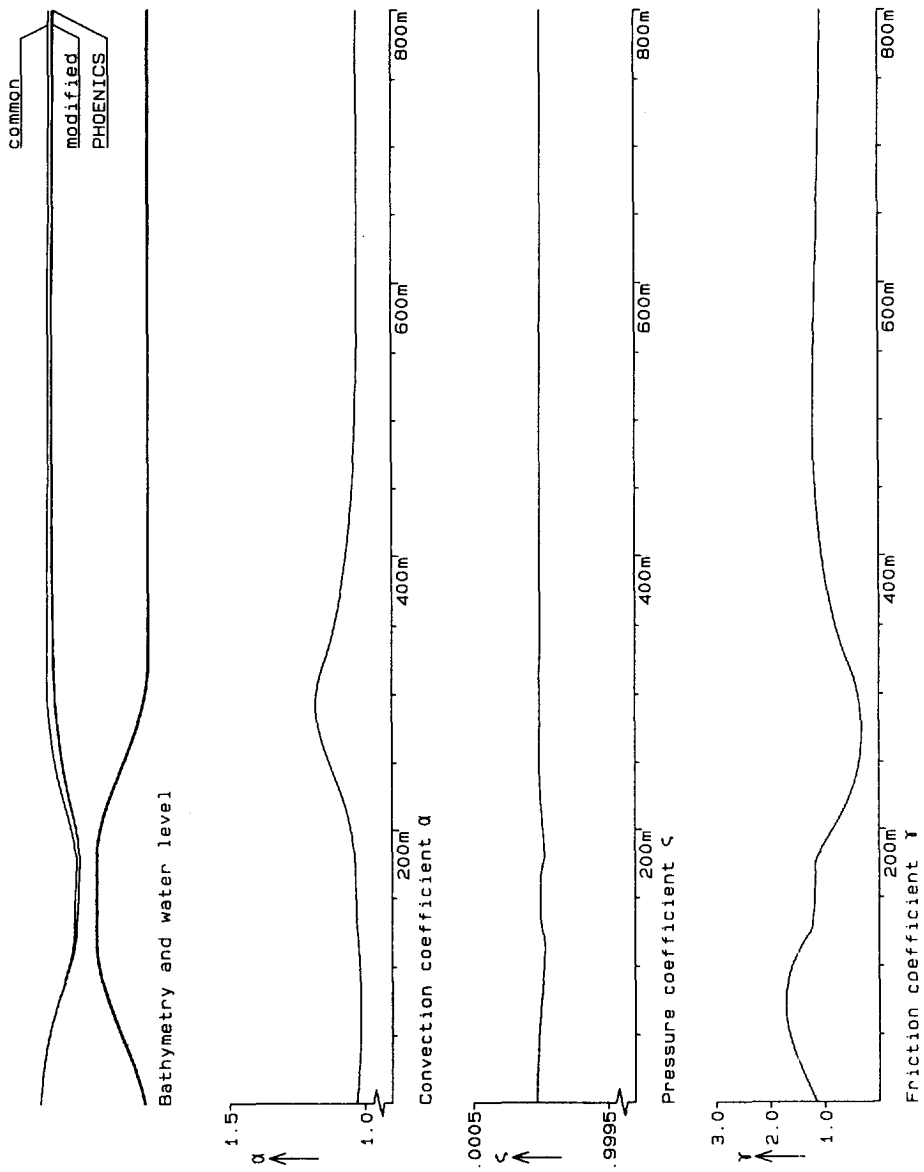

Figure 3.4.2 The situation with slopes $^1/_{10}$ (run 2)

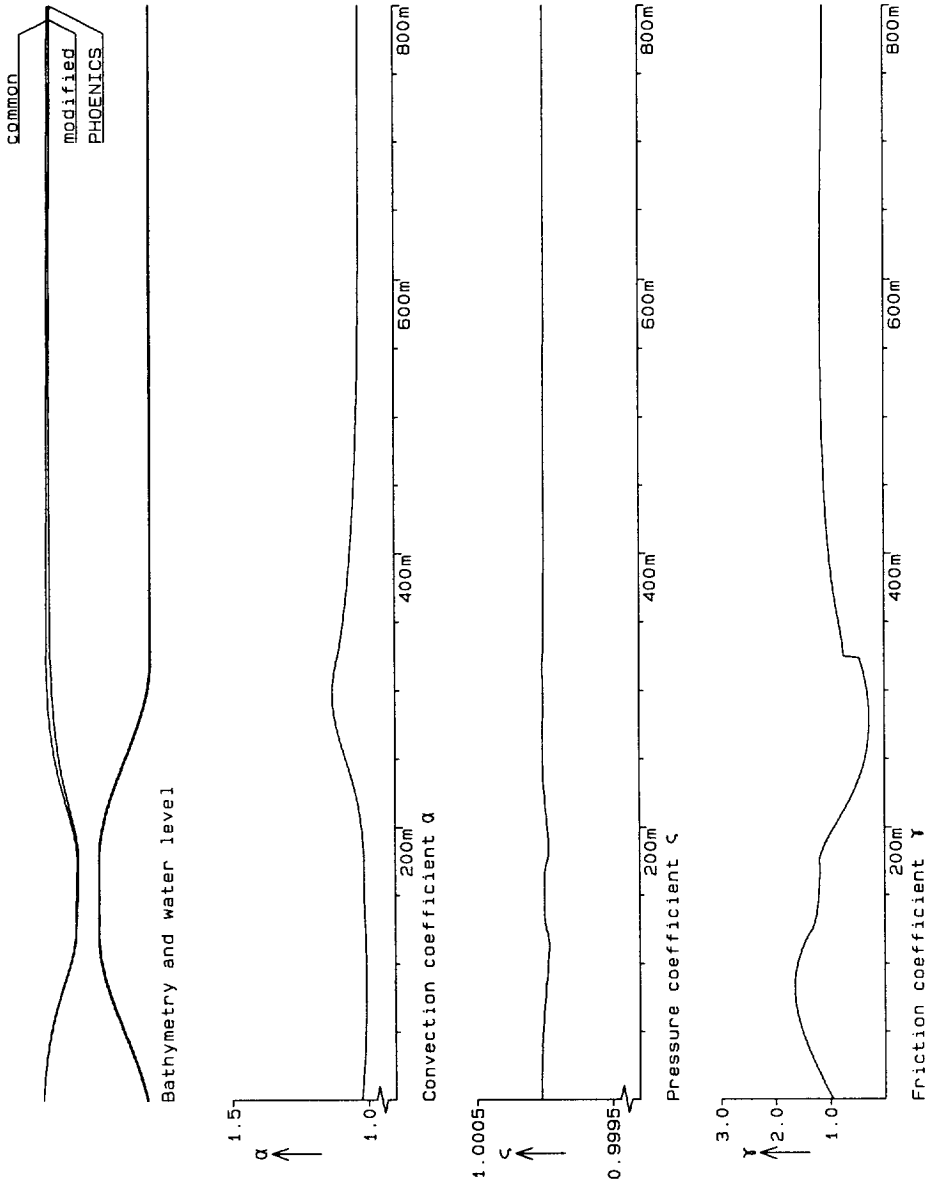

Figure 3.4.3 The situation with slopes $^1/_{10}$ and decreased roughness (run 3)

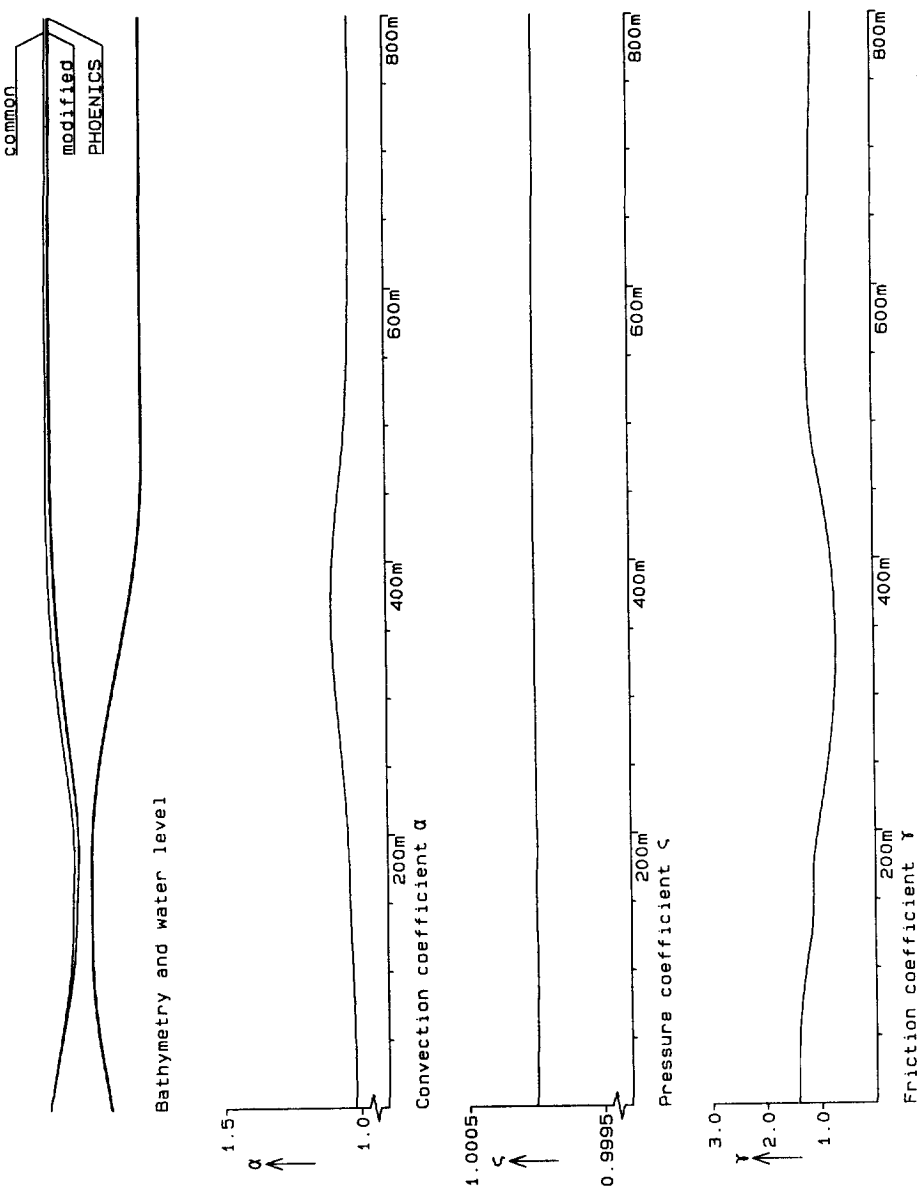

Figure 3.4.4 The situation with slopes $^1/_{20}$ (run 4)

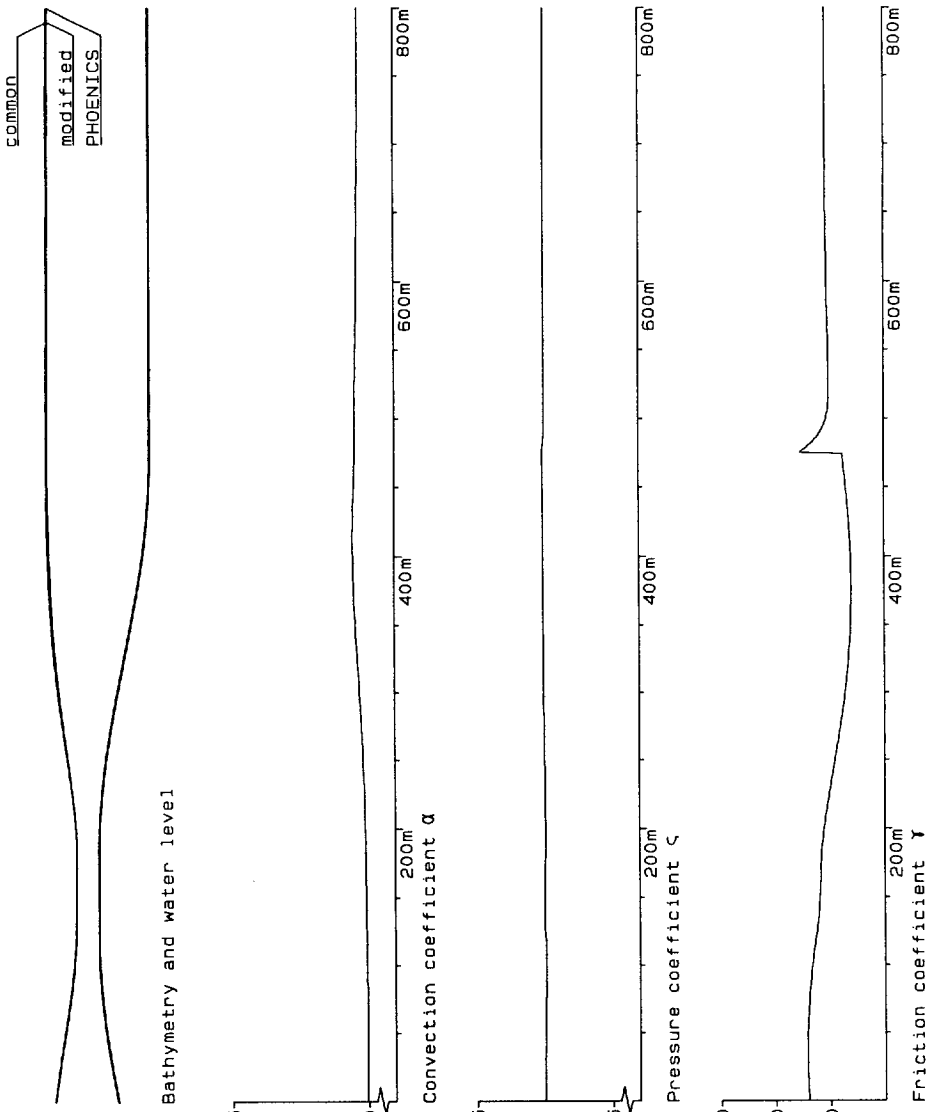

Figure 3.4.5 The situation with slopes $^1/_{20}$ and decreased roughness (run 5)

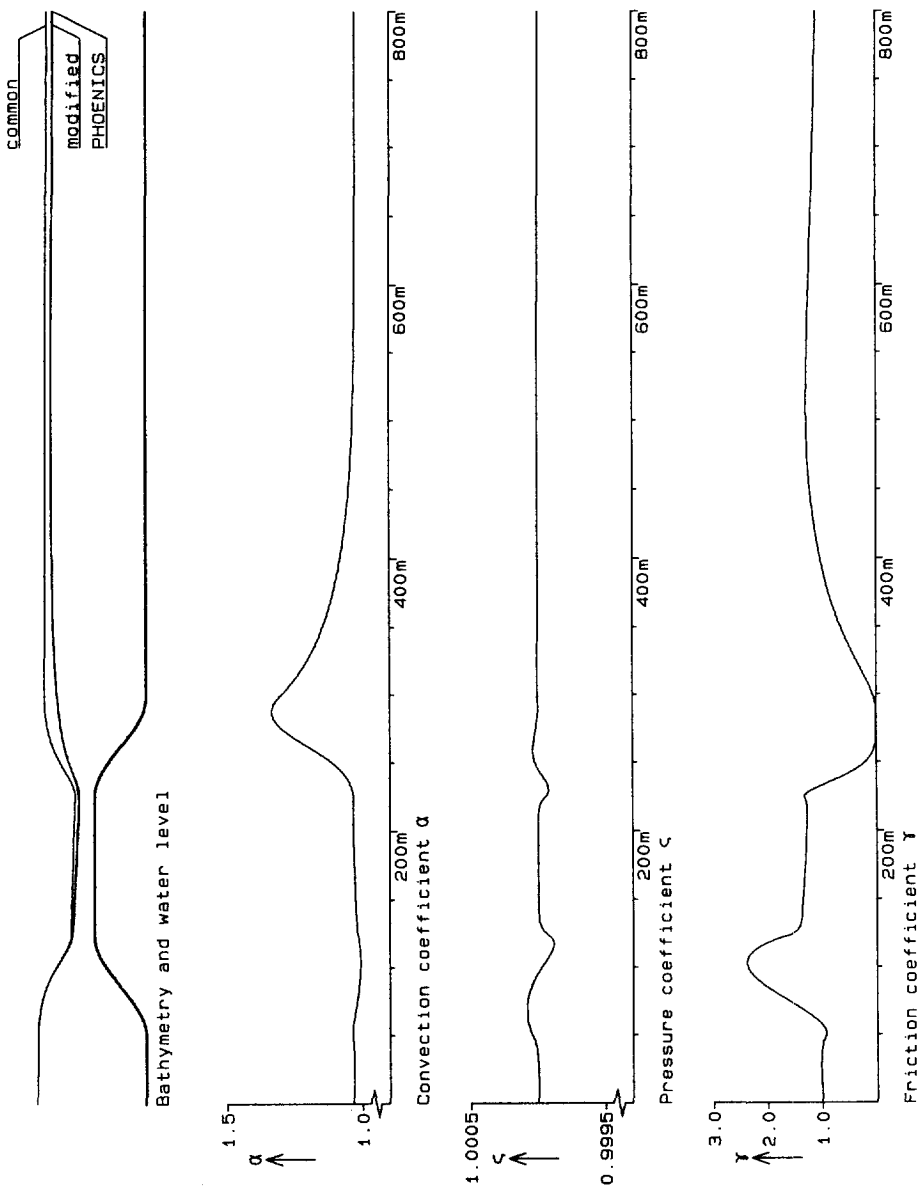

Figure 3.4.6 The situation with an increased crown length (run 6)

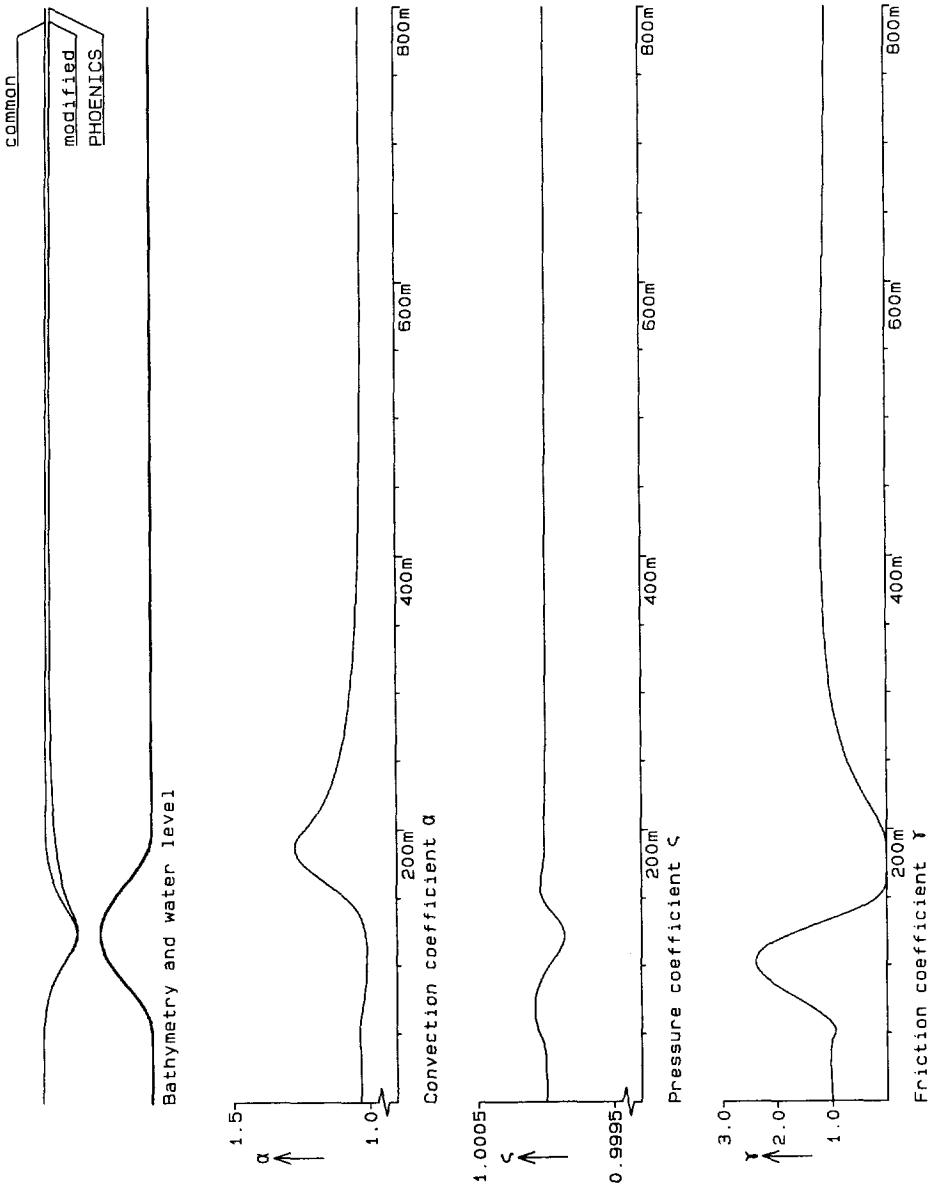

Figure 3.4.7 The situation with a decreased crown length (run 7)

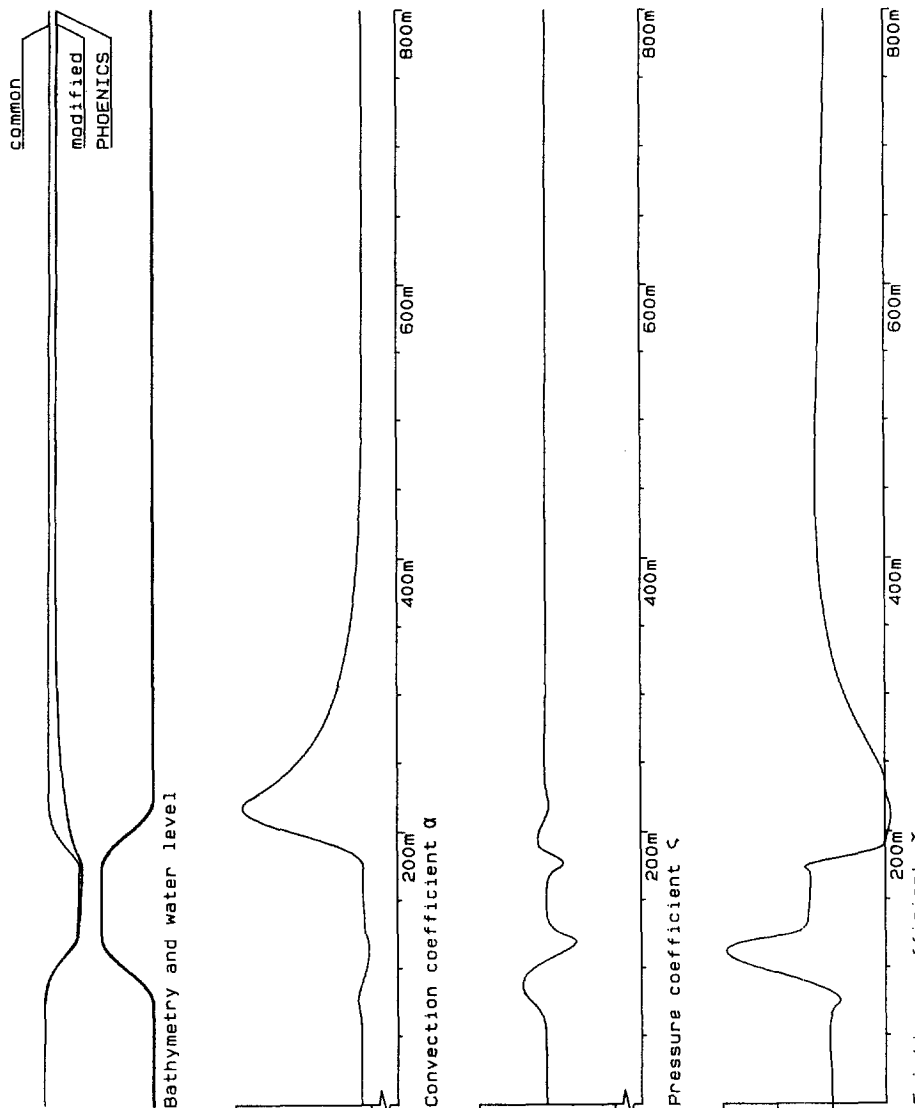

Figure 3.4.8 The situation with slopes $^{3}/_{10}$ (run 8)

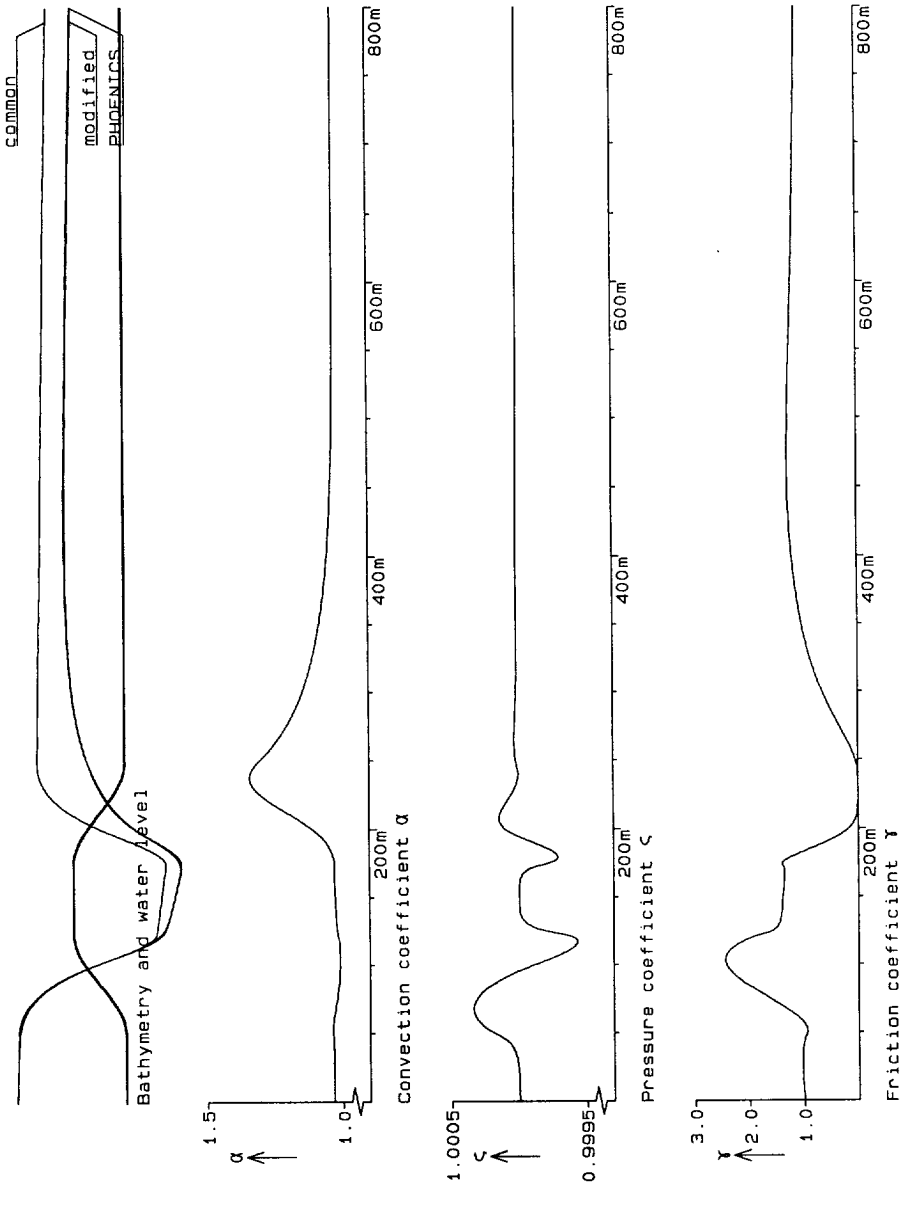

Figure 3.4.9 The basic situation with high Froude number (run 9)

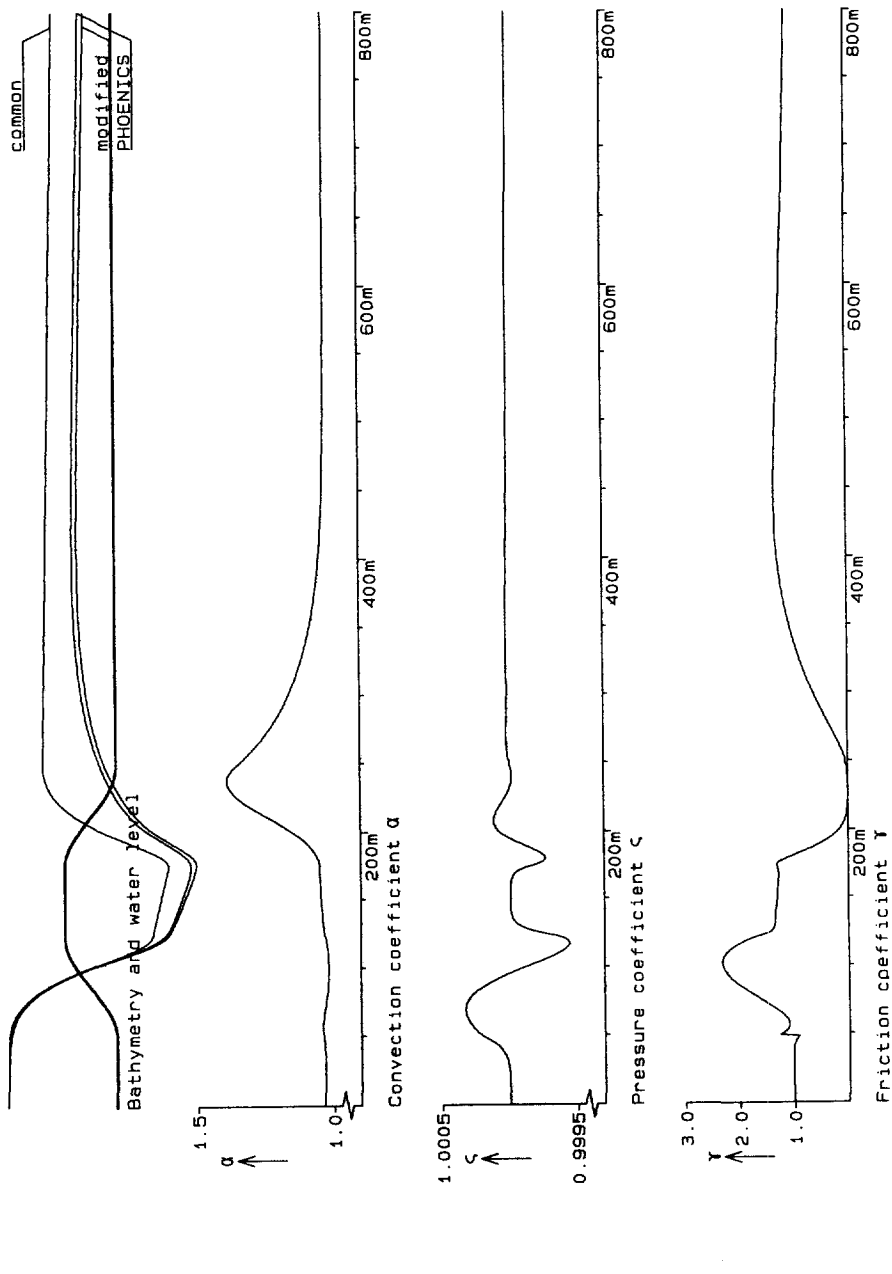

Figure 3.4.10 The situation with high Froude number and increased roughness (run 10)

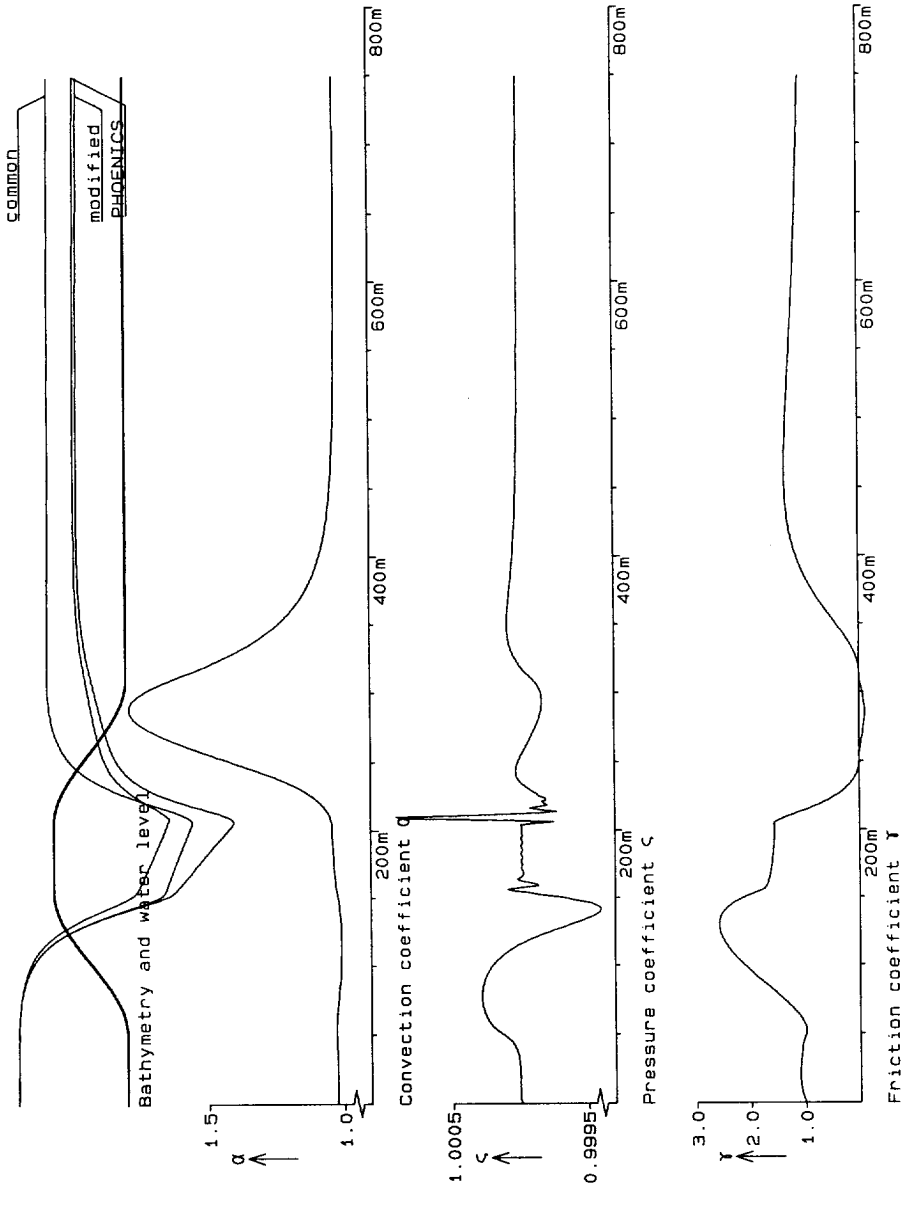

Figure 3.4.11 The situation with high Froude number and maximum height of the sill (run 11)

only 2DV calculations). Therefore, in the following section results from analytic approximations in chapter 2, derived by means of the method of weighted residuals, are used to obtain modified 1DH equations including α and γ as variables (with $\zeta=1$). A comparison of these results with those from PHOENICS is also given.

3.5 Comparison of analytic solutions with solutions of PHOENICS

In this section the analytical solutions derived in chapter 2.3 with the method of weighted residuals are compared with numerical solutions calculated with the PHOENICS flow-simulation system. In chapter 2.3 a coupled set of 1DH equations for d and Γ (eq. (2.3.34)) was derived. These equations also contain the unknown coefficients α, β, γ and γ_1, which however are known algebraic functions of Γ for given relative bottom roughness (L_{s0}) (eq. (2.3.30) through eq. (2.3.33) and eq. (2.3.37)) and a given velocity profile (eq. (2.3.25b), eq. (2.3.26) and eq. (2.3.36)).

The analytically derived horizontal velocity profiles and the convection and friction coefficients were calculated in chapter 2 using a parabolic eddy-viscosity distribution. This is in contrast with the eddy-viscosity model in the PHOENICS flow-simulation system, which is a ke-viscosity model. However, for uniform steady flow in an open channel with a horizontal bottom the eddy-viscosity profile calculated with the ke-viscosity model has almost the shape of a parabola.

The horizontal velocity profiles, water levels and convection and friction coefficients of both calculations are plotted in the Fig. 3.5.1 and Fig. 3.5.2 for maximum slope angles of $^1/_{10}$ (run 2) and $^1/_5$ (run 1), respectively.

The agreement between the two velocity profiles calculated is good for most verticals. Systematic but minor differences can be observed downstream from the sill. It cannot be expected that the velocity profiles derived analytically agree in detail with the velocity profiles derived numerically, because the eddy-viscosity models and the solution methods used are different.

The agreement between the convection coefficient, α, of both models, as calculated with the two models, is very good in the acceleration zone. In the deceleration zone the maximum value of the convection coefficient derived analytically is too large and the location of the maximum value is more downstream. (These deviations can be reduced by using

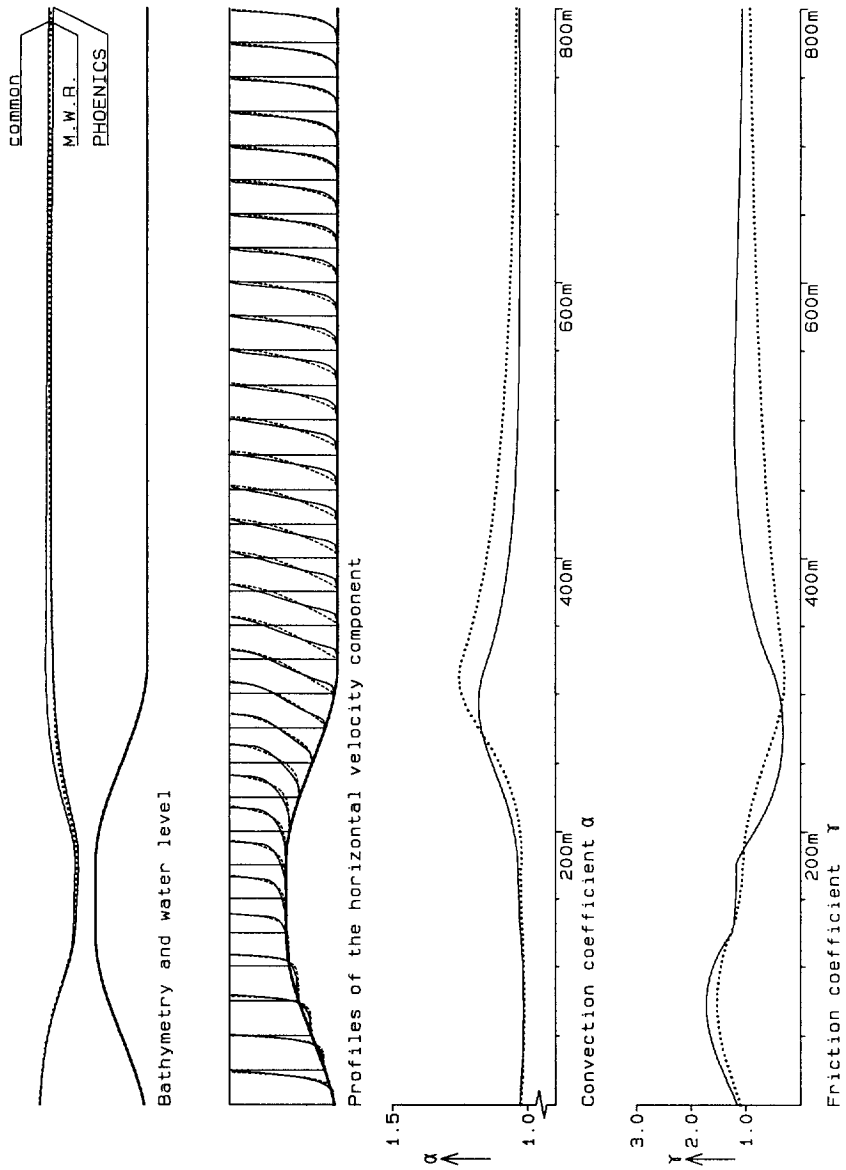

Figure 3.5.1 The velocity profiles, convection coefficient and friction coefficient. Maximum bottom slope $^1/_{10}$.
..... obtained by weighted residuals, ——— obtained by PHOENICS

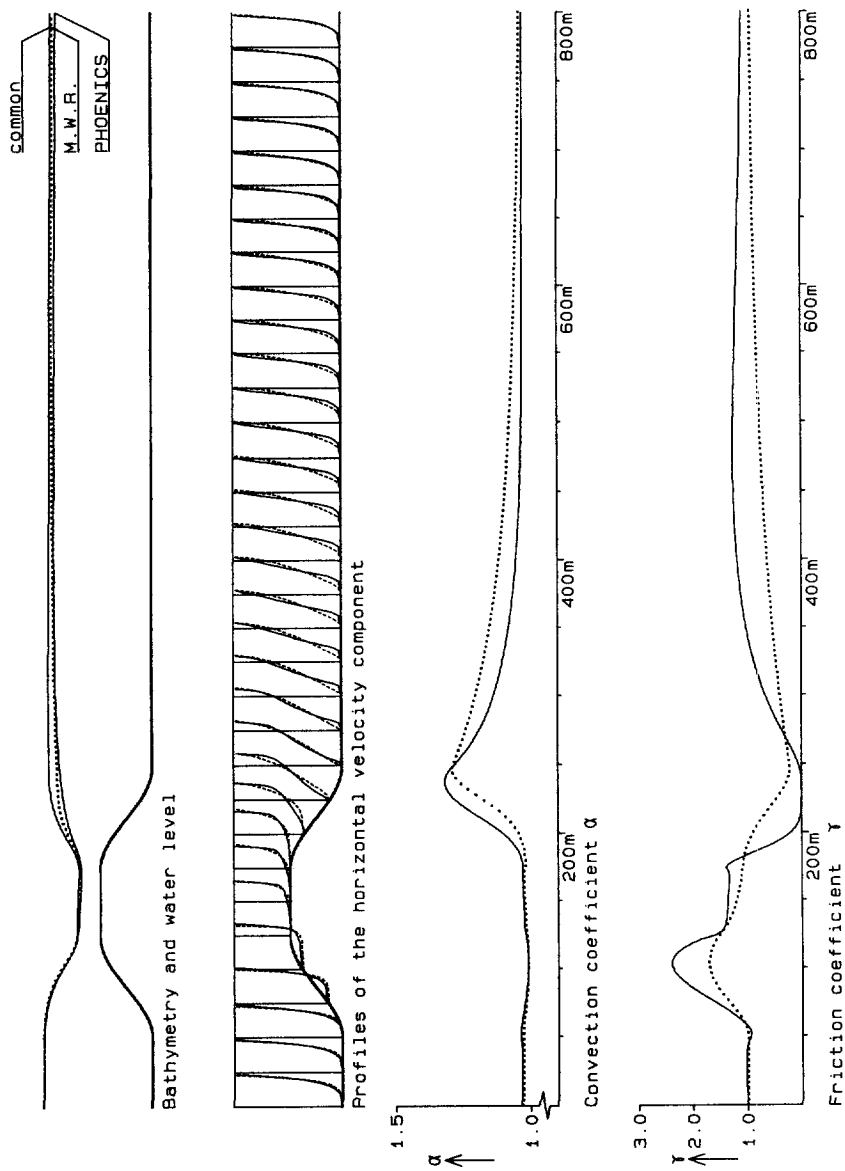

Figure 3.5.2 The velocity profiles, convection coefficient and friction coefficient. Maximum bottom slope $^1/_5$.
..... obtained by weighted residuals, ——— obtained by PHOENICS

another viscosity model, which calculates a higher viscosity in the deceleration zone; this reduces the vertical gradient in the velocity profiles, which in turn reduces the value of the convection coefficient α.)

The agreement between the graphs of the friction coefficient, γ, of both models is not so good. In the acceleration zone the maximum value calculated with the analytical model is smaller than the value calculated with PHOENICS, particularly for the $^1/_5$ slope (Fig. 3.5.2). In the deceleration zone the minimum value calculated with the analytical model is nearly the same as the minimum value calculated with solutions of PHOENICS, but it occurs further downstream. The bottom shear stress in PHOENICS is calculated with "the law of the wall" (Rodi [1980]) from the velocity in the element closest to the bottom. The bottom shear stress used in the method of weighted residuals is calculated by multiplying the eddy-viscosity with the vertical gradient of the horizontal velocity. The contribution of the perturbation velocity profile to the bottom shear stress is very small. Only the logarithmic part of the perturbation profile gives a contribution to the Reynolds shear stresses. Taking another perturbation profile, e.g. the mean first-order perturbation profiles of eq. (A.4.1), can improve the bottom shear stress.

The surface elevations obtained by both methods agree very well as shown in Fig. 3.5.1 and Fig. 3.5.2, except further downstream from the sill where the agreement for the weighted residuals with PHOENICS is not so good. But, the deviations in the water levels obtained by PHOENICS and the "common" model are not very large either. The deviations between the weighted residuals and PHOENICS are probably caused by the smaller value of γ in the weighted residuals than in PHOENICS.

In the last section of this chapter, the results presented in this and former sections are discussed and conclusions are given about this chapter.

3.6 Discussion

In this chapter the computational results from several models for flow in a vertical plane over sills are discussed.

A 2DV computer model was used, a 1DH "modified" shallow-water equations model and the 1DH "common" shallow-water equations model. The water levels calculated with the first two models agree very well for low Froude numbers, although the Reynolds normal

stress term was neglected and the water pressure at the bottom was not correctly described. The water levels derived with the common shallow-water equations model, however, show significant deviations from the water levels derived by the modified 1DH and 2DV model.

As expected, the velocity profiles become more uniform in the acceleration zone and less uniform in the deceleration zone. It takes about 60 water depths to regenerate the equilibrium profile downstream from the sill. The steepness of the sill causes a change in the shape of the velocity profile. The velocity profiles change slightly for slopes less steep than $^1/_5$, the basic slope. At slopes steeper than $^1/_5$ separation of the flow occurs. The influence of the length of the crown is negligible. The influence of the Froude numbers is only important for Froude numbers above 0.75. In that case separation occurs already for less steep slopes. The reason is the development of a jet flow at the top of the sill. The influence of the roughness length is noticeable in the velocity profile. A smaller roughness length causes a more uniform velocity profile than a larger roughness length.

To compute the water levels with the modified shallow-water equations, variable values for the convection coefficient, α, the pressure coefficient, ζ, and the friction coefficient, γ, have to be used. Changes in the velocity profiles have important influences on the coefficients α and γ, but changes in the pressure coefficient ζ can be neglected. In Fig. 3.6.1 the water surface elevations are plotted, calculated with the modified shallow-water equation with α, ζ and γ from PHOENICS, the modified shallow-water equation with α and γ from PHOENICS but $\zeta=1$, and the common shallow-water equations with $\alpha=1$, $\zeta=1$ and $\gamma=1$. The calculations are for situation 9 of Table 1. In this situation the deviations in ζ from the value $\zeta=1$ were relatively large (Fig. 3.4.9). Nevertheless the water levels obtained by the two modified models are virtually indiscernible, regardless of whether $\zeta=1$ or ζ is calculated from PHOENICS results. This shows that indeed the assumption of hydrostatic pressure is very realistic, even for this case with maximum slopes of $^1/_5$ and a relatively high Froude number.

Variation of the roughness length causes changes in the convection coefficient, α. In the acceleration zone the coefficient α approximates the value $\alpha=1$ more closely for smaller roughness lengths than for larger ones. The friction coefficient, γ, becomes larger in the acceleration zone and smaller in the deceleration zone. This coefficient even becomes negative in regions of back flow.

For mild slopes the most important coefficient used in the modified shallow-water

equations is the friction coefficient. In Fig. 3.6.2 several water levels are plotted: for the modified shallow-water equations with the coefficients α, ζ and γ as derived from 2DV PHOENICS calculations; for the modified shallow-water equations with only $\zeta=1$ and $\gamma=1$ and the convection coefficient α from PHOENICS; for the modified shallow-water equations with only $\zeta=1$ and $\alpha=1$ and the friction coefficient γ from PHOENICS, and for the conventional shallow-water equations ($\alpha=\zeta=\gamma=1$). The flow situations plotted are the situations 1, 4 and 8 of Table 1.

It appears from the plots that for the $^1/_{20}$ slope both coefficients α and γ are important (Fig. 3.6.2a), but for steep slopes ($^1/_5$ and $^3/_{10}$) only the convection coefficient, α, is important (Fig. 3.6.2b and Fig. 3.6.2c). This suggests that for slopes milder than $^1/_{20}$ the friction coefficient (γ) is the most important term.

Comparing the analytically derived horizontal velocity profiles and convection and friction coefficients with the ones derived from numerical calculations, it can be concluded that the agreement between the velocity profiles and coefficients is good, especially for mild slopes. The agreement between the convection coefficients is quite good, while the agreement between the friction coefficients is less. The agreement between the coefficients can be improved by choosing another perturbation profile. Despite the differences between the friction coefficients, the water levels obtained with the method of weighted residuals agree well with the ones obtained with PHOENICS. For steep slopes, steeper than $^1/_5$, the differences between the calculated convection and friction terms from the analytic and numerical solutions become too large, resulting in unrealistic water levels for the method of weighted residuals.

In the following chapter, measurements of flow over a sill in a flume are described. The measured velocities are compared with results from calculations with PHOENICS, based on the flow conditions in the flume.

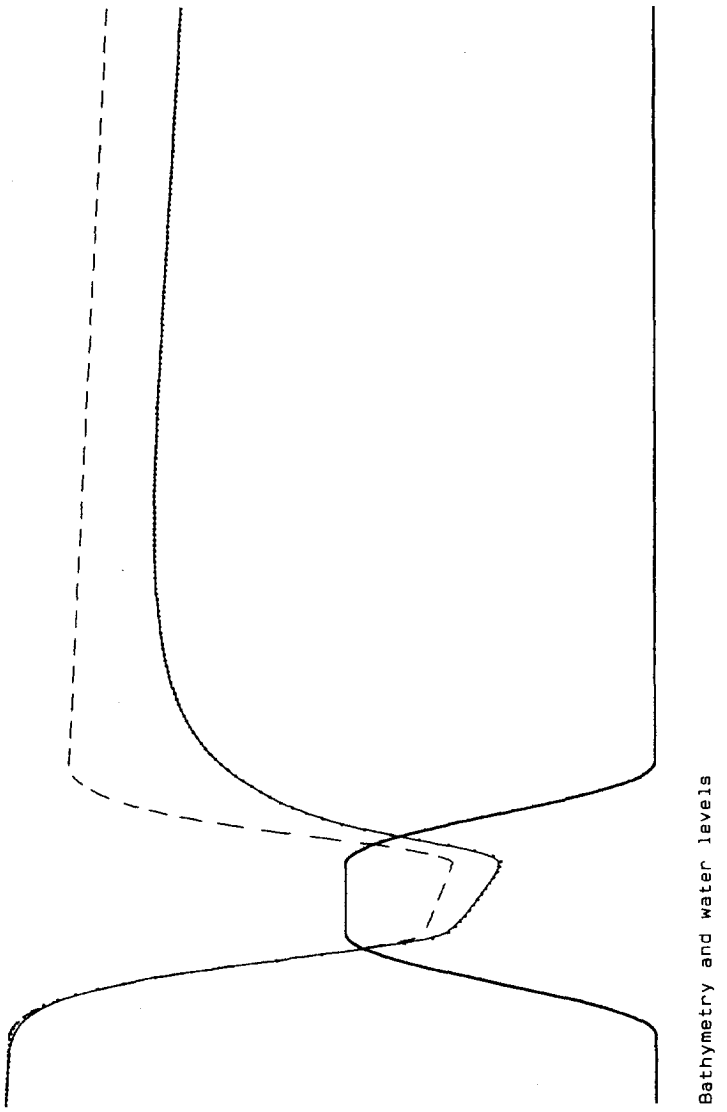

Figure 3.6.1 The influence of the coefficient ζ on the calculated water levels. The situation with slopes $^3/_{10}$. - - - $\alpha=1$, $\zeta=1$ *and* $\gamma=1$, ... $\alpha\neq1$, $\zeta=1$ *and* $\gamma\neq1$, ——— $\alpha\neq1$, $\zeta\neq1$ *and* $\gamma\neq1$. *The thick drawn line represents the bottom profile.*

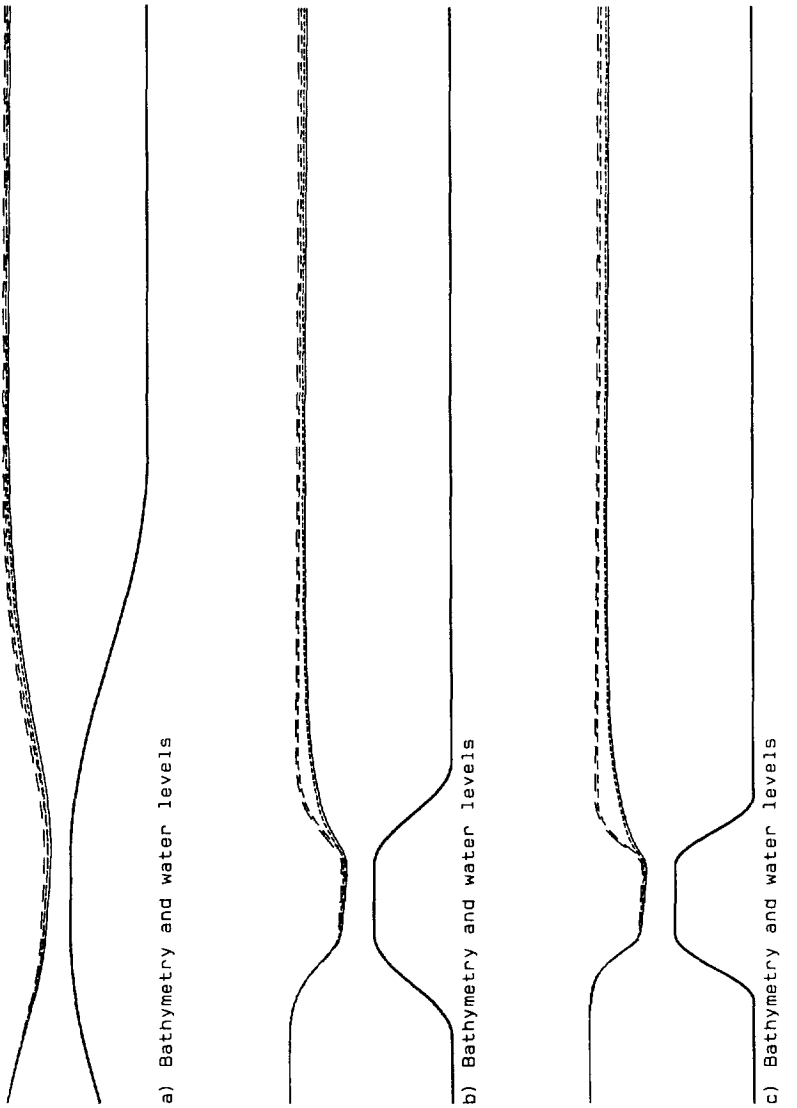

Figure 3.6.2 The influence of the coefficients α, ζ *and* γ.
a) The situation with slopes $^1/_{20}$. *b) The basic situation (slopes* $^1/_5$). *c) The situation with slopes* $^3/_{10}$.
— — — $\alpha=1,\ \zeta=1,\ \gamma=1$, – – – $\alpha=1,\ \zeta=1,\ \gamma\neq1$, - - - - - $\alpha\neq1,\ \zeta=1,\ \gamma=1$, ——— $\alpha\neq1,\ \zeta\neq1,\ \gamma\neq1$

4. Measurements

4.1 Introduction

To check the correctness of the numerical model and to get a better insight in the flow over a sill, experiments are needed.

In literature few results of measurements about flow over a sill can be found. Van Mierlo & De Ruiter [1988] carried out extensive laser-Doppler velocimeter measurements for steady flow conditions above one dune of a series of dunes in a straight sand flume. Johnson [1981] carried out measurements of mean velocities and turbulence intensities for steady flow conditions above a hill in a wind tunnel. Cardoso et al. [1991] carried out measurements of mean velocities and turbulence intensities for steady flow conditions in the acceleration zone above a sill.

The measurements of Van Mierlo & De Ruiter could not be used because their initial profiles, at the toe of the dune, are too much influenced by the upstream dunes, which causes quite different mean velocities and turbulence intensities in the acceleration zone. The measurements of Johnson could not be used because of the quite different ratio of the sill height to the total flow depth. The measurements of Cardoso et al. were quite detailed, but their measuring region, the acceleration zone, was too restricted for use in this investigation.

In order to obtain the necessary experimental data, measurements were performed in a flume. In the first section of this chapter the experimental set-up is described together with the instruments used. In the second section of this chapter the results of the measurements are presented and discussed. In the third section the measured velocities and turbulence fluctuations are compared with the values obtained with PHOENICS and values described in the literature elsewhere.

4.2 Experimental arrangement

The flume consists of two vertical, parallel glass side-walls and a horizontal bottom of smooth concrete. The width of the flume is 0.5m and the length is 22.5m (Fig. 4.2.1).

Water flows into the flume from a constant-head tank yielding a constant discharge. The required discharge was established by adjusting a valve. The water enters the flume

through a perforated bottom element to get a uniform inflow.

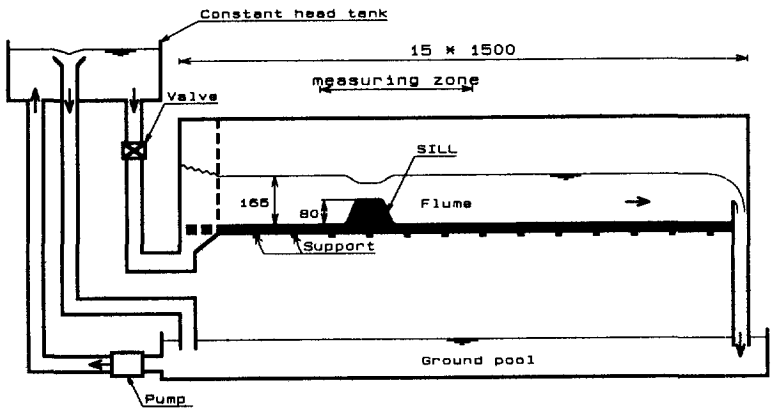

Figure 4.2.1 Schematic drawing of experimental arrangement

A sill was built in the flume with its centre 5.0m downstream from the inflow element. This distance had to be large enough to get a uniform flow situation at the toe of the sill and is taken about 30 times the initial water depth. To avoid the influence of the weir in the outflow region on the flow in the recovery zone the distance between the downstream toe of the sill and the weir is taken about 60 water depths. The shape of the sill was based on the basic situation, described in the previous chapter, although the dimensions were scaled (length scale 1:125). The maximum slope of the sill was $^1/_5$. The length of the slope was 0.6m, the length of the sill's crown was 0.4m and the height of the crown was 0.08m above the bottom.

Because of the influence of the side-walls, secondary flows appear in the flume. These secondary flows transport water with low velocity from the side-walls to the middle of the flume. To decrease these secondary flows the water depth/flume width or aspect ratio of the flow has to be small. The ratio used was about $^1/_3$ and the initial water depth chosen was therefore 0.16m. The water depth was adjusted by a weir at the outflow side. The established discharge was 17.3 l/s, measured with an orifice plate in the supply-pipe of the flume. This implies a cross-sectional average velocity of 0.22m/s in the approach flow. The Froude number upstream and downstream from the sill was $Fr \approx 0.17$ and on the sill $Fr \approx 0.49$.

The measurements were performed with a laser-Doppler velocimeter capable of measuring two perpendicular velocity components. No intentional seeding of the water was needed to carry out the measurements. Displacements of the laser-Doppler velocimeter were

executed by vertical and horizontal traversing devices. The velocity components were only measured in the middle of the flume.

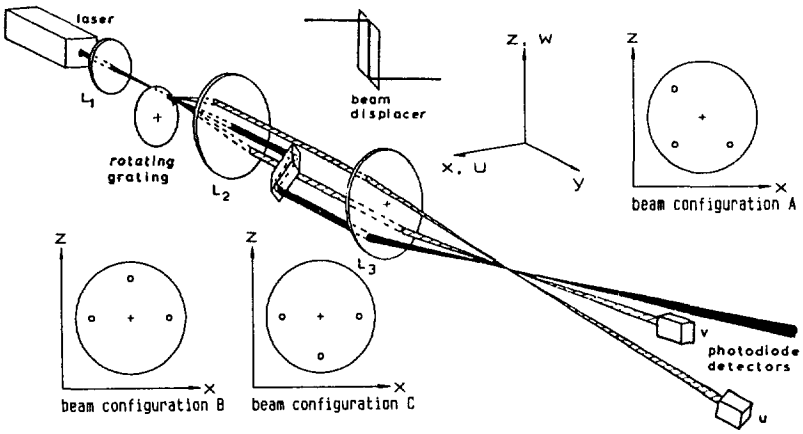

Figure 4.2.2 Optical arrangement for the orthogonal two component LDV

The optical system used consists of a 5 mW HeNe-laser, a lens to focus the laser beam on a rotating grating, a lens to make the laser beams parallel again, a beam displacer to achieve a two-dimensional beam configuration, a lens (focal length f=200mm) to create the measuring volume, formed by the intersection of the beams, and two photodiode detectors (Fig. 4.2.2).

The rotating grating diffracts the incoming laser beam into one zero order beam, the illuminating beam, and two first order diffracted beams, the reference beams. It also gives a frequency shift to detect the sign of the velocities measured and to distinguish the reference beams. With this arrangement of the laser-Doppler velocimeter (Fig. 4.2.2), it is possible to measure two orthogonal velocity components simultaneously. The beam displacing prism gives a parallel displacement of the illuminating beam in order to realize a two-dimensional beam configuration.

The configuration as shown in diagram A of Fig. 4.2.2. permits direct measurements of the horizontal and vertical velocities. A disadvantage of this geometry is that it is not possible to measure close to the bottom because one of the reference beams intersects the bottom preventing the detection of the beam. To counteract this both reference beams have to be parallel to the bottom, while the illuminating beam, which may be lost behind the measuring volume, intersects the bottom under a certain angle from above. In this

configuration (B in Fig. 4.2.2) the velocity components measured directly make angles of 45° with respect to the bottom. They are converted to vertical and horizontal components numerically. In diagram C a similar arrangement used for measurements close to the water surface is shown.

The laser-Doppler velocimeter is based on the measurement of the Doppler frequency shift in laser light scattered by small particles that are moving with the flow. The frequency shift is a measure for a component of the velocity in the measuring volume. Instantaneous records of the two velocity components were obtained by feeding the signals from the photodiode detectors to a two-channel frequency tracker. The frequency tracker converts the Doppler frequency of the bursts from the photodiode detector to an analog voltage proportional to the velocity being measured. The output of the tracker was sampled with a sample frequency of 100 Hz during 6 minutes and was recorded on floppy disks.

From the series of instantaneous velocities the average horizontal and vertical velocities $\bar{u}$ and $\overline{w}$, the turbulence energy components $\overline{u'^2}$ and $\overline{w'^2}$, and the Reynolds shear stress $\overline{u'w'}$ are calculated.

The length of the flume's section in which the measuring verticals were located was about 3.8m long. In this section the velocities were measured in 20 verticals, starting 0.5m upstream from the sill, to 1.75m downstream from the sill. The positions of the verticals are shown in Fig. 4.3.1.

The results of the measurements are discussed in the following section. In appendix D a global error estimation can be found.

4.3 Experimental results

With the laser-Doppler velocimeter described above, measurements were executed in 20 verticals in at least 10 points in each vertical. Three different measuring series were used. In the first series, it was tried to position the lowest measurement point in the vertical as close to the bottom as possible. This point was located about 1.5 cm above the bottom. The arrangement of the laser beams for this series is shown in diagram B of Fig. 4.2.2. In the second series it was tried to position the highest measurement point in the vertical as close to the water surface as possible. This point was about 0.5 cm below the water surface. The arrangement of the laser beams for this case can be seen in diagram C of Fig. 4.2.2. In the

third series some of the measurements of the first series were repeated to check the correctness of the measurements of the first series.

The signals coming from the photodiode detectors were converted to voltages using a frequency tracker and had to be filtered with a low-pass filter to eliminate the laser noise. During the first series of measurements the signals were low-pass filtered wit a too high filter cut-off frequency; in the second and third series the cut-off frequency was decreased.

The distribution of the verticals in which measurements were executed is shown in Fig. 4.3.1. In the first two verticals the measurements were used to check the uniformity of the flow. The distances between the verticals on the slopes were 0.15m, so that at least 4 such verticals were measured. On the crown of the sill this distance between the verticals could not be obtained because of the support of the flume. Downstream from the crown of the sill the verticals were spaced again at 0.15m up to vertical 17. The distance between the last four verticals increased; between the 17th and 18th verticals it was 0.30m, between the 18th and 19th verticals it was 0.45m and between the 19th and 20th verticals it was 0.60m. The results of the measurements are shown in Fig. 4.3.2 to Fig. 4.3.5.

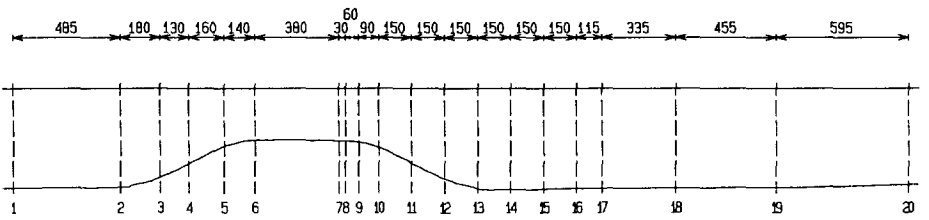

Figure 4.3.1 Location of the measuring verticals in the flume

The horizontal velocity is shown in Fig. 4.3.2. Only minor differences between the measurements of different series are noticeable in some verticals. This confirms the reproducibility of the observations.

In Fig. 4.3.3 the measured vertical velocities are shown. These velocities are difficult to determine because they are the result of subtraction of two nearly identical, large velocities. This causes large relative inaccuracies. Such errors can be seen in vertical 6 and 8. The error estimation can be found in appendix D.

In Fig. 4.3.4 the measured turbulence "energy" ($\frac{1}{2}(\overline{u'^2} + \overline{w'^2})$) profiles are shown. The differences between the first and the third series are small. In some verticals (12, 14,

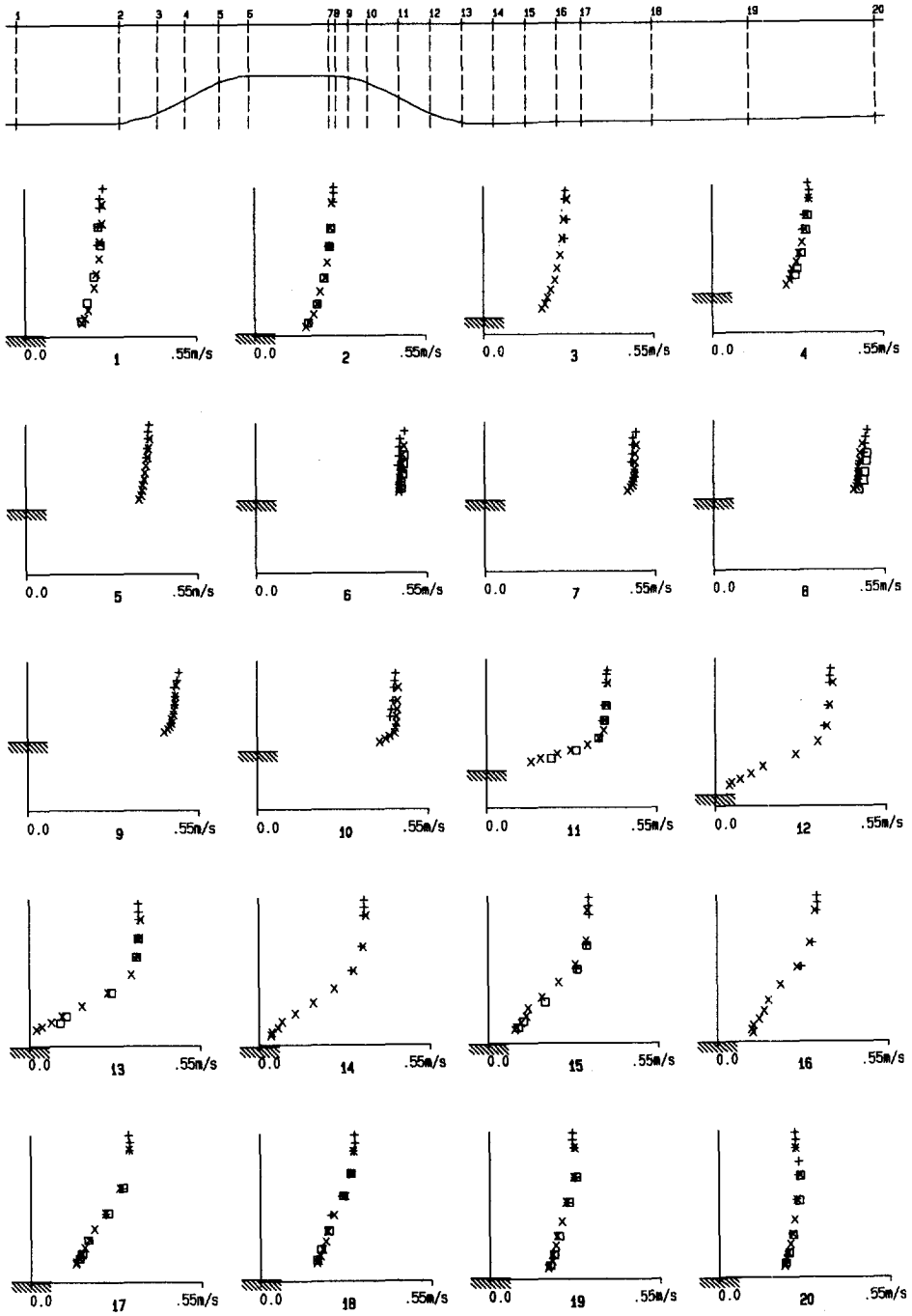

Figure 4.3.2 The measured horizontal velocity
× measurements first series, + measurements second series, □ measurements third series.

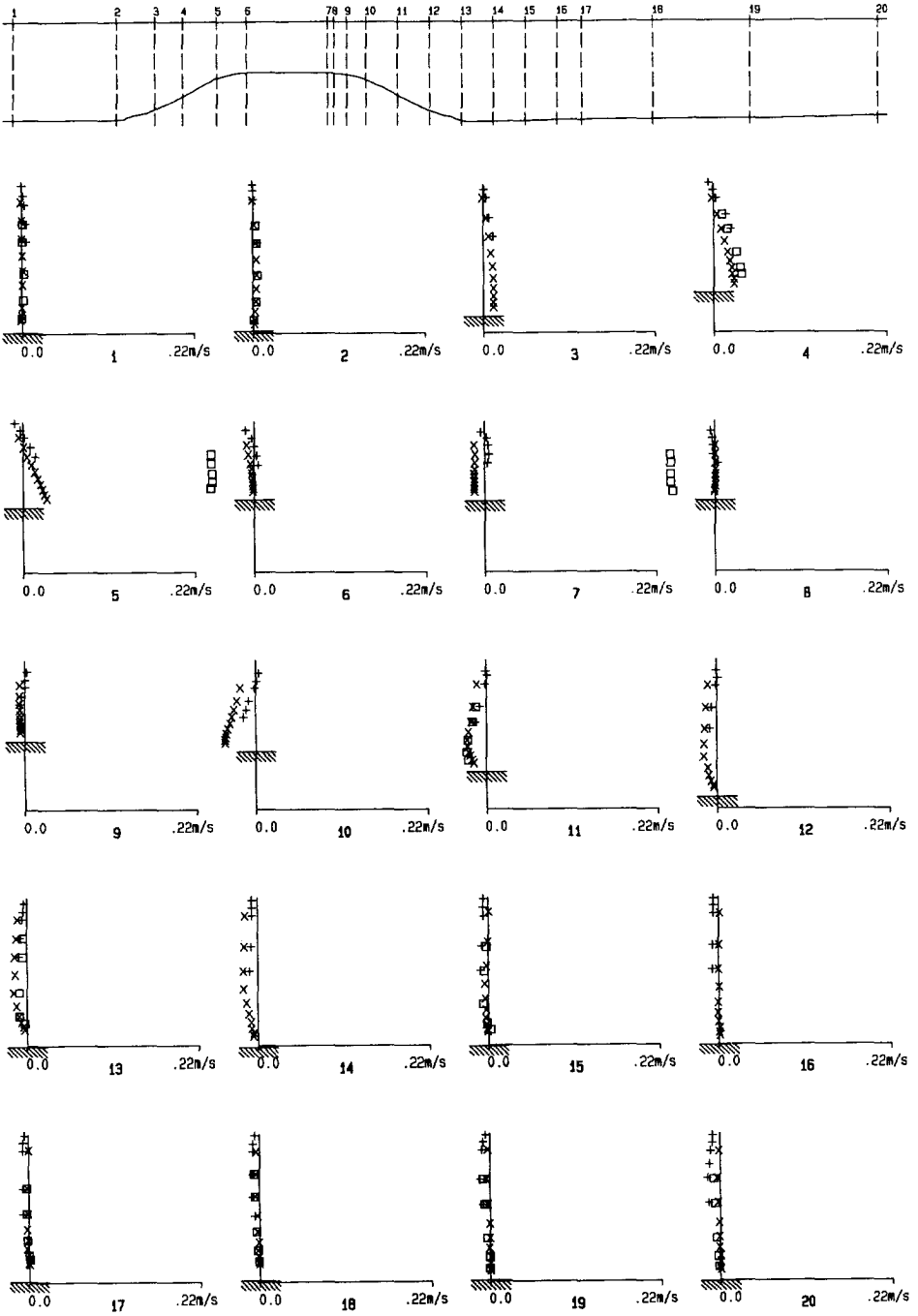

Figure 4.3.3 The measured vertical velocity
× measurements first series, + measurements second series, □ measurements third series.

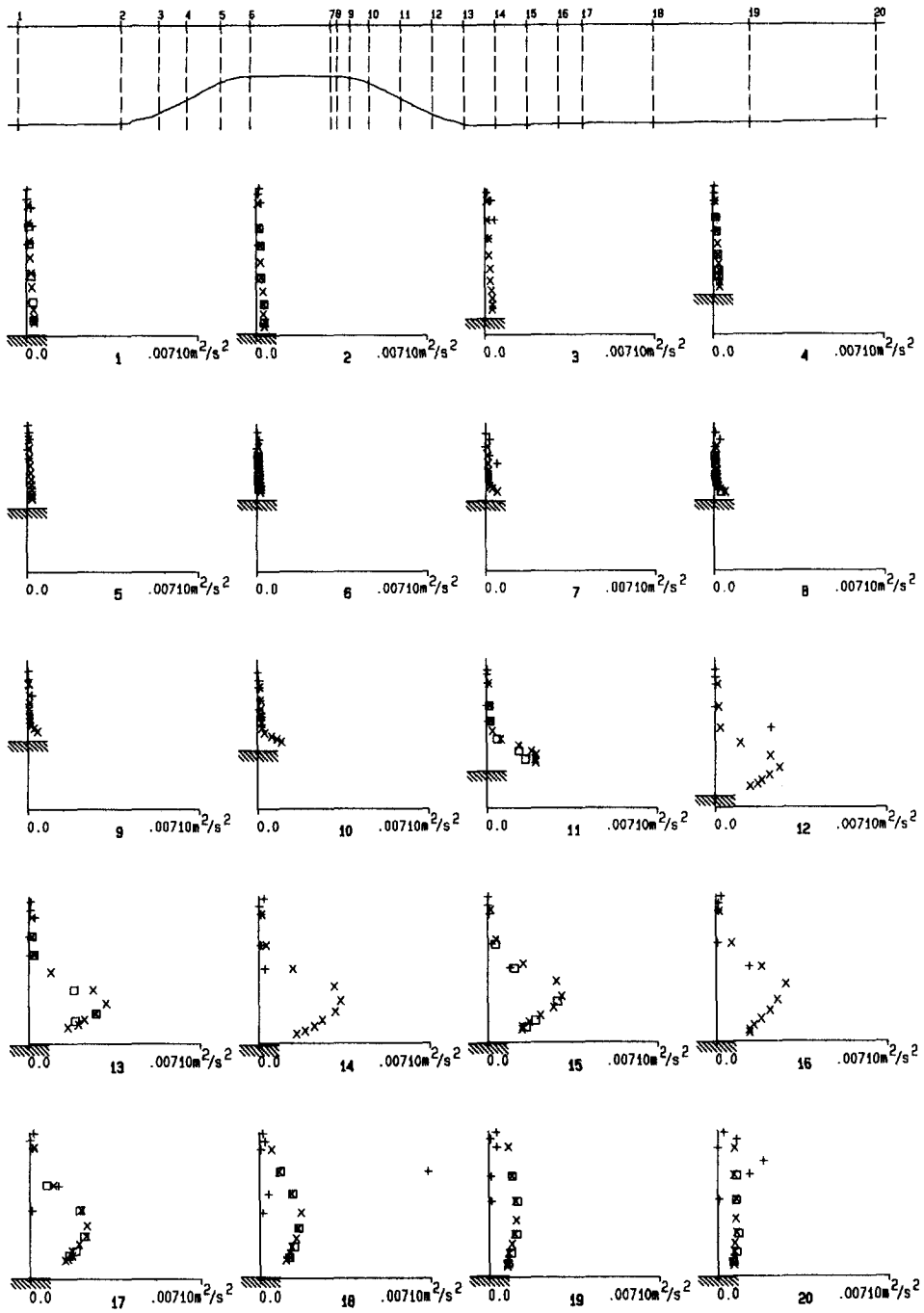

Figure 4.3.4 The measured turbulence energy
× *measurements first series,* + *measurements second series,* □ *measurements third series.*

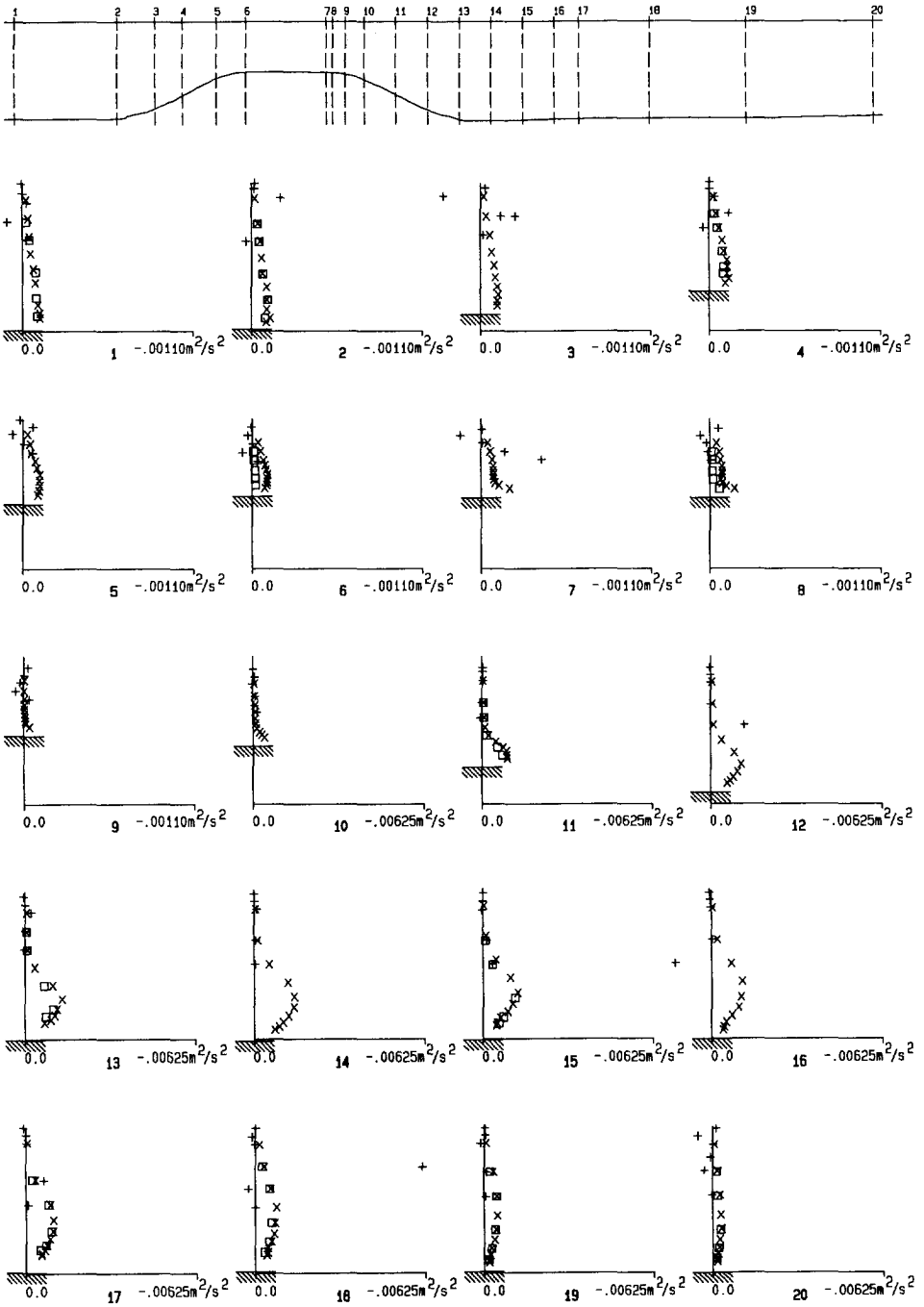

Figure 4.3.5 The measured Reynolds shear stresses
× *measurements first series,* + *measurements second series,* □ *measurements third series.*

17, 18, 19 and 20), large differences between the results of the second series and the other series are noticeable in a few points. These differences are ascribed to inaccurate measuring because the arrangement of the laser-Doppler velocimeter was not accurately adjustable.

In Fig. 4.3.5 the measured Reynolds shear stresses, $\overline{u'w'}$, are shown. Again large differences between the measurements of the first and third series and the second series are noticeable (in nearly every vertical except the verticals 10, 11, 13 and 15). In some verticals the values of the Reynolds shear stresses even become positive, which can only occur where the vertical gradient of the horizontal velocity is negative. Differences between the first and the third series exist in the verticals 6, 8 and 13, although these differences are not as large as the differences between the first and the second series.

4.4 Comparison between results of the measurements and 2DV calculations

Results of the measurements are compared with those from calculations carried out with the flow-simulation system PHOENICS to investigate the accuracy of this flow-simulation system. To this end the values of the velocities, turbulence energy and Reynolds shear stress obtained in different series at the same location are averaged. However, values in points in a vertical which have a high deviation from the values in surrounding points (see Fig. 4.3.4 vertical 18) are omitted. If, with this criterion, the value of one variable (horizontal velocity, vertical velocity, turbulence energy or Reynolds shear stress) measured in a point in a vertical is omitted, then the values of the other quantities are also omitted in that point. The results of the averaging can be seen in Fig. 4.4.4 through Fig. 4.4.7 at the end of this section.

The measured bottom profile of the sill is used for the bottom imposed in the 2DV (two-dimensional vertical) calculations. Because of the hydraulically smooth flow conditions the elevation where the horizontal velocity is zero, z_0, is calculated with eq. (A.4.1b), which yields $z_0=1.1\cdot10^{-5}$m. Although this "roughness" length is dependent on the friction velocity, the "roughness" length in the calculations is assumed to be constant to simplify the calculations. The inflow conditions were the ones described in chapter 3, except for the discharge per unit width, q. This was taken as the discharge measured with the orifice plate, Q, divided by the flume width, B.

The drawn lines in the graphs of the Fig. 4.4.4 through Fig. 4.4.7 are profiles

calculated with PHOENICS. The horizontal velocity profiles are shown in Fig. 4.4.4. The calculated velocity profiles upstream from the sill agree well with the measured velocity profiles. (This was not expected because the velocities in the middle of the flume, where the measurements took place, are expected to be larger than the velocities near the side-walls due to the influence of these side-walls as a consequence of the logarithmic distribution of the velocity profile in lateral direction near the side-walls. The discharge per unit width in the calculations is based on the one in the flume measured with the orifice plate ($q=Q/B$). Therefore the measured velocities in the centre of the flume should be larger; or, the discharge in the flume is smaller than measured with the orifice plate.) The similarity between the calculated and measured velocities is good in the acceleration zone. On top of the sill, the calculated velocities are larger than the measured velocities because due to the acceleration of the flow on the sill the velocities near the side-walls increase more than the velocities in the middle of the flume (the lateral velocity profile becomes more uniform). The average velocity in the calculation is therefore larger than the average velocity in the middle of the flume. The influence of this velocity difference is a function of the aspect ratio of the flow. If this ratio increases then the velocity differences increase too.

The differences in velocities also influence the fall of the water level. Due to the larger acceleration of the water in the calculation, the fall of the water level in the calculations is larger than the fall of the water level measured in the flume. Therefore downstream from the sill the calculated water level is lower than the water level in the flume. A larger part of the kinetic energy on the sill is dissipated in the deceleration zone in the calculations than in the flume.

In the deceleration zone there are also some minor differences in the horizontal velocity profiles.

The new bottom boundary layer (verticals 13 to 20) has almost the same dimensions in the calculations as in the measurements. This means that numerical diffusion is small.

In the last two verticals measured, the maximum velocity appears to occur slightly below the water surface. The reason is probably the transport of water with a lower velocity by the secondary flow from the side-walls to the middle of the flume. This effect is not simulated in a 2DV calculation.

In Fig. 4.4.5 the vertical velocities are shown. Although the error in the measured vertical velocities can be large (appendix D), most of the profiles of the measured and

calculated vertical velocities are almost similar. This implies that the errors in the vertical velocities measured are small and that the measurements were quite accurate. The errors in the horizontal velocities measured will be even smaller.

In Fig. 4.4.6 the measured and calculated turbulence energy profiles are shown. In most verticals the measured values are agree well with the calculated ones. The plotted values of the turbulence kinetic energy, k, are calculated from the turbulence fluctuations according to:

$$k = \frac{1}{2}\left(\overline{u'^2} + \overline{v'^2} + \overline{w'^2}\right)$$

The turbulence fluctuation $\overline{v'^2}$ is not measured, but a relation between $\overline{v'^2}$, $\overline{u'^2}$ and $\overline{w'^2}$ can be assumed. According to Nezu [1977] the component in transverse direction of the turbulence energy, $\overline{v'^2}$, is 0.17 of the entire turbulence energy; therefore, the values plotted in Fig. 4.3.4 ($\frac{1}{2}\left(\overline{u'^2} + \overline{w'^2}\right)$) were multiplied with 1.20 to get a better estimate of the turbulence energy. These values are plotted in Fig 4.4.6.

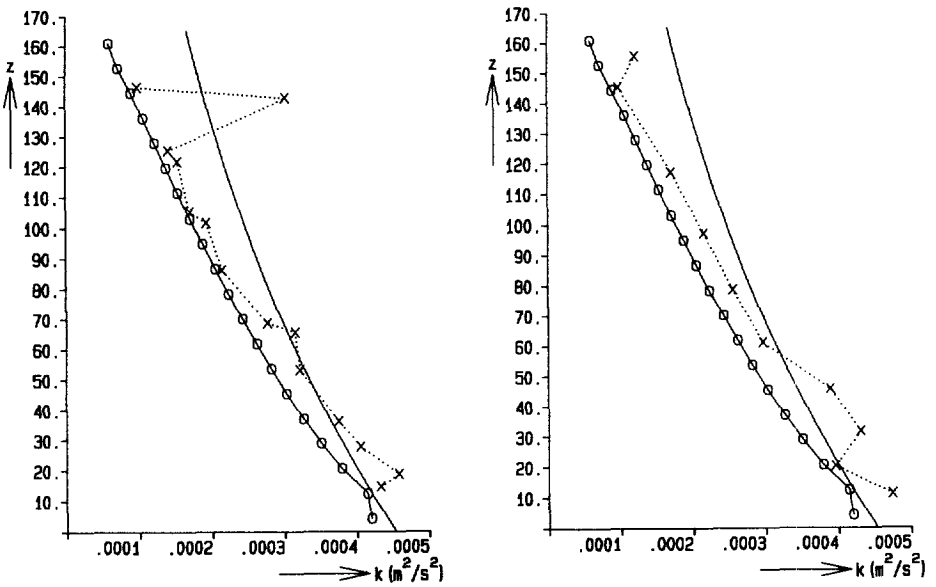

Figure 4.4.1 The turbulence kinetic energy in vertical 1 and vertical 2
×.....× measurements, ———— theoretical values (Nezu), o——o PHOENICS values

In the acceleration zone the calculated turbulence energy is too large. (The coefficients in a ke viscosity-model are tuned for gradually changing flow conditions; apparently, this does not reproduce the production of the turbulence energy very well in the zone of high acceleration.) This results in too large values of the calculated turbulence energy

on the sill in comparison with the measured values. The measured turbulence energy levels in the new boundary layer (verticals 13 to 20) agree fairly well with the calculated ones. In the most downstream verticals (18, 19 and 20) the similarity between the measured and calculated turbulence energies is not so good, probably due to three-dimensional effects. Comparing the turbulence energies measured in the verticals 1 and 20, it can be concluded that at the location of vertical 20 the flow is not nearly uniform.

The turbulence kinetic energy profiles of the verticals 1 and 2 of Fig. 4.4.6 (uniform approach flow) are replotted in Fig. 4.4.1. According to Nezu [1977] the turbulence kinetic energy increases exponentially with the distance from the bottom with the value $k = 4.8u_*^2$ (u_* is the friction velocity) at the bottom (drawn line in Fig. 4.4.1). In this figure the equilibrium turbulence kinetic energy profiles derived by the flow simulation system PHOENICS are also plotted. These values are smaller than those given by Nezu. The measured values also deviate somewhat from the exponential distribution given by Nezu, they are smaller near the water surface and larger near the bottom.

In Fig. 4.4.7 the measured and calculated Reynolds shear stresses, $\overline{u'w'}$, are shown. These stresses are compared with Reynolds stresses calculated from PHOENICS results, by taking:

$$\overline{u'w'} = \frac{\tau_{xz}}{\rho} = -\nu_t \frac{\partial u}{\partial z}$$

in which ν_t is the eddy-viscosity according to the kε viscosity-model. Although the calculated shear stresses do not exactly match the measured ones, the similarity between both stress profiles is generally good, in particular in view of the numerical differentiation of the numerically generated velocity profile.

In the acceleration zone the calculated shear stress is quite large in a small layer close to the bottom. Unfortunately, it was not possible to measure the velocities so close to the bottom.

In the deceleration zone the shear stress becomes small near the bottom and larger in the transition of the new and the old boundary layer. The shear stresses measured in the verticals 19 and 20 are smaller than the calculated ones, probably due to three-dimensional effects. Again it can be concluded that the flow is not nearly uniform at the location of vertical 20. There is a large difference between the Reynolds shear stress profile measured in vertical 20 and the one measured in vertical 1.

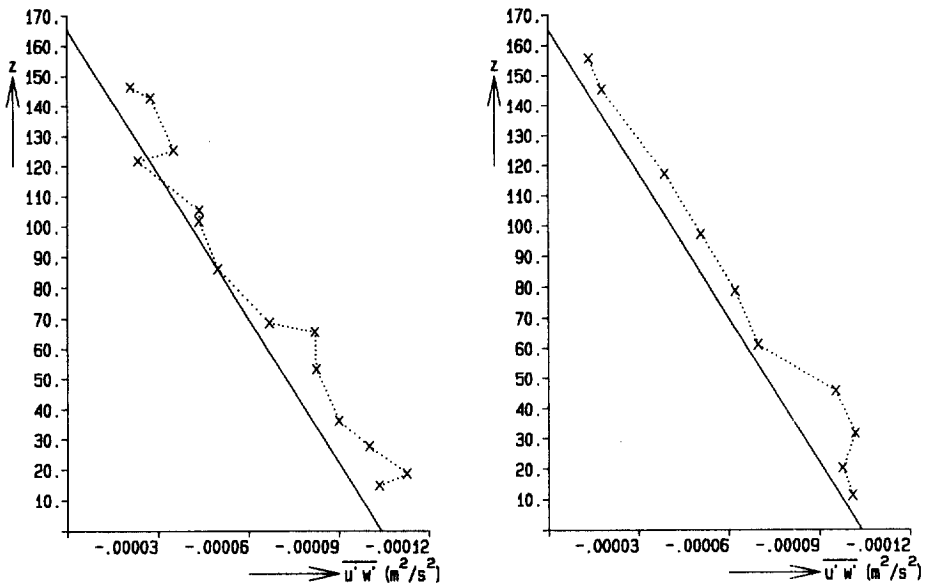

Figure 4.4.2 The Reynolds shear stress $\overline{u'w'}$ in vertical 1 and vertical 2.
× ····· × measurements, ——— theoretical values.

The Reynolds shear stresses, $\overline{u'w'}$, upstream from the sill are compared with parameterized expressions in the literature. The flow upstream from the sill is a steady uniform flow. For this flow situation it is known (Schlichting [1968], Hinze [1975]) that a linear stress distribution occurs with the value ρu_*^2 (ρ is the density) at the bottom and 0 at the water surface. The friction velocity u_* can be derived by the equilibrium of the pressure gradient (i) and the bottom friction (τ_{bx}), resulting in:

$$-\tau_{bx} = \rho u_*^2 = \rho g d i$$

or

$$u_* = \sqrt{g d i}$$

Assuming a logarithmic velocity distribution, the discharge can be expressed in terms of the friction velocity, the depth and the relative roughness:

$$q = \frac{u_*}{\kappa} d \ln\left(d\left(e z_0\right)^{-1}\right)$$

or

$$u_* = \frac{q}{d} \kappa \left(\ln\left(d\left(e z_0\right)^{-1}\right)\right)^{-1}$$

Using these expressions and the measured values of q, d and z_0, the theoretical vertical distribution of τ/ρ is shown on Fig. 4.4.2, in which also the Reynolds shear stresses

$\overline{u'w'}$ measured in the first two verticals of Fig. 4.3.1 are plotted. The measured values are slightly too large, probably due to noise (appendix D), but the vertical variation is nearly as expected.

The values of the convection coefficient, α, calculated from the measured horizontal velocities, are compared with the values calculated with PHOENICS in Fig. 4.4.3. The values do not completely agree, nevertheless the agreement is considered acceptable.

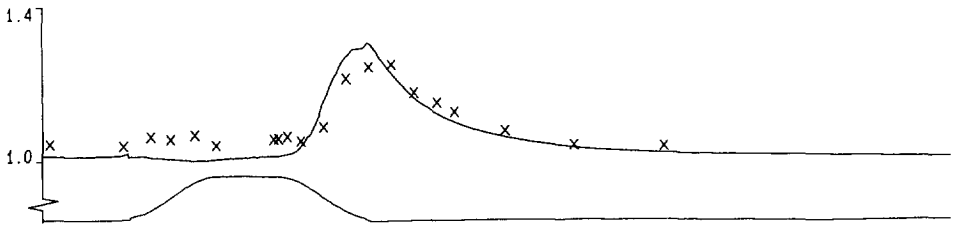

Figure 4.4.3 The measured and calculated convection coefficient α
× measurements, —— calculations PHOENICS.

Discussion

In this section the results of the measurements have been compared with the results of calculations with PHOENICS, and upstream from the sill with theoretical values. For nearly every vertical the agreements between the measured values of the horizontal and vertical velocity, turbulence energy and Reynolds shear stress and the calculated values are fairly good. Downstream from the sill in the recovery zone the similarity is not so good, possibly due to a secondary flow. This flow transports water with a lower velocity from the side-walls to the middle of the flume.

The flow is not nearly uniform in the last measured vertical. This was expected because the last vertical was only 12.5 water depth behind the sill.

The similarity between the measured and calculated boundary layer behind the sill is good. This means that the numerical diffusion in PHOENICS is small.

Comparing the measured Reynolds shear stresses and turbulence energies with theoretical values, it can be concluded that the similarity is generally good.

The measured values of the turbulence energy are too small, while the absolute values of the Reynolds shear stress are too large. This could mean that a part of the turbulence

energy contributes to the Reynolds shear stresses as determined from the velocity measurements due to alignment errors (see appendix D).

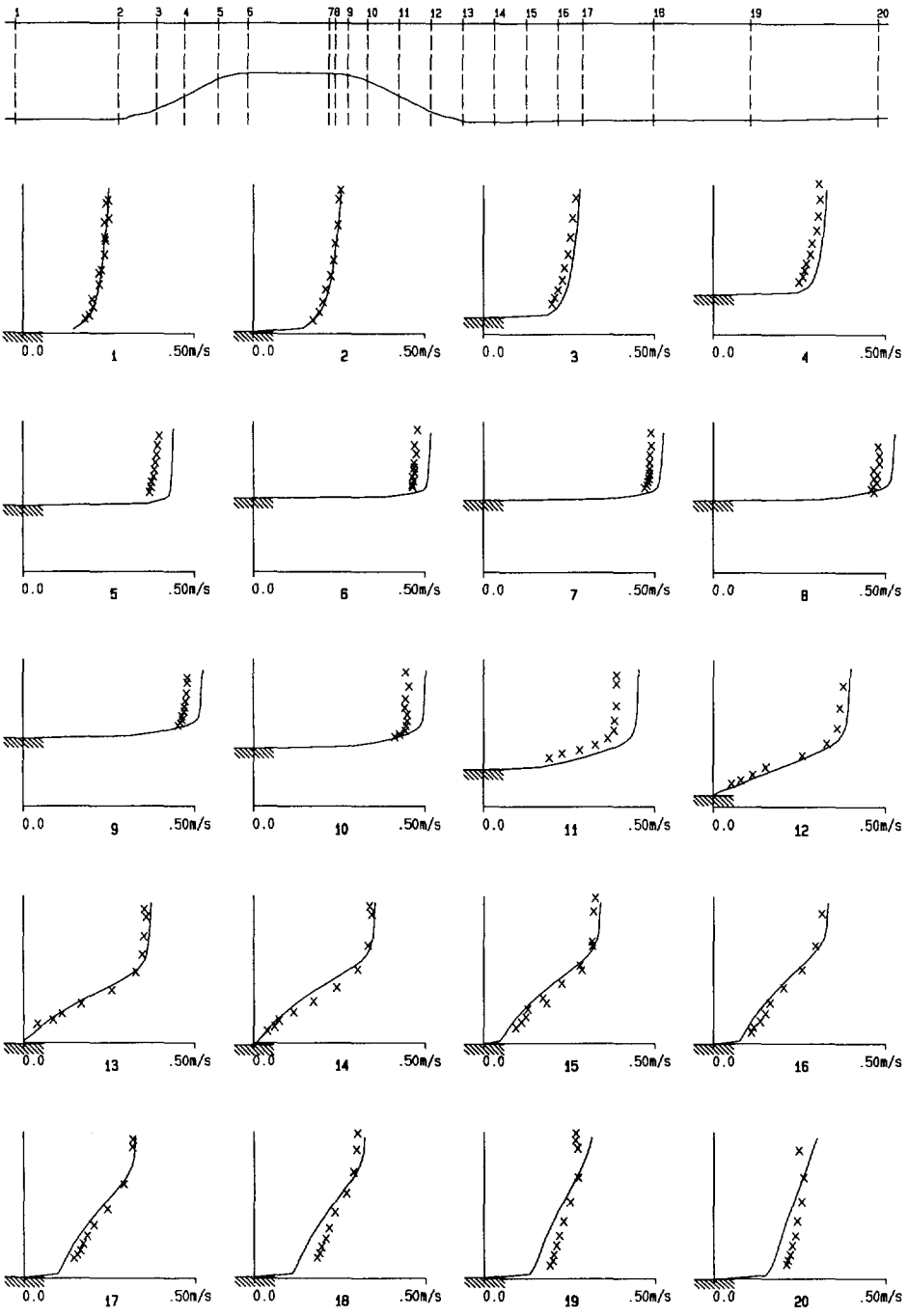

Figure 4.4.4 The measured and calculated horizontal velocity
× measurements, —— calculations PHOENICS.

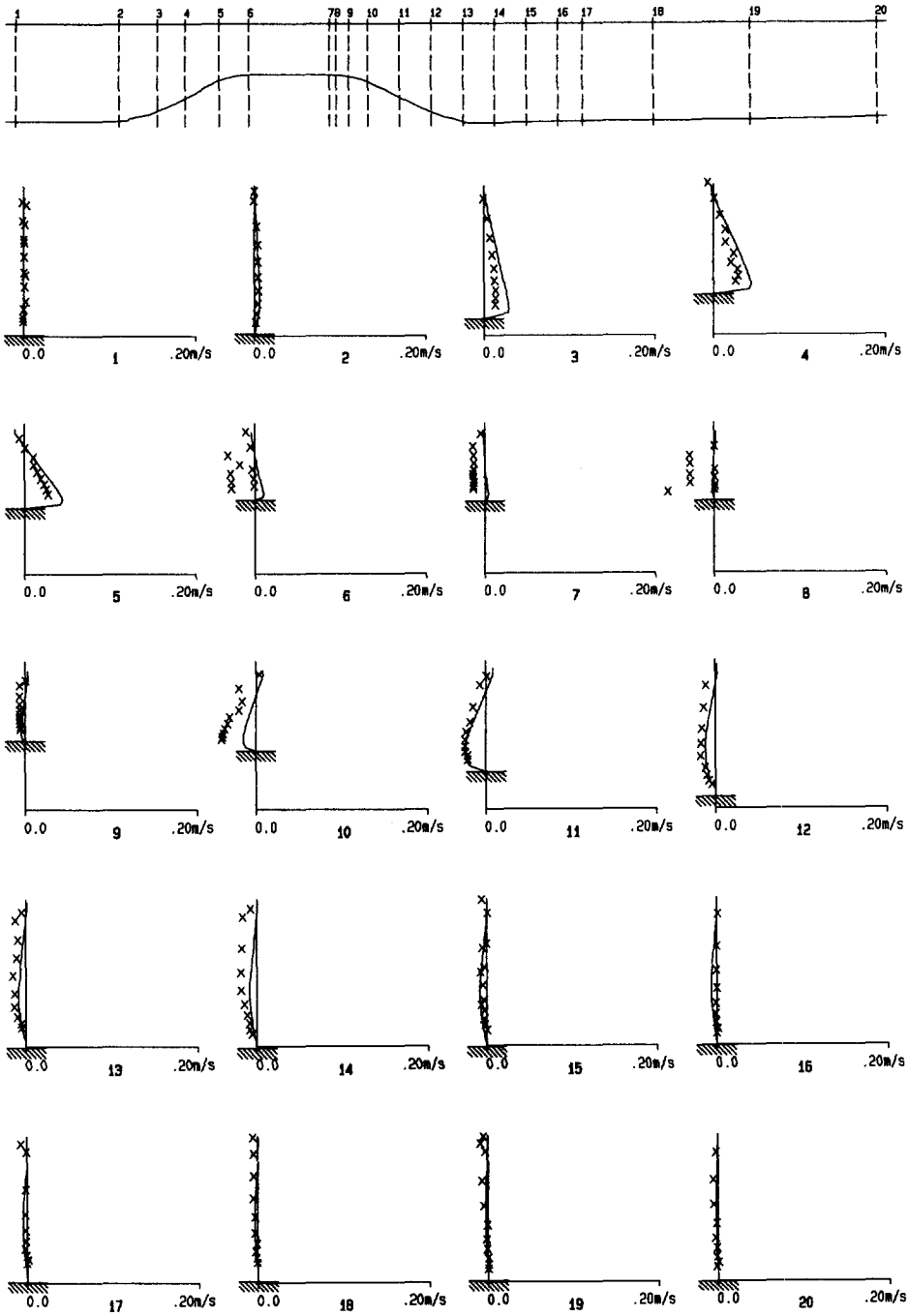

Figure 4.4.5 The measured and calculated vertical velocity
× measurements, —— calculations PHOENICS.

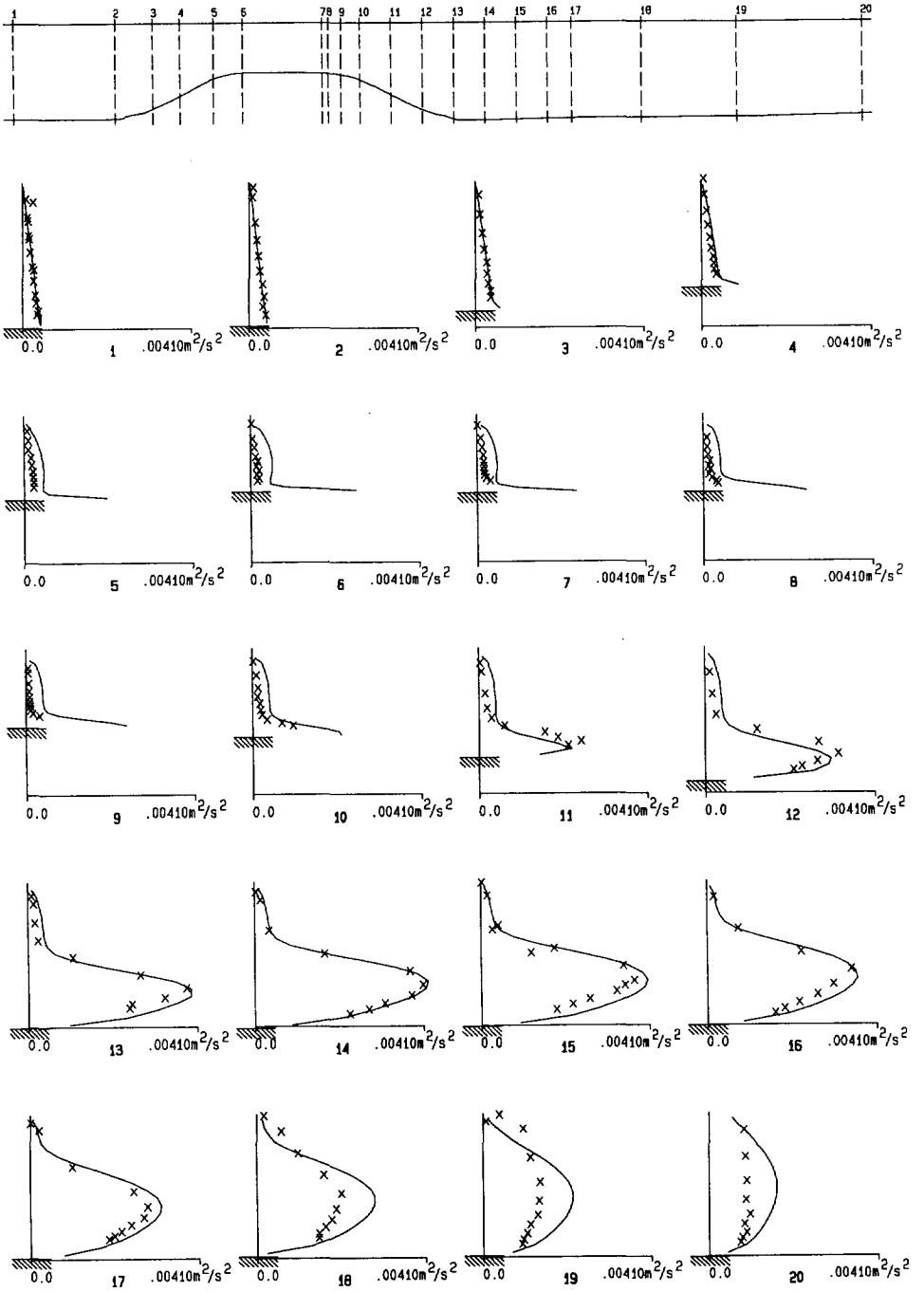

Figure 4.4.6 The measured and calculated turbulence energy
× measurements, —— calculations PHOENICS.

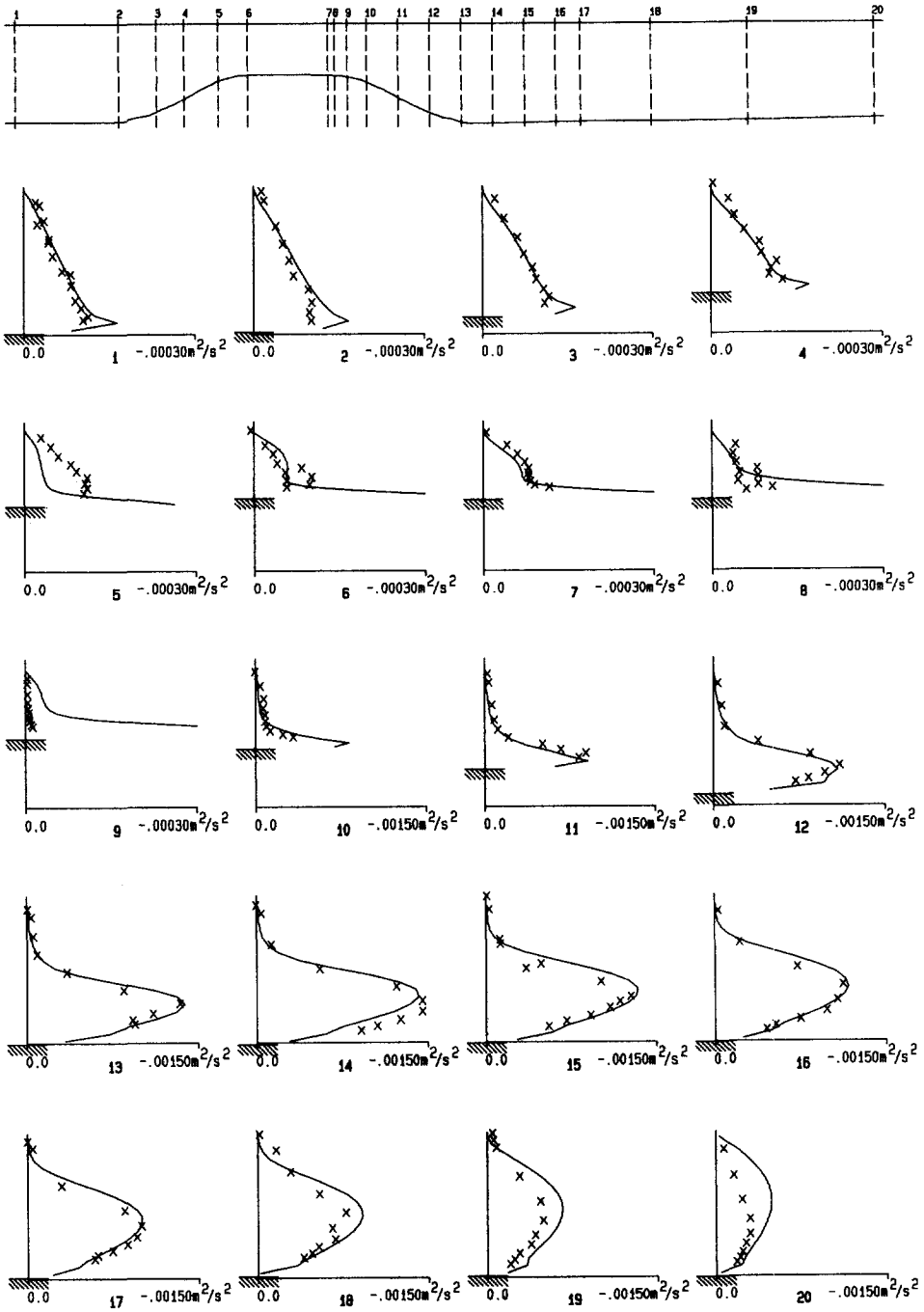

Figure 4.4.7 The measured and calculated Reynolds shear stresses
× measurements, —— calculations PHOENICS.

5. Improved 2DH shallow-water equations

5.1 Introduction

In this chapter a proposal is made to improve the 2DH (two-dimensional horizontal) shallow-water equations. These improvements are based on the results described in the previous chapters. Coefficients in the convection and friction terms of the 2DH shallow-water equations are derived by using a method based on the method of weighted residuals described in section 2.3. Only the derivation of the 2DH shallow-water equations is presented in this chapter. A verification of the 2DH solutions against the three-dimensional solutions is not carried out.

5.2 Governing equations

Starting points are the 3D (three-dimensional) continuity equation and Navier-Stokes equations. Some of the terms in these equations are neglected because they are small in comparison to the other terms; others are temporarily left out because they require no modifications (derivatives to the time, t). The neglected terms are the viscous shear stress terms, the Reynolds normal stress terms and some of the Reynolds shear stress terms. In the equation for vertical momentum the convection terms are also neglected. The remaining set of equations reads:

$$\frac{\partial u}{\partial x}+\frac{\partial v}{\partial y}+\frac{\partial w}{\partial z} = 0 \tag{5.2.1}$$

$$u\frac{\partial u}{\partial x}+v\frac{\partial u}{\partial y}+w\frac{\partial u}{\partial z}+\frac{1}{\rho}\frac{\partial p}{\partial x} = -\frac{1}{\rho}\frac{\partial \tau_{xz}}{\partial z} \tag{5.2.2a}$$

$$u\frac{\partial v}{\partial x}+v\frac{\partial v}{\partial y}+w\frac{\partial v}{\partial z}+\frac{1}{\rho}\frac{\partial p}{\partial y} = -\frac{1}{\rho}\frac{\partial \tau_{yz}}{\partial z} \tag{5.2.2b}$$

$$\frac{1}{\rho}\frac{\partial p}{\partial z}+g = 0 \tag{5.2.2c}$$

with the boundary conditions:

$$p = 0 \qquad \text{at } z = z_b+d \tag{5.2.3a}$$

$$u\frac{\partial(z_b+d)}{\partial x}+v\frac{\partial(z_b+d)}{\partial y}-w = 0 \qquad \text{at } z = z_b+d \tag{5.2.3b}$$

$$\tau_{xz} = 0 \qquad \text{at } z = z_b+d \tag{5.2.3c}$$

$$\tau_{yz} = 0 \qquad \text{at } z = z_b + d \tag{5.2.3d}$$

$$u\frac{\partial z_b}{\partial x} + v\frac{\partial z_b}{\partial y} - w = 0 \qquad \text{at } z = z_b \tag{5.2.3e}$$

plus a slip / partial-slip / no-slip condition at $z = z_b$

The coefficients needed to improve the shallow-water equations are derived by using the results of the method of weighted residuals, described in section 2.3. The logarithmic velocity profiles (eq. (2.3.25b) and eq. (2.3.26) are used in the acceleration zone, while eq. (2.3.36) is used in the deceleration zone) are used for the horizontal velocity in x-direction, u, as well as for the horizontal velocity in y-direction, v. The profile of the vertical velocity can be derived by substituting these expressions for the horizontal velocity into eq. (5.2.1). The horizontal velocity profiles used read (see eq. (2.3.25b), eq. (2.3.26) and eq. (2.3.36)):

$$u = u_0 + \Gamma_x u_1 \text{ and } v = v_0 + \Gamma_y v_1 \tag{5.2.4a}$$

$$\text{with} \quad \frac{u_0}{\bar{u}} = \frac{v_0}{\bar{v}} = \frac{\ln\left((z-z_b)/z_0\right)}{\ln\left(d/(ez_0)\right)} \tag{5.2.4b}$$

in the acceleration zone:

$$\frac{u_1}{\bar{u}} = \frac{v_1}{\bar{v}} = \frac{\ln^2\left((z-z_b)/z_0\right)}{\left(\ln^2\left(d/z_0\right) - 2\ln\left(d/z_0\right) + 2\right)} - \frac{\ln\left((z-z_b)/z_0\right)}{\ln\left(d/(ez_0)\right)} \tag{5.2.4c}$$

and in the deceleration zone:

$$\begin{aligned}\frac{u_1}{\bar{u}} = \frac{v_1}{\bar{v}} = {} & \frac{\ln^3\left((z-z_b)/z_0\right) - 5\ln^2\left((z-z_b)/z_0\right)}{3\left(\ln^3\left(d/z_0\right) - 8\ln^2\left(d/z_0\right) + 16\ln\left(d/z_0\right) - 16\right)} + \\ & + \frac{10}{9}\left(\frac{z-z_b}{d}\right)^2\left(3\left(\frac{z-z_b}{d}\right)^2 - 8\left(\frac{z-z_b}{d}\right) + 6\right) - \frac{\ln\left((z-z_b)/z_0\right)}{\ln\left(d/(ez_0)\right)}\end{aligned} \tag{5.2.4d}$$

in which $\bar{u}$ and $\bar{v}$ are the depth-averaged horizontal velocities in x- and y-direction, respectively and Γ_x and Γ_y are the parameters determining the magnitude of the perturbation profiles u_1 and v_1, respectively.

The Reynolds shear stresses are described using the Boussinesq approximation:

$$\tau_{xz} = -\rho\,\nu_t\frac{\partial u}{\partial z} \tag{5.2.5a}$$

$$\text{and} \quad \tau_{yz} = -\rho\,\nu_t\frac{\partial v}{\partial z} \tag{5.2.5b}$$

in which ν_t is the eddy-viscosity. A lot of different models can be used to prescribe the eddy-

viscosity. Here, the parabolic eddy-viscosity model is used. The 3D parabolic eddy-viscosity model is based on the 2DV (two-dimensional vertical) one described in chapter 2 (eq. (2.3.28)). The 3D eddy-viscosity used reads:

$$\nu_t = \frac{\sqrt{\bar{u}^2 + \bar{v}^2}}{\ln(d/(ez_0))} \kappa^2 (z - z_b)\left(1 - \frac{z - z_b}{d}\right)$$

Before substituting the horizontal velocity profiles and the approximations for the Reynolds shear stresses into the continuity and momentum equations, the continuity equation, eq. (5.2.1), multiplied by the horizontal velocity, u, is added to eq. (5.2.2a) and multiplied by the horizontal velocity, v, added to eq. (5.2.2b). To obtain the shallow-water equations the equations eq. (5.2.1) and eq. (5.2.2) have to be integrated with respect to the depth.

Integration of eq. (5.2.2c) yields the hydrostatic water pressure distribution:

$$p = \rho g (d + z_b - z) \tag{5.2.6}$$

Substitution of the velocity profiles, eq. (5.2.4) the Reynolds shear stresses, eq. (5.2.5), and the water pressure distribution, eq. (5.2.6), in the continuity equation, eq. (5.2.1) and in the momentum equations, eq. (5.2.2a) and eq. (5.2.2b), yields, after integration of eq. (5.2.1), eq. (5.2.2a) and eq. (5.2.2b) and substitution of the boundary conditions, eq. (5.2.3b) and eq. (5.2.3e):

$$\frac{\partial d\bar{u}}{\partial x} + \frac{\partial d\bar{v}}{\partial y} = 0 \tag{5.2.7a}$$

$$\frac{\partial}{\partial x}\left(\alpha_{xx} d \bar{u}^2\right) + \frac{\partial}{\partial y}\left(\alpha_{xy} d \bar{v} \bar{u}\right) + g d \frac{\partial (z_b + d)}{\partial x} + \gamma_x \lambda \bar{u}\sqrt{\bar{u}^2 + \bar{v}^2} = 0 \tag{5.2.7b}$$

$$\frac{\partial}{\partial x}\left(\alpha_{xy} d \bar{u} \bar{v}\right) + \frac{\partial}{\partial y}\left(\alpha_{yy} d \bar{v}^2\right) + g d \frac{\partial (z_b + d)}{\partial y} + \gamma_y \lambda \bar{v}\sqrt{\bar{u}^2 + \bar{v}^2} = 0 \tag{5.2.7c}$$

with

$$\alpha_{xx} = S_{10} + \Gamma_x S_{11} + \Gamma_x^2 S_{12} \tag{5.2.7d}$$

$$\alpha_{xy} = S_{10} + \tfrac{1}{2}(\Gamma_x + \Gamma_y) S_{11} + \Gamma_x \Gamma_y S_{12} \tag{5.2.7e}$$

$$\alpha_{yy} = S_{10} + \Gamma_y S_{11} + \Gamma_y^2 S_{12} \tag{5.2.7f}$$

$$\gamma_x = 1 - \Gamma_x \tag{5.2.7g}$$

$$\gamma_y = 1 - \Gamma_y \tag{5.2.7h}$$

in which α_{xx}, α_{xy} and α_{yy} are momentum convection coefficients, γ_x and γ_y are correction coefficients in the bottom friction terms and λ is a resistance parameter. The coefficients S_{10},

S_{11} and S_{12} are already defined in eq. (2.3.30) through eq. (2.3.33) and eq. (2.3.37) for the velocity profiles used, eq. (5.2.4). The only unknown variables are the parameters Γ_x and Γ_y, determining the magnitude of the perturbation terms in u and v, respectively. In the following a method is described to estimate these parameters.

5.3 Determination of velocity profile parameters

The set of modified shallow-water equations, eq. (5.2.7), contains only three equations for five unknown variables; the water depth d, the depth-averaged horizontal velocities $\bar{u}$ and $\bar{v}$, and the profile parameters Γ_x and Γ_y. Therefore two additional equations are needed to solve for these two parameters, but only one equation is available, the energy equation. However, an approximate solution, valid for mild slopes, can be obtained. The method of weighted residuals is only valid for mild slopes, with a maximum slope gradient of $^1/_5$, say. For such slopes the assumption is made that the velocities in all points of each vertical are coplanar. This implies that the two parameters Γ_x and Γ_y have the same value, $\Gamma_x = \Gamma_y = \Gamma$, and only one additional differential equation is required to solve for this parameter. This simplification also influences the momentum equations. These equations now read:

$$\alpha\left(\bar{u}\frac{\partial \bar{u}}{\partial x}+\bar{v}\frac{\partial \bar{u}}{\partial y}\right)+\bar{u}^2\frac{\partial \alpha}{\partial x}+\bar{u}\,\bar{v}\frac{\partial \alpha}{\partial y}+g\frac{\partial(z_b+d)}{\partial x}+\gamma\frac{\lambda\,\bar{u}\sqrt{\bar{u}^2+\bar{v}^2}}{d}=0 \qquad (5.3.1a)$$

$$\alpha\left(\bar{u}\frac{\partial \bar{v}}{\partial x}+\bar{v}\frac{\partial \bar{v}}{\partial y}\right)+\bar{u}\,\bar{v}\frac{\partial \alpha}{\partial x}+\bar{v}^2\frac{\partial \alpha}{\partial y}+g\frac{\partial(z_b+d)}{\partial y}+\gamma\frac{\lambda\,\bar{v}\sqrt{\bar{u}^2+\bar{v}^2}}{d}=0 \qquad (5.3.1b)$$

with $$\alpha = S_{10}+\Gamma S_{11}+\Gamma^2 S_{12} \qquad (5.3.1c)$$

$$\gamma = 1-\Gamma \qquad (5.3.1d)$$

The 3D energy equation reads:

$$u^2\frac{\partial u}{\partial x}+u\,v\frac{\partial u}{\partial y}+uw\frac{\partial u}{\partial z}+\frac{u}{\rho}\frac{\partial p}{\partial x}+\frac{u}{\rho}\frac{\partial \tau_{xz}}{\partial z}+vu\frac{\partial v}{\partial x}+$$
$$+v^2\frac{\partial v}{\partial y}+vw\frac{\partial v}{\partial z}+\frac{v}{\rho}\frac{\partial p}{\partial y}+\frac{v}{\rho}\frac{\partial \tau_{yz}}{\partial z}+\frac{w}{\rho}\frac{\partial p}{\partial z}+wg=0$$

To integrate this equation with respect to the depth, the continuity equation, eq. (5.2.1), multiplied by the term $\left(\frac{1}{2}u^2+\frac{1}{2}v^2+g(z_b+d)\right)$ is added. This yields:

$$\int_{z_b}^{z_b+d}\left\{\frac{1}{2}\left(\frac{\partial u^3}{\partial x}+\frac{\partial u^2 v}{\partial y}+\frac{\partial u^2 w}{\partial z}+\frac{\partial u v^2}{\partial x}+\frac{\partial v^3}{\partial y}+\frac{\partial v^2 w}{\partial z}\right)+\right.$$

$$\left.+g\frac{\partial(z_b+d)u}{\partial x}+g\frac{\partial(z_b+d)v}{\partial y}+\frac{u}{\rho}\frac{\partial \tau_{xz}}{\partial z}+\frac{v}{\rho}\frac{\partial \tau_{yz}}{\partial z}+g(z_b+d)\frac{\partial w}{\partial z}\right\}dz=0$$

Simplification of this equation and substitution of the boundary conditions, eq. (5.2.3b) and eq. (5.2.3e), yields:

$$\frac{1}{2}\left(\frac{\partial}{\partial x}\int_{z_b}^{z_b+d}u^3dz+\frac{\partial}{\partial y}\int_{z_b}^{z_b+d}u^2 v dz+\frac{\partial}{\partial x}\int_{z_b}^{z_b+d}u v^2 dz+\frac{\partial}{\partial y}\int_{z_b}^{z_b+d}v^3 dz\right)+$$

$$+g\frac{\partial}{\partial x}\int_{z_b}^{z_b+d}(z_b+d)u dz+g\frac{\partial}{\partial y}\int_{z_b}^{z_b+d}(z_b+d)v dz+\int_{z_b}^{z_b+d}\frac{u}{\rho}\frac{\partial \tau_{xz}}{\partial z}dz+\int_{z_b}^{z_b+d}\frac{v}{\rho}\frac{\partial \tau_{yz}}{\partial z}dz=0$$

Substitution of the velocity profiles, eq. (5.2.4), gives the depth-averaged energy equation:

$$\beta\left(\bar{u}^2\frac{\partial \bar{u}}{\partial x}+\bar{u}\bar{v}\frac{\partial \bar{u}}{\partial y}+\bar{u}\bar{v}\frac{\partial \bar{v}}{\partial x}+\bar{v}^2\frac{\partial \bar{v}}{\partial y}\right)+\frac{1}{2}(\bar{u}^3+\bar{u}\bar{v}^2)\frac{\partial \beta}{\partial x}+$$

$$+\frac{1}{2}(\bar{v}^3+\bar{u}^2\bar{v})\frac{\partial \beta}{\partial y}+g\bar{u}\frac{\partial(z_b+d)}{\partial x}+g\bar{v}\frac{\partial(z_b+d)}{\partial y}+\frac{\gamma_1\lambda}{d}(\bar{u}^2+\bar{v}^2)^{(3/2)}=0 \qquad (5.3.2a)$$

with $\beta = S_{20}+\Gamma S_{21}+\Gamma^2 S_{22}+\Gamma^3 S_{23}$ (5.3.2b)

$\gamma_1 = S_{30}+\Gamma S_{31}+\Gamma^2 S_{32}$ (5.3.2c)

The four differential equations (5.2.7a), (5.3.1) and (5.3.2) together form a set of modified 2DH equations, from which the four unknown variables $\bar{u}$, $\bar{v}$, d and Γ can be solved.

5.4 Generalisation

The modified shallow-water equations presented above are for steady flow, derived from the three-dimensional Navier-Stokes and continuity equations. In this derivation some terms in the Navier-Stokes equations are neglected because these terms are small in comparison to the others: others are temporarily left out. In this section the terms temporarily left out are added to the shallow-water equations and the neglected terms are discussed.

In case of unsteady flow situations the transient terms have to be included, but these do not require modifications due to flow non-uniformity.

In the equation of vertical momentum nearly all the terms are neglected. Only the pressure term and the gravitational acceleration remain. Solving this momentum equation yields the hydrostatic pressure distribution. Adding the convection and Reynolds stress terms gives a slight change of the hydrostatic pressure distribution. The momentum equation containing these terms is solved in the flow-simulation system PHOENICS. In calculations of 2DV flows the deviations from the hydrostatic pressure are very small (chapter 3). This deviation is expressed in the pressure coefficient, ζ. The values of ζ hardly differ from the value $\zeta=1$, which value corresponds to the hydrostatic pressure distribution. Therefore it is not necessary to use this coefficient and the pressure can be approximated as hydrostatic.

Some of the Reynolds stress terms are also neglected in the derivation of the shallow-water equations. This simplification is not allowed in all cases. The so-called effective stresses (Flokstra [1977]), τ_{xx}, τ_{xy} and τ_{yy}, have to be used in flows to improve the horizontal diffusion. These effective stresses are important in flows with circulation (Flokstra [1977]). The effective stresses consist of three distribution: viscous stresses, Reynolds stresses (the ones omitted in the previous sections) and stresses due to depth integration of the tree-dimensional convective terms. The first part can be neglected while the third part is already taken into account using the convection coefficients α and β. The remaining part of the effective stresses can be approximated by:

$$\frac{1}{\rho}\tau_{ij} = \nu_L\left(\frac{\partial \bar{u}_i}{\partial x_j}+\frac{\partial \bar{u}_j}{\partial x_i}-\frac{1}{2}\frac{\partial \bar{u}_i}{\partial x_i}\delta_{ij}\right)$$

in which i and j stand for x or y in the summation convention, and δ_{ij} is the Kronecker delta. The ν_L is horizontal viscosity, of which the value is not exactly known.

The boundary values chosen for the Reynolds shear stresses τ_{xz} and τ_{yz} at the water surface are $\tau_{xz}=\tau_{yz}=0$. This boundary value is not correct in all situations, because the wind can exert a shear stress on the water surface. This can be taken into account by adding a water surface stress term to the equations.

Due to the rotation of the earth a translation acceleration occurs in the flow, yielding an extra term in both momentum equations in horizontal direction. This acceleration is called the Coriolis acceleration.

Substitution of the transient terms, the neglected Reynolds stress terms (the effective stress terms), the Coriolis acceleration, but still assuming hydrostatic water pressure distribution, yields for the 2DH shallow-water equations:

$$\frac{\partial d}{\partial t}+\frac{\partial d\bar{u}}{\partial x}+\frac{\partial d\bar{v}}{\partial y}=0$$

$$\frac{\partial d\bar{u}}{\partial t}+\frac{\partial \alpha d\bar{u}^2}{\partial x}+\frac{\partial \alpha d\bar{v}\bar{u}}{\partial y}-f\bar{v}+gd\frac{\partial(z_b+d)}{\partial x}-\frac{1}{\rho}\tau_{wx}+\gamma\lambda\bar{u}\sqrt{\bar{u}^2+\bar{v}^2}+\frac{1}{\rho}\left(\frac{\partial d\tau_{xx}}{\partial x}+\frac{\partial d\tau_{xy}}{\partial y}\right)=0$$

$$\frac{\partial d\bar{v}}{\partial t}+\frac{\partial \alpha d\bar{u}\bar{v}}{\partial x}+\frac{\partial \alpha d\bar{v}^2}{\partial y}+f\bar{u}+gd\frac{\partial(z_b+d)}{\partial y}-\frac{1}{\rho}\tau_{wy}+\gamma\lambda\bar{v}\sqrt{\bar{u}^2+\bar{v}^2}+\frac{1}{\rho}\left(\frac{\partial d\tau_{xy}}{\partial x}+\frac{\partial d\tau_{yy}}{\partial y}\right)=0$$

$$\frac{1}{2}\left(\frac{\partial \alpha d\bar{u}^2}{\partial t}+\frac{\partial \alpha d\bar{v}^2}{\partial t}+\frac{\partial \beta d\bar{u}^3}{\partial x}+\frac{\partial \beta d\bar{u}^2\bar{v}}{\partial y}+\frac{\partial \beta d\bar{u}\bar{v}^2}{\partial x}+\frac{\partial \beta d\bar{v}^3}{\partial y}\right)+gd\bar{u}\frac{\partial d+z_b}{\partial x}+gd\bar{v}\frac{\partial d+z_b}{\partial y}+$$
$$+\frac{\bar{u}d}{\rho}\tau_{wx}+\frac{\bar{v}d}{\rho}\tau_{wy}+\gamma_1\lambda\left(\bar{u}^2+\bar{v}^2\right)^{(3/2)}+\frac{\bar{u}}{\rho}\left(\frac{\partial d\tau_{xx}}{\partial x}+\frac{\partial d\tau_{xy}}{\partial y}\right)+\frac{\bar{v}}{\rho}\left(\frac{\partial d\tau_{xy}}{\partial x}+\frac{\partial d\tau_{yy}}{\partial y}\right)=0$$

with $\alpha = S_{10}+\Gamma S_{11}+\Gamma^2 S_{12}$

$\gamma = 1-\Gamma$

$\beta = S_{20}+\Gamma S_{21}+\Gamma^2 S_{22}+\Gamma^3 S_{23}$

$\gamma_1 = S_{30}+\Gamma S_{31}+\Gamma^2 S_{32}$

$\tau_{xx} = -\rho\nu_L\left(\frac{3}{2}\frac{\partial\bar{u}}{\partial x}\right)$

$\tau_{xy} = -\rho\nu_L\left(\frac{\partial\bar{u}}{\partial y}+\frac{\partial\bar{v}}{\partial x}\right)$

$\tau_{yy} = -\rho\nu_L\left(\frac{3}{2}\frac{\partial\bar{v}}{\partial y}\right)$

The coefficients S_{10} until S_{32} are defined in eq. (2.3.30) through eq. (2.3.33) and eq. (2.3.37) for the velocity profiles used, eq. (5.2.4).

Discussion

In this chapter a method has been described to improve the 2DH shallow-water equations. The principal advantage of the method developed here is that the water levels just downstream from the sill can be simulated more realistically in comparison to water levels calculated using a method based on the ordinary shallow-water equations. Due to the more realistic water levels the depth-averaged velocities calculated are more realistic too. The parameter Γ also appears in the friction terms, causing additional dependency of the bottom friction on the bottom bathymetry. This is relevant to sediment transport modelling.

The solutions found for the convection and friction coefficients are dependent on the velocity profiles chosen a priori. Additional research has still to be done to find improved estimates for these velocity profiles.

The coefficients of the friction terms can be improved by the choice of a better eddy-viscosity model in the description of the Reynolds shear stress terms. The parabolic viscosity model used is dependent on the depth-averaged velocity. In flows over sills the depth-averaged velocity increases in the acceleration zone, yielding an increased value of the eddy-viscosity. This effect is in contrast to the effect appearing in numerical calculations, carried out with the flow-simulation system PHOENICS (chapter 3) using a ke-viscosity model. In these calculations the maximum value of the eddy-viscosity in a vertical decreases in the acceleration zone due to the suppression of the turbulence fluctuations in this zone. The bottom shear stress derived by a ke-viscosity model is larger than the one derived by a parabolic viscosity model in the acceleration zone. In the deceleration zone the maximum value of the eddy-viscosity in a particular vertical, calculated with the flow-simulation system PHOENICS, increases downstream but using a parabolic eddy-viscosity this maximum value decreases. In the deceleration zone the smaller eddy-viscosity causes a too slow conversion from a less uniform velocity profile to a more logarithm-like velocity profile.

6. Summary, conclusions and recommendations

Summary

The aims of this study were:

- To explain the differences in the water levels and flow velocities calculated with 2DH numerical models and the measured ones for flow over a sill,
- To modify the shallow-water equations (SWE) for flow over a sill.

In two-dimensional flow, uniform in transverse-direction (2DV flow), the most important effects of flow over a sill, adaptation of the velocity profile and separation, also appear. This flow was studied in this investigation. Conclusions from this investigation are given in this chapter. At the end of this chapter some recommendations are described.

Explanation

The SWE used nowadays, the "common" SWE, are derived for quasi-uniform flow situations, which means that the velocity profile occurring in uniform flows is assumed. In flow over sills the velocity profile changes (chapter 2,3,4). The vertical profile of the velocity becomes more uniform in the acceleration zone and less uniform in the deceleration zone. These changes also influence the pressure distribution, because the velocities appear in the Navier-Stokes equation in vertical direction. Changes in the velocity and pressure distribution cause adaptations of the depth-integrated terms in the Navier-Stokes equations, which can be expressed as modifications of the terms in the SWE.

Upstream from the sill, the velocity profile becomes more uniform. This influences the momentum flux as well as the bottom friction.

These influences are not described in the common SWE. Nevertheless, the water levels derived with these SWE agree well with the measured levels in the acceleration zone of the sill (chapter 1). Therefore, the overestimation of the increase in momentum flux in the acceleration zone appears to balance the underestimation of the friction in the common SWE. However, the changes in the velocity profile due to the acceleration can only be small because the velocity profile for uniform flow is a nearly constant profile in vertical direction. (For uniform turbulent flows the velocity profile can be described by a logarithm.) This means that the changes in the friction term in the SWE in the acceleration zone are not very important in comparison to the changes in the convective term.

The changes in the velocity profile can be large in the deceleration zone. On steep

slopes the velocity profile can be come nearly triangular. In this zone the convective terms in the SWE should be much larger than the convective terms in the common SWE, due to these changes in the velocity profile. This means that the momentum flux in the common SWE is underestimated, while the friction is overestimated. (The gradient of the velocity profile near the bottom is smaller than assumed, which causes smaller values for the friction.) But the influence of the changes in the bottom friction is less important. Therefore the adverse pressure gradient in the deceleration zone is overestimated, resulting in too high water levels just behind the sill.

Modifications of shallow-water equations.

In the present study, modifications of the common SWE have been attempted so as to increase the similarity between the predicted water levels and the ones measured in the prototype. Only modifications for the 1DH SWE were derived. These modifications were expressed in coefficients: α in the convective term, ζ in the pressure term, and γ in the friction term (eq. (3.4.2)). Different methods are used to obtain these coefficients: two analytic methods in chapter 2, one numerical method in chapter 3.

The first analytic method used was the method of asymptotic expansions. Coefficients derived with this method were only valid for extremely mild slopes.

The second analytic method used was the method of weighted residuals. In this method the velocity profile is prescribed by a parabolic or a logarithmic zeroth-order velocity profile for uniform flow to which a first-order perturbation velocity profile is added. The magnitude of this first-order profile is determined by a profile parameter. The magnitude of this profile parameter and the elevation of the water level are obtained from a set of coupled differential equation. These differential equations arose by rewriting the depth-integrated momentum and energy equations. This method is applicable up to slopes of $^1/_5$.

The numerical method was described in chapter 3. The velocity and pressure distributions needed to calculate the coefficients were obtained from 2DV computations with the flow-simulation system PHOENICS of CHAM Ltd.

To verify the flow-simulation system PHOENICS, results of a computation were compared with results of laser-Doppler velocity measurements in a flume (chapter 4). The agreement between the measured and the calculated velocities is good, which proves the reliability of the velocities and water levels obtained from the 2DV numerical model.

The water levels calculated with modified SWE (i.e. the SWE in which the coefficients obtained from the 2DV numerical calculations were applied) agree very well with

the water levels obtained from the 2DV numerical model (chapter 3).

The influence of the pressure coefficient is very small, even for steep slopes or high Froude numbers. This means that the pressure distribution on the sill can be approximated by the hydrostatic pressure distribution, despite local accelerations or decelerations.

The agreement between the convection coefficient obtained analytically and the one obtained with results from the 2DV numerical model is quite good. The agreement between the friction coefficients is not so good. Despite the deviations between the modification coefficients derived in different ways, the agreement between the water levels was good.

Finally, a tentative proposal has been made to improve the 2DH SWE (chapter 5).

Conclusions

In brief the main conclusions of this investigation are:

- The reproduction of the water levels with the common SWE is good in the acceleration zone because the underestimation of the bottom friction balances the overestimation of the change in momentum flux. The reproduction of the water levels in the deceleration zone with the common SWE is not good because the underestimation of the momentum flux is not balanced by the overestimation of the bottom friction. This underestimation of the convective terms causes an overestimation of the upward pressure gradient, which leads to too high water levels downstream from the sill and to wrong depth-averaged velocities.
- The pressure distribution on the sill can very well be approximated by the hydrostatic pressure distribution, even for slopes up to $^1/_5$ and high Froude numbers. This means that the pressure coefficient can be taken equal to 1.
- Modifications of the SWE with convection and friction coefficients improve the water levels in the deceleration zone in comparison to the water levels derived with the common SWE.
- For mild slopes (up to about $^1/_{20}$) the friction coefficient is the most important coefficient to be applied in the modified SWE. For steep slopes (maximum slope steeper than $^1/_{10}$) the convection coefficient is the most important coefficient to be applied in these SWE.
- The method of weighted residuals gives a fairly good approximation for the convection and friction coefficients. This method is applicable up to slopes $^1/_5$.

The method of weighted residuals has only been applied for 1DH SWE with a few, velocity profiles. Additional work has still to be done to find improved estimates for the

velocity profiles and to make this method suitable for 2DH SWE. Therefore some recommendations are given.

Recommendations.

The 1DH SWE with modifications obtained from results of 2DV calculations has been proven to represent the physics in an acceptable manner. Consequently it was justified to enter the next phase of application, the analytical derivation of these modification in the SWE. At this stage a method to obtain the modifications has been presented, the method of weighted residuals.

The modifications in the 1DH SWE obtained from the method of weighted residuals are dependent on the assumed velocity profile and eddy-viscosity model. In the deceleration zone the horizontal velocity near the bottom obtained from the method of weighted residuals was too large and downstream from the sill the bottom shear stress obtained by this method was too small in comparison to these quantities obtained from 2DV calculations. Therefore it will be necessary to investigate:

- The similarity velocity profiles to be used in the method of weighted residuals.
- The improvement of the bottom shear stress by means of other eddy-viscosity models, allowing for acceleration or deceleration of the flow.

In chapter 5 a proposal is presented to apply the method of weighted residuals for 2DH SWE. The shape of the velocity profile in this method is determined by a profile parameter. The additional equation to derive this profile parameter is the depth-integrated energy equation. Unfortunately, only one profile parameter can be solved using this energy equation, while two velocity profiles have to be obtained, one in x-direction and one in y-direction. The simplifying assumption was made that the velocities in all points of each vertical are in one plane. To relax this restriction a second profile parameter has to be derived analytically, or additional coefficients or terms, like the effective stresses, have to be introduced. Therefore it will be necessary to investigate:

- The method of weighted residuals for 2DH flows.
- Analytic approximations for the profile parameter.
- The use of two differently derived profile parameters.
- The use of additional coefficients or terms to simulate non-planar vertical velocity distribution.

7. References

Abramovich, G.N. (1963). *The theory of turbulent jets.* MIT Press.

Akkermans, G.J. (1984). *Discharge characteristics and flow pattern near barriers* (in Dutch). Report S431/S643, Delft Hydraulics.

Blom, P. (1988). *The one-dimensional steady-state shallow-water equation.* Internal Report, Delft University of Technology.

Boussinesq, J. (1877). "Test on the theory of flowing waters." (in French) *Mémoires présentés par divers savants à l'académie royale des science de l'institute imperial de France*, Paris, **23**, 46.

Cardoso, A.H., Graf, W.H. & Gust, G. (1991). "Steady gradually accelerating flow in a smooth open channel." *Journal of hydraulic research*, Vol. 29, **4**, 525-543.

Dyke, M. van (1963). *Perturbation methods in fluid mechanics.* Parabolic Press.

Elvius, T. & Sundström, A. (1973). "Computationally efficient schemes and boundary conditions for a fine-mesh barotropic model based on the shallow-water equations." *Tellus XXV*, **25**, 132-156.

Fischer, H.B., List, E.J., Koh, R.C.Y., Imberger, J. & Brooks, N.H. (1979). *Mixing in inland and coastal waters.* Academic Press.

Flokstra, C. (1977). "The closure problem for depth-averaged two-dimensional flow." *Proceedings XVIIth IAHR Congress*, Baden-Baden, Vol 2, **A106**, 247-257.

Gustafssen, B. (1971). "An alternating implicit method for solving the shallow-water equations." *Journal of Computational Physics*, **7**, 239-254.

Hinze, J.O. (1975). *Turbulence.* McGraw-Hill Book Company.

Hossain, M.S. (1980). *Mathematical modelling of turbulent buoyancy flows.* (in German) Ph. D. Thesis, University of Karlsruhe.

Jackson, P.S. & Hunt, J.C.R. (1975). "Turbulent wind flow over a low hill." *Quarterly Journal of the Royal Meteorologic Society*, **101**, 929-955.

Johnson, R. (1981). *Three-dimensional wind flow over hills; model tests in a boundary layer wind tunnel*, Ph. D. Thesis, Cranfield Institute of Technology, Aerodynamics Department.

Kármán, T. von (1930). "Mechanical similarity and turbulence." (in German) *Nachrichten von der Gesellschalten der Wissenschaften zu Göttingen*, Mathematisch Physikalische Klasse, 56-76.

Launder, B.E. & Spalding, D.B. (1972). *Mathematical models of Turbulence.* Academic Press.

Leendertse, J.J. (1970). *A water-quality simulation model for well-mixed estuaries and coastal seas.* Volume I, Principles of Computation. Rand Corporation, Memorandum RM-6230-RC, Santa Monica.

Liepmann, H.W. & Laufer, J. (1947). "Investigation of free turbulent mixing." *N.A.C.A.* Tech. Note **1257**.

Madsen, P.A. & Svendsen I.A. (1983). "Turbulent bores and hydraulic jumps." *Journal of Fluid Mechanics*, **129**, 1-25.

Mierlo, M.C.L.M. van & Ruiter, J.C.C. de (1988). *Turbulence measurements above dunes.* Report Q789, Vol. I and II, Delft Hydraulics.

Nezu, I., (1977). *Turbulent Structures in open channel flow.* Ph. D. Thesis, Kyoto University.

Phillips, N.A. (1957). "A coordinate system having some special advantages for numerical forecasting." *Journal of Meteorology*, **14**, 184-185.

Rajaratnam, N. (1976). *Turbulent jets.* Elsevier.

Rodi W. (1980). *Turbulence models and their application in hydraulics.* State-of-the-art paper IAHR.

Rosten, H.I. & Spalding, D.B. (1987). *The PHOENICS reference manual.* Report TR/200, CHAM.

Rijkswaterstaat, (1989). *Storm surge barrier Eastern Scheldt.* Evaluation of water movement studies and construction of the barrier. Report PEGESS-N-89011, Rijkswaterstaat

Rijkswaterstaat, (1988). *Division of the Eastern Scheldt into compartments* (in Dutch). Evaluation of two-dimensional flow-calculations. Report Q 528, Vol IV, Rijkswaterstaat.

Schlichting, H. (1968). *Boundary layer theory.* Pergamson Press Ltd.

Stelling, G.S. (1984). *On the construction of computational methods for shallow-water flow problems.* Ph. D. Thesis. Delft University of Technology.

APPENDIX A Analytic approximations for the 2DV Navier-Stokes and the 1DH shallow-water equations by means of the method of asymptotic expansions

A.1 Introduction

In this appendix solutions of the 2DV (two-dimensional vertical) Navier-Stokes and continuity equations are determined using the method of asymptotic expansions. The 1DH (one-dimensional horizontal) shallow-water equations are derived by substituting these solutions into the Navier-Stokes and continuity equations, and integrating these equations with respect to the depth.

This appendix has been divided into four parts. The first part is this introduction. In the second part sets of equations with different orders of magnitude are derived. These sets are solved in the third and fourth parts. The difference between these last two parts is the eddy-viscosity model used in the computations. In the third part a constant eddy-viscosity model is used, while in the fourth part a model with a parabolic eddy-viscosity distribution is used. Both parts are divided into a section in which the equations are solved and into a section in which the 1DH shallow-water equations are derived.

A.2 Determination of the sets of equations with different order of magnitude.

To get these different sets of equations the set of equations (2.2.1) and (2.2.2) has to be written as a set of dimensionless equations. The dependent variables of this set of dimensionless equations are written as asymptotic expansions, through which it is possible to split this set of equations in sets of equations with different orders of magnitude. To simplify the calculations of the water depth, water pressure distributions and velocities a transformation is introduced.

The used set of dimensionless equations is the one in which the pressure term and the Reynolds shear stress terms are supposed to be of the same order of magnitude, the one valid for **gradually varied flows**. The used perturbation quantity is $\varepsilon = D/(\chi L)$. Therefore variables are scaled in the following way (see eq. (2.2.7)):

$$x^* = \frac{x}{L} \tag{A.2.1a}$$

$$z^* = \frac{z}{D} \tag{A.2.1b}$$

$$z_b^* = \frac{z_b}{D} \tag{A.2.1c}$$

$$d^* = \frac{d}{D} \tag{A.2.1d}$$

$$p^* = \frac{p}{P} = \frac{p}{\frac{\rho \chi L U^2}{D}} \tag{A.2.1e}$$

$$u^* = \frac{u}{U} \tag{A.2.1f}$$

$$w^* = \frac{w}{\frac{D}{L}U} \tag{A.2.1g}$$

$$\nu_t^* = \frac{\nu_t}{\chi U D} \tag{A.2.1h}$$

$$g^* = \frac{g}{\frac{\chi L U^2}{D^2}} \tag{A.2.1i}$$

Introducing these dimensionless variables, the dimensionless equations become (omitting the *) (see eq.(2.2.8) and eq. (2.2.9)):

$$\frac{\partial u}{\partial x} + \frac{\partial w}{\partial z} = 0 \tag{A.2.2}$$

$$\varepsilon\left(u\frac{\partial u}{\partial x} + w\frac{\partial u}{\partial z}\right) + \frac{\partial p}{\partial x} = 2\chi^2\varepsilon^2\frac{\partial}{\partial x}\left(\nu_t\frac{\partial u}{\partial x}\right) + \frac{\partial}{\partial z}\left(\nu_t\left(\frac{\partial u}{\partial z} + \chi^2\varepsilon^2\frac{\partial w}{\partial x}\right)\right) \tag{A.2.3a}$$

$$\chi^2\varepsilon^3\left(u\frac{\partial w}{\partial x} + w\frac{\partial w}{\partial z}\right) + \frac{\partial p}{\partial z} + g = \chi^2\varepsilon^2\frac{\partial}{\partial x}\left(\nu_t\left(\frac{\partial u}{\partial z} + \chi^2\varepsilon^2\frac{\partial w}{\partial x}\right)\right) + 2\chi^2\varepsilon^2\frac{\partial}{\partial z}\left(\nu_t\frac{\partial w}{\partial z}\right) \tag{A.2.3b}$$

Writing the variables u, w and p as asymptotic expansions (see eq. (2.1.1)), yields:

$$\frac{\partial}{\partial x}\left(u_0 + \varepsilon u_1 + \varepsilon^2 u_2 + \cdots\right) + \frac{\partial}{\partial z}\left(w_0 + \varepsilon w_1 + \varepsilon^2 w_2 + \cdots\right) = 0 \tag{A.2.4}$$

$$\begin{aligned}\varepsilon\Big[&(u_0 + \varepsilon u_1 + \varepsilon^2 u_2 + \cdots)\frac{\partial}{\partial x}\left(u_0 + \varepsilon u_1 + \varepsilon^2 u_2 + \cdots\right) + \\ &+ (w_0 + \varepsilon w_1 + \varepsilon^2 w_2 + \cdots)\frac{\partial}{\partial z}\left(u_0 + \varepsilon u_1 + \varepsilon^2 u_2 + \cdots\right)\Big] + \\ &+ \frac{\partial}{\partial x}\left(p_0 + \varepsilon p_1 + \varepsilon^2 p_2 + \cdots\right) = 2\chi^2\varepsilon^2\frac{\partial}{\partial x}\left(\nu_t\frac{\partial}{\partial x}\left(u_0 + \varepsilon u_1 + \varepsilon^2 u_2 + \cdots\right)\right) + \\ &+ \frac{\partial}{\partial z}\left(\nu_t\left(\frac{\partial}{\partial z}\left(u_0 + \varepsilon u_1 + \varepsilon^2 u_2 + \cdots\right) + \chi^2\varepsilon^2\frac{\partial}{\partial x}\left(w_0 + \varepsilon w_1 + \varepsilon^2 w_2 + \cdots\right)\right)\right)\end{aligned} \tag{A.2.5a}$$

$$\chi^2\varepsilon^3\Big((u_0+\varepsilon u_1+\varepsilon^2u_2+\cdots)\frac{\partial}{\partial x}\Big(w_0+\varepsilon w_1+\varepsilon^2w_2+\cdots\Big)+$$
$$+(w_0+\varepsilon w_1+\varepsilon^2w_2+\cdots)\frac{\partial}{\partial z}\Big(w_0+\varepsilon w_1+\varepsilon^2w_2+\cdots\Big)\Big)+$$
$$+\frac{\partial}{\partial z}\Big(p_0+\varepsilon p_1+\varepsilon^2p_2+\cdots\Big)+g\;=\qquad\text{(A.2.5b)}$$
$$=\chi^2\varepsilon^2\frac{\partial}{\partial x}\Big(\nu_t\Big(\frac{\partial}{\partial z}\Big(u_0+\varepsilon u_1+\varepsilon^2u_2+\cdots\Big)+\chi^2\varepsilon^2\frac{\partial}{\partial x}\Big(w_0+\varepsilon w_1+\varepsilon^2w_2+\cdots\Big)\Big)\Big)+$$
$$+2\chi^2\varepsilon^2\frac{\partial}{\partial z}\Big(\nu_t\frac{\partial}{\partial z}\Big(w_0+\varepsilon w_1+\varepsilon^2w_2+\cdots\Big)\Big)$$

The boundary conditions and the discharge condition, written in a dimensionless form, also have to be decomposed into asymptotic expansions. This yields for the boundary conditions:

$$p_0+\varepsilon p_1+\varepsilon^2p_2+\cdots\;=0\qquad\text{at } z=z_b+d_0+\varepsilon d_1+\varepsilon^2d_2+\cdots\qquad\text{(A.2.6a)}$$

$$(u_0+\varepsilon u_1+\varepsilon^2u_2+\cdots)\frac{\mathrm{d}}{\mathrm{d}x}\Big(z_b+d_0+\varepsilon d_1+\varepsilon^2d_2+\cdots\Big)-(w_0+\varepsilon w_1+\varepsilon^2w_2+\cdots)=0$$
$$\text{at } z=z_b+d_0+\varepsilon d_1+\varepsilon^2d_2+\cdots\qquad\text{(A.2.6b)}$$

$$\tau_{xz_0}+\varepsilon\tau_{xz_1}+\varepsilon^2\tau_{xz_2}+\cdots=0\quad\text{at } z=z_b+d_0+\varepsilon d_1+\varepsilon^2d_2+\cdots\qquad\text{(A.2.6c)}$$

$$(u_0+\varepsilon u_1+\varepsilon^2u_2+\cdots)\frac{\mathrm{d}z_b}{\mathrm{d}x}-(w_0+\varepsilon w_1+\varepsilon^2w_2+\cdots)=0\quad\text{at } z=z_b\qquad\text{(A.2.6d)}$$

No-slip condition $u_0+\varepsilon u_1+\varepsilon^2u_2+\cdots=w_0+\varepsilon w_1+\varepsilon^2w_2+\cdots=0$ at $z=z_b$ (A.2.6e)

and for the discharge:

$$\int_{z_b}^{z_b+d_0+\varepsilon d_1+\varepsilon^2d_2+\cdots}(u_0+\varepsilon u_1+\varepsilon^2u_2+\cdots)\,\mathrm{d}z=q\qquad\text{(A.2.7)}$$

In the boundary conditions (A.2.6a), (A.2.6b) and the discharge condition (A.2.7) the boundary $z=z_b+d$ is written as $z=z_b+d_0+\varepsilon d_1+\varepsilon^2d_2+\cdots$. It is required that $|d_0|\gg|\varepsilon d_1|\gg|\varepsilon^2d_2|\gg\cdots$. Substitution of the boundary $z=z_b+d_0+\varepsilon d_1+\varepsilon^2d_2+\cdots$ into the calculated solutions and using the Taylor series around the point $z=z_b+d_0$ give terms in these solutions located at $z=z_b+d_0$ which are multiplied by powers of the perturbation quantity, ε, higher than or equal to one. These multiplied terms are one or more orders of magnitude smaller than the term that is not multiplied with a power of ε. Hence, it is allowed to choose the boundary at $z=z_b+d_0$.

The expansion of the depth-integrated velocity, eq. (A.2.7), needs a closer examination. It can be written as:

$$\int_{z_b}^{z_b+d_0} u_0\,dz + \varepsilon d_1 u_0\Big|_{z=z_b+d_0} + \varepsilon^2\left(d_2 u_0\Big|_{z=z_b+d_0} + \frac{1}{2}d_1^2\frac{\partial u_0}{\partial z}\Big|_{z=z_b+d_0}\right)+\cdots+$$
$$+\varepsilon\left(\int_{z_b}^{z_b+d_0} u_1\,dz + \varepsilon d_1 u_1\Big|_{z=z_b+d_0} + \varepsilon^2\left(d_2 u_1\Big|_{z=z_b+d_0} + \frac{1}{2}d_1^2\frac{\partial u_1}{\partial z}\Big|_{z=z_b+d_0}\right)+\cdots\right)+ \qquad \text{(A.2.8)}$$
$$+\varepsilon^2\left(\int_{z_b}^{z_b+d_0} u_2\,dz + \varepsilon d_1 u_2\Big|_{z=z_b+d_0} + \varepsilon^2\left(d_2 u_2\Big|_{z=z_b+d_0} + \frac{1}{2}d_1^2\frac{\partial u_2}{\partial z}\Big|_{z=z_b+d_0}\right)+\cdots\right) = q$$

Rewriting eq. (A.2.8) as asymptotic expansions and choosing the zeroth-order term equal to q, $\int_{z_b}^{z_b+d_0} u_0\,dz = q$, yields that the first- and higher-order discharges are zero:

$$\varepsilon\left(d_1 u_0\Big|_{z=z_b+d_0} + \int_{z_b}^{z_b+d_0} u_1\,dz\right)+\varepsilon^2\left(d_1 u_1\Big|_{z=z_b+d_0} + \left(d_2 u_0\Big|_{z=z_b+d_0} + \frac{1}{2}d_1^2\frac{\partial u_0}{\partial z}\Big|_{z=z_b+d_0}\right) + \int_{z_b}^{z_b+d_0} u_2\,dz\right)+\cdots = 0$$

At this moment the terms with the same order of magnitude have to be collected and the equations have to be split to obtain sets of equations with the same order of magnitude.

Before collecting the terms it is convenient to introduce a transformation. This transformation simplifies the integration of the equations. The transformation is:

$$\sigma = \frac{z - z_b}{d}$$

in which σ is the new vertical coordinate, z is the old vertical coordinate, z_b is the bottom level and d is the water depth. Due to this transformation the boundaries are located at $\sigma=0$, which is equal to $z=z_b$, and $\sigma=1$, which is equal to $z=z_b+d$. This transformation is called the σ-transformation and was first used by Phillips [1957].

Using the method of asymptotic expansions, it is more feasible to introduce a slightly different transformation:

$$\sigma = \frac{z - z_b}{d_0} \qquad \text{(A.2.9)}$$

in which d_0 is the zeroth-order water depth. The advantage of the transformation of eq. (A.2.9) is that no extra terms are introduced due to the higher-order water depths.

Applying the transformation of eq. (A.2.9) and collecting the terms with the same order of magnitude, gives the sets of equations to be solved. It will become clear that it is only necessary to solve the first three sets of equations.

The set of the zeroth-order equations:

$$\frac{\partial u_0}{\partial x} - \frac{1}{d_0}\left(\frac{\mathrm{d}z_b}{\mathrm{d}x} + \sigma\frac{\mathrm{d}d_0}{\mathrm{d}x}\right)\frac{\partial u_0}{\partial \sigma} + \frac{1}{d_0}\frac{\partial w_0}{\partial \sigma} = 0 \tag{A.2.10}$$

$$\frac{\partial p_0}{\partial x} - \frac{1}{d_0}\left(\frac{\mathrm{d}z_b}{\mathrm{d}x} + \sigma\frac{\mathrm{d}d_0}{\mathrm{d}x}\right)\frac{\partial p_0}{\partial \sigma} = \frac{1}{d_0}\frac{\partial}{\partial \sigma}\left(\frac{\nu_t}{d_0}\frac{\partial u_0}{\partial \sigma}\right) \tag{A.2.11a}$$

$$\frac{1}{d_0}\frac{\partial p_0}{\partial \sigma} + g = 0 \tag{A.2.11b}$$

$$p_0 = 0 \qquad \text{at } \sigma = 1 \tag{A.2.12a}$$

$$u_0\frac{\mathrm{d}(z_b + d_0)}{\mathrm{d}x} - w_0 = 0 \qquad \text{at } \sigma = 1 \tag{A.2.12b}$$

$$\tau_{xz_0} = 0 \qquad \text{at } \sigma = 1 \tag{A.2.12c}$$

$$u_0\frac{\mathrm{d}z_b}{\mathrm{d}x} - w_0 = 0 \qquad \text{at } \sigma = 0 \tag{A.2.12d}$$

$$u_0 = w_0 = 0 \qquad \text{at } \sigma = 0 \tag{A.2.12e}$$

$$d_0\int_0^1 u_0\,\mathrm{d}\sigma = q \tag{A.2.13}$$

The set of the first-order equations:

$$\frac{\partial u_1}{\partial x} - \frac{1}{d_0}\left(\frac{\mathrm{d}z_b}{\mathrm{d}x} + \sigma\frac{\mathrm{d}d_0}{\mathrm{d}x}\right)\frac{\partial u_1}{\partial \sigma} + \frac{1}{d_0}\frac{\partial w_1}{\partial \sigma} = 0 \tag{A.2.14}$$

$$u_0\frac{\partial u_0}{\partial x} - \frac{u_0}{d_0}\left(\frac{\mathrm{d}z_b}{\mathrm{d}x} + \sigma\frac{\mathrm{d}d_0}{\mathrm{d}x}\right)\frac{\partial u_0}{\partial \sigma} + \frac{w_0}{d_0}\frac{\partial u_0}{\partial \sigma} + \frac{\partial p_1}{\partial x} + \\ - \frac{1}{d_0}\left(\frac{\mathrm{d}z_b}{\mathrm{d}x} + \sigma\frac{\mathrm{d}d_0}{\mathrm{d}x}\right)\frac{\partial p_1}{\partial \sigma} = \frac{1}{d_0}\frac{\partial}{\partial \sigma}\left(\frac{\nu_t}{d_0}\frac{\partial u_1}{\partial \sigma}\right) \tag{A.2.15a}$$

$$\frac{1}{d_0}\frac{\partial p_1}{\partial \sigma} = 0 \tag{A.2.15b}$$

$$p_1 + \frac{d_1}{d_0}\frac{\partial p_0}{\partial \sigma} = 0 \qquad \text{at } \sigma = 1 \tag{A.2.16a}$$

$$u_0\frac{\mathrm{d}d_1}{\mathrm{d}x} + u_1\frac{\mathrm{d}z_b + d_0}{\mathrm{d}x} + \frac{d_1}{d_0}\frac{\mathrm{d}z_b + d_0}{\mathrm{d}x}\frac{\partial u_0}{\partial \sigma} - w_1 - \frac{d_1}{d_0}\frac{\partial w_0}{\partial \sigma} = 0 \qquad \text{at } \sigma = 1 \tag{A.2.16b}$$

$$\tau_{xz_1} + \frac{d_1}{d_0}\frac{\partial \tau_{xz_0}}{\partial \sigma} = 0 \qquad \text{at } \sigma = 1 \tag{A.2.16c}$$

$$u_1\frac{\mathrm{d}z_b}{\mathrm{d}x} - w_1 = 0 \qquad \text{at } \sigma = 0 \tag{A.2.16d}$$

$$u_1 = w_1 = 0 \qquad \text{at } \sigma = 0 \tag{A.2.16e}$$

$$d_0 \int_0^1 u_1 \, d\sigma + d_1 u_0 \Big|_{\sigma=1} = 0 \qquad \text{(A.2.17)}$$

The set of the second-order equations:

$$\frac{\partial u_2}{\partial x} - \frac{1}{d_0}\left(\frac{dz_b}{dx} + \sigma \frac{dd_0}{dx}\right)\frac{\partial u_2}{\partial \sigma} + \frac{1}{d_0}\frac{\partial w_2}{\partial \sigma} = 0 \qquad \text{(A.2.18)}$$

$$u_0 \frac{\partial u_1}{\partial x} - \frac{u_0}{d_0}\left(\frac{dz_b}{dx} + \sigma \frac{dd_0}{dx}\right)\frac{\partial u_1}{\partial \sigma} + u_1 \frac{\partial u_0}{\partial x} - \frac{u_1}{d_0}\left(\frac{dz_b}{dx} + \sigma \frac{dd_0}{dx}\right)\frac{\partial u_0}{\partial \sigma} + \frac{w_0}{d_0}\frac{\partial u_1}{\partial \sigma} + \frac{w_1}{d_0}\frac{\partial u_0}{\partial \sigma} +$$

$$+ \frac{\partial p_2}{\partial x} - \frac{1}{d_0}\left(\frac{dz_b}{dx} + \sigma \frac{dd_0}{dx}\right)\frac{\partial p_2}{\partial \sigma} = 2\chi^2 \frac{\partial}{\partial x}\left(\nu_t \frac{\partial u_0}{\partial x} - \frac{\nu_t}{d_0}\left(\frac{dz_b}{dx} + \sigma \frac{dd_0}{dx}\right)\frac{\partial u_0}{\partial \sigma}\right) + \qquad \text{(A.2.19a)}$$

$$-\chi^2 \frac{2}{d_0}\left(\frac{dz_b}{dx} + \sigma \frac{dd_0}{dx}\right)\frac{\partial}{\partial \sigma}\left(\nu_t \frac{\partial u_0}{\partial x} - \frac{\nu_t}{d_0}\left(\frac{dz_b}{dx} + \sigma \frac{dd_0}{dx}\right)\frac{\partial u_0}{\partial \sigma}\right) +$$

$$+ \frac{1}{d_0}\frac{\partial}{\partial \sigma}\left(\nu_t\left(\frac{1}{d_0}\frac{\partial u_2}{\partial \sigma} + \chi^2 \frac{\partial w_0}{\partial x} - \frac{\chi^2}{d_0}\left(\frac{dz_b}{dx} + \sigma \frac{dd_0}{dx}\right)\frac{\partial w_0}{\partial \sigma}\right)\right)$$

$$\frac{1}{d_0}\frac{\partial p_2}{\partial \sigma} = \chi^2 \frac{\partial}{\partial x}\left(\frac{\nu_t}{d_0}\frac{\partial u_0}{\partial \sigma}\right) - \chi^2 \frac{1}{d_0}\left(\frac{dz_b}{dx} + \sigma \frac{dd_0}{dx}\right)\frac{\partial}{\partial \sigma}\left(\frac{\nu_t}{d_0}\frac{\partial u_0}{\partial \sigma}\right) + \chi^2 \frac{2}{d_0}\frac{\partial}{\partial \sigma}\left(\frac{\nu_t}{d_0}\frac{\partial w_0}{\partial \sigma}\right) \qquad \text{(A.2.19b)}$$

$$p_2 + \frac{d_2}{d_0}\frac{\partial p_0}{\partial \sigma} + \frac{d_1}{d_0}\frac{\partial p_1}{\partial \sigma} + \frac{1}{2}\left(\frac{d_1}{d_0}\right)^2 \frac{\partial^2 p_0}{\partial \sigma^2} = 0 \qquad \text{at } \sigma = 1 \qquad \text{(A.2.20a)}$$

$$u_0 \frac{dd_2}{dx} + u_1 \frac{dd_1}{dx} + u_2 \frac{dz_b + d_0}{dx} + \frac{d_1}{d_0}\frac{dd_1}{dx}\frac{\partial u_0}{\partial \sigma} + \frac{d_1}{d_0}\frac{dx_b + d_0}{dx}\frac{\partial u_1}{\partial \sigma} +$$

$$+ \frac{1}{2}\left(\frac{d_1}{d_0}\right)^2 \frac{dd_0}{dx}\frac{\partial^2 u_0}{\partial \sigma^2} + \frac{d_2}{d_0}\frac{dz_b + d_0}{dx}\frac{\partial u_0}{\partial \sigma} - w_2 - \frac{d_1}{d_0}\frac{\partial w_1}{\partial \sigma} - \frac{d_2}{d_0}\frac{\partial w_0}{\partial \sigma} - \frac{1}{2}\left(\frac{d_1}{d_0}\right)^2 \frac{\partial^2 w_0}{\partial \sigma^2} = 0$$

$$\text{at } \sigma = 1 \qquad \text{(A.2.20b)}$$

$$\tau_{xz_2} + \frac{d_2}{d_0}\frac{\partial \tau_{xz_0}}{\partial \sigma} + \frac{d_1}{d_0}\frac{\partial \tau_{xz_1}}{\partial \sigma} + \frac{1}{2}\left(\frac{d_1}{d_0}\right)^2 \frac{\partial^2 \tau_{xz_0}}{\partial \sigma^2} = 0 \qquad \text{at } \sigma = 1 \qquad \text{(A.2.20c)}$$

$$u_2 \frac{dz_b}{dx} - w_2 = 0 \qquad \text{at } \sigma = 0 \qquad \text{(A.2.20d)}$$

$$u_2 = w_2 = 0 \qquad \text{at } \sigma = 0 \qquad \text{(A.2.20e)}$$

$$d_0 \int_0^1 u_2 \, d\sigma + d_2 u_0 \Big|_{\sigma=1} + d_1 u_1 \Big|_{\sigma=1} + \frac{1}{2}\left(\frac{d_1}{d_0}\right)^2 \frac{\partial u_0}{\partial \sigma}\Big|_{\sigma=1} = 0 \qquad \text{(A.2.21)}$$

In the next sections these sets of equations are solved using a constant eddy-viscosity (section A.3) and a parabolic eddy-viscosity (section A.4). The solutions of these sets are substituted in the continuity and Navier-Stokes equations, which integrated over the depth yield the modified 1DH shallow-water equations.

A.3 The constant eddy-viscosity

In this section the different sets of equations are solved for a constant eddy-viscosity starting with the zeroth-order set of equations.

Before solving the set of zeroth-order equations it is convenient to simplify the Reynolds stress terms. The approximation of the eddy-viscosity with a constant value makes it possible to simplify the Reynolds stress terms, because the eddy-viscosity is no longer a function of the x- and σ-coordinates. The Reynolds stress term in the zeroth-order equation, eq. (A.2.11a), changes into:

$$\frac{1}{d_0}\frac{\partial}{\partial\sigma}\left(\frac{\nu_t}{d_0}\frac{\partial u_0}{\partial\sigma}\right) = \frac{\nu_t}{d_0^2}\frac{\partial^2 u_0}{\partial\sigma^2} \tag{A.3.1}$$

and in the first-order equation, eq. (A.2.15a):

$$\frac{1}{d_0}\frac{\partial}{\partial\sigma}\left(\frac{\nu_t}{d_0}\frac{\partial u_1}{\partial\sigma}\right) = \frac{\nu_t}{d_0^2}\frac{\partial^2 u_1}{\partial\sigma^2} \tag{A.3.2}$$

The Reynolds stress terms in the second-order equations, eq. (A.2.19a) and eq. (A.2.19b), simplify also. Using eq. (A.2.10), the Reynolds stress terms in eq. (A.2.19a) become:

$$2\chi^2\frac{\partial}{\partial x}\left(\nu_t\frac{\partial u_0}{\partial x}-\frac{\nu_t}{d_0}\left(\frac{\mathrm{d}z_b}{\mathrm{d}x}+\sigma\frac{\mathrm{d}d_0}{\mathrm{d}x}\right)\frac{\partial u_0}{\partial\sigma}\right)-2\frac{\chi^2}{d_0}\left(\frac{\mathrm{d}z_b}{\mathrm{d}x}+\sigma\frac{\mathrm{d}d_0}{\mathrm{d}x}\right)\frac{\partial}{\partial\sigma}\left(\nu_t\frac{\partial u_0}{\partial x}-\frac{\nu_t}{d_0}\left(\frac{\mathrm{d}z_b}{\mathrm{d}x}+\sigma\frac{\mathrm{d}d_0}{\mathrm{d}x}\right)\frac{\partial u_0}{\partial\sigma}\right)+$$
$$+\frac{1}{d_0}\frac{\partial}{\partial\sigma}\left(\nu_t\left(\frac{1}{d_0}\frac{\partial u_2}{\partial\sigma}+\chi^2\frac{\partial w_0}{\partial x}-\frac{\chi^2}{d_0}\left(\frac{\mathrm{d}z_b}{\mathrm{d}x}+\sigma\frac{\mathrm{d}d_0}{\mathrm{d}x}\right)\frac{\partial w_0}{\partial\sigma}\right)\right) =$$

$$= \chi^2 \frac{\partial}{\partial x}\left(\nu_t \frac{\partial u_0}{\partial x} - \frac{\nu_t}{d_0}\left(\frac{dz_b}{dx} + \sigma \frac{dd_0}{dx}\right)\frac{\partial u_0}{\partial \sigma}\right) - \frac{\chi^2}{d_0}\left(\frac{dz_b}{dx} + \sigma \frac{dd_0}{dx}\right)\frac{\partial}{\partial \sigma}\left(\nu_t \frac{\partial u_0}{\partial x} - \frac{\nu_t}{d_0}\left(\frac{dz_b}{dx} + \sigma \frac{dd_0}{dx}\right)\frac{\partial u_0}{\partial \sigma}\right) +$$

$$+ \frac{\nu_t}{d_0^2}\frac{\partial^2 u_2}{\partial \sigma^2} + \chi^2 \frac{\partial}{\partial x}\left(\nu_t \frac{\partial u_0}{\partial x} - \frac{\nu_t}{d_0}\left(\frac{dz_b}{dx} + \sigma \frac{dd_0}{dx}\right)\frac{\partial u_0}{\partial \sigma}\right) + \chi^2 \frac{\nu_t}{d_0}\frac{\partial^2 w_0}{\partial \sigma \partial x} - \chi^2 \frac{\nu_t}{d_0^2}\frac{\partial w_0}{\partial \sigma}\frac{dd_0}{dx} +$$

$$- \frac{\chi^2}{d_0}\left(\frac{dz_b}{dx} + \sigma \frac{dd_0}{dx}\right)\frac{\partial}{\partial \sigma}\left(\nu_t \frac{\partial u_0}{\partial x} - \frac{\nu_t}{d_0}\left(\frac{dz_b}{dx} + \sigma \frac{dd_0}{dx}\right)\frac{\partial u_0}{\partial \sigma}\right) - \frac{\chi^2}{d_0}\left(\frac{dz_b}{dx} + \sigma \frac{dd_0}{dx}\right)\frac{\partial^2 w_0}{\partial \sigma^2} =$$

$$= \chi^2 \frac{\partial}{\partial x}\left(\nu_t \frac{\partial u_0}{\partial x} - \frac{\nu_t}{d_0}\left(\frac{dz_b}{dx} + \sigma \frac{dd_0}{dx}\right)\frac{\partial u_0}{\partial \sigma}\right) - \frac{\chi^2}{d_0}\left(\frac{dz_b}{dx} + \sigma \frac{dd_0}{dx}\right)\frac{\partial}{\partial \sigma}\left(\nu_t \frac{\partial u_0}{\partial x} - \frac{\nu_t}{d_0}\left(\frac{dz_b}{dx} + \sigma \frac{dd_0}{dx}\right)\frac{\partial u_0}{\partial \sigma}\right) +$$

$$+ \frac{\nu_t}{d_0^2}\frac{\partial^2 u_2}{\partial \sigma^2} + \chi^2 \frac{\partial}{\partial x}\left(\nu_t \frac{\partial u_0}{\partial x} - \frac{\nu_t}{d_0}\left(\frac{dz_b}{dx} + \sigma \frac{dd_0}{dx}\right)\frac{\partial u_0}{\partial \sigma} + \frac{\nu_t}{d_0}\frac{\partial w_0}{\partial \sigma}\right) +$$

$$- \frac{\chi^2}{d_0}\left(\frac{dz_b}{dx} + \sigma \frac{dd_0}{dx}\right)\frac{\partial}{\partial \sigma}\left(\nu_t \frac{\partial u_0}{\partial x} - \frac{\nu_t}{d_0}\left(\frac{dz_b}{dx} + \sigma \frac{dd_0}{dx}\right)\frac{\partial u_0}{\partial \sigma} + \frac{\nu_t}{d_0}\frac{\partial w_0}{\partial \sigma}\right) =$$

$$= \chi^2 \nu_t \frac{\partial}{\partial x}\left(\frac{\partial u_0}{\partial x} - \frac{1}{d_0}\left(\frac{dz_b}{dx} + \sigma \frac{dd_0}{dx}\right)\frac{\partial u_0}{\partial \sigma}\right) + \tag{A.3.3}$$

$$- \chi^2 \frac{\nu_t}{d_0}\left(\frac{dz_b}{dx} + \sigma \frac{dd_0}{dx}\right)\frac{\partial}{\partial \sigma}\left(\frac{\partial u_0}{\partial x} - \frac{1}{d_0}\left(\frac{dz_b}{dx} + \sigma \frac{dd_0}{dx}\right)\frac{\partial u_0}{\partial \sigma}\right) + \frac{\nu_t}{d_0^2}\frac{\partial^2 u_2}{\partial \sigma^2}$$

and the Reynolds stress terms in eq. (A.2.19b) become:

$$\chi^2 \frac{\partial}{\partial x}\left(\frac{\nu_t}{d_0}\frac{\partial u_0}{\partial \sigma}\right) - \frac{\chi^2}{d_0}\left(\frac{\partial z_b}{\partial x} + \sigma \frac{\partial d_0}{\partial x}\right)\frac{\partial}{\partial \sigma}\left(\frac{\nu_t}{d_0}\frac{\partial u_0}{\partial \sigma}\right) + \chi^2 \frac{2}{d_0}\frac{\partial}{\partial \sigma}\left(\frac{\nu_t}{d_0}\frac{\partial w_0}{\partial \sigma}\right) =$$

$$= \chi^2 \frac{\nu_t}{d_0}\frac{\partial^2 u_0}{\partial x \partial \sigma} - \chi^2 \frac{\nu_t}{d_0^2}\frac{\partial u_0}{\partial \sigma}\frac{dd_0}{dx} - \chi^2 \frac{\nu_t}{d_0^2}\frac{\partial^2 u_0}{\partial \sigma^2}\frac{dz_b}{dx} - \chi^2 \sigma \frac{\nu_t}{d_0^2}\frac{\partial^2 u_0}{\partial \sigma^2}\frac{dd_0}{dx} + \chi^2 2 \frac{\nu_t}{d_0^2}\frac{\partial^2 w_0}{\partial \sigma^2}$$

$$= \chi^2 \frac{\nu_t}{d_0}\frac{\partial}{\partial \sigma}\left(\frac{\partial u_0}{\partial x} - \frac{1}{d_0}\left(\frac{dz_b}{dx} + \sigma \frac{dd_0}{dx}\right)\frac{\partial u_0}{\partial \sigma} + \frac{1}{d_0}\frac{\partial w_0}{\partial \sigma}\right) + \chi^2 \frac{\nu_t}{d_0^2}\frac{\partial^2 w_0}{\partial \sigma^2}$$

$$= \chi^2 \frac{\nu_t}{d_0^2}\frac{\partial^2 w_0}{\partial \sigma^2} \tag{A.3.4}$$

Solving the set of equations starts with the solution of the pressure from the Navier-Stokes equation in σ-direction. This pressure is then substituted into the Navier-Stokes equation in x-direction to solve for the horizontal velocity. The horizontal velocity is

substituted into the continuity equation to solve for the vertical velocity. This yields for the zeroth-order equations:

$$p_0 = g d_0 (1 - \sigma) \tag{A.3.5}$$

This is the hydrostatic distribution of the water pressure. This result is substituted into eq. (A.2.11a). Integrating twice with respect to σ and substituting the conditions (A.2.12c) and (A.2.12d), yields:

$$u_0 = \frac{g d_0^2}{\nu_t} \frac{1}{2}\left((\sigma - 1)^2 - 1\right) \frac{\mathrm{d}(z_b + d_0)}{\mathrm{d}x} \tag{A.3.6}$$

The solution of u_0 shows a parabolic velocity profile, but it still contains the variable d_0, which dependency on the x-coordinate is not known. This dependency is determined by making use of the discharge condition, (A.2.13).

$$d_0 \int_0^1 \frac{g d_0^2}{\nu_t} \frac{1}{2}\left((\sigma - 1)^2 - 1\right) \frac{\mathrm{d}(z_b + d_0)}{\mathrm{d}x} \mathrm{d}\sigma = -\frac{g d_0^3}{3\nu_t} \frac{\mathrm{d}(z_b + d_0)}{\mathrm{d}x} = q$$

this gives:

$$\frac{\mathrm{d}(z_b + d_0)}{\mathrm{d}x} = -\frac{3 q \nu_t}{g d_0^3} \tag{A.3.7}$$

This differential equation describes the water level slope as function of the water depth. The solution of the water level can be substituted into eq. (A.3.6), to obtain a more common solution for the velocity:

$$u_0 = \frac{3}{2} \frac{q}{d_0} \left(1 - (\sigma - 1)^2\right) \tag{A.3.8}$$

The expression (A.3.8) for u_0 gives a parabolic velocity profile. This profile only depends on the discharge, q, and the water depth, d_0. The velocity profile adapts itself to the changes of the bottom profile while the discharge is imposed by the depth-averaged continuity equation.

The velocity w_0 is calculated from eq. (A.2.10) by substituting expression (A.3.8) and condition (A.2.12e). This yields:

$$w_0 = \frac{3}{2} \frac{q}{d_0} \left(-\sigma^3 + 2\sigma^2\right) \frac{\mathrm{d}d_0}{\mathrm{d}x} + \frac{3}{2} \frac{q}{d_0} \left(1 - (\sigma - 1)^2\right) \frac{\mathrm{d}z_b}{\mathrm{d}x} \tag{A.3.9}$$

The same kind of analysis can be carried out with the set of first-order equations, eq. (A.2.14) and eq. (A.2.15), in which the zeroth-order velocities and pressure are substituted. It yields for the pressure:

$$p_1 = g d_1 \tag{A.3.10}$$

in which the first-order water depth can be calculated from eq. (A.2.15a), using the boundary

values (A.2.16c) and (A.2.16d) and the depth-integrated continuity equation (A.2.17):

$$\frac{\mathrm{d}d_1}{\mathrm{d}x} = 3\frac{q\nu_t}{gd_0^3}\left(\tfrac{18}{35}\frac{q}{\nu_t}\frac{\mathrm{d}d_0}{\mathrm{d}x}+3\frac{d_1}{d_0}\right) \tag{A.3.11}$$

The analysis yields for the horizontal velocity:

$$u_1 = \tfrac{3}{2}\frac{q}{d_0}\frac{d_1}{d_0}\left(3\sigma^2-4\sigma\right)-\tfrac{9}{4}\frac{q^2}{d_0\nu_t}\frac{\mathrm{d}d_0}{\mathrm{d}x}\left(\frac{7\sigma^6-42\sigma^5+70\sigma^4-72\sigma^2+32\sigma}{210}\right) \tag{A.3.12}$$

and for the vertical velocity:

$$\begin{aligned} w_1 = {} & -\tfrac{3}{2}\frac{q}{d_0}\left(\frac{\mathrm{d}d_1}{\mathrm{d}x}-2\frac{d_1}{d_0}\frac{\mathrm{d}d_0}{\mathrm{d}x}\right)\left(\sigma^3-2\sigma^2\right)+\tfrac{9}{4}\frac{q^2}{\nu_t}\left(\frac{\mathrm{d}^2d_0}{\mathrm{d}x^2}-\frac{1}{d_0}\left(\frac{\mathrm{d}d_0}{\mathrm{d}x}\right)^2\right)\left(\frac{\sigma^7-7\sigma^6+14\sigma^5-24\sigma^3+16\sigma^2}{210}\right)+ \\ & +\tfrac{3}{2}\frac{q}{d_0}\frac{\mathrm{d}z_b}{\mathrm{d}x}\frac{d_1}{d_0}\left(3\sigma^2-4\sigma\right)-\tfrac{9}{4}\frac{q^2}{d_0\nu_t}\frac{\mathrm{d}d_0}{\mathrm{d}x}\frac{\mathrm{d}z_b}{\mathrm{d}x}\left(\frac{7\sigma^6-42\sigma^5+70\sigma^4-72\sigma^2+32\sigma}{210}\right)+ \\ & +\tfrac{3}{2}\frac{q}{d_0}\frac{\mathrm{d}d_0}{\mathrm{d}x}\frac{d_1}{d_0}\left(2\sigma^3-2\sigma^2\right)-\tfrac{9}{4}\frac{q^2}{d_0\nu_t}\left(\frac{\mathrm{d}d_0}{\mathrm{d}x}\right)^2\left(\frac{6\sigma^7-35\sigma^6+56\sigma^5-48\sigma^3+16\sigma^2}{210}\right) \end{aligned} \tag{A.3.13}$$

To obtain the second-order solutions, the first-order and the zeroth-order solutions have to be substituted into the second-order set of equations and the analysis is to be repeated. The second-order pressure is derived from eq. (A.2.19b), after integrating with respect to σ and using condition (A.2.20a):

$$p_2 = \tfrac{3}{2}\frac{\chi^2 q\nu_t}{d_0^2}\left(\left(-3\sigma^2+4\sigma-1\right)\frac{\mathrm{d}d_0}{\mathrm{d}x}+2\left(1-\sigma\right)\frac{\mathrm{d}z_b}{\mathrm{d}x}\right)+gd_2 \tag{A.3.14}$$

with the differential equation for d_2:

$$\begin{aligned} \frac{\mathrm{d}d_2}{\mathrm{d}x} = {} & 3\frac{q\nu_t}{gd_0^3}\left(-6\left(\frac{d_1}{d_0}\right)^2+3\frac{d_2}{d_0}-\tfrac{54}{35}\frac{q}{\nu_t}\frac{d_1}{d_0}\frac{\mathrm{d}d_0}{\mathrm{d}x}+\tfrac{13}{5}\chi^2\left(\frac{\mathrm{d}d_0}{\mathrm{d}x}\right)^2+2\chi^2\frac{\mathrm{d}d_0}{\mathrm{d}x}\frac{\mathrm{d}z_b}{\mathrm{d}x}-2\chi^2\left(\frac{\mathrm{d}z_b}{\mathrm{d}x}\right)^2+\right. \\ & \left.-\tfrac{7}{5}\chi^2 d_0\frac{\mathrm{d}^2d_0}{\mathrm{d}x^2}-\tfrac{3}{2}\chi^2 d_0\frac{\mathrm{d}^2z_b}{\mathrm{d}x^2}+\tfrac{18}{35}\frac{q}{\nu_t}\frac{\mathrm{d}d_1}{\mathrm{d}x}-\tfrac{156}{13475}\left(\frac{q}{\nu_t}\right)^2 d_0\frac{\mathrm{d}^2d_0}{\mathrm{d}x^2}+\tfrac{208}{13475}\left(\frac{q}{\nu_t}\frac{\mathrm{d}d_0}{\mathrm{d}x}\right)^2\right) \end{aligned} \tag{A.3.15}$$

Eq. (A.3.15) is derived from eq. (A.2.19a) by integrating it twice with respect to σ and substitution of the boundary conditions (A.2.20c) and (A.2.20d) and the depth-averaged continuity equation (A.2.21). This solution also determines the second-order horizontal velocity, which reads:

$$
\begin{aligned}
u_2 = &-9\frac{q}{d_0}\left(\frac{d_1}{d_0}\right)^2(\sigma^2-2\sigma)+\frac{3}{2}\frac{q}{d_0}\frac{d_2}{d_0}(3\sigma^2-4\sigma)-\frac{9}{4}\frac{q^2}{d_0\nu_t}\frac{\mathrm{d}d_1}{\mathrm{d}x}\left(\frac{7\sigma^6-42\sigma^5+70\sigma^4-72\sigma^2+32\sigma}{210}\right)+\\
&+\frac{9}{4}\frac{q^2}{d_0\nu_t}\frac{d_1}{d_0}\frac{\mathrm{d}d_0}{\mathrm{d}x}\left(\frac{49\sigma^6-252\sigma^5+350\sigma^4-216\sigma^2+64\sigma}{210}\right)-q\chi^2\frac{\mathrm{d}^2d_0}{\mathrm{d}x^2}\left(\frac{15\sigma^4-40\sigma^3+57\sigma^2-24\sigma}{20}\right)+\\
&-q\chi^2\frac{\mathrm{d}^2z_b}{\mathrm{d}x^2}\left(\frac{4\sigma^3-3\sigma^2}{4}\right)+\frac{3}{5}\chi^2\frac{q}{d_0}\left(\frac{\mathrm{d}d_0}{\mathrm{d}x}\right)^2(5\sigma^4-10\sigma^3+9\sigma^2-3\sigma)+3\chi^2\frac{q}{d_0}\frac{\mathrm{d}d_0}{\mathrm{d}x}\frac{\mathrm{d}z_b}{\mathrm{d}x}(2\sigma^3-3\sigma^2+\sigma)+\\
&+\frac{q^3}{\nu_t^2}\frac{\mathrm{d}^2d_0}{\mathrm{d}x^2}\left(\frac{385\sigma^{10}-3850\sigma^9+13860\sigma^8-18480\sigma^7-5544\sigma^6+33264\sigma^5-18480\sigma^4-7488\sigma^2+5150\sigma}{431200}\right)+\\
&-\frac{q^3}{\nu_t^2 d_0}\left(\frac{\mathrm{d}d_0}{\mathrm{d}x}\right)^2\left(\frac{1078\sigma^{10}-10780\sigma^9+38115\sigma^8-46200\sigma^7-33264\sigma^6+121968\sigma^5-73920\sigma^4-9984\sigma^2+10112\sigma}{431200}\right)
\end{aligned}
\qquad \text{(A.3.16)}
$$

In this equation parts of the zeroth-order and first-order velocity profiles can be recognised. The first two terms on the right hand side are from the second-order solution of u_0, the third and the fourth terms on the right hand side from the first-order solution of u_1. Due to the decomposition of the water depth these terms arise in the second-order velocity profile.

The second-order vertical velocity can be derived from eq. (A.2.26) by substituting the second-order horizontal velocity profile into this equation, integrating this equation with respect to σ and using boundary condition (A.2.28e). This is not carried out in this thesis because the solution of this velocity is not used in the derivation of the 1DH shallow-water equation.

Derivation of the 1DH shallow-water equations.

At this time the horizontal velocity and the pressure are known to second order. To derive the 1DH shallow-water equations, valid for flows over sills, these solutions have to be substituted, with the appropriate power of the perturbation quantity, in the 2DV continuity and the Navier-Stokes equation in flow direction, eq. (A.2.4) and eq. (A.2.5a). The equations, generated in this way, have to be integrated from the bottom to the water surface as approximated in the second-order solution.

Determining the shallow-water equations by using the zeroth-order solutions only yields a shallow-water equation without a convective term. Determining the shallow-water equations using the zeroth-order and first-order solutions yields a shallow-water equation containing a convective term which is only dependent on the average velocity. Using at least three orders of solutions yields a convective term which is dependent on the bottom slope. Therefore only the zeroth-order, first-order and second-order sets of equations are solved. Higher-order solutions than the second-order solutions are not determined because the

contributions of these solutions to the total are supposed to be very small and in addition the derivation of these solutions is very time-consuming.

The first equation to be solved is the continuity equation:

$$\int_0^{d_r}\left(d_0\frac{\partial}{\partial x}\left(u_0+\varepsilon u_1+\varepsilon^2 u_2\right)-\left(\frac{\mathrm{d}z_b}{\mathrm{d}x}+\sigma\frac{\mathrm{d}d_0}{\mathrm{d}x}\right)\frac{\partial}{\partial\sigma}\left(u_0+\varepsilon u_1+\varepsilon^2 u_2\right)+\frac{\partial}{\partial\sigma}\left(w_0+\varepsilon w_1+\varepsilon^2 w_2\right)\right)\mathrm{d}\sigma=0$$

in which d_r is the scaled water depth (to second order):

$$d_r = 1+\varepsilon\frac{d_1}{d_0}+\varepsilon^2\frac{d_2}{d_0}$$

After straightforward but tedious calculations, which are not presented here, the result of integration is:

$$\frac{\mathrm{d}q}{\mathrm{d}x} = O(\varepsilon^3)$$

or, to second order in ε,

$$\frac{\mathrm{d}q}{\mathrm{d}x} = 0 \qquad \text{(A.3.17)}$$

The shallow-water equation of motion.

This equation is obtained from the depth-integrated Navier-Stokes equation in flow direction. To obtain this equation the different magnitudes of the horizontal velocities and pressures, with the perturbation quantity, are substituted in the original Navier-Stokes equation, which gives:

$$d_0\int_0^{d_r}\Bigg(\underbrace{\varepsilon\left(u_0\frac{\partial u_0}{\partial x}-\frac{u_0}{d_0}\left(\frac{\mathrm{d}z_b}{\mathrm{d}x}+\sigma\frac{\mathrm{d}d_0}{\mathrm{d}x}\right)\frac{\partial u_0}{\partial\sigma}+\frac{w_0}{d_0}\frac{\partial u_0}{\partial\sigma}\right)}_{A_1}+$$

$$\underbrace{+\varepsilon^2\left(u_0\frac{\partial u_1}{\partial x}-\frac{u_0}{d_0}\left(\frac{\mathrm{d}z_b}{\mathrm{d}x}+\sigma\frac{\mathrm{d}d_0}{\mathrm{d}x}\right)\frac{\partial u_1}{\partial\sigma}+u_1\frac{\partial u_0}{\partial x}-\frac{u_1}{d_0}\left(\frac{\mathrm{d}z_b}{\mathrm{d}x}+\sigma\frac{\mathrm{d}d_0}{\mathrm{d}x}\right)\frac{\partial u_0}{\partial\sigma}+\frac{w_0}{d_0}\frac{\partial u_1}{\partial\sigma}+\frac{w_1}{d_0}\frac{\partial u_0}{\partial\sigma}\right)}_{A_2}+$$

$$\underbrace{+\frac{\partial}{\partial x}\left(p_0+\varepsilon p_1+\varepsilon^2 p_2\right)-\frac{1}{d_0}\left(\frac{\mathrm{d}z_b}{\mathrm{d}x}+\sigma\frac{\mathrm{d}d_0}{\mathrm{d}x}\right)\frac{\partial}{\partial\sigma}\left(p_0+\varepsilon p_1+\varepsilon^2 p_2\right)}_{B}\Bigg)\mathrm{d}\sigma = \qquad \text{(A.3.18)}$$

$$= \int_0^{d_r} \underbrace{\frac{\nu_t}{d_0}\left(\frac{\partial^2 u_0}{\partial \sigma^2} + \varepsilon \frac{\partial^2 u_1}{\partial \sigma^2} + \varepsilon^2 d_0^2 \left(\chi^2 \frac{\partial^2 u_0}{\partial x^2} - \chi^2 \frac{\partial}{\partial x}\left(\frac{1}{d_0}\left(\frac{dz_b}{dx} + \sigma \frac{dd_0}{dx}\right)\frac{\partial u_0}{\partial \sigma}\right)\right.\right.}_{C_1} +$$

$$\underbrace{\left.\left. - \frac{\chi^2}{d_0}\left(\frac{dz_b}{dx} + \sigma \frac{dd_0}{dx}\right)\frac{\partial}{\partial \sigma}\left(\frac{\partial u_0}{\partial x} - \frac{1}{d_0}\left(\frac{dz_b}{dx} + \sigma \frac{dd_0}{dx}\right)\frac{\partial u_0}{\partial \sigma}\right) + \frac{1}{d_0^2}\frac{\partial^2 u_2}{\partial \sigma^2}\right)\right)}_{C_2} d\sigma \qquad \text{(A.3.18)}$$

This equation is divided into three parts; part A contains the convective terms, part B contains the pressure terms and part C contains the turbulent stress terms. All parts are evaluated separately, starting with part A of eq. (A.3.18). To integrate this part the following equations are added:

$(\varepsilon u_0 + \varepsilon^2 u_1) \cdot$ (continuity eq. (A.2.10)) and $(\varepsilon^2 u_0) \cdot$ (continuity eq. (A.2.14)

This yields:

$$d_0 \int_0^{d_r} \left(\varepsilon \left(2u_0 \frac{\partial u_0}{\partial x} - 2\frac{u_0}{d_0}\left(\frac{dz_b}{dx} + \sigma \frac{dd_0}{dx}\right)\frac{\partial u_0}{\partial \sigma} + \frac{w_0}{d_0}\frac{\partial u_0}{\partial \sigma} + \frac{u_0}{d_0}\frac{\partial w_0}{\partial \sigma} \right) + \right.$$

$$+ \varepsilon^2 \left(2u_0 \frac{\partial u_1}{\partial x} - 2\frac{u_0}{d_0}\left(\frac{dz_b}{dx} + \sigma \frac{dd_0}{dx}\right)\frac{\partial u_1}{\partial \sigma} + 2u_1 \frac{\partial u_0}{\partial x} - 2\frac{u_1}{d_0}\left(\frac{dz_b}{dx} + \sigma \frac{dd_0}{dx}\right)\frac{\partial u_0}{\partial \sigma} + \right.$$

$$\left.\left. + \frac{w_0}{d_0}\frac{\partial u_1}{\partial \sigma} + \frac{u_0}{d_0}\frac{\partial w_1}{\partial \sigma} + \frac{w_1}{d_0}\frac{\partial u_0}{\partial \sigma} + \frac{u_1}{d_0}\frac{\partial w_0}{\partial \sigma} \right) \right) d\sigma =$$

$$= \varepsilon \left(d_0 \frac{d}{dx}\left(\int_0^{d_r} u_0^2 \, d\sigma \right) + \frac{dd_0}{dx}\left(\int_0^{d_r} u_0^2 \, d\sigma \right) - u_0(d_r)\left(d_0 \frac{dd_r}{dx} u_0(d_r) + d_r \frac{dd_0}{dx} u_0(d_r) + \frac{dz_b}{dx} u_0(d_r) - w_0(d_r) \right) + \right.$$

$$\left. + u_0(0)\left(u_0(0)\frac{dz_b}{dx} - w_0(0) \right) \right) + \qquad \text{(A.3.19)}$$

$$+ \varepsilon^2 \left(2d_0 \frac{d}{dx}\left(\int_0^{d_r} u_0 u_1 \, d\sigma \right) + 2\frac{dd_0}{dx} \int_0^{d_r} u_0 u_1 \, d\sigma - u_0(d_r)\left(d_0 \frac{dd_r}{dx} u_1(d_r) + d_r \frac{dd_0}{dx} u_1(d_r) + \frac{dz_b}{dx} u_1(d_r) - w_0(d_r) \right) + \right.$$

$$- u_1(d_r)\left(d_0 \frac{dd_r}{dx} u_0(d_r) + d_r \frac{dd_0}{dx} u_0(d_r) + \frac{dz_b}{dx} u_0(d_r) - w_0(d_r) \right) +$$

$$\left. + u_0(0)\left(u_1(0)\frac{dz_b}{dx} - w_1(0) \right) + u_1(0)\left(u_0(0)\frac{dz_b}{dx} - w_0(0) \right) \right)$$

In eq. (A.3.19) the boundary condition (A.2.12b), (A.2.16b), (A.2.12d) and (A.2.16d) can be recognized. Substituting these into eq. (A.3.19) yields for the convective terms of eq. (A.3.18):

$$\varepsilon\left(\frac{\mathrm{d}}{\mathrm{d}x}\left(d_0\int_0^1 u_0^2\,\mathrm{d}\sigma + 2\varepsilon d_1\left(u_0(1)\right)^2 + \text{H.O.T}\right)\right) + \varepsilon^2\left(2\frac{\mathrm{d}}{\mathrm{d}x}\left(d_0\int_0^1 u_0u_1\,\mathrm{d}\sigma + \text{H.O.T.}\right)\right)$$

in which H.O.T. stands for Higher Order Terms in ε. Substitution of eq. (A.3.8) and eq. (A.3.12), integrating over the depth and omitting the H.O.T., yields for the convection term (A):

$$\varepsilon\frac{\mathrm{d}}{\mathrm{d}x}\left(\tfrac{6}{5}\frac{q^2}{d_0} + \varepsilon\tfrac{9}{4}d_1\frac{q^2}{d_0^2}\right) + \varepsilon^2\frac{\mathrm{d}}{\mathrm{d}x}\left(-\tfrac{69}{20}d_1\frac{q^2}{d_0^2} + \tfrac{4}{175}\frac{q}{\nu_t}\frac{q^2}{d_0}\frac{\mathrm{d}d_0}{\mathrm{d}x}\right) \qquad \text{(A.3.20)}$$

The next part of eq. (A.3.18) to be evaluated is part B, the part with the pressure terms:

$$d_0\int_0^{d_r}\left(\frac{\partial p_0}{\partial x} + \varepsilon\frac{\partial p_1}{\partial x} + \varepsilon^2\frac{\partial p_2}{\partial x} - \frac{1}{d_0}\left(\frac{\mathrm{d}z_b}{\mathrm{d}x} + \sigma\frac{\mathrm{d}d_0}{\mathrm{d}x}\right)\frac{\partial}{\partial\sigma}\left(p_0 + \varepsilon p_1 + \varepsilon^2 p_2\right)\right)\mathrm{d}\sigma =$$

$$= d_0\frac{\mathrm{d}}{\mathrm{d}x}\left(\int_0^{d_r}\left(p_0 + \varepsilon p_1 + \varepsilon^2 p_2\right)\mathrm{d}\sigma\right) - d_0\frac{\mathrm{d}d_r}{\mathrm{d}x}\left(p_0(d_r) + \varepsilon p_1(d_r) + \varepsilon^2 p_2(d_r)\right) +$$

$$- \frac{\mathrm{d}z_b}{\mathrm{d}x}\left[p_0 + \varepsilon p_1 + \varepsilon^2 p_2\right]_0^{d_r} - \frac{\mathrm{d}d_0}{\mathrm{d}x}\left[\sigma\left(p_0 + \varepsilon p_1 + \varepsilon^2 p_2\right)\right]_0^{d_r} + \frac{\mathrm{d}d_0}{\mathrm{d}x}\int_0^{d_r}\left(p_0 + \varepsilon p_1 + \varepsilon^2 p_2\right)\mathrm{d}\sigma$$

Substitution of the solutions for the pressure, eq. (A.3.5), eq. (A.3.10) and eq. (A.3.14), yields:

$$\frac{\mathrm{d}}{\mathrm{d}x}\left(d_0\int_0^{d_r}\left(p_0+\varepsilon p_1+\varepsilon^2 p_2\right)\mathrm{d}\sigma\right) - \frac{\mathrm{d}}{\mathrm{d}x}\left(z_b + d_0 + \varepsilon d_1 + \varepsilon^2 d_2\right)\left(p_0(d_r) + \varepsilon p_1(d_r) + \varepsilon^2 p_2(d_r)\right) +$$

$$+ \frac{\mathrm{d}z_b}{\mathrm{d}x}\left(p_0(0) + \varepsilon p_1(0) + \varepsilon^2 p_2(0)\right) =$$

$$= \frac{\mathrm{d}}{\mathrm{d}x}\left(d_0\int_0^1 p_0\mathrm{d}\sigma + \varepsilon d_1 p_0(1) + \varepsilon^2\left(d_2 p_0(1) + \tfrac{1}{2}\frac{d_1^2}{d_0}\frac{\partial p_0}{\partial\sigma}\right) + \varepsilon d_0\int_0^1 p_1\,\mathrm{d}\sigma + \varepsilon^2 d_1 p_1(1) + \varepsilon^2 d_0\int_0^1 p_2\,\mathrm{d}\sigma\right) +$$

$$- \frac{\mathrm{d}}{\mathrm{d}x}\left(z_b + d_0 + \varepsilon d_1 + \varepsilon^2 d_2\right)\left(p_0(1) + \varepsilon\frac{d_1}{d_0}\frac{\partial p_0}{\partial\sigma} + \varepsilon^2\frac{d_2}{d_0}\frac{\partial p_0}{\partial\sigma} + \tfrac{1}{2}\varepsilon^2\left(\frac{d_1}{d_0}\right)^2\frac{\partial^2 p_0}{\partial\sigma^2} + \varepsilon p_1(1) + \varepsilon^2\frac{d_1}{d_0}\frac{\partial p_1}{\partial\sigma} + \varepsilon^2 p_2(1)\right) +$$

$$+ \frac{\mathrm{d}z_b}{\mathrm{d}x}\left(p_0(0) + \varepsilon p_1(0) + \varepsilon^2 p_2(0)\right) =$$

$$=g\frac{\mathrm{d}}{\mathrm{d}x}\left(\tfrac{1}{2}d_0^{\,2}+\varepsilon d_1 d_0+\varepsilon^2\left(d_2 d_0+\tfrac{3}{2}\frac{\chi^2 q\nu_t}{g d_0}\frac{\mathrm{d}z_b}{\mathrm{d}x}\right)\right)+g\frac{\mathrm{d}z_b}{\mathrm{d}x}\left(d_0+\varepsilon d_1+\varepsilon^2 d_2+\varepsilon^2\frac{\chi^2}{g}\left(-\tfrac{3}{2}\frac{q\nu_t}{d_0^{\,2}}\frac{\mathrm{d}d_0}{\mathrm{d}x}+3\frac{q\nu_t}{d_0^{\,2}}\frac{\mathrm{d}z_b}{\mathrm{d}x}\right)\right)=$$

$$=g\left(d_0+\varepsilon d_1+\varepsilon^2 d_2\right)\frac{\mathrm{d}}{\mathrm{d}x}\left(z_b+d_0+\varepsilon d_1+\varepsilon^2 d_2\right)+\varepsilon^2\tfrac{3}{2}\frac{\chi^2 q\nu_t}{d_0^{\,2}}\left(d_0\frac{\mathrm{d}^2 z_b}{\mathrm{d}x^2}+2\left(\frac{\mathrm{d}z_b}{\mathrm{d}x}\right)^2-2\frac{\mathrm{d}z_b}{\mathrm{d}x}\frac{\mathrm{d}d_0}{\mathrm{d}x}\right) \qquad \text{(A.3.21)}$$

The last part of eq. (A.3.18) to be evaluated is part C, which consists of the turbulent stress terms:

$$\int_0^{d_t}\frac{\nu_t}{d_0}\left(\frac{\partial^2 u_0}{\partial\sigma^2}+\varepsilon\frac{\partial^2 u_1}{\partial\sigma^2}+\varepsilon^2 d_0^{\,2}\left(\chi^2\frac{\partial^2 u_0}{\partial x^2}-\chi^2\frac{\partial}{\partial x}\left(\frac{1}{d_0}\left(\frac{\mathrm{d}z_b}{\mathrm{d}x}+\sigma\frac{\mathrm{d}d_0}{\mathrm{d}x}\right)\frac{\partial u_0}{\partial\sigma}\right)+\right.\right.$$

$$\left.\left.-\frac{\chi^2}{d_0}\left(\frac{\mathrm{d}z_b}{\mathrm{d}x}+\sigma\frac{\mathrm{d}d_0}{\mathrm{d}x}\right)\frac{\partial}{\partial\sigma}\left(\frac{\partial u_0}{\partial x}-\frac{1}{d_0}\left(\frac{\mathrm{d}z_b}{\mathrm{d}x}+\sigma\frac{\mathrm{d}d_0}{\mathrm{d}x}\right)\frac{\partial u_0}{\partial\sigma}\right)+\frac{1}{d_0^{\,2}}\frac{\partial^2 u_2}{\partial\sigma^2}\right)\right)\mathrm{d}\sigma=$$

$$=\frac{\nu_t}{d_0}\left(\left[\frac{\partial u_0}{\partial\sigma}\right]_0^1+\varepsilon\frac{d_1}{d_0}\frac{\partial^2 u_0}{\partial\sigma^2}+\varepsilon^2\left(\frac{d_2}{d_0}\frac{\partial^2 u_0}{\partial\sigma^2}+\tfrac{1}{2}\left(\frac{d_1}{d_0}\right)^2\frac{\partial^3 u_0}{\partial\sigma^3}\right)+\varepsilon\left[\frac{\partial u_1}{\partial\sigma}\right]_0^1+\varepsilon^2\frac{d_1}{d_0}\frac{\partial^2 u_1}{\partial\sigma^2}+\right.$$

$$+\varepsilon^2 d_0^{\,2}\left(\chi^2\frac{\mathrm{d}^2}{\mathrm{d}x^2}\left(\int_0^1 u_0\mathrm{d}\sigma\right)-\chi^2\frac{\mathrm{d}}{\mathrm{d}x}\left(\frac{1}{d_0}\left(\frac{\mathrm{d}z_b}{\mathrm{d}x}[u_0]_0^1+\frac{\mathrm{d}d_0}{\mathrm{d}x}\left[\sigma u_0\right]_0^1-\int_0^1 u_0\mathrm{d}\sigma\right)\right)\right)+$$

$$-\frac{\chi^2}{d_0}\left(\frac{\mathrm{d}z_b}{\mathrm{d}x}\left[\frac{\partial u_0}{\partial x}-\frac{1}{d_0}\left(\frac{\mathrm{d}z_b}{\mathrm{d}x}+\sigma\frac{\mathrm{d}d_0}{\mathrm{d}x}\right)\frac{\partial u_0}{\partial\sigma}\right]_0^1-\frac{\mathrm{d}d_0}{\mathrm{d}x}\left(\left[\sigma\frac{\partial u_0}{\partial x}-\frac{\sigma}{d_0}\left(\frac{\mathrm{d}z_b}{\mathrm{d}x}+\sigma\frac{\mathrm{d}d_0}{\mathrm{d}x}\right)\frac{\partial u_0}{\partial\sigma}\right]_0^1+\right.\right.$$

$$\left.\left.\left.-\frac{\mathrm{d}}{\mathrm{d}x}\left(\int_0^1 u_0\mathrm{d}\sigma\right)-\frac{1}{d_0}\left[\frac{\mathrm{d}z_b}{\mathrm{d}x}u_0+\frac{\mathrm{d}d_0}{\mathrm{d}x}\sigma u_0\right]_0^1+\frac{1}{d_0}\frac{\mathrm{d}d_0}{\mathrm{d}x}\left(\int_0^1 u_0\mathrm{d}\sigma\right)\right)\right)+\frac{1}{d_0^{\,2}}\left[\frac{\partial u_2}{\partial\sigma}\right]_0^1\right)\right)$$

Substitution of the velocity profiles, eq. (A.3.8), eq. (A.3.12) and eq. (A.3.16) and the boundary conditions (A.2.12c), (A.2.16c) and (A.2.20c) yields the bottom shear stress for part C of eq. (A.3.18):

$$\frac{1}{\rho}\tau_{xb} = 3\frac{q\nu_t}{d_0^2}\left(-1+2\varepsilon\frac{d_1}{d_0}+\varepsilon^2\left(2\frac{d_2}{d_0}-3\left(\frac{d_1}{d_0}\right)^2\right)+\varepsilon\tfrac{4}{35}\frac{q}{\nu_t}\frac{dd_0}{dx}\left(1-2\varepsilon\frac{d_1}{d_0}\right)+\varepsilon^2\tfrac{4}{35}\frac{q}{\nu_t}\frac{dd_1}{dx}+\right.$$
$$+\varepsilon^2\chi^2\left(-d_0\frac{d^2d_0}{dx^2}-\tfrac{3}{5}d_0\frac{d^2z_b}{dx^2}+3\left(\frac{dd_0}{dx}\right)^2+\frac{dz_b}{dx}\frac{dd_0}{dx}-\tfrac{3}{2}\left(\frac{dz_b}{dx}\right)^2\right)+ \quad \text{(A.3.22)}$$
$$\left.+\varepsilon^2\left(\frac{q}{\nu_t}\right)^2\left(-\tfrac{32}{8085}d_0\frac{d^2d_0}{dx^2}+\tfrac{316}{13475}\left(\frac{dd_0}{dx}\right)^2\right)+\text{H.O.T}\right)$$

in which the H.O.T. can be neglected.

The depth-averaged Navier-Stokes equation in flow direction or the shallow-water equation of motion is derived by adding the convective part, eq. (A.3.20), the pressure part, eq. (A.3.21), and the friction part, eq. (A.3.22). The result is:

$$\varepsilon\frac{d}{dx}\left(\tfrac{6}{5}\frac{q^2}{d_0}+\varepsilon\tfrac{9}{4}d_1\frac{q^2}{d_0^2}\right)+\varepsilon^2\frac{d}{dx}\left(-\tfrac{69}{20}d_1\frac{q^2}{d_0^2}+\tfrac{4}{175}\frac{q}{\nu_t}\frac{q^2}{d_0^2}\frac{dd_0}{dx}\right)+$$
$$+g\left(d_0+\varepsilon d_1+\varepsilon^2 d_2\right)\frac{d}{dx}\left(z_b+d_0+\varepsilon d_1+\varepsilon^2 d_2\right)+\varepsilon^2\tfrac{3}{2}\frac{\chi^2 q\nu_t}{d_0^2}\left(\underline{d_0\frac{d^2z_b}{dx^2}}+\underline{2\left(\frac{dz_b}{dx}\right)^2}-\underline{2\frac{dz_b}{dx}\frac{dd_0}{dx}}\right)=$$
$$=3\frac{q\nu_t}{d_0^2}\left(-1+2\varepsilon\frac{d_1}{d_0}+\varepsilon^2\left(2\frac{d_2}{d_0}-3\left(\frac{d_1}{d_0}\right)^2\right)+\varepsilon\tfrac{4}{35}\frac{q}{\nu_t}\frac{dd_0}{dx}\left(1-2\varepsilon\frac{d_1}{d_0}\right)+\varepsilon^2\tfrac{4}{35}\frac{q}{\nu_t}\frac{dd_1}{dx}+\right.$$
$$+\varepsilon^2\chi^2\left(-d_0\frac{d^2d_0}{dx^2}-\underline{\tfrac{3}{5}d_0\frac{d^2z_b}{dx^2}}+3\left(\frac{dd_0}{dx}\right)^2+\underline{\frac{dz_b}{dx}\frac{dd_0}{dx}}-\underline{\tfrac{3}{2}\left(\frac{dz_b}{dx}\right)^2}\right)+$$
$$\left.+\varepsilon^2\left(\frac{q}{\nu_t}\right)^2\left(-\tfrac{32}{8085}d_0\frac{d^2d_0}{dx^2}+\tfrac{316}{13475}\left(\frac{dd_0}{dx}\right)^2\right)\right)$$

The underlined terms can be taken together. This yields:

$$\varepsilon\frac{\mathrm{d}}{\mathrm{d}x}\left(\tfrac{6}{5}\frac{q^2}{d_0}+\varepsilon\tfrac{9}{4}d_1\frac{q^2}{d_0^2}\right)+\varepsilon^2\frac{\mathrm{d}}{\mathrm{d}x}\left(-\tfrac{69}{20}d_1\frac{q^2}{d_0^2}+\tfrac{4}{175}\frac{q}{\nu_t}\frac{q^2}{d_0^2}\frac{\mathrm{d}d_0}{\mathrm{d}x}\right)+g\left(d_0+\varepsilon d_1+\varepsilon^2 d_2\right)\frac{\mathrm{d}}{\mathrm{d}x}\left(z_b+d_0+\varepsilon d_1+\varepsilon^2 d_2\right)=$$

$$=3\frac{q\nu_t}{d_0^2}\left(-1+2\varepsilon\frac{d_1}{d_0}+\varepsilon^2\left(2\frac{d_2}{d_0}-3\left(\frac{d_1}{d_0}\right)^2\right)+\varepsilon\tfrac{4}{35}\frac{q}{\nu_t}\frac{\mathrm{d}d_0}{\mathrm{d}x}\left(1-2\varepsilon\frac{d_1}{d_0}\right)+\varepsilon^2\tfrac{4}{35}\frac{q}{\nu_t}\frac{\mathrm{d}d_1}{\mathrm{d}x}+\right.$$

$$+\varepsilon^2\chi^2\left(-d_0\frac{\mathrm{d}^2d_0}{\mathrm{d}x^2}-\tfrac{11}{10}d_0\frac{\mathrm{d}^2z_b}{\mathrm{d}x^2}+3\left(\frac{\mathrm{d}d_0}{\mathrm{d}x}\right)^2+2\frac{\mathrm{d}z_b}{\mathrm{d}x}\frac{\mathrm{d}d_0}{\mathrm{d}x}-\tfrac{5}{2}\left(\frac{\mathrm{d}z_b}{\mathrm{d}x}\right)^2\right)+ \qquad \text{(A.3.23)}$$

$$\left.\left.+\varepsilon^2\left(\frac{q}{\nu_t}\right)^2\left(-\tfrac{32}{8085}d_0\frac{\mathrm{d}^2d_0}{\mathrm{d}x^2}+\tfrac{316}{13475}\left(\frac{\mathrm{d}d_0}{\mathrm{d}x}\right)^2\right)\right)\right)$$

In this equation the water depth has still to be approximated by the solutions of the water depth:

$$d = d_0+\varepsilon d_1+\varepsilon^2 d_2$$

or for the reciprocal value:

$$\frac{1}{d}=\frac{1}{d_0+\varepsilon d_1+\varepsilon^2 d_2}=\frac{1}{d_0\left(1+\varepsilon\frac{d_1}{d_0}+\varepsilon^2\frac{d_2}{d_0}\right)}$$

$$=\frac{1}{d_0}\left(1-\varepsilon\frac{d_1}{d_0}+\varepsilon^2\left(\left(\frac{d_1}{d_0}\right)^2-\frac{d_2}{d_0}\right)+\cdots\right)$$

Substitution of both approximations in eq. (A.3.23) and omitting the H.O.T., yields the dimensionless equation for motion of the 1DH shallow-water equations:

$$\varepsilon\frac{\mathrm{d}}{\mathrm{d}x}\left(\tfrac{6}{5}\frac{q^2}{d}\right)+\varepsilon^2\frac{\mathrm{d}}{\mathrm{d}x}\left(\tfrac{4}{175}\frac{q}{\nu_t}\frac{q^2}{d}\frac{\mathrm{d}d}{\mathrm{d}x}\right)+gd\frac{\mathrm{d}}{\mathrm{d}x}\left(z_b+d\right)=$$

$$=-3\frac{q\nu_t}{d^2}\left(1-\varepsilon\tfrac{4}{35}\frac{q}{\nu_t}\frac{\mathrm{d}d}{\mathrm{d}x}+\varepsilon^2\chi^2\left(d\frac{\mathrm{d}^2d}{\mathrm{d}x^2}+\tfrac{11}{10}d\frac{\mathrm{d}^2z_b}{\mathrm{d}x^2}-3\left(\frac{\mathrm{d}d}{\mathrm{d}x}\right)^2-2\frac{\mathrm{d}z_b}{\mathrm{d}x}\frac{\mathrm{d}d}{\mathrm{d}x}+\tfrac{5}{2}\left(\frac{\mathrm{d}z_b}{\mathrm{d}x}\right)^2\right)+\right. \qquad \text{(A.3.24)}$$

$$\left.+\varepsilon^2\left(\frac{q}{\nu_t}\right)^2\left(\tfrac{32}{8085}d\frac{\mathrm{d}^2d}{\mathrm{d}x^2}-\tfrac{316}{13475}\left(\frac{\mathrm{d}d}{\mathrm{d}x}\right)^2\right)\right)$$

Eq. (A.3.24) and eq. (A.3.17) are the dimensionless depth-integrated equation of motion and continuity equation. Together these equations are called the steady shallow-water equations. To get these equations in dimensional form, the characteristic values of eq. (A.2.1) have to be substituted in these equations. This yields the modified 1DH steady shallow-water

equations:

Continuity equation: $$\frac{dq}{dx} = 0 \qquad \text{(A.3.25a)}$$

Equation of motion: $$\frac{d}{dx}\left(\alpha \frac{q^2}{d}\right) + gd\frac{d}{dx}(z_b + d) = -\gamma 3\frac{q\nu_t}{d^2} \qquad \text{(A.3.25b)}$$

with: $$\alpha = \frac{6}{5} + \frac{4}{175}\frac{q}{\nu_t}\frac{dd}{dx} \qquad \text{(A.3.25c)}$$

$$\gamma = 1 - \frac{4}{35}\frac{q}{\nu_t}\frac{dd}{dx} + d\frac{d^2d}{dx^2} + \frac{11}{10}d\frac{d^2z_b}{dx^2} - 3\left(\frac{dd}{dx}\right)^2 - 2\frac{dz_b}{dx}\frac{dd}{dx} + \frac{5}{3}\left(\frac{dz_b}{dx}\right)^2 + \left(\frac{q}{\nu_t}\right)^2\left(\frac{32}{8085}d\frac{d^2d}{dx^2} - \frac{316}{13475}\left(\frac{dd}{dx}\right)^2\right) \qquad \text{(A.3.25d)}$$

The first term in the equation of motion is the convective term. In this term the coefficient α is the so-called convection coefficient. This convection coefficient is often taken $\alpha = 1$ for quasi-uniform flows. In open channels the value $\alpha = 1$ is a good approximation for turbulent flows over horizontal bottoms, because of the logarithmic velocity profile, which is almost a uniform velocity profile. For uniform, laminar flows, as well as for uniform, turbulent flows modeled with a constant eddy-viscosity, the value for α is equal to $\alpha = 1.2$. The value for the convection coefficient α in non-uniform flow, eq. (A.3.25c), is dependent on the derivative of the water depth.

The second term of eq. (A.3.25b) is the hydrostatic pressure-gradient term which exists already in the ordinary shallow-water equations.

The third term is the friction term. This term, expression (A.3.25d), is dependent on the fluctuating water depth and the bathymetry. For uniform flow with a constant eddy-viscosity, the bed shear stress is:

$$\frac{1}{\rho}\tau_{bx} = -3\frac{q\nu_t}{d^2} \qquad \text{(A.3.25)}$$

This is multiplied by a friction coefficient, γ, dependent on changes of the bottom level. Graphs of the convection and friction coefficients are shown in Fig. A.3.4. The flow situation is based on a situation in which the average velocity is 1. m/s, the water depth, d, is 20 m, the length of the sinusoidal sill, L, is 6500 m and the sill height, D, is 7.5 m. The perturbation quantity ε is in this situation $\varepsilon = 1/3$. Steeper slopes are not allowed because the perturbation quantity becomes too large in such cases. For larger perturbation quantities it is not allowed to cut the series of solutions after the second-order solutions because the influence on the zeroth-order solutions of these higher-order solutions can be large. The sill height is chosen quite high to make the influences on the fall and raise of the water level due

to the acceleration and deceleration visible. The velocity profiles and water levels calculated in this section are plotted in Fig. A.3.1 through Fig. A.3.3 for above-described flow characteristics.

In Fig. A.3.1 the horizontal velocity profiles are shown. The first-order and second-order profiles are plotted with the same velocity scale as the profiles of the zeroth-order and the overall velocity profiles.

The main part of the first-order velocity profile is proportional to the first-order derivative of the bottom (eq. A.3.12). As expected, it makes the profile more uniform where the bottom slopes upward in the flow direction (accelerating flow) and less uniform where the bottom slopes downward (decelerating flow). The second-order velocity is dependent on the first-order as well as on the second-order derivative of the bottom elevation. This means that there is some "remembrance" on the sill's crown and in the valley about the acceleration or deceleration phase just before, respectively. As shown in this figure, the first-order and second-order discharges are not zero, due to the dominance of the zeroth-order velocity part (adaptation of the zeroth-order water depth) in the first-order and second-order velocity profiles. Due to the large perturbation quantity the influence of the first-order and second-order velocity profiles are visible in the overall velocity profiles.

Graphs of the vertical velocities are shown in Fig. A.3.2. For the vertical velocities the same scales as for the horizontal velocities in the previous figure are used. The plot of the zeroth-order vertical velocity shows upward flow in the acceleration zone and downward flow in the deceleration zone. Adaptation of the direction of the flow to the fall of the water level is recognisable in the first-order velocity profiles.

The water depths are plotted in Fig. A.3.3. The zeroth-order water depth is not influenced by the fall of water surface due to the changes in the velocity profiles. This fall of the water surface is recognisable in the first-order and second-order water depth. The value of the second-order water depth at x=0 deviates from zero, because the presented values of the horizontal velocities, vertical velocities and water depths are the values at the end of a calculation domain to avoid inflow phenomena.

In Fig. A.3.4 the convection coefficient and friction coefficient calculated with eq. (A.3.25c) and (A.3.25d) are plotted. The convection coefficient, α, increases in the deceleration zone and decreases in the accelerating zone. The deviation from the value for uniform flow, α=1.2, is small. The friction coefficient, γ, increases in the acceleration zone

and decreases in the deceleration zone. The deviation from the value for uniform flow, $\gamma = 1$, is small.

Although the method of asymptotic expansion for the scaling used in this investigation is only valid for unrealistically mild slopes, it is nevertheless also applied in the following section to determine solutions for the velocities and water depth for the case of a parabolic eddy-viscosity distribution instead of the constant eddy-viscosity. A parabolic eddy-viscosity profile gives a logarithmic velocity profile for uniform flow conditions, which is better in agreement with measurements (chapter 4).

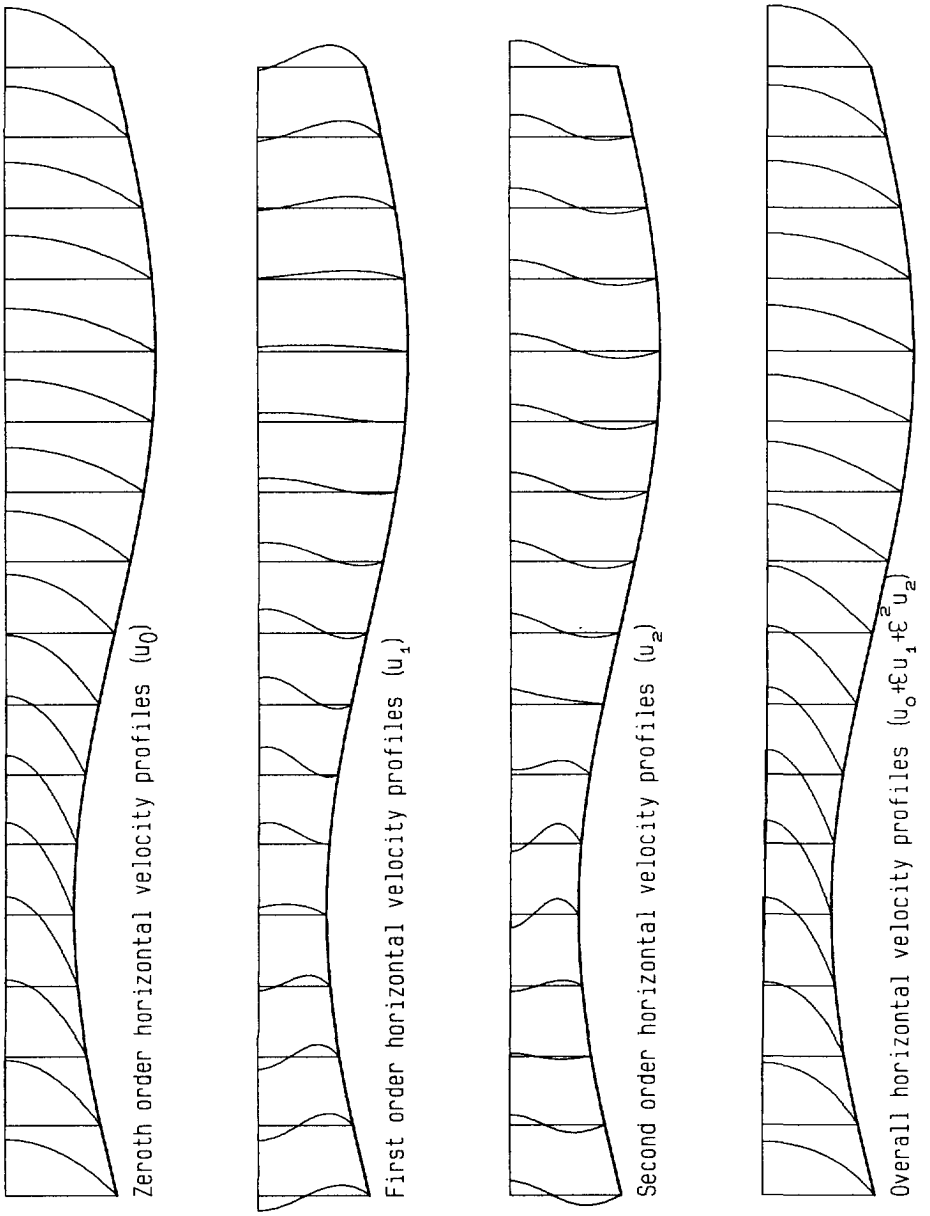

Figure A.3.1 The zeroth-order, first-order, second-order and overall horizontal velocity profiles

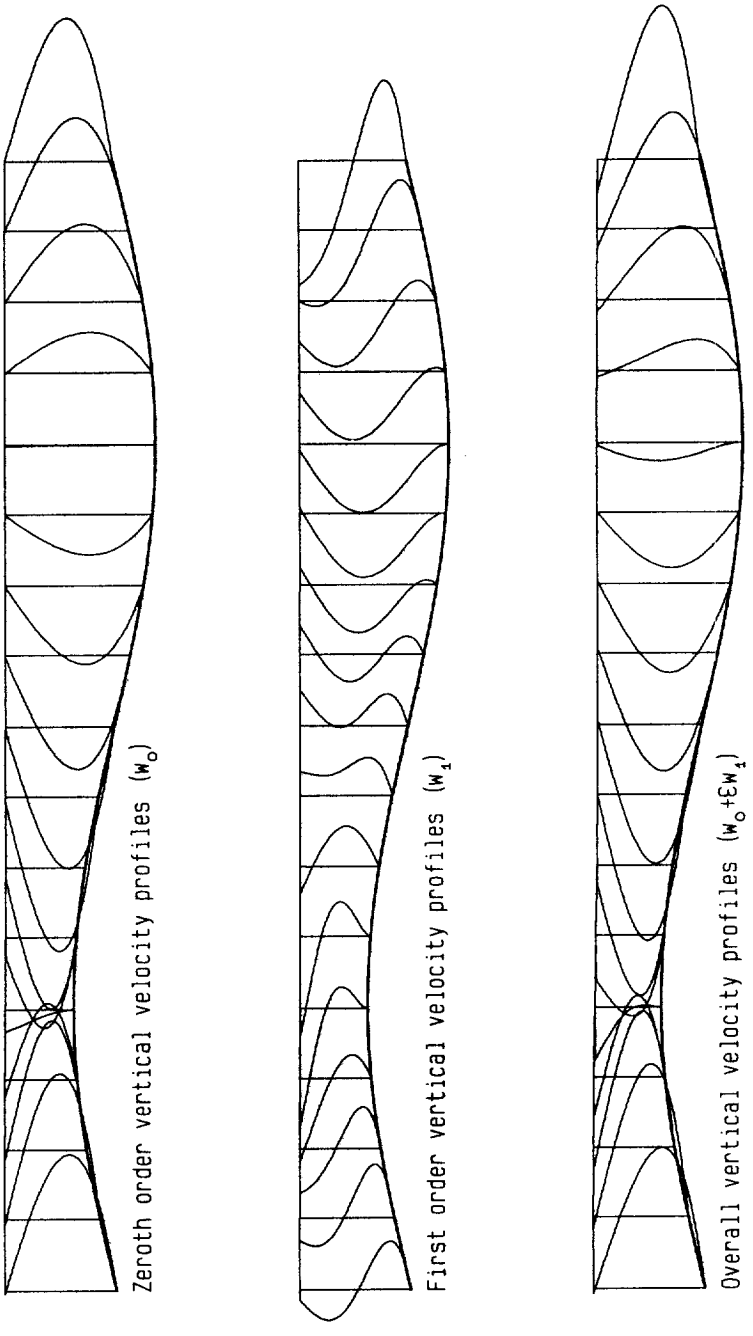

Figure A.3.2 The zeroth-order, first-order and overall vertical velocity profiles

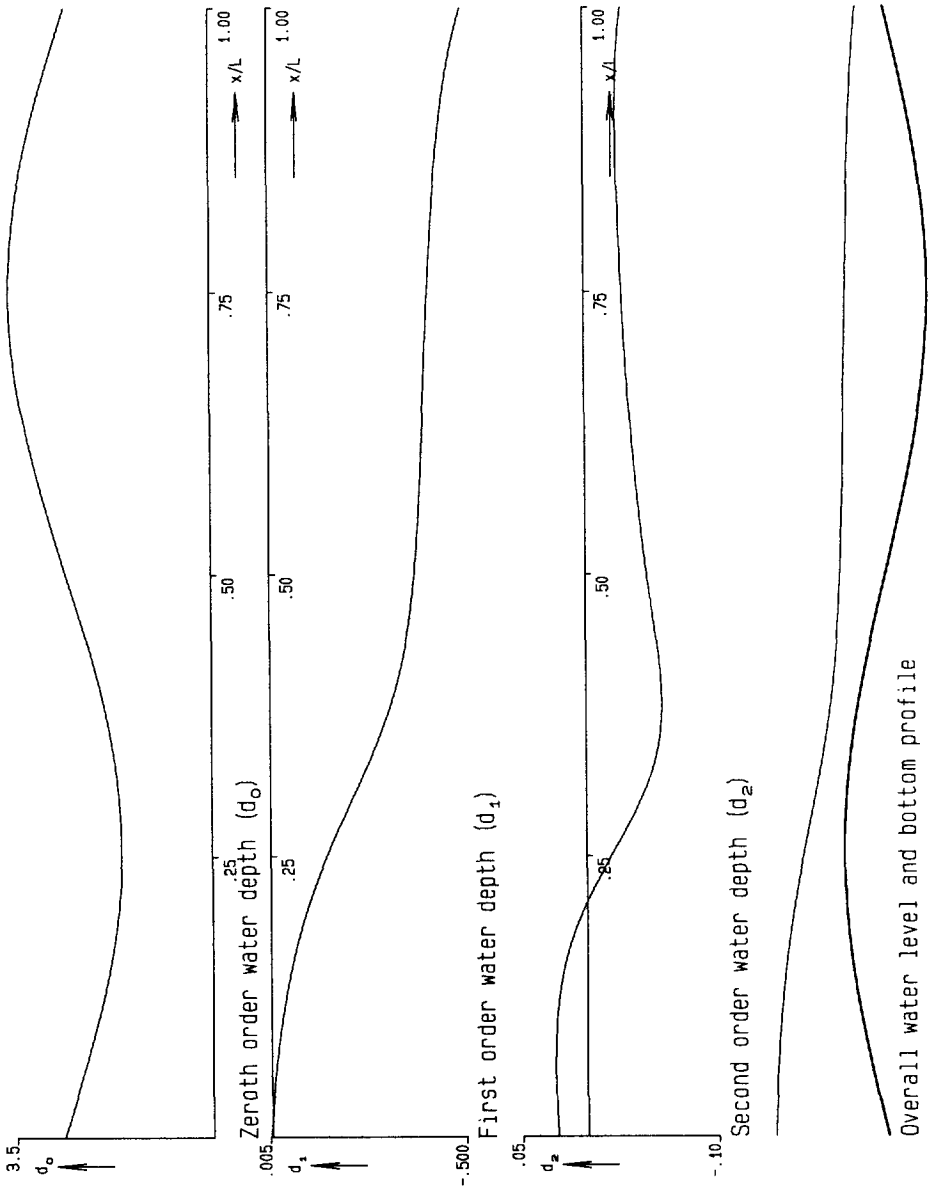

Figure A.3.3 The zeroth-order, first-order, second-order and overall water depths

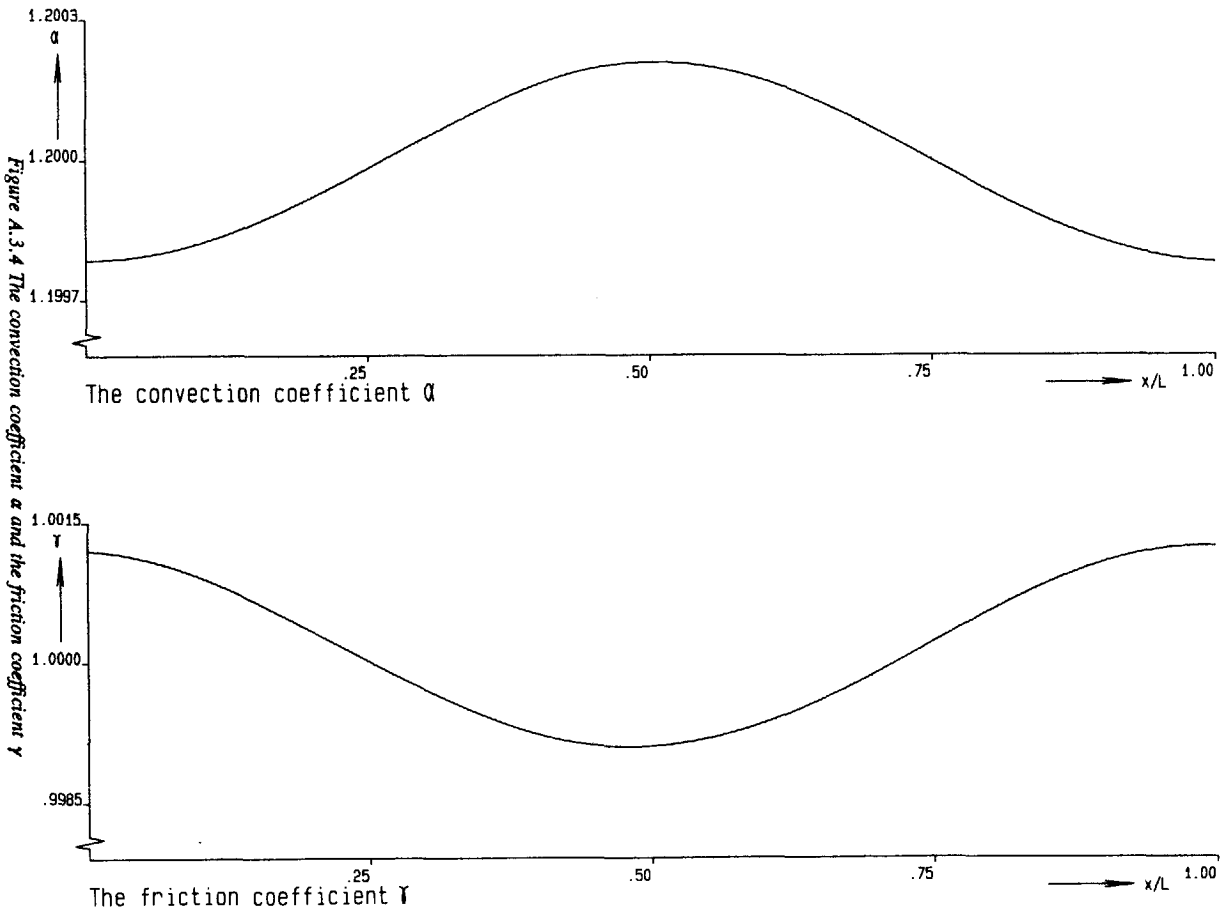

Figure A.3.4 The convection coefficient α and the friction coefficient γ

A.4 The parabolic eddy-viscosity distribution

In this section the analysis of section A.3 is repeated for a parabolic eddy-viscosity profile. Substitution of such an eddy-viscosity in the Navier-Stokes equations gives a logarithmic horizontal velocity profile when uniform flow is considered. The zero value of these velocity profiles is taken a small distance (z_0) above the bottom.

For hydraulic rough flow conditions this characteristic length is dependent on the roughness of the bottom as in:

$$z_0 = \frac{k_N}{30} \tag{A.4.1a}$$

in which k_N is the roughness according to Nikuradse. For hydraulic smooth flow conditions this length is:

$$z_0 = 0.11 \frac{\nu}{u_*} \tag{A.4.1b}$$

in which ν is the kinematic viscosity and u_* is the friction velocity (defined as $u_* = \sqrt{|\tau_{bx}|/\rho}$).

The roughness length, z_0, is used by Jackson & Hunt [1975] as a perturbation quantity to investigate wind flow over a hill. In the present investigation z_0 is not used as a perturbation quantity. Just as in the previous chapter $\frac{D}{L}$ is used as the only perturbation quantity. Unfortunately, it is no longer possible to derive the second-order velocity profiles. As will become clear the expressions of the first-order velocities contain series. To derive the expressions for the second-order velocities every term of the series in the expressions for the first-order velocities has to be written as a series. This makes the determination of the second-order velocities very time-consuming, and besides it will be difficult to understand the meaning of these second-order velocities.

The equations for the roughness length z_0, eq. (A.4.1), are still written in a dimensional form. From this point in this section only dimensionless expressions are used. This means that the roughness according to Nikuradse, k_N, and the roughness length, z_0, are scaled with the vertical characteristic length D. The eddy viscosity, ν_t, is scaled with the characteristic velocity multiplied by the vertical characteristic length and the small coefficient, with χUD. The friction velocity, u_*, is scaled with the characteristic velocity multiplied with the square root of χ, while the Von Kármán parameter, κ, is scaled with the square root of χ. This looks strange but it is a consequence of the used definition of u_*, as

will become clear below.

The dimensionless parabolic eddy-viscosity distribution is written as:

$$\nu_t = u_* \kappa (z - z_b)\left(\frac{d - (z - z_b)}{d}\right)$$

Due to the dependence of the eddy-viscosity on the water depth d, the eddy-viscosity has to be written as an asymptotic expansion too. This yields:

$$\begin{aligned}
\nu_t &= u_* \kappa (z - z_b)\left(1 - \left(\frac{z - z_b}{d}\right)\right) \\
&= u_* \kappa (z - z_b)\left(1 - \left(\frac{(z - z_b)}{d_0}\left(1 - \varepsilon \frac{d_1}{d_0} + \varepsilon^2 \left(\frac{d_1^2}{d_0^2} - \frac{d_2}{d_0}\right) + \cdots\right)\right)\right) \\
&= u_* \kappa (z - z_b)\left(\left(1 - \left(\frac{(z - z_b)}{d_0}\right)\right) + \varepsilon \left(\frac{(z - z_b)}{d_0}\frac{d_1}{d_0}\right) + \varepsilon^2 \frac{(z - z_b)}{d_0}\left(\frac{d_2}{d_0} - \frac{d_1^2}{d_0^2}\right) + \cdots\right) \\
&= u_* \kappa d_0 \sigma \left((1 - \sigma) + \varepsilon \frac{d_1}{d_0}\sigma + \varepsilon^2 \left(\frac{d_2}{d_0} - \frac{d_1^2}{d_0^2}\right)\sigma + \cdots\right) \\
&= \nu_{t_0} + \varepsilon \nu_{t_1} + \varepsilon^2 \nu_{t_2} + \cdots
\end{aligned} \tag{A.4.2}$$

Due to the decomposition of the eddy-viscosity the equations of motion change slightly. The equations eq. (A.2.11a) and eq. (A.2.15a) become:

$$\frac{\partial p_0}{\partial x} - \frac{1}{d_0}\left(\frac{dz_b}{dx} + \sigma \frac{dd_0}{dx}\right)\frac{\partial p_0}{\partial \sigma} = \frac{1}{d_0}\frac{\partial}{\partial \sigma}\left(\frac{\nu_{t_0}}{d_0}\frac{\partial u_0}{\partial \sigma}\right) \tag{A.4.3}$$

$$\begin{aligned}
u_0 \frac{\partial u_0}{\partial x} - \frac{u_0}{d_0}\left(\frac{dz_b}{dx} + \sigma \frac{dd_0}{dx}\right)\frac{\partial u_0}{\partial \sigma} + \frac{w_0}{d_0}\frac{\partial u_0}{\partial \sigma} + \frac{\partial p_1}{\partial x} + \\
- \frac{1}{d_0}\left(\frac{dz_b}{dx} + \sigma \frac{dd_0}{dx}\right)\frac{\partial p_1}{\partial \sigma} = \frac{1}{d_0}\frac{\partial}{\partial \sigma}\left(\frac{\nu_{t_0}}{d_0}\frac{\partial u_1}{\partial \sigma} + \frac{\nu_{t_1}}{d_0}\frac{\partial u_0}{\partial \sigma}\right)
\end{aligned} \tag{A.4.4}$$

Solutions of the zeroth- and first-order sets of equations.

Just as was done in the previous section the first variables to be determined are the zeroth-order variables, the zeroth-order water pressure distribution first, then the zeroth-order horizontal velocity and at last the zeroth-order vertical velocity. These zeroth-order solutions are substituted into the first-order equations. The first-order water pressure distribution is the first first-order variable to be solved, then the first-order horizontal velocity and at last the first-order vertical velocity.

From eq. (A.2.11b) the zeroth-order water pressure can be derived. It reads:

$$p_0 = g d_0 (1 - \sigma) \tag{A.4.5}$$

This is again the hydrostatic water pressure distribution and is equal to eq. (A.3.5). This result can be substituted in the Navier-Stokes equation in x-direction. After substitution of the zeroth-order viscosity and integrating twice with respect to σ, the zeroth-order horizontal velocity is derived:

$$u_0 = \frac{g d_0}{u_* \kappa} \frac{\mathrm{d}(d_0 + z_b)}{\mathrm{d}x} \ln(\sigma/\sigma_0)$$

in which σ_0 is the dimensionless roughness length, defined as the dimensionless roughness length of expression (A.4.1) divided by the zeroth-order water depth:

$$\sigma_0 = \frac{z_0}{d_0}$$

The solution of u_0 shows a logarithmic velocity profile, which contains the still unknown zeroth-order water depth. The expression for the water depth can be derived by using the discharge condition (A.2.13), which yields the differential equation for the zeroth-order water depth:

$$\frac{\mathrm{d}d_0}{\mathrm{d}x} = -\frac{u_* \kappa q}{g d_0^2 (L_{\sigma 0} - 1)} - \frac{\mathrm{d}z_b}{\mathrm{d}x} \tag{A.4.6}$$

in which $L_{\sigma 0}=\ln(1/\sigma_0)$.

Substitution of eq. (A.4.6) into the expression for the zeroth-order horizontal velocity gives:

$$u_0 = \frac{q}{d_0} \frac{\ln(\sigma/\sigma_0)}{L_{\sigma 0} - 1} \tag{A.4.7}$$

in which q is the discharge, d_0 is the zeroth-order water depth and σ_0 is the dimensionless roughness length.

Expression (A.4.6) contains the unknown friction velocity u_*. The friction velocity can be obtained from the Reynolds shear stress distribution, which can be derived from the right hand term of eq. (A.4.3). After substitution of the expressions for u_0, eq. (A.4.7), and ν_{t0}, eq. (A.4.2), the Reynolds shear stress reads:

$$\tau_{xz} = \frac{u_* \kappa q}{d_0 (L_{\sigma 0} - 1)} (\sigma - 1)$$

Substitution of $\sigma=0$ yields the bottom friction which is equal to u_*^2. From this equalization the expression for the friction velocity can be derived:

$$u_* = \frac{q\,\kappa}{d_0}\frac{1}{(L_{\sigma 0}-1)}\,^{\dagger} \qquad \text{(A.4.8)}$$

This expression can also be substituted into the expression for the viscosity, eq. (A.4.2), into the equation for the zeroth-order water depth, eq. (A.4.6), and into the expression for the zeroth-order velocity, eq. (A.4.5). The water depth, written in this way, follows from:

$$\frac{\mathrm{d}d_0}{\mathrm{d}x} = -\frac{\kappa^2 q^2}{g d_0^3}\frac{1}{(L_{\sigma 0}-1)^2} - \frac{\mathrm{d}z_b}{\mathrm{d}x} = -\frac{u_*^2}{g d_0} - \frac{\mathrm{d}z_b}{\mathrm{d}x}$$

This expression shows that the pressure gradient due to the fall of the water level, $\mathrm{d}(d_0+z_b)/\mathrm{d}x$, is in equilibrium with the bottom friction, u_*^2.

Substitution of expression (A.4.8) into eq. (A.4.7) yields:

$$u_0 = \frac{u_*}{\kappa}\ln(\sigma/\sigma_0)$$

This expression is a commonly used expression for the horizontal velocity. However, in this investigation the zeroth-order velocity written in this way is not used.

The last zeroth-order variable to be determined is the vertical velocity. This is derived by substituting the expression for the zeroth-order horizontal velocity, eq. (A.4.7), into the continuity equation, eq. (A.2.10). This equation has to be integrated using the boundary equation, eq. (A.2.12e). The result is:

$$w_0 = \frac{q}{d_0}\frac{L_{\sigma 0}}{(L_{\sigma 0}-1)}\sigma\left(\ln(\sigma/\sigma_0)-1\right)\frac{\mathrm{d}d_0}{\mathrm{d}x} + \frac{q}{d_0}\frac{1}{L_{\sigma 0}-1}\ln(\sigma/\sigma_0)\frac{\mathrm{d}z_b}{\mathrm{d}x} \qquad \text{(A.4.9)}$$

The zeroth-order variables are known and the expressions of these variable can be substituted into the set of first-order equations.

To obtain the first-order water level and first-order horizontal and vertical velocities the analysis as was used before to obtain the zeroth-order water depth and velocities has to be repeated. The first-order water pressure can be derived from eq. (A.2.15b). After the derivation of the first-order water pressure, the first-order horizontal velocity can be calculated by substituting the zeroth-order horizontal and vertical velocities and the first-order water pressure into eq. (A.4.4). This equation has to be integrated twice with respect to σ. Using the boundary equations (A.2.16c) and (A.2.16b) the expression for the first-order

---

†This expression gives the reason for scaling u_* with $\chi^{1/2}U$. The dimensionless u_* has to be of order 1. The dimensionless discharge, q, and dimensionless water depth, d, are of order 1, while $L_{\sigma 0}$ is of order 7. Scaling κ^* with $\chi^{1/2}$, with κ=0.4 and $\chi={}^1/_{225}$, provides that the fraction $\kappa/(L_{\sigma 0}-1)$ and κ^* are of order 1.

horizontal velocity is found. However, the horizontal velocity is still dependent on the first-order water depth, d_1, which at this time is still unknown. To solve this water depth the discharge condition (A.2.17) is used. This gives a differential equation for the first-order water level which can be substituted into the horizontal velocity. The last first-order variable to be solved is the first-order vertical velocity. This velocity is solved by using the continuity equation, eq. (A.2.14), and the boundary condition, eq. (A.2.16e).

Unfortunately, terms exist in the Navier-Stokes equation in x-direction which are not solvable analytically in this way. Terms containing logarithms are divided by the eddy-viscosity, which value is zero at the water surface, eq. (A.4.2). This gives very large values near the water level for these logarithmic terms and causes insolvability of the first-order velocity. The terms making the horizontal velocity unsolvable are:

$$\frac{\ln\left(\frac{\sigma}{\sigma_0}\right)-\ln\left(\frac{1}{\sigma_0}\right)}{1-\sigma} \qquad \text{and} \qquad \frac{\ln^2\left(\frac{\sigma}{\sigma_0}\right)-\ln^2\left(\frac{1}{\sigma_0}\right)}{1-\sigma}$$

Hence, to determine the horizontal velocity these terms are written as Taylor series around the water level, $\sigma=1$ (Appendix B):

$$\frac{\ln\left(\frac{\sigma}{\sigma_0}\right)-\ln\left(\frac{1}{\sigma_0}\right)}{1-\sigma} = -\sum_{i=1}^{\infty}\frac{(1-\sigma)^{i-1}}{i} \tag{B.6}$$

and

$$\frac{\ln^2\left(\frac{\sigma}{\sigma_0}\right)-\ln^2\left(\frac{1}{\sigma_0}\right)}{1-\sigma} = -2\sum_{i=1}^{\infty}\frac{(1-\sigma)^{i-1}}{i}\left(\ln\left(\frac{1}{\sigma_0}\right)-\sum_{k=1}^{i-1}\frac{1}{k}\right) \tag{B.10}$$

In the first-order horizontal velocity these series appear integrated with respect to the σ coordinate. Due to the used continuity equation these series also appear in depth-integrated form in the first-order horizontal velocity. These depth-integrated forms are approximated by fractions.

The expression for the first-order horizontal velocity is derived by substitution of the zeroth-order horizontal and vertical velocities and the first-order water depth into eq. (A.4.4) and by twice integrating this equation. After once integrating eq. (A.4.4) the equations (B.6) and (B.10) are substituted. The expression for the first-order horizontal velocity reads:

$$u_1 = -\frac{q}{d_0\kappa^2}\frac{L_{\sigma 0}}{(L_{\sigma 0}-1)^2}\frac{\mathrm{d}d_0}{\mathrm{d}x}\left(\sum_{i=1}^{\infty}\frac{(1-\sigma)^i-1}{i^2}\left(2L_{\sigma 0}-3-2\sum_{k=1}^{i-1}\frac{1}{k}\right)+2\ln\left(\frac{\sigma}{\sigma_0}\right)\frac{L_{\sigma 0}-b}{L_{\sigma 0}-1}\right)+ \\ -\frac{q}{d_0}\frac{d_1}{d_0}\frac{L_{\sigma 0}}{(L_{\sigma 0}-1)^2}\ln\left(\frac{\sigma}{\sigma_0}\right) \tag{A.4.10}$$

with b=2.4995.

In the first term of the right hand side of this expression parts of eq. (B.6) and eq. (B.10) are recognizable. The second term contains depth-integrated expressions of integrated equations (B.6) and (B.10). The third term is the correction of the zeroth-order horizontal velocity for changes in the water depth due to the first-order water depth.

The differential equation for the first-order water depth is derived from the discharge condition, eq. (A.2.17). It reads:

$$\frac{\mathrm{d}d_1}{\mathrm{d}x} = \frac{q^2}{g d_0^3}\frac{L_{\sigma 0}}{(L_{\sigma 0}-1)^4}\frac{\mathrm{d}d_0}{\mathrm{d}x}\left(2(L_{\sigma 0}-b)+(L_{\sigma 0}-1)\left(L_{\sigma 0}^2-3L_{\sigma 0}+4\right)\right) - \frac{\mathrm{d}(d_0+z_b)}{\mathrm{d}x}\frac{d_1}{d_0}\left(\frac{2L_{\sigma 0}-1}{L_{\sigma 0}-1}\right) \tag{A.4.11}$$

The expression for the first-order water pressure is the same expression as the expression for the first-order water pressure in the previous section using a constant eddy-viscosity:

$$p_1 = g d_1 \tag{A.4.12}$$

while the expression for the first-order vertical velocity is given by:

$$\begin{aligned}
w_1 = {} & \frac{q}{d_0\kappa^2}\left(\frac{L_{\sigma 0}^2+1}{(L_{\sigma 0}-1)^3}\left(\frac{\mathrm{d}d_0}{\mathrm{d}x}\right)^2 - \frac{L_{\sigma 0}}{(L_{\sigma 0}-1)}d_0\frac{\mathrm{d}^2 d_0}{\mathrm{d}x^2}\right)\cdot \\
& \cdot\left(\sum_{i=1}^{\infty}\left(\frac{(1-\sigma)^{i+1}-1}{i^2(i+1)}+\frac{\sigma}{i^2}\right)\left(2L_{\sigma 0}-3-2\sum_{k=1}^{i-1}\frac{1}{k}\right)-2\sigma\left(\ln\left(\frac{\sigma}{\sigma_0}\right)-1\right)\left(\frac{L_{\sigma 0}-b}{L_{\sigma 0}-1}\right)\right)+ \\
& +\frac{q}{d_0\kappa^2}\frac{L_{\sigma 0}}{(L_{\sigma 0}-1)^2}\left(\frac{\mathrm{d}d_0}{\mathrm{d}x}\right)^2\left(2\sum_{i=1}^{\infty}\left(\frac{1-(1-\sigma)^{i+1}}{i^2(i+1)}-\frac{\sigma}{i^2}\right)+2\sigma\left(\frac{L_{\sigma 0}-b}{L_{\sigma 0}-1}\right)-\sigma\left(\ln\left(\frac{\sigma}{\sigma_0}\right)-1\right)\frac{2b-2}{(L_{\sigma 0}-1)^2}\right)+ \\
& -\frac{q}{d_0\kappa^2}\frac{L_{\sigma 0}}{(L_{\sigma 0}-1)^2}\frac{\mathrm{d}d_0}{\mathrm{d}x}\left(\frac{\mathrm{d}d_0}{\mathrm{d}x}+\frac{\mathrm{d}z_b}{\mathrm{d}x}\right)\left(\sum_{i=1}^{\infty}\frac{(1-\sigma)^i-1}{i^2}\left(2L_{\sigma 0}-3-2\sum_{k=1}^{i-1}\frac{1}{k}\right)+2\ln\left(\frac{\sigma}{\sigma_0}\right)\frac{L_{\sigma 0}-b}{L_{\sigma 0}-1}\right)+ \\
& -\frac{q}{d_0\kappa^2}\frac{L_{\sigma 0}}{(L_{\sigma 0}-1)^2}\left(\frac{\mathrm{d}d_0}{\mathrm{d}x}\right)^2\left(\sum_{i=1}^{\infty}\frac{1-(1-\sigma)^{i+1}}{i(i+1)}\left(2L_{\sigma 0}-3-2\sum_{k=1}^{i-1}\frac{1}{k}\right)+2\left(\ln\left(\frac{\sigma}{\sigma_0}\right)-\sigma\right)\frac{L_{\sigma 0}-b}{(L_{\sigma 0}-1)}\right)+ \\
& +\frac{q}{d_0}\left(\frac{d_1}{d_0}\left(\frac{-L_{\sigma 0}^2+L_{\sigma 0}-1}{(L_{\sigma 0}-1)^3}\right)\frac{\mathrm{d}d_0}{\mathrm{d}x}+\frac{L_{\sigma 0}}{L_{\sigma 0}-1}\frac{\mathrm{d}d_1}{\mathrm{d}x}\right)\sigma\left(\ln\left(\frac{\sigma}{\sigma_0}\right)-1\right)-\frac{q}{d_0}\frac{d_1}{d_0}\frac{L_{\sigma 0}}{(L_{\sigma 0}-1)^2}\ln\left(\frac{\sigma}{\sigma_0}\right)\frac{\mathrm{d}z_b}{\mathrm{d}x}
\end{aligned} \tag{A.4.13}$$

Graphs of the horizontal velocity profiles and the water levels are shown in Fig. A.4.1 and

Fig. A.4.2. The same flow characteristics are used as in the previous section. The average velocity is 1. m/s, the water depth at the inflow boundary, d, is 20 m, the length of the sinusoidal sill, L, is 6500 m and the sill height, D, is 7.5 m.

The first-order velocities plotted in Fig. A.4.1 have the same velocity scale as the first-order velocities of Fig. A.4.1. The first-order velocity is proportional to the first-order derivative of the water depth (eq. (A.4.10)). The zeroth-order velocity profile is logarithmic. The maximum velocity in a vertical is dependent on the water depth. No other adaptations to the bottom profile are present. The overall velocity profiles hardly differ from the zeroth-order velocity profiles.

The water depths are plotted in Fig. A.4.2. In the zeroth-order water depth the fall of the water surface due to the acceleration is nearly absent. The gradient of the zeroth-order water level, $\mathrm{d}(z_b+d_0)/\mathrm{d}x$, has the same value as the gradient of the water level for uniform flow over a horizontal bottom. The zeroth-order water level is dependent on the bottom geometry only through changes in the friction velocity. In contrast to the zeroth-order water depth, the first-order water depth is dependent on the bottom slope. Nevertheless the first-order water depth is hardly recognizable in the overall water depth.

Derivation of the shallow-water equations.

To obtain the modified shallow-water equations the expressions for the zeroth-order and first-order horizontal velocities and water depths have to be substituted into the continuity equation, eq. (A.2.2) and the Navier-Stokes equation in x-direction, eq. (A.2.3a). The continuity equation is not worked out because the analysis is the same as described in the previous section. It reads:

$$\frac{\mathrm{d}q}{\mathrm{d}x} = 0 \qquad \text{(A.4.14)}$$

The shallow-water equation of motion is obtained from the Navier-Stokes equation for the x-direction. In this case the convective part of the Navier-Stokes equation only contains the zeroth-order horizontal velocity. Integration of this part gives a convective term which is only dependent on changes in the bottom profile only through the depth-averaged velocity. This convective term also appears in the ordinary shallow-water equations, the ones derived for quasi-uniform flow over horizontal bottoms. One of the goals of this investigation is to find modifications of these shallow-water equations for the convective term. Therefore

the second-order part of the convective terms is taken into account. This is a second-order term while the other terms are zeroth-order or first-order terms. In the friction term, derived in the previous section for a constant eddy-viscosity, the second-order terms are hardly visible. In Fig. A.3.4 the friction coefficient, γ, derived with a constant eddy-viscosity is plotted. In this plot only the first-order derivative of the bottom is noticeable, which appears in the first-order friction term (eq. (A.3.25)). The second-order terms in the friction are dependent on the second-order derivative and the first-order derivative squared. These terms containing derivatives are so small that they are hardly visible in Fig. A.3.4. Therefore the second-order convective terms are taken into account, while the second-order pressure and viscous terms are neglected.

Therefore the equation to be solved reads:

$$\int_0^{d_r} \underbrace{\left(\varepsilon\left(d_0 u_0 \frac{\partial u_0}{\partial x} - u_0\left(\frac{dz_b}{dx} + \sigma\frac{dd_0}{dx}\right)\frac{\partial u_0}{\partial \sigma} + w_0\frac{\partial u_0}{\partial \sigma}\right)\right.}_{A_1} +$$

$$\underbrace{+\varepsilon^2\left(d_0 u_0 \frac{\partial u_1}{\partial x} - u_0\left(\frac{dz_b}{dx} + \sigma\frac{dd_0}{dx}\right)\frac{\partial u_1}{\partial \sigma} + d_0 u_1 \frac{\partial u_0}{\partial x} - u_1\left(\frac{dz_b}{dx} + \sigma\frac{dd_0}{dx}\right)\frac{\partial u_0}{\partial \sigma} + w_0\frac{\partial u_1}{\partial \sigma} + w_1\frac{\partial u_0}{\partial \sigma}\right) +}_{A_2}$$

$$\underbrace{\left. + d_0\frac{\partial p_0}{\partial x} + d_0\varepsilon\frac{\partial p_1}{\partial x} - \left(\frac{dz_b}{dx} + \sigma\frac{dd_0}{dx}\right)\left(\frac{\partial p_0}{\partial \sigma} + \varepsilon\frac{\partial p_1}{\partial \sigma}\right)\right)}_{B} d\sigma =$$

$$= \underbrace{\int_0^{d_r} \frac{\partial}{\partial \sigma}\left(\frac{\nu_{t0}}{d_0}\frac{\partial u_0}{\partial \sigma} + \varepsilon\left(\frac{\nu_{t0}}{d_0}\frac{\partial u_1}{\partial \sigma} + \frac{\nu_{t1}}{d_0}\frac{\partial u_0}{\partial \sigma}\right)\right) d\sigma}_{C} \qquad \text{(A.4.15)}$$

in which now $d_r = 1 + \varepsilon\frac{d_0}{d_1}$.

This equation is divided into three parts, part A containing the convective terms, part B the pressure terms and part C the friction terms. All parts are again evaluated separately, starting with part A of eq. (A.4.15).

To integrate part A the following equation is added:

$(\varepsilon u_0 + \varepsilon^2 u_1)$ · (continuity eq. (A.2.10)) and $(\varepsilon^2 u_0)$ · (continuity eq. (A.2.14))

This yields:

$$\int_0^{d_r}\left(\varepsilon\left(d_0 2u_0\frac{\partial u_0}{\partial x}-2u_0\left(\frac{dz_b}{dx}+\sigma\frac{dd_0}{dx}\right)\frac{\partial u_0}{\partial\sigma}+w_0\frac{\partial u_0}{\partial\sigma}+u_0\frac{\partial w_0}{\partial\sigma}\right)+\right.$$

$$+\varepsilon^2\left(d_0 2u_0\frac{\partial u_1}{\partial x}-2u_0\left(\frac{dz_b}{dx}+\sigma\frac{dd_0}{dx}\right)\frac{\partial u_1}{\partial\sigma}+d_0 2u_1\frac{\partial u_0}{\partial x}+\right.$$

$$\left.\left.-2u_1\left(\frac{dz_b}{dx}+\sigma\frac{dd_0}{dx}\right)\frac{\partial u_0}{\partial\sigma}+w_0\frac{\partial u_1}{\partial\sigma}+u_0\frac{\partial w_1}{\partial\sigma}+w_1\frac{\partial u_0}{\partial\sigma}+u_1\frac{\partial w_0}{\partial\sigma}\right)\right)d\sigma =$$

$$=\varepsilon\left(d_0\frac{d}{dx}\left(\int_0^{d_r}u_0^2 d\sigma\right)+\frac{dd_0}{dx}\left(\int_0^{d_r}u_0^2 d\sigma\right)+\right.$$

$$-u_0(d_r)\left(d_0\frac{dd_r}{dx}u_0(d_r)+d_r\frac{dd_0}{dx}u_0(d_r)+\frac{dz_b}{dx}u_0(d_r)-w_0(d_r)\right)+ \qquad \text{(A.4.16)}$$

$$\left.+u_0(0)\left(u_0(0)\frac{dz_b}{dx}-w_0(0)\right)\right)$$

$$+\varepsilon^2\left(2d_0\frac{d}{dx}\left(\int_0^{d_r}u_0u_1 d\sigma\right)+2\frac{dd_0}{dx}\left(\int_0^{d_r}u_0u_1 d\sigma\right)+\right.$$

$$-u_0(d_r)\left(d_0\frac{dd_r}{dx}u_1(d_r)+d_r\frac{dd_0}{dx}u_1(d_r)+\frac{dz_b}{dx}u_1(d_r)-w_1(d_r)\right)+$$

$$-u_1(d_r)\left(d_0\frac{dd_r}{dx}u_0(d_r)+d_r\frac{dd_0}{dx}u_0(d_r)+\frac{dz_b}{dx}u_0(d_r)-w_0(d_r)\right)+$$

$$\left.+u_0(0)\left(u_1(0)\frac{dz_b}{dx}-w(0)\right)+u_1(0)\left(u_0(0)\frac{dz_b}{dx}-w_0(0)\right)\right)$$

In eq. (A.4.16) the boundary conditions (A.2.12b), (A.2.16b), (A.2.12d) and (A.2.16d) can be recognized. Substitutions of these boundary conditions into eq. (A.4.16) yields for the convective part of eq. (A.4.15):

$$\varepsilon\left(\frac{d}{dx}\left(d_0\int_0^1 u_0^2 d\sigma+2\varepsilon d_1(u_0(1))^2+\text{H.O.T.}\right)\right)+\varepsilon^2\left(2\frac{d}{dx}\left(d_0\int_0^1 u_0u_1 d\sigma+\text{H.O.T.}\right)\right)$$

Substitution of eq. (A.4.7) and eq. (A.4.10), integration over the depth and omitting the H.O.T., yields:

$$\varepsilon\frac{d}{dx}\left(\frac{q^2}{d_0}\left(1+\frac{1}{(L_{\sigma 0}-1)^2}+\varepsilon\frac{d_1}{d_0}\frac{L_{\sigma 0}{}^2}{(L_{\sigma 0}-1)^2}\right)\right)-2\varepsilon^2\frac{d}{dx}\left(\frac{d_1}{d_0}\frac{q^2}{d_0}\frac{L_{\sigma 0}{}^3-2L_{\sigma 0}{}^2+2L_{\sigma 0}}{(L_{\sigma 0}-1)^3}\right)+$$

$$+\varepsilon^2 2\frac{d}{dx}\left(\frac{q^2}{d_0\kappa^2}\frac{dd_0}{dx}\left(\frac{a_{10}L_{\sigma 0}{}^3-a_{11}L_{\sigma 0}{}^2+a_{12}L_{\sigma 0}}{(L_{\sigma 0}-1)^3}+2\frac{L_{\sigma 0}{}^4-a_{20}L_{\sigma 0}{}^3+a_{21}L_{\sigma 0}{}^2-a_{22}L_{\sigma 0}}{(L_{\sigma 0}-1)^4}\right)\right) \qquad \text{(A.4.17)}$$

with $a_{10} = 1.1016$

$a_{11} = 4.0160$

$a_{12} = 3.5460$

$a_{20} = 4.9995$

$a_{21} = 6.9990$

$a_{22} = 4.9990$

The coefficients a_{10} until a_{22} are derived by numerical calculations of the series appearing in the integrated velocities.

The next part of eq. (A.4.15) to be evaluated is part B, the part with the pressure terms:

$$\int_0^{d_r}\left(d_0\frac{\partial p_0}{\partial x}+d_0\varepsilon\frac{\partial p_1}{\partial x}-\left(\frac{dz_b}{dx}+\sigma\frac{dd_0}{dx}\right)\left(\frac{\partial p_0}{\partial\sigma}+\varepsilon\frac{\partial p_1}{\partial\sigma}\right)\right)d\sigma =$$

$$= d_0\frac{d}{dx}\left(\int_0^{d_r}(p_0+\varepsilon p_1)d\sigma\right)-d_0\frac{dd_1}{dx}(p_0(d_r)+\varepsilon p_1(d_r))+$$

$$-\frac{dz_b}{dx}[p_0+\varepsilon p_1]_0^{d_r}-\frac{dd_0}{dx}[\sigma(p_0+\varepsilon p_1)]_0^{d_r}+\frac{dd_0}{dx}\int_0^{d_r}(p_0+\varepsilon p_1)d\sigma$$

Substitution of the solutions for the zeroth- and first-order pressure, eq. (A.4.5) and eq. (A.4.12), yields:

$$\frac{d}{dx}\left(d_0\int_0^{d_r}(p_0+\varepsilon p_1)d\sigma\right)-\frac{d}{dx}(z_b+d_0+\varepsilon d_1)(p_0(d_r)+\varepsilon p_1(d_r))+\frac{dz_b}{dx}(p_0(0)+\varepsilon p_1(0))=$$

$$=\frac{d}{dx}\left(d_0\int_0^1(p_0+\varepsilon p_1)d\sigma+\varepsilon\frac{d_1}{d_0}p_0(1)\right)-\frac{d}{dx}(z_b+d_0+\varepsilon d_1)\left(p_0(1)+\varepsilon\frac{d_1}{d_0}\frac{\partial p_0}{\partial\sigma}\bigg|_{\sigma=1}+\varepsilon p_1(1)\right)+$$

$$+\frac{dz_b}{dx}(p_0(0)+\varepsilon p_1(0))=$$

$$=g\frac{d}{dx}\left(\tfrac{1}{2}d_0^2+\varepsilon d_1d_0\right)+g\frac{dz_b}{dx}(d_0+\varepsilon d_1)=$$

$$=g(d_0+\varepsilon d_1)\frac{d}{dx}(z_b+d_0+\varepsilon d_1) \qquad \text{(A.4.18)}$$

The last part of eq. (A.4.15) to be solved is part C, the part with the Reynolds stress terms. This part yields:

$$\int_0^{d_r}\frac{\partial}{\partial\sigma}\left(\frac{\nu_{t0}}{d_0}\frac{\partial u_0}{\partial\sigma}+\varepsilon\left(\frac{\nu_{t0}}{d_0}\frac{\partial u_1}{\partial\sigma}+\frac{\nu_{t1}}{d_0}\frac{\partial u_0}{\partial\sigma}\right)\right)d\sigma =$$

$$=\left[\frac{\nu_{t0}}{d_0}\frac{\partial u_0}{\partial\sigma}\right]_0^1+\varepsilon\frac{d_1}{d_0}\frac{\partial}{\partial\sigma}\left(\frac{\nu_{t0}}{d_0}\frac{\partial u_0}{\partial\sigma}\right)\bigg|_{\sigma=1}+\varepsilon\left[\frac{\nu_{t0}}{d_0}\frac{\partial u_1}{\partial\sigma}+\frac{\nu_{t1}}{d_0}\frac{\partial u_0}{\partial\sigma}\right]_0^1$$

Substitution of the zeroth- and first-order velocity profiles, eq. (A.4.7) and eq. (A.4.10), and

the zeroth- and first-order eddy-viscosity, eq. (A.4.2), yields, after omitting the H.O.T.:

$$\frac{1}{\rho}\tau_{bx} = -\frac{u_* q \kappa}{d_0(L_{\sigma 0}-1)}\left(1-\varepsilon\frac{d_1}{d_0}\frac{L_{\sigma 0}}{(L_{\sigma 0}-1)}\right)-\varepsilon\frac{2}{\kappa^2}\frac{u_* q\kappa}{d_0(L_{\sigma 0}-1)}\left(\frac{L_{\sigma 0}^{\,2}-bL_{\sigma 0}}{(L_{\sigma 0}-1)^2}\right)\frac{\mathrm{d}d_0}{\mathrm{d}x} \qquad \text{(A.4.19)}$$

The shallow-water equation of motion can be derived by adding the convective terms, eq. (A.4.17), the pressure terms, eq. (A.4.18), and the turbulent friction terms, eq. (A.4.19). The dimensionless shallow-water equation reads:

$$\varepsilon\frac{\mathrm{d}}{\mathrm{d}x}\left(\frac{q^2}{d_0}\left(1+\frac{1}{(L_{\sigma 0}-1)^2}+\varepsilon\frac{d_1}{d_0}\frac{L_{\sigma 0}^{\,2}}{(L_{\sigma 0}-1)^2}\right)\right)-2\varepsilon^2\frac{\mathrm{d}}{\mathrm{d}x}\left(\frac{d_1}{d_0}\frac{q^2}{d_0}\frac{L_{\sigma 0}^{\,3}-2L_{\sigma 0}^{\,2}+2L_{\sigma 0}}{(L_{\sigma 0}-1)^3}\right)+$$

$$+\varepsilon^2 2\frac{\mathrm{d}}{\mathrm{d}x}\left(\frac{q^2}{d_0\kappa^2}\frac{\mathrm{d}d_0}{\mathrm{d}x}\left(\frac{a_1L_{\sigma 0}^{\,4}-a_2L_{\sigma 0}^{\,3}+a_3L_{\sigma 0}^{\,2}-a_4L_{\sigma 0}}{(L_{\sigma 0}-1)^4}\right)\right)+g(d_0+\varepsilon d_1)\frac{\mathrm{d}}{\mathrm{d}x}(z_b+d_0+\varepsilon d_1) = \text{(A.4.20)}$$

$$= -\frac{u_* q\kappa}{d_0(L_{\sigma 0}-1)}\left(1-\varepsilon\frac{d_1}{d_0}\frac{L_{\sigma 0}}{(L_{\sigma 0}-1)}\right)-\varepsilon\frac{2}{\kappa^2}\frac{u_* q\kappa}{d_0(L_{\sigma 0}-1)}\left(\frac{L_{\sigma 0}^{\,2}-bL_{\sigma 0}}{(L_{\sigma 0}-1)^2}\right)\frac{\mathrm{d}d_0}{\mathrm{d}x}$$

in which $a_1 = 3.1016$

$a_2 = 14.117$

$a_3 = 21.560$

$a_4 = 3.5440$

$b = 2.4995$

In eq. (A.4.20) the water depth is approximated by the first two orders of the water depth, which means that $d=d_0+\varepsilon d_1$. This yields for the reciprocal value of d:

$$\frac{1}{d} = \frac{1}{d_0}\left(1-\varepsilon\frac{d_1}{d_0}+\cdots\right)$$

The variable $L_{\sigma 0}$ contains the zeroth-order water depth. In the dimensional form of the shallow-water equations terms containing zeroth-order variables have to be replaced by terms containing only non-expanded variables. The variable $L_{\sigma 0}$ is a term in a Taylor series around the point $\sigma=1$ of the non-expanded variable L_0, which reads:

$$L_0 = \ln\left(\frac{d}{z_0}\right) = \ln\left(\frac{d_0+\varepsilon d_1+\varepsilon^2 d_0+\cdots}{z_0}\right) = \ln\left(1+\varepsilon\frac{d_1}{d_0}+\varepsilon^2\frac{d_2}{d_0}+\cdots\right)+\ln\left(\frac{1}{\sigma_0}\right)$$

$$= \ln(1)+\varepsilon\frac{d_1}{d_0}+\varepsilon^2\left(\frac{d_2}{d_0}-\tfrac{1}{2}\left(\frac{d_1}{d_0}\right)^2\right)+\cdots+\ln\left(\frac{1}{\sigma_0}\right)$$

$$= L_{\sigma 0}+\varepsilon\frac{d_1}{d_0}+\varepsilon^2\left(\frac{d_2}{d_0}-\tfrac{1}{2}\left(\frac{d_1}{d_0}\right)^2\right)+\cdots$$

Substitution of these two into eq. (A.4.20) and omitting the H.O.T. yields the dimensionless shallow-water equation of motion in the following form:

$$\varepsilon \frac{\mathrm{d}}{\mathrm{d}x}\left(\frac{q^2}{d}\left(1+\frac{1}{(L_0-1)^2}\right)\right)+2\varepsilon^2\frac{\mathrm{d}}{\mathrm{d}x}\left(\frac{q^2}{d\kappa^2}\frac{\mathrm{d}d}{\mathrm{d}x}\left(\frac{a_1L_0^4-a_2L_0^3+a_3L_0^2-a_4L_0}{(L_0-1)^4}\right)\right)+$$
$$+gd\frac{\mathrm{d}}{\mathrm{d}x}(z_b+d) = -\frac{u_*q\kappa}{d(L_0-1)}-\varepsilon\frac{2}{\kappa^2}\frac{u_*q\kappa}{d(L_0-1)}\left(\frac{L_0^2-bL_0}{(L_0-1)^2}\right)\frac{\mathrm{d}d}{\mathrm{d}x} \qquad \text{(A.4.21)}$$

in which $L_0=\ln(d/z_0)$.

Eq. (A.4.14) and eq. (A.4.21) are the modified shallow-water equations, using a parabolic eddy-viscosity. To obtain the shallow-water equations in dimensional form, the characteristic values of eq. (A.2.1) have to be substituted in these equations. This yields the modified 1DH shallow-water equations:

Continuity equation: $$\frac{\mathrm{d}q}{\mathrm{d}x} = 0 \qquad \text{(A.4.22a)}$$

Equation of motion: $$\frac{\mathrm{d}}{\mathrm{d}x}\left(\alpha\frac{q^2}{d}\right)+gd\frac{\mathrm{d}}{\mathrm{d}x}(z_b+d) = -\gamma\lambda\left(\frac{q}{d}\right)^2 \qquad \text{(A.4.22b)}$$

in which $$\alpha = \left(1+\frac{1}{(L_0-1)^2}+\frac{2}{\kappa^2}\left(\frac{a_1L_0^4-a_2L_0^3+a_3L_0^2-a_4L_0}{(L_0-1)^4}\right)\frac{\mathrm{d}d}{\mathrm{d}x}\right)$$

$$\gamma = \left(1+\frac{2}{\kappa^2}\left(\frac{L_0^2-bL_0}{(L_0-1)^2}\right)\frac{\mathrm{d}d}{\mathrm{d}x}\right)$$

with $L_0 = \ln(d/z_0)$

$a_1 = 3.1016$

$a_2 = 14.117$

$a_3 = 21.560$

$a_4 = 3.5440$

$b = 2.4995$

$\lambda = \kappa^2/(L_0\text{-}1)^2$

In the first term of eq. (A.4.22b), the convective term, the convection coefficient α is introduced. For uniform, turbulent flows over horizontal bottoms the velocity profile is approximately logarithmic. The convection coefficient for such a profile reads:

$$\alpha = \left(1+\frac{1}{(L_0-1)^2}\right)$$

The value for α in eq. (A.4.22b) is dependent on the bathymetry through the first-order

derivative of the water depth.

The second term is the conventional hydrostatic pressure term.

The third term is the bottom friction term. In this term the friction parameter λ and the friction coefficient γ appear. For uniform, turbulent flow the bottom friction can be written as: $\tau_{bx} = -\rho u_*^2 = -\lambda (q/d)^2$. Substitution of the dimensional form of eq. (A.4.8) yields the expression for λ used here. The friction coefficient, γ, expresses the influence of flow non-uniformity on the bed shear stress. This coefficient is dependent on the bathymetry through the first-order derivative of the water depth.

Graphs of the convection and friction coefficients, α and γ, are plotted in Fig. A.4.3. The flow characteristics are the same as the ones for the analytical solutions of the horizontal and water depths of Fig. A.4.1 and Fig. A.4.2. The average velocity is 1. m/s, the water depth, d, is 20 m, the length of the sinusoidal sill, L, is 6500 m and the sill height, D, is 7.5 m. The convection coefficient, α, increases in the deceleration zone and decreases in the deceleration zone. The deviation from the value for uniform flow is small. The friction coefficient, γ, increases in the acceleration zone and decreases in the deceleration zone. The deviation from the value for uniform flow is also small for this coefficient.

Modifying the shallow-water equations with coefficients calculated with analytical solutions of the Navier-Stokes equations, using the method of the asymptotic expansions, turned out to be possible only for very mild slopes. The convective terms, which are assumed to be smaller than the friction and the pressure terms, become more important at steeper slopes. The set of equations expanded in such a way that the convective terms and the pressure term are important and the Reynolds stress terms are less important is a non-linear set of zeroth-order differential equations. Such a set is not easy to solve.

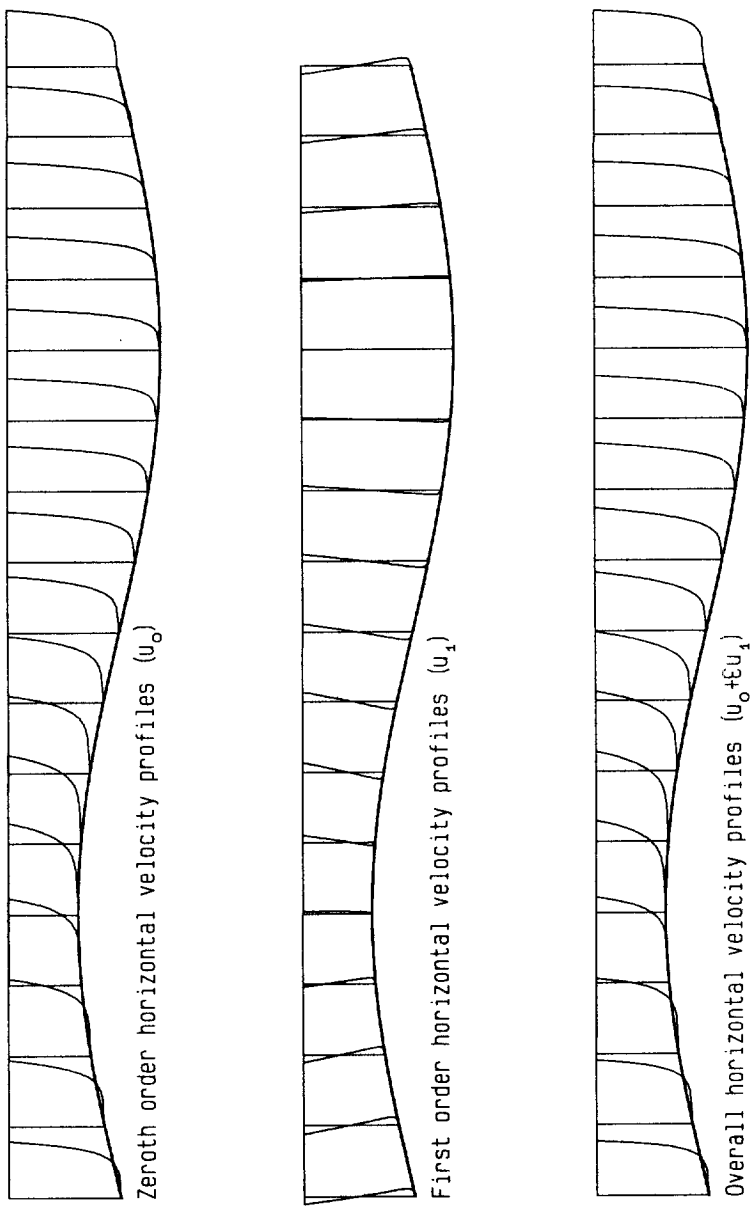

Figure A.4.1 The zeroth-order, first-order and overall horizontal velocity profiles

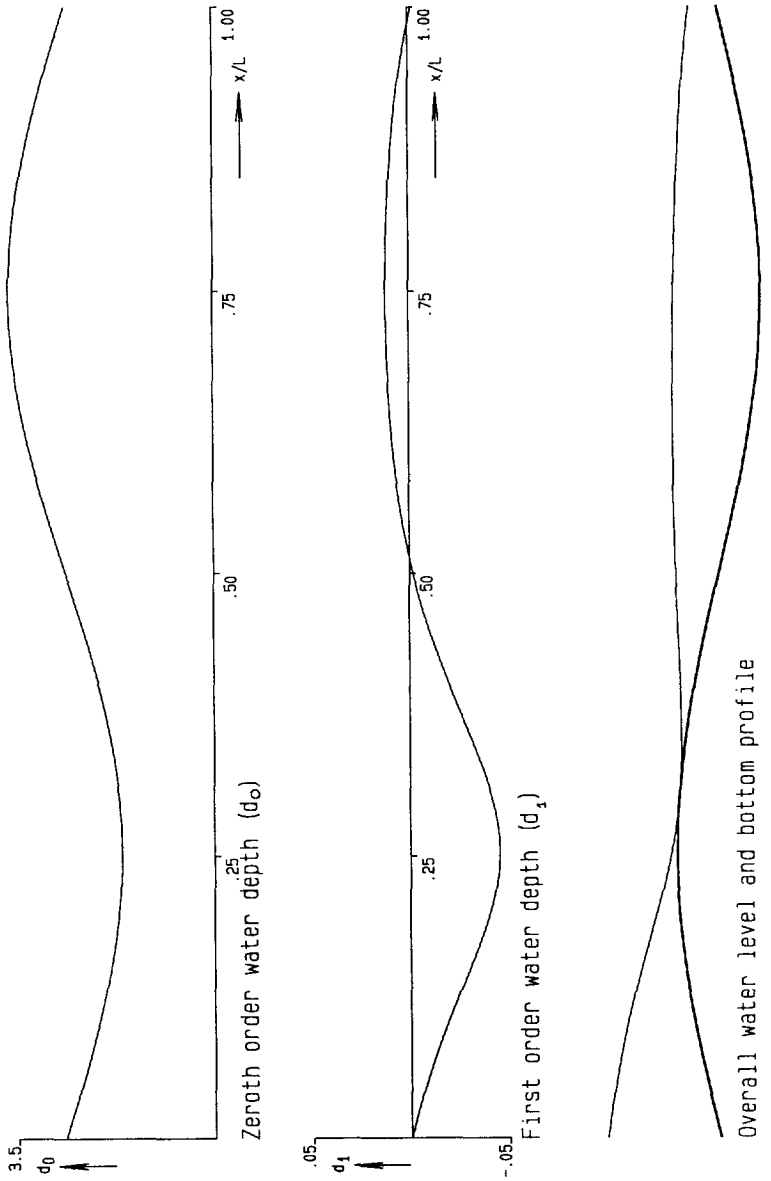

Figure A.4.2 The zeroth-order, first-order and overall water depths

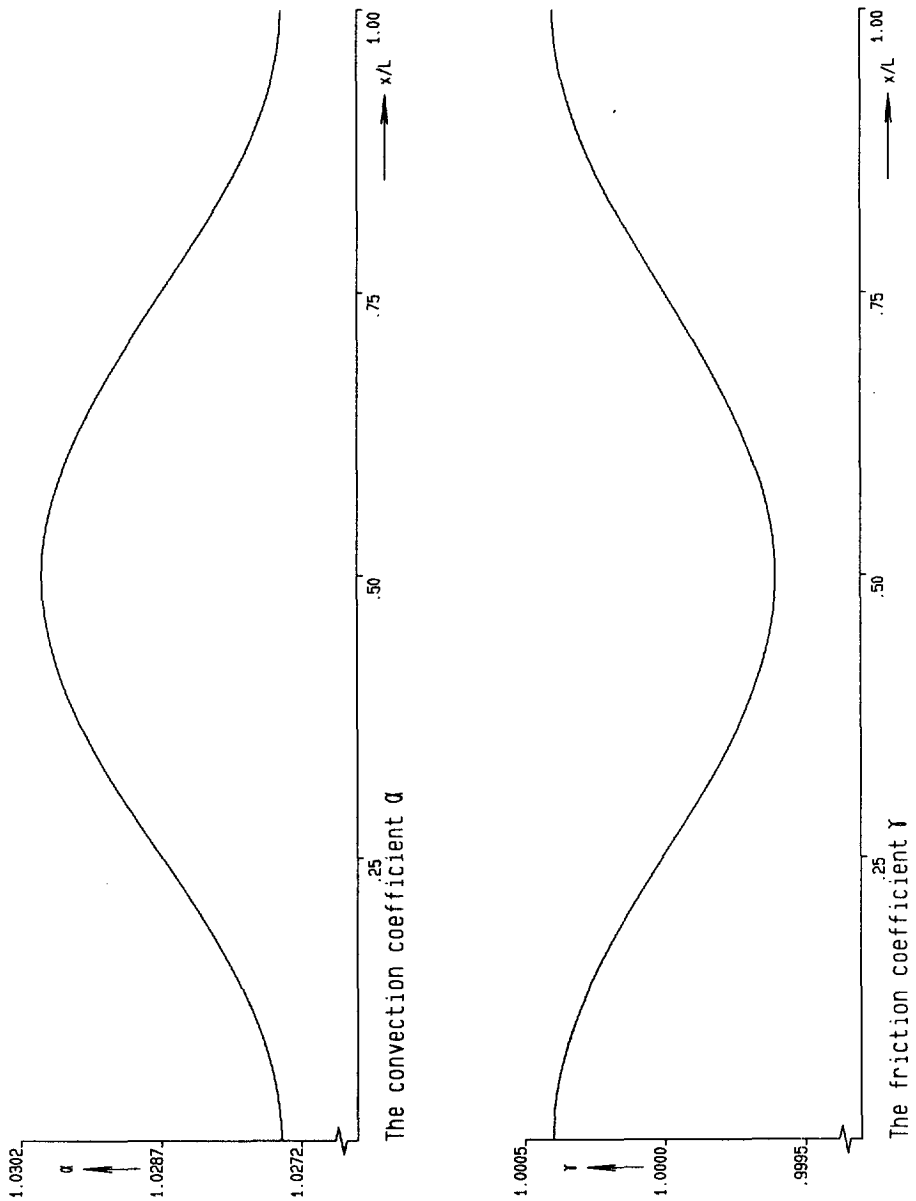

Figure A.4.3 The convection coefficient α and the friction coefficient γ

APPENDIX B: An expression for some logarithmic terms written as Taylor series

To derive the shallow-water equations, using the method of asymptotic expansions, it is necessary to solve different orders of perturbation velocities. In the calculation of the first-order horizontal velocity, logarithmic terms appear. These terms are divided by the eddy-viscosity and have to be integrated. Using a parabolic eddy-viscosity this division gives some difficulties because the eddy-viscosity is zero at the water surface and at the bottom. Especially the fact that the eddy-viscosity is also zero at the water surface makes it impossible to evaluate the logarithmic terms exactly. Therefore these terms have to be approximated by series. These terms read:

$$\frac{\ln(\sigma/\sigma_0) - \ln(1/\sigma_0)}{1-\sigma} \tag{B.1a}$$

and

$$\frac{\ln^2(\sigma/\sigma_0) - \ln^2(1/\sigma_0)}{1-\sigma} \tag{B.1b}$$

An arbitrary function, f, dependent on the arbitrary variable, x, can be written as a Taylor series around an arbitrary point, a, as:

$$f(x+a) = f(a) + xf'(a) + \tfrac{1}{2!}x^2 f''(a) + \tfrac{1}{3!}x^3 f'''(a) + \cdots$$

or

$$f(x+a) = f(a) + \sum_{i=0}^{\infty} \tfrac{1}{i!} x^i f^{(i)}(a) \tag{B.2}$$

This series contains derivatives of the function $f(x)$. The first equation chosen for $f(x)$ is the logarithmic part of eq. (B.1a), dependent on the variable σ:

$$f(x) = \ln(x/\sigma_0) \tag{B.3}$$

The i^{th} order derivative of f is:

$$\frac{d^i f}{dx^i} = -(i-1)!\,(-1)^i x^{-i} \tag{B.4}$$

Substitution of eq. (B.3) and eq. (B.4) into eq. (B.2) yields:

$$\ln((x+a)/\sigma_0) = \ln(a/\sigma_0) - \sum_{i=0}^{\infty} \tfrac{1}{i!} x^i \left((i-1)!\,(-1)^i a^{-i}\right)$$

Substitution of $x=(\sigma-1)$ and $a=1$ yields:

$$\ln(\sigma/\sigma_0) = \ln(1/\sigma_0) - \sum_{i=0}^{\infty} \frac{(\sigma-1)^i (-1)^i (1)^{-i}}{i}$$

$$= \ln(1/\sigma_0) - \sum_{i=0}^{\infty} \frac{(1-\sigma)^i}{i} \qquad \text{(B.5)}$$

Substitution of eq. (B.5) into eq. (B.1a) yields:

$$\frac{\ln(\sigma/\sigma_0) - \ln(1/\sigma_0)}{1-\sigma} = \frac{\ln(1/\sigma_0) - \sum_{i=0}^{\infty} \frac{(1-\sigma)^i}{i} - \ln(1/\sigma_0)}{1-\sigma} = -\sum_{i=0}^{\infty} \tfrac{1}{i}(1-\sigma)^{i-1} \qquad \text{(B.6)}$$

The same analysis can be done with eq. (B.1b). The function chosen for $f(x)$ is:

$$f(x) = \ln^2(x/\sigma_0) \qquad \text{(B.7)}$$

The first order derivative of f is:

$$\frac{df}{dx} = 2\frac{1}{x}\ln(x/\sigma_0)$$

The second order derivative of f is:

$$\frac{d^2f}{dx^2} = 2\left(-x^{-2}\ln(x/\sigma_0) + x^{-2}\right)$$

In general the i^{th} order derivative of f is:

$$\frac{d^if}{dx^i} = 2\left(-(i-1)!(-1)^i x^{-i}\ln(x/\sigma_0) + (i-1)!(-1)^i x^{-i}\sum_{k=1}^{i-1}\frac{1}{k}\right) \qquad \text{(B.8)}$$

Substitution of eq. (B.7) and eq. (B.8) into eq. (B.2) yields:

$$\ln^2((x+a)/\sigma_0) = \ln^2(a/\sigma_0) - 2\sum_{i=1}^{\infty}\tfrac{1}{i!}x^i\left((i-1)!(-1)^i a^{-i}\ln(a/\sigma_0) - (i-1)!(-1)^i a^{-i}\sum_{k=1}^{i-1}\frac{1}{k}\right)$$

Substitution of $x=(\sigma-1)$ and $a=1$ yields:

$$\ln^2(\sigma/\sigma_0) = \ln^2(1/\sigma_0) - 2\sum_{i=1}^{\infty}\left((-1)^i\frac{(\sigma-1)^i}{i}\ln(1/\sigma_0) - (-1)^i\frac{(\sigma-1)^i}{i}\sum_{k=1}^{i-1}\frac{1}{k}\right) \qquad \text{(B.9)}$$

Substitution of eq. (B.9) into eq. (B.1b) yields:

$$\frac{\ln^2(\sigma/\sigma_0)-\ln^2(1/\sigma_0)}{1-\sigma} = \frac{\ln^2(1/\sigma_0)-2\sum_{i=1}^{\infty}\left(\frac{(1-\sigma)^i}{i}\ln(1/\sigma_0)-\frac{(1-\sigma)^i}{i}\sum_{k=1}^{i-1}\frac{1}{k}\right)-\ln^2(1/\sigma_0)}{1-\sigma}$$

$$= -2\sum_{i=1}^{\infty}\left(\frac{(1-\sigma)^{i-1}}{i}\ln(1/\sigma_0)-\frac{(1-\sigma)^{i-1}}{i}\sum_{k=1}^{i-1}\frac{1}{k}\right) \qquad \text{(B.10)}$$

Eq. (B.6) and eq. (B.10) are substituted into the solution for the first-order Reynolds stresses. To obtain the first-order horizontal velocity, u_1, the expression for the Reynolds shear stress, containing the expressions (B.6) and (B.10), has to be divided by the parabolic eddy-viscosity and integrated with respect to σ. The first-order velocity is given by eq. (A.4.10) in which the integrated expressions (B.6) and (B.10) are recognisable.

APPENDIX C: An approximation for the first-order perturbation profile

The velocity profiles which can be used in the method of weighted residuals can be derived from the velocity profiles calculated with the method of asymptotic expansions. For a parabolic viscosity-model the zeroth-order velocity profile, derived by the method of asymptotic expansions, is logarithmic (eq. (A.4.7)). The first-order velocity profile, eq. (A.4.10), also contains a logarithmic shaped part, but it also contains a part with series in $(1-\sigma)$. Just like the main part of the first-order velocity of eq. (A.3.12) was used for the velocity profile of eq. (2.3.20), the main part of eq. (A.4.10) should be used for the first-order velocity profile of eq. (2.3.25a). It satisfies the boundary condition, $u(0)=0$ and $du/d\sigma=0$ at $\sigma=1$, and the discharge condition, $\int_0^1 u_1 d\sigma = 0$. But, if this first-order profile is used in the method of weighted residuals the part with the series causes many time-consuming calculations. To avoid these time-consuming calculations the part with the series is approximated with higher-order power terms of logarithms. Here only terms with logarithms to the power two and three are used.

The main part of eq. (A.4.10) reads:

$$u_1 = \frac{q}{d_0\kappa^2}\frac{L_{\sigma 0}}{(L_{\sigma 0}-1)^2}\frac{dd_0}{dx}\left(-\sum_{i=1}^{\infty}\frac{(1-\sigma)^i-1}{i^2}\left(2L_{\sigma 0}-3-2\sum_{k=1}^{i-1}\frac{1}{k}\right)-\ln(\sigma/\sigma_0)\frac{2(L_{\sigma 0}-b)}{L_{\sigma 0}-1}\right) \tag{C.1}$$

in which $L_{\sigma 0}$ stands for $\ln(1/\sigma_0)$ and $b=2.4995$.

The expression in the large brackets is proportional to:

$$\frac{-\sum_{i=1}^{\infty}\frac{(1-\sigma)^i-1}{i^2}\left(2L_{\sigma 0}-3-2\sum_{k=1}^{i-1}\frac{1}{k}\right)}{2(L_{\sigma 0}-b)}-\frac{\ln\sigma/\sigma_0}{L_{\sigma 0}-1} \tag{C.2}$$

Approximating eq. (C.1) with series in logarithms of powers up to two means that the first term of expression (C.2) is replaced by $\ln^2(\sigma/\sigma_0)$ times a normalisation factor such that the depth-integral of u_1 is zero. This yields the following result for the first-order velocity profile to be used in the method of the weighted residuals:

$$u_1 = \frac{q}{d}\left(\frac{\ln^2(\sigma/\sigma_0)}{L_{\sigma 0}^2-2L_{\sigma 0}+2}-\frac{\ln(\sigma/\sigma_0)}{L_{\sigma 0}-1}\right) \tag{C.3}$$

Graphs of the velocity profile of eq. (C.3) and eq. (C.1) are plotted in Fig. C.1.

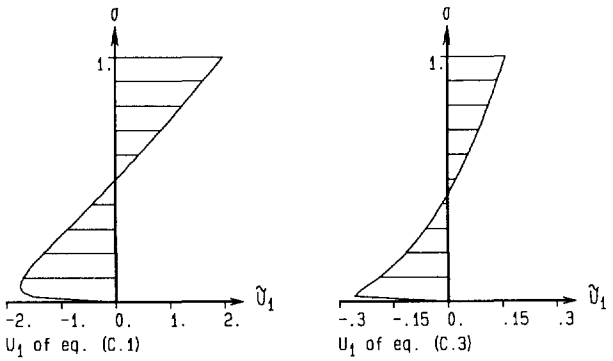

Figure C.1 The velocity profiles of eq. (C.1) and eq. (C.3) ($\tilde{u}$=ud/q)

To approximate eq. (C.1) with series of powers in logarithms up to three, these series are written as Taylor series around the value $\sigma=1$, in the following way:

$$\ln^3(\sigma/\sigma_0) = L_{\sigma 0}{}^3+(\sigma-1)\left(3L_{\sigma 0}{}^2\right)+(\sigma-1)^2\left(-\tfrac{3}{2}L_{\sigma 0}{}^2+3L_{\sigma 0}\right)+(\sigma-1)^3\left(L_{\sigma 0}{}^2-3L_{\sigma 0}+1\right)+\cdots \quad \text{(C.4)}$$

$$\ln^2(\sigma/\sigma_0) = L_{\sigma 0}{}^2+(\sigma-1)(2L_{\sigma 0})+(\sigma-1)^2(-L_{\sigma 0}+1)+(\sigma-1)^3\left(\tfrac{2}{3}L_{\sigma 0}-1\right)+\cdots \quad \text{(C.5)}$$

A linear combination of these two series has to be equal to the series of eq. (C.1), which reads:

$$\sum_{i=1}^{\infty}\frac{1-(1-\sigma)^i}{i^2}\left(2L_{\sigma 0}-3-2\sum_{k=1}^{i-1}\frac{1}{k}\right) = -\sigma(2L_{\sigma 0}-3)+\frac{(1-\sigma)^2-1}{4}(2L_{\sigma 0}-5)+\frac{(\sigma-1)^3-1}{9}(2L_{\sigma 0}-6)+\cdots \quad \text{(C.6)}$$

This means that:

$$a\cdot\{\text{eq. (C.4)}\}+b\cdot\{\text{eq. (C.5)}\} = \{\text{eq. (C.6)}\} \quad \text{(C.7)}$$

in which a and b are proportionality constants. Equating terms of equal power of σ on both sides of eq. (C.7) yields:

$$a = \frac{-2L_{\sigma 0}{}^2+5L_{\sigma 0}-3}{L_{\sigma 0}{}^3}$$

and

$$b = \frac{2L_{\sigma 0}{}^2-7L_{\sigma 0}+6}{L_{\sigma 0}{}^2}$$

Substitution of the values for a, b, eq. (C.4) and eq. (C.5) into eq. (C.6) yields:

$$\sum_{i=1}^{\infty}\frac{1-(1-\sigma)^i}{i^2}\left(2L_{\sigma 0}-3-2\sum_{k=1}^{i-1}\frac{1}{k}\right) = \frac{-2L_{\sigma 0}{}^2+5L_{\sigma 0}-3}{L_{\sigma 0}{}^3}\ln^3(\sigma/\sigma_0)+\frac{2L_{\sigma 0}{}^2-7L_{\sigma 0}+6}{L_{\sigma 0}{}^2}\ln^2(\sigma/\sigma_0) \quad \text{(C.8)}$$

The discharge of the first-order velocity profile used in the method of weighted

residuals has to be zero. This can be obtained by subtracting a logarithmic shaped profile from eq. (C.8). The values of profiles integrated with respect to the depth must have the same value. Therefore eq. (C.8) is written as:

$$\sum_{i=1}^{\infty} \frac{1-(1-\sigma)^i}{i^2}\left(2L_{\sigma 0}-3-2\sum_{k=1}^{i-1}\frac{1}{k}\right) = \ln^3(\sigma/\sigma_0)-\frac{L_{\sigma 0}(L_{\sigma 0}-2)}{L_{\sigma 0}-1}\ln^2(\sigma/\sigma_0)$$

Substitution of σ_0=0.001 in the factor containing $L_{\sigma 0}$, a value often used for flows in estuaries (Blom [1988]), yields:

$$\sum_{i=1}^{\infty} \frac{(1-\sigma)^i-1}{i^2}\left(2L_{\sigma 0}-3-2\sum_{k=1}^{i-1}\frac{1}{k}\right) = \ln^3(\sigma/\sigma_0)-5\ln^2(\sigma/\sigma_0)$$

Integration with respect to the water depth, yields:

$$\int_0^1 \ln^3(\sigma/\sigma_0)-5\ln^2(\sigma/\sigma_0)\,d\sigma = L_{\sigma 0}{}^3-8L_{\sigma 0}{}^2+16L_{\sigma 0}-16$$

The corresponding first-order velocity profile is:

$$u_1 = \frac{q}{d}\left(\frac{\ln^3(\sigma/\sigma_0)-5\ln^2(\sigma/\sigma_0)}{L_{\sigma 0}{}^3-8L_{\sigma 0}{}^2+16L_{\sigma 0}-16}-\frac{\ln(\sigma/\sigma_0)}{L_{\sigma 0}-1}\right) \qquad \text{(C.9)}$$

Graphs of the velocity profile of eq. (C.9) and eq. (C.1) are plotted in Fig. C.2.

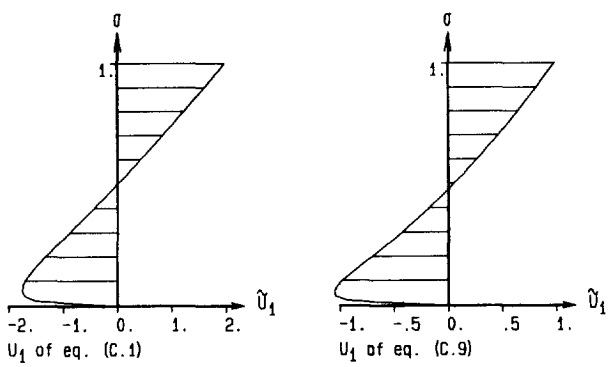

Figure C.2 The velocity profiles of eq. (C.1) and eq. (C.9) ($\bar{u}$=ud/q)

The first-order velocity profiles of the expressions (C.3) and (C.9) are applied in the method of weighted residuals (eq. (2.3.28), eq. (2.3.29) and eq. (2.3.37)).

APPENDIX D: The relative errors in the measured velocities

The velocities measured with a laser-Doppler velocimeter are dependent on the configuration of the laser beams. In the configurations B and C (Fig. 4.1.2), the laser-Doppler velocimeter is supposed to measure two orthogonal velocities in the measuring volume, formed by the intersection of the laser beams, in two directions making angles of 45° with respect to the horizontal plane. The real configuration deviates from this ideal configuration, causing errors. The most likely errors are caused by:

- Rotation of the beam configuration.
- Deviations in the angles between the plane of the reference beam and the illuminating beam and the horizontal plane causing deviations in the direction of the velocity components.
- Deviations in the angle between the reference beam and the illuminating beam causing deviations in the values of the velocities.

In addition to these geometric errors other errors are possible such as errors caused by:

- Changes in the zero adjustment of the laser-Doppler velocimeter.
- Noise.

The importance of these errors is discussed below.

Rotation of the beam configuration.

To estimate the errors due to the rotation of the configuration the assumption is made that the plane of the reference beam and the illuminating beam is not parallel to the bottom, as it should, but makes a small angle, α, with it. The velocity component measured is perpendicular to the optical axis and directed from one reference beam towards the illuminating beam for one channel, and from the illuminating beam towards the other reference beam for the other channel (Fig. D.1). The measured velocity components are recombined into horizontal and vertical components.

The error of the horizontal velocity component is for small α proportional to the vertical velocity. The error of the vertical velocity is proportional to the horizontal velocity. The relative error in the horizontal velocity is negligible when the vertical velocity is small. But in that case, the relative error in the vertical velocity can be large.

The error in the turbulence energy is proportional to the turbulence energy, and is

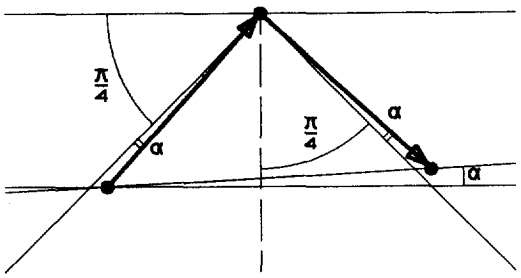

Figure D.1 The influence on the velocities due to the rotation of the beam configuration.

generally small. The relative error in the Reynolds shear stress is also proportional to the turbulence energy, but can be relatively large, because the turbulence energy is larger than the Reynolds shear stress.

Deviation in the angle between the planes of the reference beam and the illuminating beam and the horizontal.

If the angle between the planes of the reference beam and the illuminating beam and the horizontal deviates from 45°, errors are recognizable in the average vertical velocity, the turbulence energy and the Reynolds shear stress. In the error estimation for this case the assumption is made that only one of the angles deviate from the angle 45°, say that the angle between the plane of the illuminating beam and the reference beam and the horizontal is $45° + \beta$ (Fig. D.2).

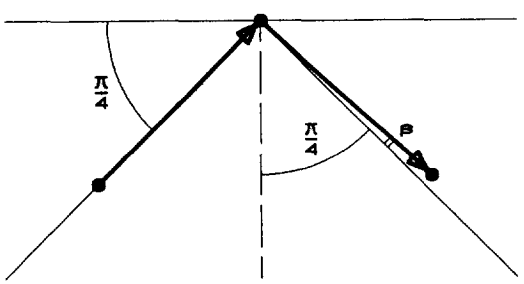

Figure D.2 The influence on the velocities due to a small angle.

The errors in the horizontal and vertical velocities are proportional to the horizontal velocity minus the vertical velocity. If the vertical velocity is small then the error in the horizontal velocity is again negligible, while the error in the vertical velocity can be large.

The error in the turbulence energy is again proportional to the turbulence energy, and

is small. The error in the Reynolds shear stress is also proportional to the turbulence energy, but can be relatively large, because the turbulence energy is much larger then the Reynolds shear stress.

Errors in the angle between the reference beam and the illuminating beam.

The doppler frequency has to be transformed to a velocity. The equation describing the relation between the Doppler frequency and the velocity reads:

$$u = \frac{\lambda \Delta f}{2 \sin \varphi}$$

in which u is the velocity, λ is the laser wave length (λ = 632.8 nm), Δf the frequency and φ is half the angle between the illuminating beam and the reference beam. Due to the inaccuracies in the configuration an error can also appear in the angle between reference beam and the illuminating beam. The influence on the velocities and turbulence fluctuations is small. Assuming an error in φ of γ, with γ very small, yields:

$$\Delta u = \frac{\lambda \Delta f}{2 \sin(\varphi + \gamma)} = \frac{\lambda \Delta f}{2 \sin \varphi}(1 - \gamma)$$

This error is only important for the vertical velocity component, when this component is small, because this vertical component is derived by subtraction of two nearly the same velocities, in which both channels can have different values for γ.

Quantitative estimate of geometric errors.

The overall velocity error due to the geometric effects mentioned above has been estimated quantitatively by projecting the laser beams on a vertical plane. The angles between the laser beams are determined by measuring the distances between the projected beams and the distance between the projection plane and intersection of the beams. Only the distances between the laser beams of two of the three measurement series were measured. The distances in the first series were not measured.

The error in the measured velocities are due to inaccuracies in the measurements of the location of the projected laser beams. The assumption is made that the error in the distances measured in the projection plane is 20 mm (the projection of the illuminating beam has a diameter of about 20 mm and of the reference beam of about 15 mm), and in the distance between the measuring volume and the projection plane is 20 mm. The maximum error in the velocity is then 5%. The errors in the velocities of the first series could not be

determined because the locations of the projected beams were not measured. These errors are assumed to be in the same range as the errors of the other series.

Changes in the zero adjustment.

Due to changes in the temperature and humidity, vibrations, etc. the zero adjustment of the laser-Doppler velocimeter, the value measured when the velocity is zero, can vary. An error in the zero adjustment gives an error of the average velocity. The influence on the turbulence intensities is generally small.

Errors due to noise.

Errors due to a difference of the noise level in the two channels can play an dominant part in the measured values of the Reynolds shear stresses. For an ideal laser beam configuration the Reynolds shear stress is the difference between the Reynolds normal stress measured in both channels.

If the noise of the channels is unequal, then this difference is not equal to zero so the noise influences the measured Reynolds shear stress. This phenomenon manifests itself generally in a constant added to the Reynolds shear stress, as can be seen in Fig. 4.3.1. In the turbulence energy noise is not clearly recognizable because the mean square velocities of the channels are added.

Curriculum Vitae

Pieter Blom werd op 29 januari 1959 in Schiedam geboren. In zijn vierde levensjaar verhuisde hij naar 's-Gravenhage alwaar hij een groot deel van zijn lagere school opleiding volgde. In zijn tiende levensjaar verhuisde hij naar Pijnacker alwaar hij het lager onderwijs vervolgde en zijn middelbare school opleiding genoot. In 1976 behaalde hij daar het Mavo diploma.

Vervolgens studeerde hij "Weg- en Waterbouwkunde" aan de MTS te 's-Gravenhage, alwaar hij in 1978 het getuigschrift behaalde. Hij vervolgde zijn technische studie aan de HTS te 's-Gravenhage, die hij in 1980 verliet om in Delft aan de Technische Hogeschool "Civiele Techniek" te gaan studeren. In 1987 werd deze studie afgerond bij de vakgroep constructieleer, sectie funderingstechniek.

In dat zelfde jaar trad hij in dienst van de Technische Universiteit Delft als Assistent in opleiding.